Supporting Information: Ga and Zn Increase the Oxygen Affinity of Cu-based Catalysts for the CO_x Hydrogenation According to Ab Initio Atomistic Thermodynamics

Andreas Müller,[†] Aleix Comas-Vives,[*,‡,¶] and Christophe Copéret[*,†]

†*Department of Chemistry and Applied Biosciences, ETH Zürich, 8093 Zurich, Switzerland*

‡*Institute of Materials Chemistry, TU Wien, 1060 Vienna, Austria*

¶*Departament de Química, Universitat Autònoma de Barcelona, 08193 Cerdanyola del Vallès, Catalonia, Spain*

E-mail: Aleix.Comas@uab.cat; ccoperet@ethz.ch

1 Computational Details

1.1 Typical INCAR File

System = "System Name"

LCHARG = .FALSE.

Electronic minimization

PREC = NORMAL

GGA = PE

EDIFF = 1E-5

ENCUT = 400

ALGO = VeryFast

VOSKOWN = 1

LREAL = Auto

Ionic relaxation

EDIFFG = -0.01

NSW = 5000

IBRION = 2

ISIF = 0

POTIM = 0.5

DOS related values

ISMEAR = 1

SIGMA = 0.2

Parallelization etc.

NPAR = 1

1.2 Typical KPOINTS File

K-Points

0

Monkhorst-Pack

3 3 1

0 0 0

2 *Ab Initio* Thermodynamics

2.1 Chemical Potential in Solids and Gas Phase

The chemical potential of a substance at a temperature of 0 K and standard pressure, μ_i^0 at 0 K, is the electronic energy of the substance as calculated by DFT-based calculations. For an atom X in a bulk structure consisting of k atoms X, it is defined as the contribution of a single atom to the bulk internal energy (and thus the k^{th} part of the electronic energy of the substance as calculated by DFT). As vibrational, rotational, and other temperature-dependent contributions to the chemical potential of a bulk material are small (when the temperature is much lower than the melting temperature of the bulk), the temperature-dependency of the bulk chemical potential can be safely neglected.

$$\mu_{X,bulk}(T) \approx \mu_{X,bulk}(0\text{K}) = \mu^0_{X,bulk} = \frac{E_{X_k,bulk}}{k} \tag{1}$$

If the bulk consists of multiple elements (i.e. alloys), it is important to differentiate between the individual pure chemical potentials, which are defined according to equation (1), and the chemical potential of the elements in the alloy bulk structure, which also contains the mixing energy of the system. For systems consisting of two elements, the bulk internal

energy $E_{X_{n_X},Y_{n_Y},bulk}$ can be expressed as a function of the individual chemical potentials:

$$E_{X_nY_k,bulk} = n_X \cdot \mu^0_{X,X_nY_k,bulk} + n_Y \cdot \mu^0_{Y,X_nY_k,bulk} \tag{2}$$

For an equilibrium structure (energetic minima), the individual chemical potentials are related according to the Gibbs–Duhem equation:

$$d\mu_X = -\frac{n_X}{n_Y} d\mu_Y \tag{3}$$

But since the Gibbs–Duhem equation only relates the individual chemical potentials, at least one chemical potential has to be known to determine the chemical potentials in the bulk structure. Alternatively, the individual bulk internal energies can be calculated explicitly without knowing the individual chemical potentials for each configuration, which can then be used to estimate the mixing energy according to equation (4) and used to correct the surface energy of the alloy slabs:

$$\Delta E^{Mixing}_{n_X,n_Y} = E_{X_nY_k,bulk} - n_X \cdot \mu^0_{X,bulk} - n_Y \cdot \mu^0_{Y,bulk} \tag{4}$$

Any gas can be approximated as an ideal gas for sufficiently large temperatures and sufficiently low partial pressures. The chemical potential of an ideal gas Z can be written as the sum of the chemical potential at zero temperature and standard pressure $\mu_{Z,gas}(0\mathrm{K})$ ($\mu^0_{Z,gas}$) and the pressure and temperature dependent change of the chemical potential $\Delta\mu_{Z,gas}(T, p_Z)$. The vibrational, rotational, and other temperature-dependent, but pressure-independent contributions $\Delta G_Z(T)$ can be calculated according to the following formula using the values in the thermochemical Tables.[S1]

$$\Delta G_Z(T) = \Delta H_Z(T) - T \cdot \Delta S_Z(T) = H_Z(T) - H_Z(0K) - T \cdot S_Z(T) \tag{5}$$

The pressure-dependent term is based on the ideal gas law and has the following form:

$$k_B \cdot T \cdot \ln\left\{\frac{p_Z}{p^0}\right\} \tag{6}$$

Combining these terms together gives the following equation describing the temperature- and pressure-dependency of the chemical potential of an atom in the gas phase:

$$\mu_{Z,gas} = \mu_{Z,gas}(0\mathrm{K}) + \Delta\mu_{Z,gas} = \mu^0_{Z,gas} + \Delta G_Z(T) + k_B \cdot T \cdot \ln\left\{\frac{p_Z}{p^0}\right\} \tag{7}$$

For molecular gases, the chemical potential of a single atom can be calculated using one of the two following methods. For molecules constructed only from multiples of the same atom, such as dioxygen (O_2), the chemical potential of a single atom is the atomic fraction of the molecular chemical potential. For O* in O_2, the chemical potential of O* (μ_{O,O_2}) is half of the chemical potential of O_2 (μ_{O_2}).

$$\mu_{O,O_2} = \frac{\mu_{O_2}}{2} = \frac{1}{2} \cdot \left[\mu^0_{O_2} + \Delta G_{O_2}(T) + k_B \cdot T \cdot \ln\left\{\frac{p_{O_2}}{p^0}\right\}\right] \tag{8}$$

For gases consisting of multiple different atoms, such as CO_2, the chemical potential of a single atom is defined as the difference of the chemical potential of the whole molecule and the chemical potential of the remaining molecule without that specific atom. As an example, the chemical potential of O* in CO_2 is the difference between the chemical potential of CO_2 and the chemical potential of CO.

$$\begin{aligned}\mu_{O,CO_2} &= \mu_{CO_2} - \mu_{CO} \\ &= [\mu^0_{CO_2} - \mu^0_{CO}] + [\Delta G_{CO_2}(T) - \Delta G_{CO}(T)] + k_B \cdot T \cdot \ln\left\{\frac{p_{CO_2}}{p_{CO}}\right\}\end{aligned} \tag{9}$$

As seen in equations (8) and (9), the chemical potential for any atom/molecule Z directly in the gas phase or a in gas containing Z can be represented by an equation of the following

form:

$$\mu_{Z,Gas} = a_Z + b_Z(T) + c_Z(T,p) \tag{10}$$

where a_Z contains all the constant terms, $b_Z(T)$ contains all temperature-dependent but pressure-independent terms and $c_Z(T,p)$ contains all both temperature- and pressure-depending terms. For a fixed temperature T_{fix}, the expression in equation (10) can be further simplified into the following equation depending linearly on the logarithm of the individual partial pressures of each gas:

$$\mu_{Z,Gas} = d_Z(T_{fix}) + e_Z(T_{fix}) \cdot \left[\ln\left\{ \frac{p_Z}{p^0} \right\} \quad \text{or} \quad \ln\left\{ \frac{p_{M-Z}}{p_M} \right\} \right] \tag{11}$$

where the chemical potential of an atom/molecule Z in the gas phase for a fixed temperature T_{fix} depends only on the partial pressure of the atoms/molecules in the gas phase.

2.2 Surface Energy

The surface energy γ is defined as the energy generated by a surface relative to the energy of the bulk, normalized by the surface area. The bulk energy can be expressed using the bulk chemical potential as described in equation (1). This gives as a result the following equation for the surface energy (n_X atoms of bulk material X):

$$\gamma_{n_X} = \frac{E_{tot,Surface} - E_{Bulk,n_X}}{A} = \frac{E_{tot,Surface} - n_X \cdot \mu_{X,bulk}}{A} \tag{12}$$

If the bulk material consists of multiple elements, the energy of the bulk can be expressed as the individual bulk chemical potential (n_X atoms of bulk material X, n_Y atoms of bulk material Y) assuming ideal solids:

$$\gamma_{n_X,n_Y} = \frac{E_{tot,Surface} - n_X \cdot \mu_{X,bulk} - n_Y \cdot \mu_{Y,bulk}}{A} \tag{13}$$

If real solids are used, the chemical potential of the atoms in the alloy bulk structure must be used, which can be represented by the energy of an equivalent bulk structure:

$$\begin{aligned}\gamma_{n_X,n_Y} &= \frac{E_{tot,Surface} - n_X \cdot \mu_{X,n_X,n_Y} - n_Y \cdot \mu_{Y,n_X,n_Y}}{A} \\ &= \frac{E_{tot,Surface} - E_{X_nY_k,bulk}}{A}\end{aligned} \tag{14}$$

If an atom Z is adsorbed from the gas phase (the source of adsorbates Z), the chemical potential of the atom in the gas phase must also be subtracted giving the following equation as a result:

$$\gamma_{n_X,n_Y,n_Z} = \frac{1}{A} \cdot (E_{Surface,n_X,n_Y,n_Z} - n_X \cdot \mu_{X,n_X,n_Y} - n_Y \cdot \mu_{Y,n_X,n_Y} - n_Z \cdot \mu_{Z,Gas}) \tag{15}$$

Equation (15) shows the dependency of the surface energy on the chemical potential of both the individual bulk metals as well the gas phase molecules. If the individual chemical potentials are replaced by the chemical potential of an ideal bulk structure with the same stoichiometry using equation (1), equation (15) further simplifies to the following expression, which now only has the gas phase chemical potential $\mu_{Z,Gas}$ as a variable:

$$\gamma_{n_X,n_Y,n_Z} = \frac{1}{A} \cdot (E_{Surface,n_X,n_Y,n_Z} - E_{X_nY_k,bulk} - n_Z \cdot \mu_{Z,Gas}) \tag{16}$$

Inserting the expression in equation (11) into equation (16) results in a expression depending linearly on the logarithm of the different partial pressures, as follows:

$$\begin{aligned}\gamma_{n_X,n_Y,n_Z}(T_{fix},p) = &\frac{1}{A} \cdot f_{X,Y,Z}(T_{fix}) \\ &- \frac{1}{A} \cdot g_{X,Y,Z}(T_{fix}) \cdot \ln\left[\left\{\frac{p_Z}{p^0}\right\} \quad \text{or} \quad \ln\left\{\frac{p_{M-Z}}{p_M}\right\}\right]\end{aligned} \tag{17}$$

where the surface energy of a model $\gamma_{n_X,n_Y,n_Z}(T,p)$ for a fixed temperature T_{fix} depends only on the partial pressure of the adsorbate atoms/molecules in the gas phase.

2.3 Oxygen Chemical Potential for Different Starting Conditions

Figure 1 in the main text shows the chemical potential of oxygen (μ_O) under CO_x hydrogenation conditions depending on the molar ratio of CO_2 in the feedstock (X_{CO_2}). It was constructed by first plotting μ_O as a function of the chemical potentials of CO_2, CO, H_2O and H_2 under reaction conditions based on the different starting conditions and the RWGS conversion (ξ_{RWGS}) as a single parameter (compare equations (9) and (10) in the main text. Several of these plots for different starting conditions are shown in Figures S1 (feed of 75 % H_2 and 25 % CO_2), S2 (feed of 75 % H_2, 12.5 % CO and 12.5 % CO_2), S3 (feed of 75 % H_2, 23.75 % CO and 1.25 % CO_2) and S4 (feed of 75 % H_2 and 25 % CO). Table **S1** shows the range of accessible chemical potentials of the three main adsorbates under reaction conditions based on the different starting conditions, summarising the results shown in Figures S1-S4.

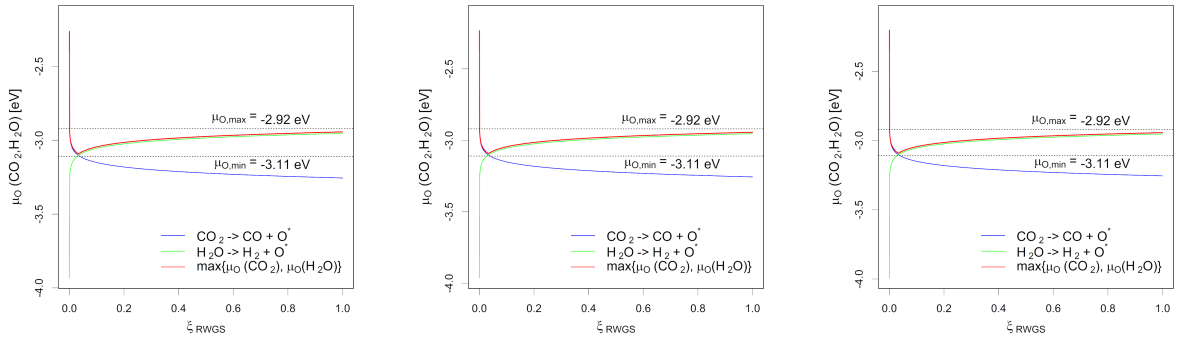

(a) $p^0_{H_2}$ = 15 bar, p^0_{CO} = 0 bar, $p^0_{CO_2}$ = 5 bar

(b) $p^0_{H_2}$ = 30 bar, p^0_{CO} = 0 bar, $p^0_{CO_2}$ = 10 bar

(c) $p^0_{H_2}$ = 60 bar, p^0_{CO} = 0 bar, $p^0_{CO_2}$ = 20 bar

Figure S1: Chemical potential of oxygen depending on the chemical potentials of CO_2, CO, H_2O and H_2 under reaction conditions with starting conditions of 75 % H_2, 0 % CO, 25 % CO_2 and p^0_{tot} = 20 bar (a), 40 bar (b) and 80 bar (c).

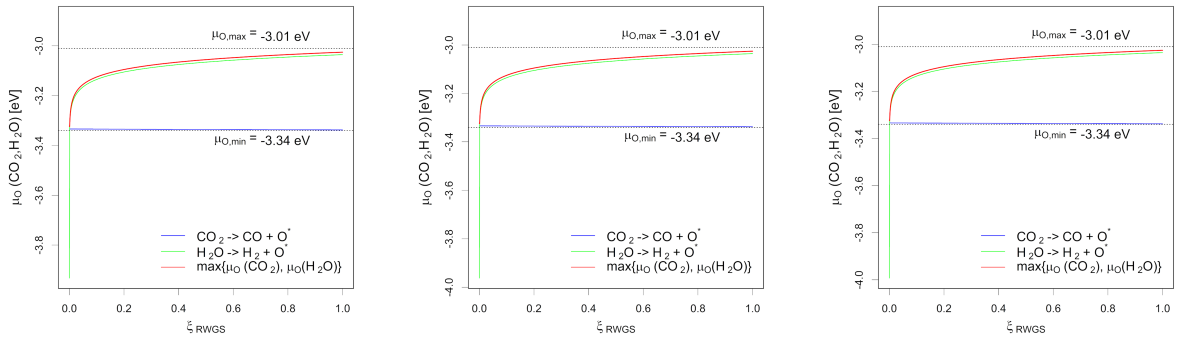

(a) $p^0_{H_2}$ = 15 bar, p^0_{CO} = 2.5 bar, $p^0_{CO_2}$ = 2.5 bar

(b) $p^0_{H_2}$ = 30 bar, p^0_{CO} = 5 bar, $p^0_{CO_2}$ = 5 bar

(c) $p^0_{H_2}$ = 60 bar, p^0_{CO} = 10 bar, $p^0_{CO_2}$ = 10 bar

Figure S2: Chemical potential of oxygen depending on the chemical potentials of CO_2, CO, H_2O and H_2 under reaction conditions with starting conditions of 75 % H_2, 12.5 % CO, 12.5 % CO_2 and p^0_{tot} = 20 bar (a), 40 bar (b) and 80 bar (c).

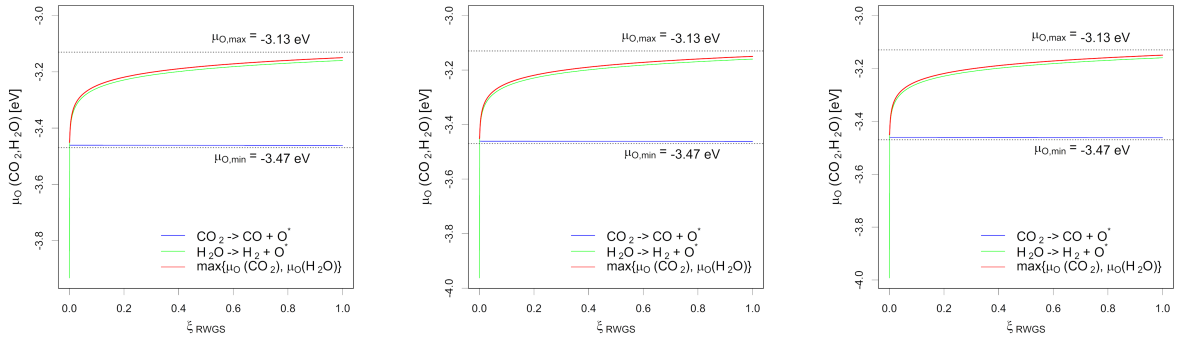

(a) $p^0_{H_2}$ = 15 bar, p^0_{CO} = 4.75 bar, $p^0_{CO_2}$ = 0.25 bar

(b) $p^0_{H_2}$ = 30 bar, p^0_{CO} = 9.5 bar, $p^0_{CO_2}$ = 0.5 bar

(c) $p^0_{H_2}$ = 60 bar, p^0_{CO} = 19 bar, $p^0_{CO_2}$ = 1 bar

Figure S3: Chemical potential of oxygen depending on the chemical potentials of CO_2, CO, H_2O and H_2 under reaction conditions with starting conditions of 75 % H_2, 23.75 % CO, 1.25 % CO_2 and p^0_{tot} = 20 bar (a), 40 bar (b) and 80 bar (c).

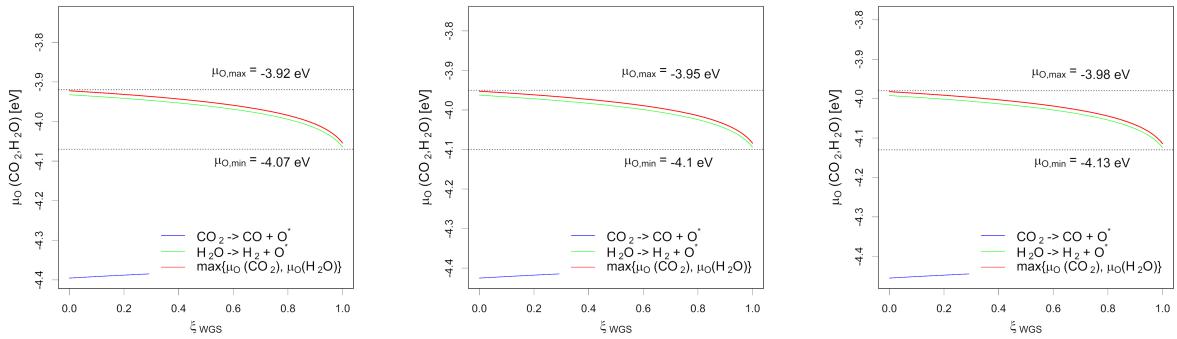

(a) $p^0_{H_2}$ = 15 bar, p^0_{CO} = 5 bar, $p^0_{CO_2}$ = 0 bar

(b) $p^0_{H_2}$ = 30 bar, p^0_{CO} = 10 bar, $p^0_{CO_2}$ = 0 bar

(c) $p^0_{H_2}$ = 60 bar, p^0_{CO} = 20 bar, $p^0_{CO_2}$ = 0 bar

Figure S4: Chemical potential of oxygen depending on the chemical potentials of CO_2, CO, H_2O and H_2 under reaction conditions with starting conditions of 75 % H_2, 25 % CO, 0 % CO_2 and p^0_{tot} = 20 bar (a), 40 bar (b) and 80 bar (c).

Table S1: Chemical potentials of hydrogen, CO and oxygen for selected initial hydrogen, CO and CO_2-partial pressures (assuming a least minimal RWGS-conversion) at 230 °C. The influence of the ratio of CO_2 to CO onto μ_O can clearly be seen. The influence of the hydrogen partial pressure onto μ_H is quite small. μ_{CO} already increases quite strongly when small quantities of CO are added to the feedstock gas.

$p_{H_2}^{init}$ [bar]	p_{CO}^{init} [bar]	$p_{CO_2}^{init}$ [bar]	μ_H [eV]	μ_{CO} [eV]	μ_O [eV]
15	10^{-10}	5	-0.246 to -0.245	-1.944 to -0.967	-3.11 to -2.92
30	10^{-10}	10	-0.231 to -0.230	-1.944 to -0.937	-3.11 to -2.92
60	10^{-10}	20	-0.216 to -0.215	-1.944 to -0.907	-3.11 to -2.92
15	2.5	2.5	-0.245	-0.912 to -0.910	-3.34 to -3.01
30	5	5	-0.230	-0.882 to -0.880	-3.34 to -3.01
60	10	10	-0.215	-0.852 to -0.850	-3.34 to -3.01
15	4.75	0.25	-0.245	-0.884	-3.47 to -3.13
30	9.5	0.5	-0.230	-0.854	-3.47 to -3.13
60	19	1	-0.215	-0.825	-3.47 to -3.13
15	5	10^{-10}	-0.245	-0.882	-4.07 to -3.92
30	10	10^{-10}	-0.230	-0.852	-4.10 to -3.95
60	20	10^{-10}	-0.215	-0.822	-4.13 to -3.98

Figure S5 shows how μ_O under CO_x hydrogenation reaction conditions depends not linearly on ξ_{RWGS}, but changes increases rather strongly as soon as small quantities of H_2O is formed by the RWGS reaction while not changing strongly after this initial increase of μ_O.

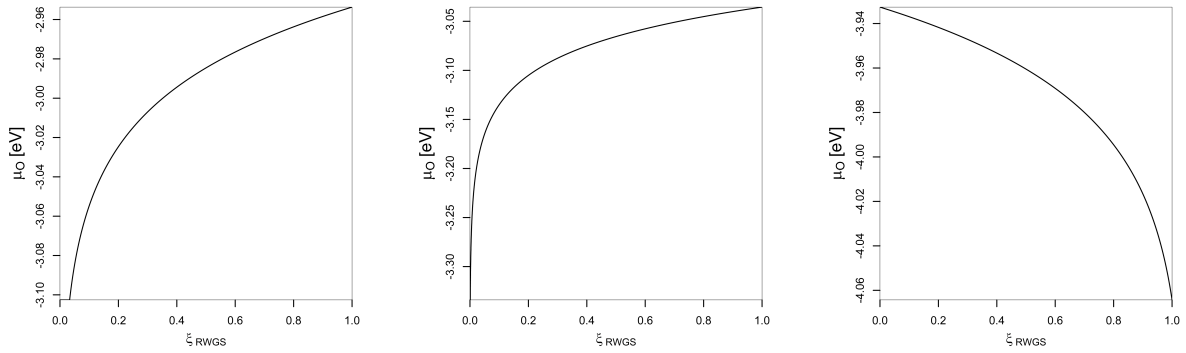

Figure S5: Chemical potential of oxygen (μ_O) depending on the chemical potentials of CO_2, CO, H_2O and H_2 under reaction conditions with starting conditions of 15 bar H_2 and 5 bar CO_X (Mixture of CO_2 and CO at specific values of X_{CO_2}) at 230 °C with the colour gradient indicating the progressing (R)WGS-conversion.
(a) Pure CO_2 hydrogenation ($X_{CO_2} = 1$, $X_{CO} = 0$).
(b) CO_2/CO hydrogenation ($X_{CO_2} = 0.5$, $X_{CO} = 0.5$).
(c) Pure CO hydrogenation ($X_{CO_2} = 0$, $X_{CO} = 1$).
It can be seen that the oxygen chemical potential does not depend linearly on the (R)WGS-conversion.

3 Surface Stability Diagrams in Oxygen Atmosphere

3.1 Individual Surface Stability Diagrams in Oxygen Atmosphere

(100)-Facet

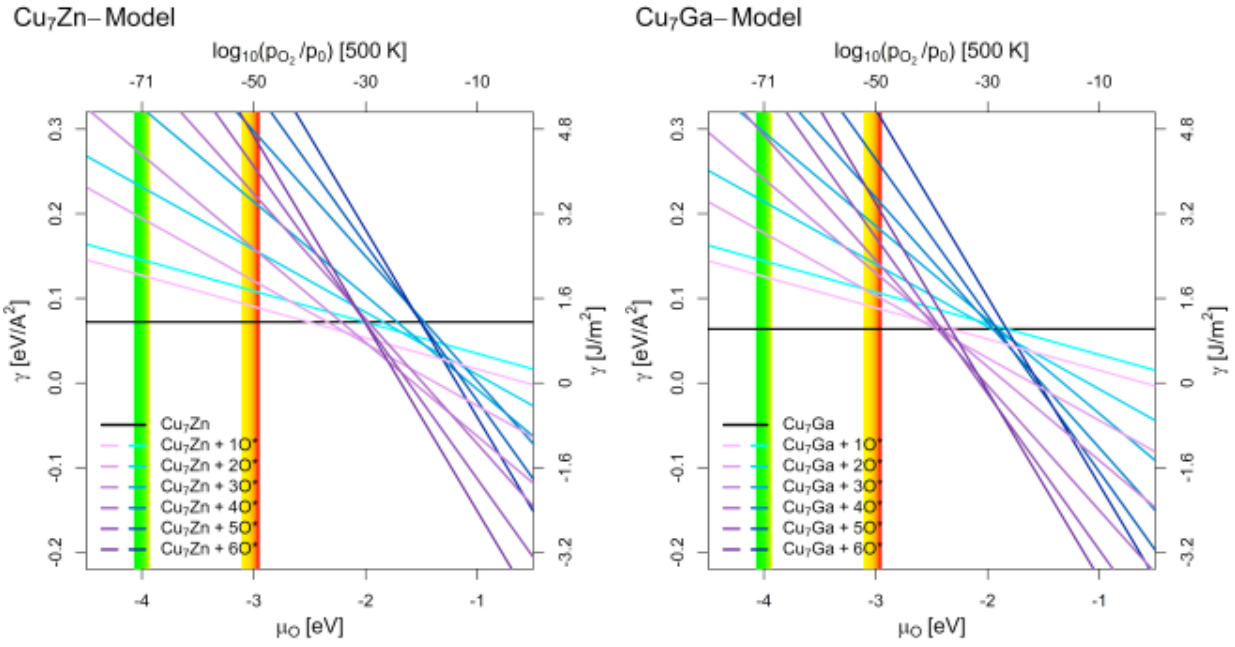

(a) (b)

(c) (d)

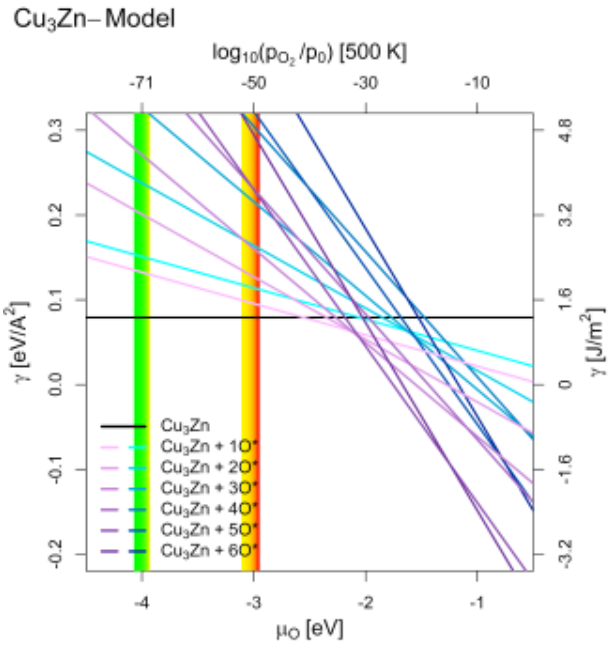
Cu3Zn−Model
log10(pO2/p0) [500 K]
-71
-50
-30
-10
γ [eV/Å2]
γ [J/m2]
μO [eV]
Cu3Zn
Cu3Zn + 1O*
Cu3Zn + 2O*
Cu3Zn + 3O*
Cu3Zn + 4O*
Cu3Zn + 5O*
Cu3Zn + 6O*

(e)

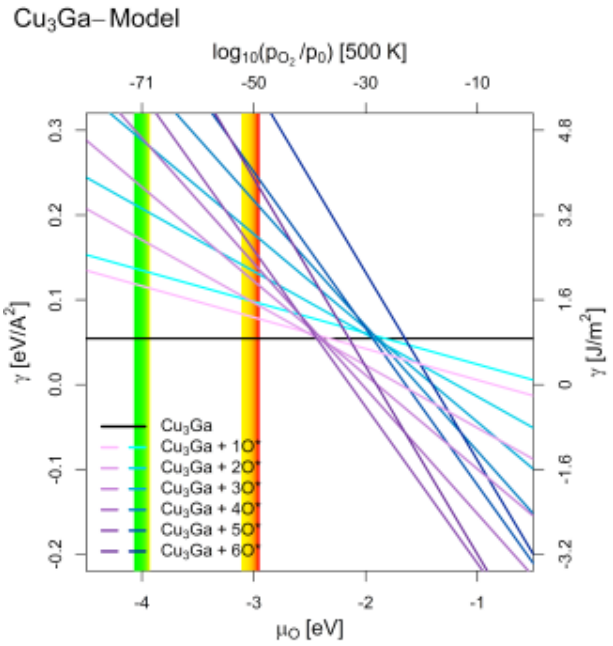
Cu3Ga−Model
log10(pO2/p0) [500 K]
-71
-50
-30
-10
γ [eV/Å2]
γ [J/m2]
μO [eV]
Cu3Ga
Cu3Ga + 1O*
Cu3Ga + 2O*
Cu3Ga + 3O*
Cu3Ga + 4O*
Cu3Ga + 5O*
Cu3Ga + 6O*

(f)

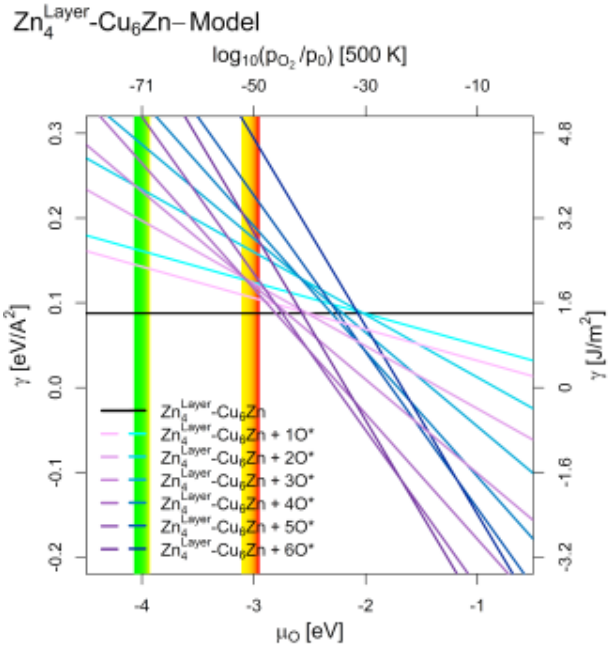
Zn4Layer-Cu6Zn−Model
log10(pO2/p0) [500 K]
-71
-50
-30
-10
γ [eV/Å2]
γ [J/m2]
μO [eV]
Zn4Layer-Cu6Zn
Zn4Layer-Cu6Zn + 1O*
Zn4Layer-Cu6Zn + 2O*
Zn4Layer-Cu6Zn + 3O*
Zn4Layer-Cu6Zn + 4O*
Zn4Layer-Cu6Zn + 5O*
Zn4Layer-Cu6Zn + 6O*

(g)

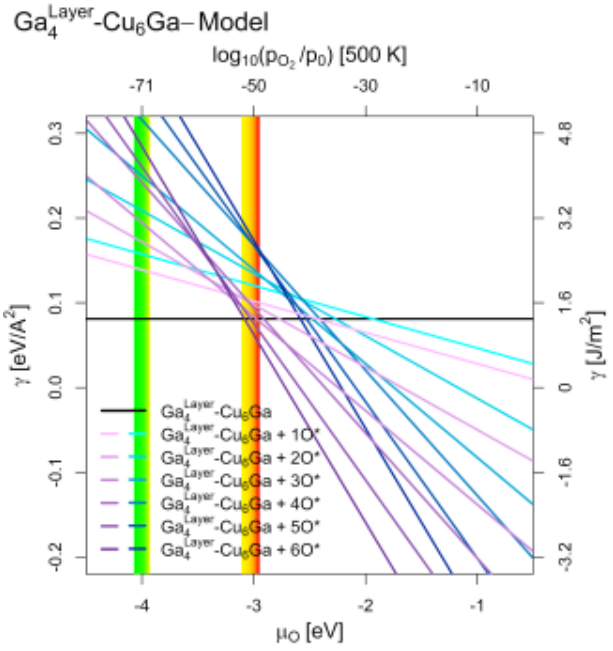
Ga4Layer-Cu6Ga−Model
log10(pO2/p0) [500 K]
-71
-50
-30
-10
γ [eV/Å2]
γ [J/m2]
μO [eV]
Ga4Layer-Cu6Ga
Ga4Layer-Cu6Ga + 1O*
Ga4Layer-Cu6Ga + 2O*
Ga4Layer-Cu6Ga + 3O*
Ga4Layer-Cu6Ga + 4O*
Ga4Layer-Cu6Ga + 5O*
Ga4Layer-Cu6Ga + 6O*

(h)

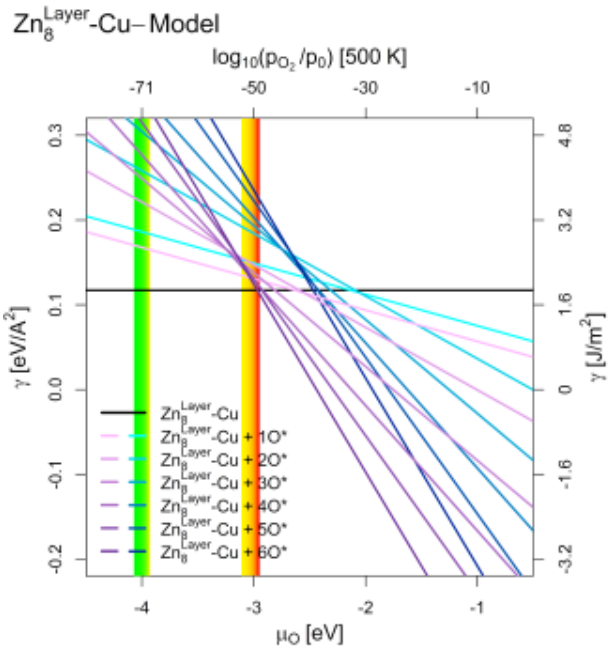
Zn_8^{Layer}-Cu– Model
$\log_{10}(p_{O_2}/p_0)$ [500 K]
-71
-50
-30
-10
0.3
0.2
0.1
0.0
-0.1
-0.2
4.8
3.2
1.6
0
-1.6
-3.2
γ [eV/A²]
γ [J/m²]
Zn_8^{Layer}-Cu
Zn_8^{Layer}-Cu + 1O*
Zn_8^{Layer}-Cu + 2O*
Zn_8^{Layer}-Cu + 3O*
Zn_8^{Layer}-Cu + 4O*
Zn_8^{Layer}-Cu + 5O*
Zn_8^{Layer}-Cu + 6O*
-4
-3
-2
-1
μ_O [eV]

(i)

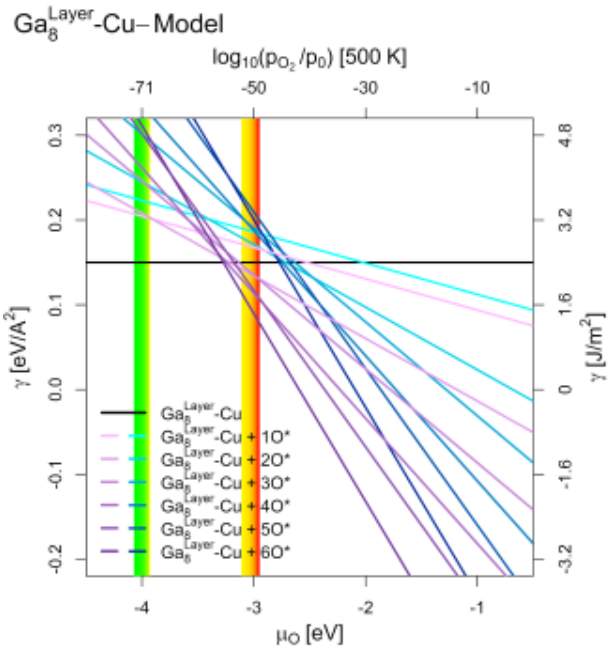
Ga_8^{Layer}-Cu– Model
$\log_{10}(p_{O_2}/p_0)$ [500 K]
-71
-50
-30
-10
0.3
0.2
0.1
0.0
-0.1
-0.2
4.8
3.2
1.6
0
-1.6
-3.2
γ [eV/A²]
γ [J/m²]
Ga_8^{Layer}-Cu
Ga_8^{Layer}-Cu + 1O*
Ga_8^{Layer}-Cu + 2O*
Ga_8^{Layer}-Cu + 3O*
Ga_8^{Layer}-Cu + 4O*
Ga_8^{Layer}-Cu + 5O*
Ga_8^{Layer}-Cu + 6O*
-4
-3
-2
-1
μ_O [eV]

(j)

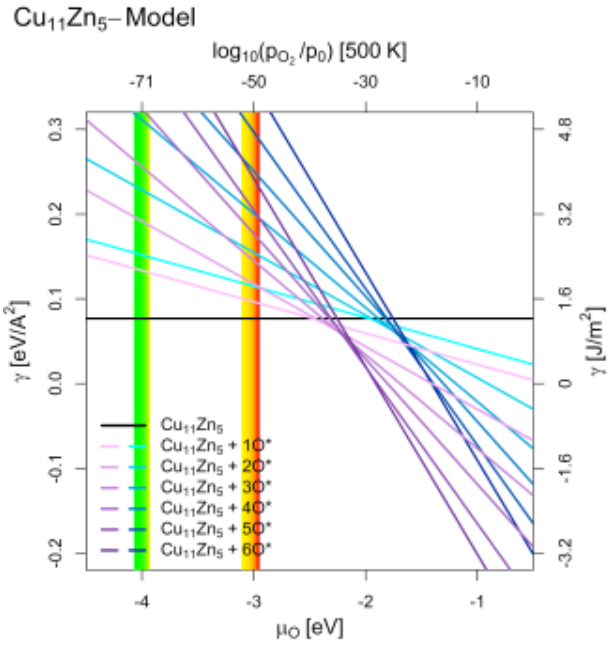
$Cu_{11}Zn_5$– Model
$\log_{10}(p_{O_2}/p_0)$ [500 K]
-71
-50
-30
-10
0.3
0.2
0.1
0.0
-0.1
-0.2
4.8
3.2
1.6
0
-1.6
-3.2
γ [eV/A²]
γ [J/m²]
$Cu_{11}Zn_5$
$Cu_{11}Zn_5$ + 1O*
$Cu_{11}Zn_5$ + 2O*
$Cu_{11}Zn_5$ + 3O*
$Cu_{11}Zn_5$ + 4O*
$Cu_{11}Zn_5$ + 5O*
$Cu_{11}Zn_5$ + 6O*
-4
-3
-2
-1
μ_O [eV]

(k)

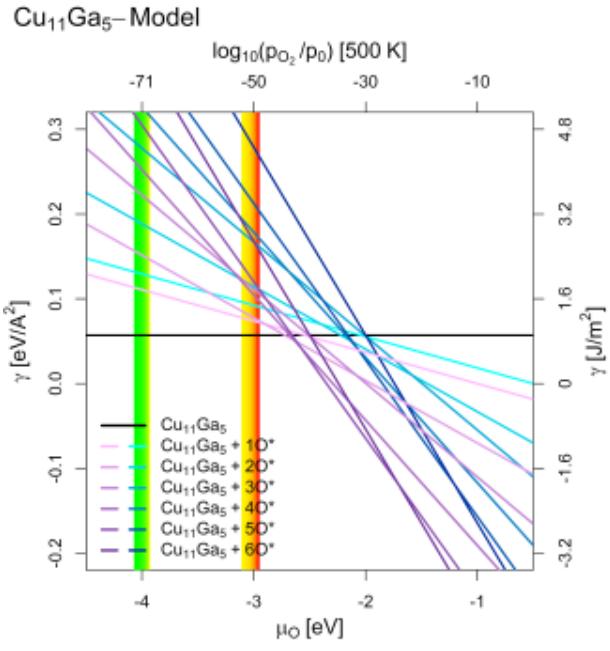
$Cu_{11}Ga_5$– Model
$\log_{10}(p_{O_2}/p_0)$ [500 K]
-71
-50
-30
-10
0.3
0.2
0.1
0.0
-0.1
-0.2
4.8
3.2
1.6
0
-1.6
-3.2
γ [eV/A²]
γ [J/m²]
$Cu_{11}Ga_5$
$Cu_{11}Ga_5$ + 1O*
$Cu_{11}Ga_5$ + 2O*
$Cu_{11}Ga_5$ + 3O*
$Cu_{11}Ga_5$ + 4O*
$Cu_{11}Ga_5$ + 5O*
$Cu_{11}Ga_5$ + 6O*
-4
-3
-2
-1
μ_O [eV]

(l)

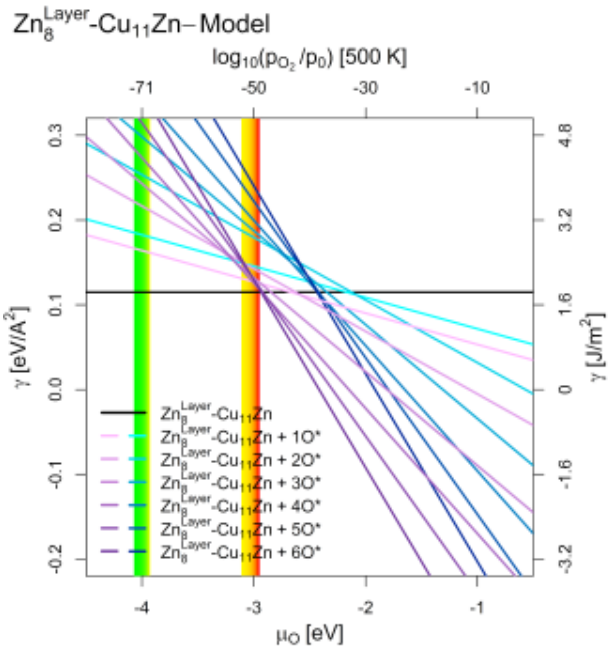
Zn_8^{Layer}-$Cu_{11}Zn$ – Model
$\log_{10}(p_{O_2}/p_0)$ [500 K]
-71
-50
-30
-10
γ [eV/Å^2]
γ [J/m^2]
μ_O [eV]
Zn_8^{Layer}-$Cu_{11}Zn$
Zn_8^{Layer}-$Cu_{11}Zn$ + 1O*
Zn_8^{Layer}-$Cu_{11}Zn$ + 2O*
Zn_8^{Layer}-$Cu_{11}Zn$ + 3O*
Zn_8^{Layer}-$Cu_{11}Zn$ + 4O*
Zn_8^{Layer}-$Cu_{11}Zn$ + 5O*
Zn_8^{Layer}-$Cu_{11}Zn$ + 6O*

(m)

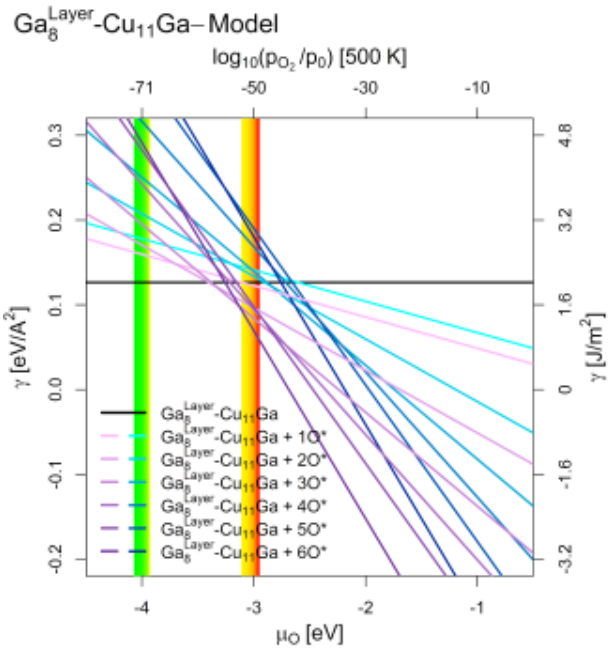
Ga_8^{Layer}-$Cu_{11}Ga$ – Model
$\log_{10}(p_{O_2}/p_0)$ [500 K]
-71
-50
-30
-10
γ [eV/Å^2]
γ [J/m^2]
μ_O [eV]
Ga_8^{Layer}-$Cu_{11}Ga$
Ga_8^{Layer}-$Cu_{11}Ga$ + 1O*
Ga_8^{Layer}-$Cu_{11}Ga$ + 2O*
Ga_8^{Layer}-$Cu_{11}Ga$ + 3O*
Ga_8^{Layer}-$Cu_{11}Ga$ + 4O*
Ga_8^{Layer}-$Cu_{11}Ga$ + 5O*
Ga_8^{Layer}-$Cu_{11}Ga$ + 6O*

(n)

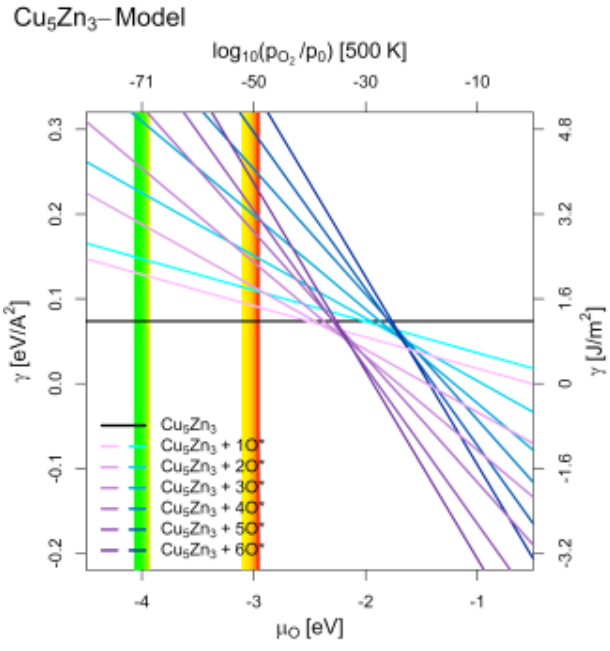
Cu_5Zn_3 – Model
$\log_{10}(p_{O_2}/p_0)$ [500 K]
-71
-50
-30
-10
γ [eV/Å^2]
γ [J/m^2]
μ_O [eV]
Cu_5Zn_3
Cu_5Zn_3 + 1O*
Cu_5Zn_3 + 2O*
Cu_5Zn_3 + 3O*
Cu_5Zn_3 + 4O*
Cu_5Zn_3 + 5O*
Cu_5Zn_3 + 6O*

(o)

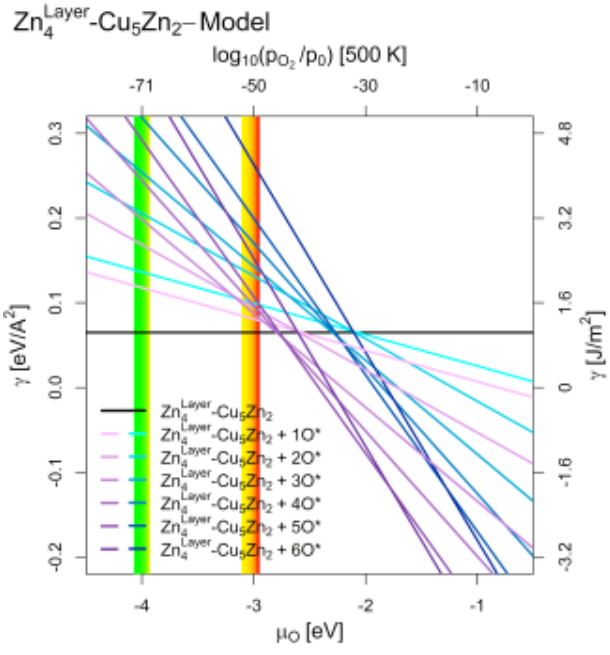
Zn_4^{Layer}-Cu_5Zn_2 – Model
$\log_{10}(p_{O_2}/p_0)$ [500 K]
-71
-50
-30
-10
γ [eV/Å^2]
γ [J/m^2]
μ_O [eV]
Zn_4^{Layer}-Cu_5Zn_2
Zn_4^{Layer}-Cu_5Zn_2 + 1O*
Zn_4^{Layer}-Cu_5Zn_2 + 2O*
Zn_4^{Layer}-Cu_5Zn_2 + 3O*
Zn_4^{Layer}-Cu_5Zn_2 + 4O*
Zn_4^{Layer}-Cu_5Zn_2 + 5O*
Zn_4^{Layer}-Cu_5Zn_2 + 6O*

(p)

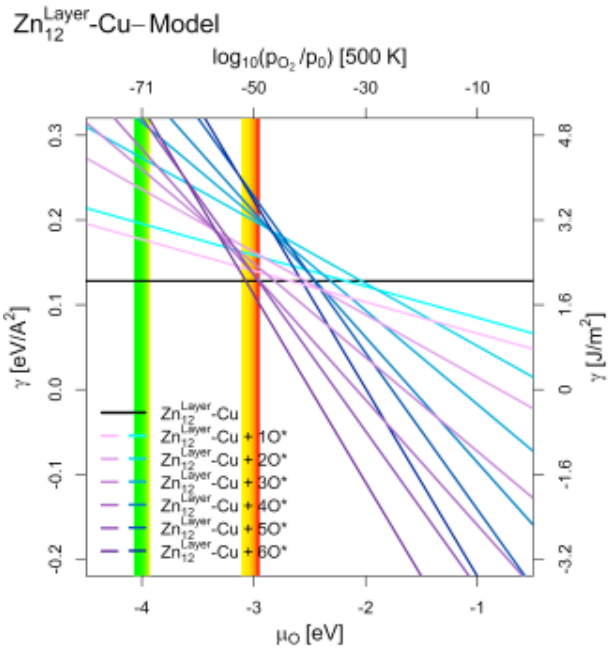
Zn12Layer-Cu− Model
log10(pO2/p0) [500 K]
-71
-50
-30
-10
0.3
0.2
0.1
0.0
-0.1
-0.2
γ [eV/A2]
4.8
3.2
1.6
0
-1.6
-3.2
γ [J/m2]
Zn12Layer-Cu
Zn12Layer-Cu + 1O*
Zn12Layer-Cu + 2O*
Zn12Layer-Cu + 3O*
Zn12Layer-Cu + 4O*
Zn12Layer-Cu + 5O*
Zn12Layer-Cu + 6O*
-4
-3
-2
-1
μO [eV]

(q)

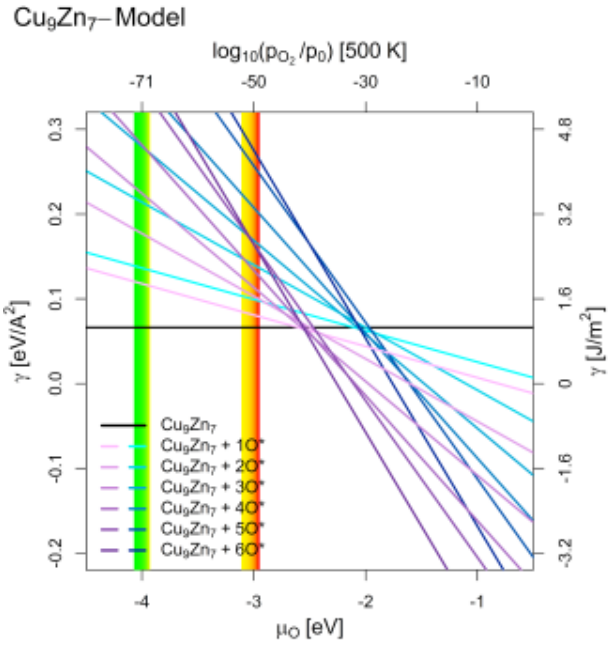
Cu9Zn7− Model
log10(pO2/p0) [500 K]
-71
-50
-30
-10
0.3
0.2
0.1
0.0
-0.1
-0.2
γ [eV/A2]
4.8
3.2
1.6
0
-1.6
-3.2
γ [J/m2]
Cu9Zn7
Cu9Zn7 + 1O*
Cu9Zn7 + 2O*
Cu9Zn7 + 3O*
Cu9Zn7 + 4O*
Cu9Zn7 + 5O*
Cu9Zn7 + 6O*
-4
-3
-2
-1
μO [eV]

(r)

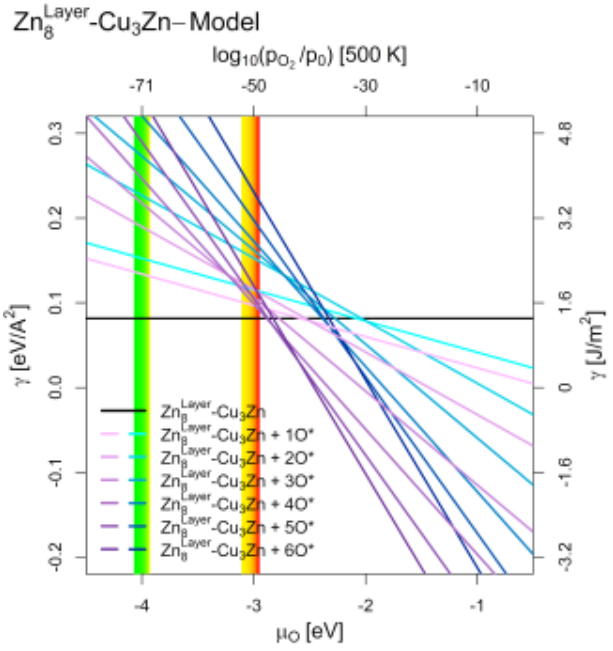
Zn8Layer-Cu3Zn− Model
log10(pO2/p0) [500 K]
-71
-50
-30
-10
0.3
0.2
0.1
0.0
-0.1
-0.2
γ [eV/A2]
4.8
3.2
1.6
0
-1.6
-3.2
γ [J/m2]
Zn8Layer-Cu3Zn
Zn8Layer-Cu3Zn + 1O*
Zn8Layer-Cu3Zn + 2O*
Zn8Layer-Cu3Zn + 3O*
Zn8Layer-Cu3Zn + 4O*
Zn8Layer-Cu3Zn + 5O*
Zn8Layer-Cu3Zn + 6O*
-4
-3
-2
-1
μO [eV]

(s)

Figure S6: Surface stability diagram of the (100)-facet of the investigated CuGa-/CuZn-models with both uncorrected surface energies (in blue) and corrected surface energies (in violet) depending on the chemical potential of oxygen (μ_O in eV) and the equivalent oxygen partial pressure at 500 K. The yellow-red area indicates the expected oxygen chemical potential (μ_O) under CO_2 hydrogenation conditions (-3.11 eV $< \mu_O <$ -2.92 eV, corresponding to an equivalent O_2 partial pressure bellow 10^{-48} bar) while the green-yellow area indicates the expected μ_O CO hydrogenation conditions (-4.07 eV $< \mu_O <$ -3.93 eV, equivalent to an O_2 partial pressure bellow 10^{-69} bar) with the colour gradient indicating the progressing (R)WGS reaction (yellow for low conversion, red/green for high conversion; compare Figure 1 in the main text as well as Figures S1 and S4 in the SI). Used slab models for the (100)-facet used are:
(a/b) Unlayered substoichiometric fcc-Cu_3Ga/-Cu_3Zn (12.5 % Zn/Ga).
(c/d) One Ga/Zn surface layer on pure fcc-Cu (12.5 % Ga/Zn).
(e/f) Unlayered stoichiometric fcc-Cu_3Ga/-Cu_3Zn (25 % Ga/Zn).
(g/h) One Ga/Zn surface layer on substoichiometric fcc-Cu_3Ga/-Cu_3Zn (25 % Ga/Zn).
(i/j) Two Ga/Zn surface layers on pure fcc-Cu (25 % Ga/Zn).
(k/l) Unlayered superstoichiometric fcc-Cu_3Ga/-Cu_3Zn (31.25 % Ga/Zn).
(m/n) Two Ga/Zn surface layers on substoichiometric fcc-Cu_3Ga/-Cu_3Zn (31.25 % Ga/Zn).
(o) Unlayered supersubstoichiometric fcc-Cu_3Zn (37.5 % Zn).
(p) One Zn surface layer on fcc-Cu_3Zn (37.5 % Ga/Zn).
(q) Three Zn surface layers on pure fcc-Cu (37.5 % Ga/Zn).
(r) Unlayered supersubstoichiometric fcc-Cu_3Zn (43.75 % Zn).
(s) Two Zn surface layers on fcc-Cu_3Zn (43.75 % Ga/Zn).

(110)-Facet

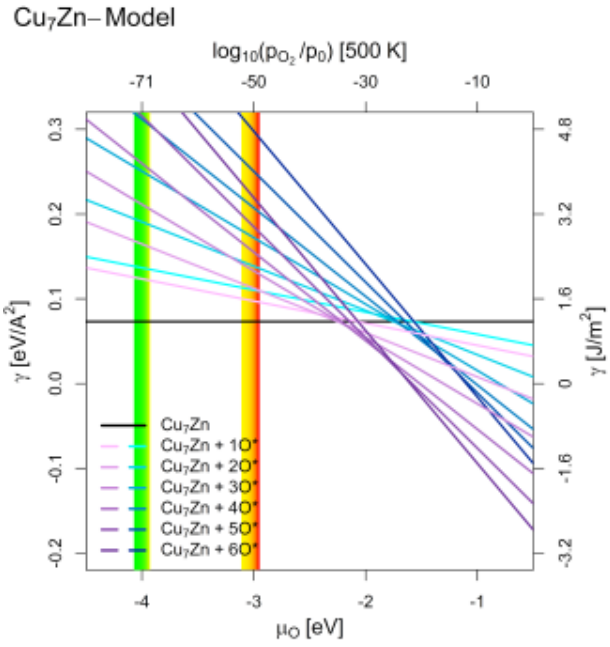

(a)

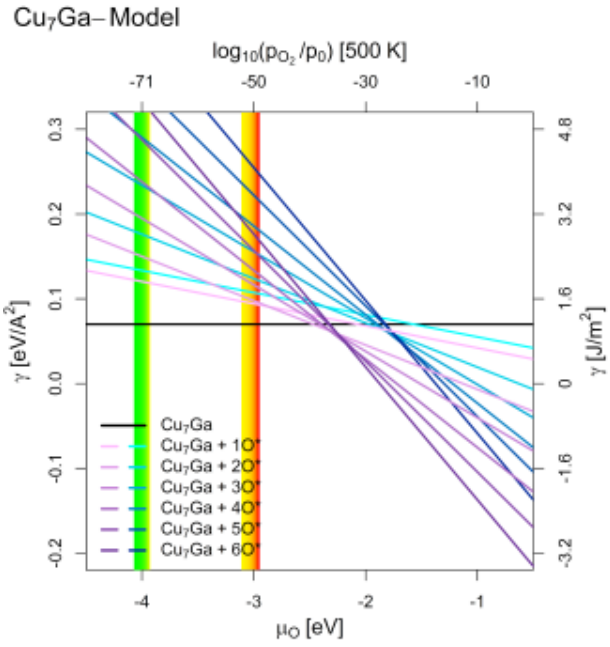

(b)

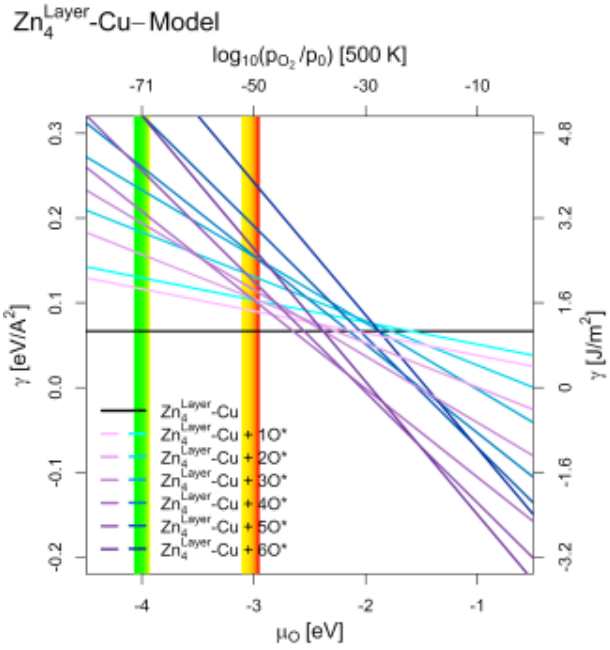

(c)

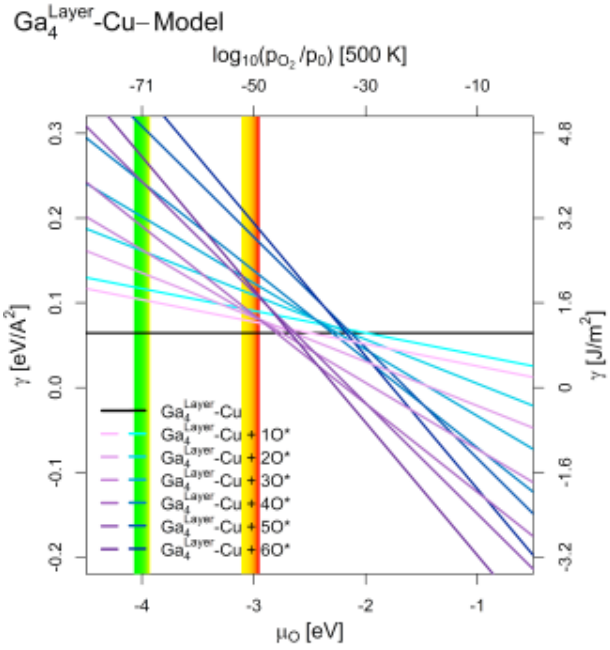

(d)

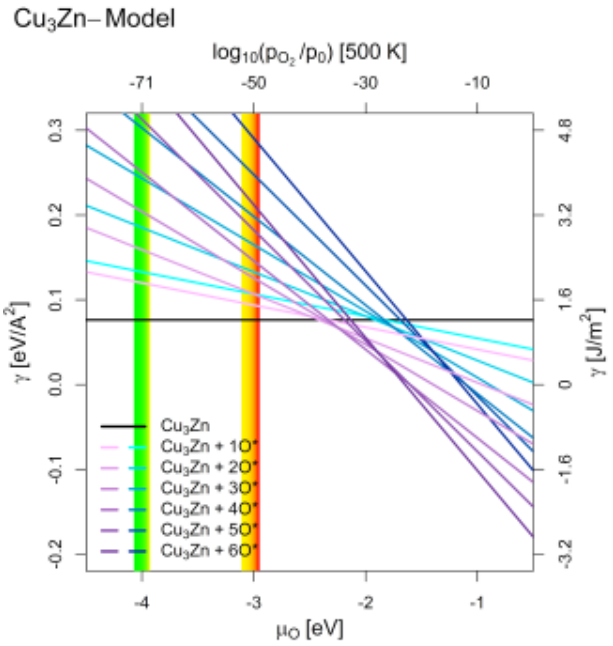
Cu3Zn– Model
log10(pO2/p0) [500 K]
-71
-50
-30
-10
γ [eV/A2]
γ [J/m2]
μO [eV]
Cu3Zn
Cu3Zn + 1O*
Cu3Zn + 2O*
Cu3Zn + 3O*
Cu3Zn + 4O*
Cu3Zn + 5O*
Cu3Zn + 6O*

(e)

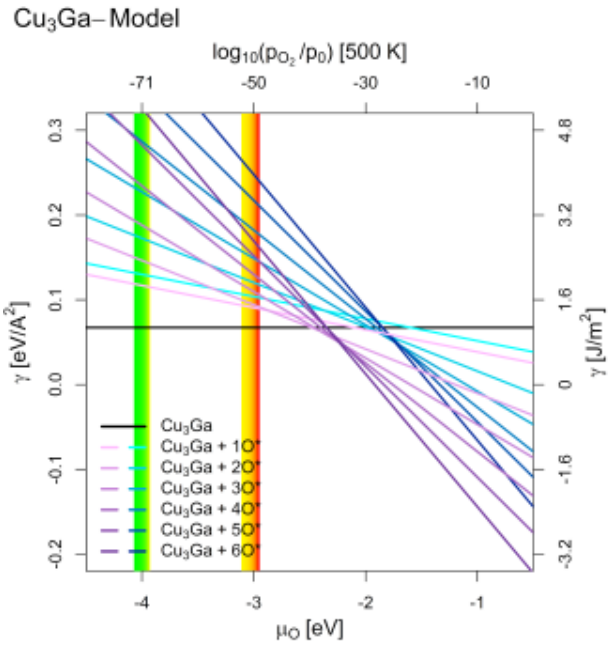
Cu3Ga– Model
log10(pO2/p0) [500 K]
-71
-50
-30
-10
γ [eV/A2]
γ [J/m2]
μO [eV]
Cu3Ga
Cu3Ga + 1O*
Cu3Ga + 2O*
Cu3Ga + 3O*
Cu3Ga + 4O*
Cu3Ga + 5O*
Cu3Ga + 6O*

(f)

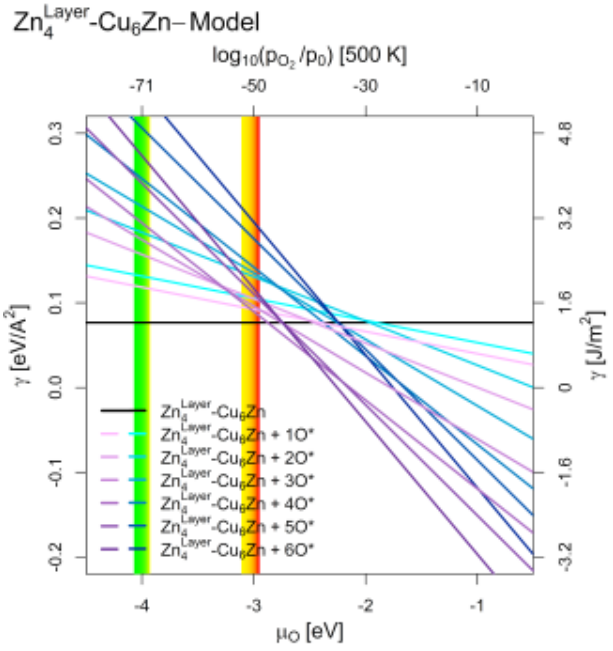
Zn4Layer-Cu6Zn– Model
log10(pO2/p0) [500 K]
-71
-50
-30
-10
γ [eV/A2]
γ [J/m2]
μO [eV]
Zn4Layer-Cu6Zn
Zn4Layer-Cu6Zn + 1O*
Zn4Layer-Cu6Zn + 2O*
Zn4Layer-Cu6Zn + 3O*
Zn4Layer-Cu6Zn + 4O*
Zn4Layer-Cu6Zn + 5O*
Zn4Layer-Cu6Zn + 6O*

(g)

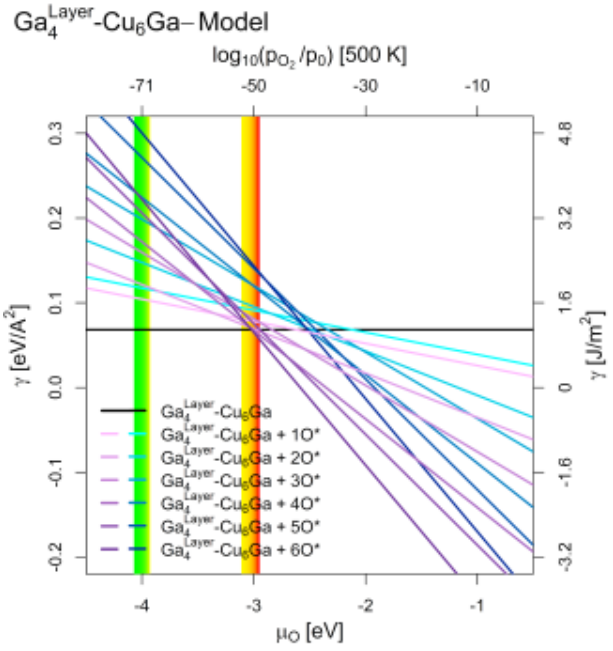
Ga4Layer-Cu6Ga– Model
log10(pO2/p0) [500 K]
-71
-50
-30
-10
γ [eV/A2]
γ [J/m2]
μO [eV]
Ga4Layer-Cu6Ga
Ga4Layer-Cu6Ga + 1O*
Ga4Layer-Cu6Ga + 2O*
Ga4Layer-Cu6Ga + 3O*
Ga4Layer-Cu6Ga + 4O*
Ga4Layer-Cu6Ga + 5O*
Ga4Layer-Cu6Ga + 6O*

(h)

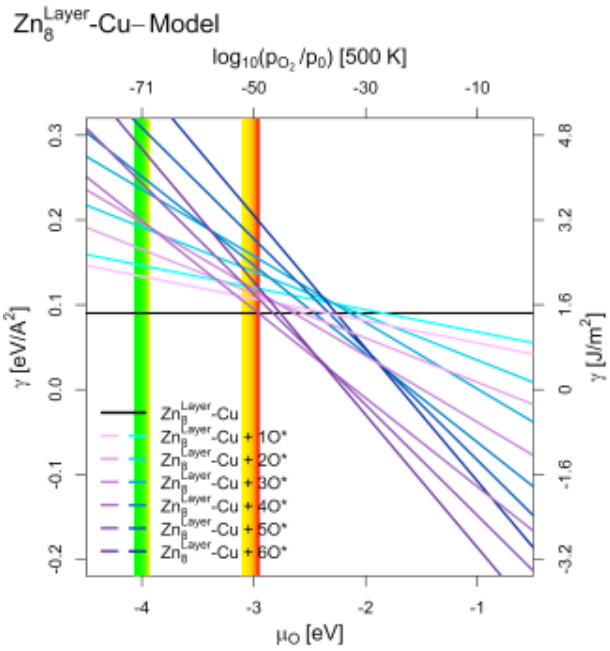
Zn_8^{Layer}-Cu– Model
$\log_{10}(p_{O_2}/p_0)$ [500 K]
-71
-50
-30
-10
0.3
0.2
0.1
0.0
-0.1
-0.2
4.8
3.2
1.6
0
-1.6
-3.2
γ [eV/A²]
γ [J/m²]
Zn_8^{Layer}-Cu
Zn_8^{Layer}-Cu + 1O*
Zn_8^{Layer}-Cu + 2O*
Zn_8^{Layer}-Cu + 3O*
Zn_8^{Layer}-Cu + 4O*
Zn_8^{Layer}-Cu + 5O*
Zn_8^{Layer}-Cu + 6O*
-4
-3
-2
-1
μ_O [eV]

(i)

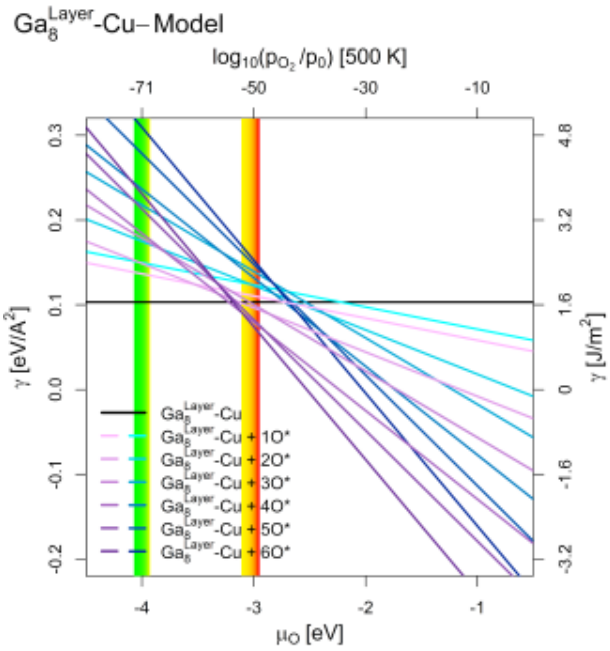
Ga_8^{Layer}-Cu– Model
$\log_{10}(p_{O_2}/p_0)$ [500 K]
-71
-50
-30
-10
0.3
0.2
0.1
0.0
-0.1
-0.2
4.8
3.2
1.6
0
-1.6
-3.2
γ [eV/A²]
γ [J/m²]
Ga_8^{Layer}-Cu
Ga_8^{Layer}-Cu + 1O*
Ga_8^{Layer}-Cu + 2O*
Ga_8^{Layer}-Cu + 3O*
Ga_8^{Layer}-Cu + 4O*
Ga_8^{Layer}-Cu + 5O*
Ga_8^{Layer}-Cu + 6O*
-4
-3
-2
-1
μ_O [eV]

(j)

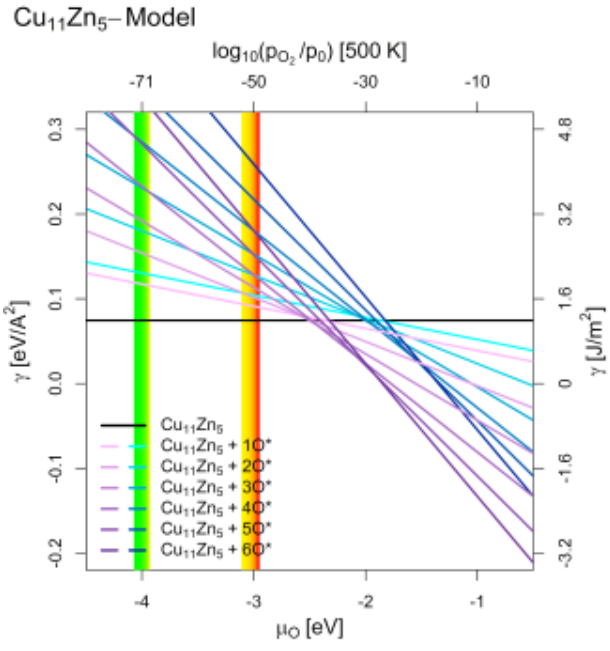
$Cu_{11}Zn_5$– Model
$\log_{10}(p_{O_2}/p_0)$ [500 K]
-71
-50
-30
-10
0.3
0.2
0.1
0.0
-0.1
-0.2
4.8
3.2
1.6
0
-1.6
-3.2
γ [eV/A²]
γ [J/m²]
$Cu_{11}Zn_5$
$Cu_{11}Zn_5$ + 1O*
$Cu_{11}Zn_5$ + 2O*
$Cu_{11}Zn_5$ + 3O*
$Cu_{11}Zn_5$ + 4O*
$Cu_{11}Zn_5$ + 5O*
$Cu_{11}Zn_5$ + 6O*
-4
-3
-2
-1
μ_O [eV]

(k)

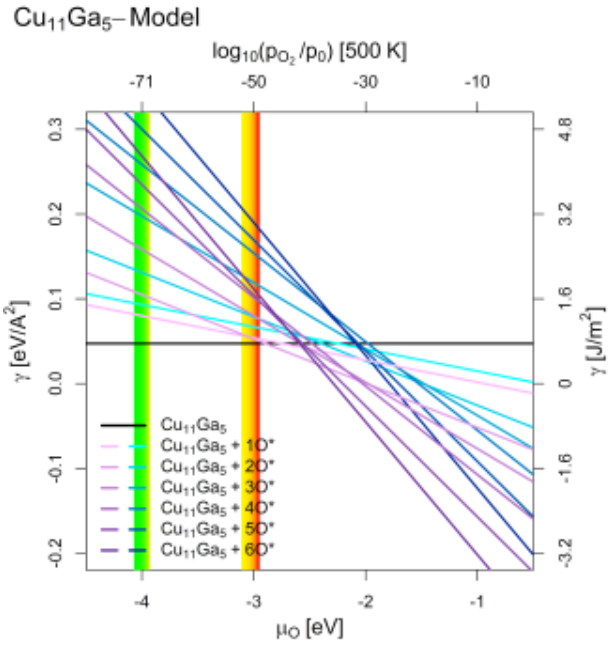
$Cu_{11}Ga_5$– Model
$\log_{10}(p_{O_2}/p_0)$ [500 K]
-71
-50
-30
-10
0.3
0.2
0.1
0.0
-0.1
-0.2
4.8
3.2
1.6
0
-1.6
-3.2
γ [eV/A²]
γ [J/m²]
$Cu_{11}Ga_5$
$Cu_{11}Ga_5$ + 1O*
$Cu_{11}Ga_5$ + 2O*
$Cu_{11}Ga_5$ + 3O*
$Cu_{11}Ga_5$ + 4O*
$Cu_{11}Ga_5$ + 5O*
$Cu_{11}Ga_5$ + 6O*
-4
-3
-2
-1
μ_O [eV]

(l)

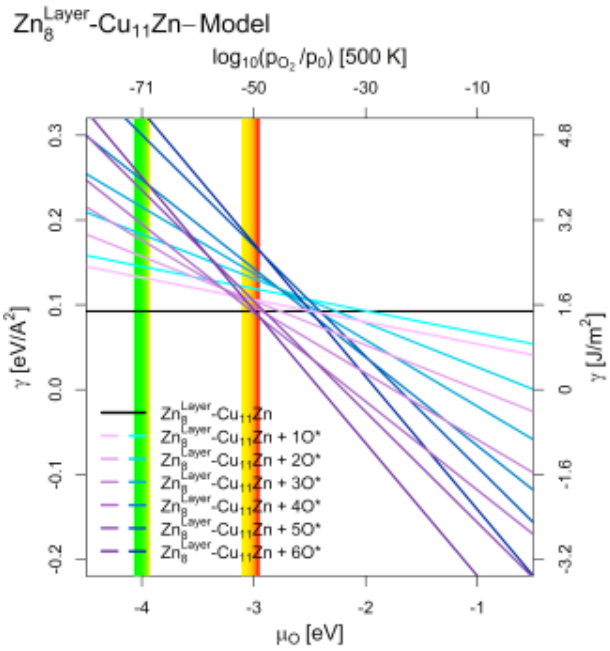
Zn8Layer-Cu11Zn– Model
log10(pO2/p0) [500 K]
-71
-50
-30
-10
γ [eV/A2]
γ [J/m2]
μO [eV]
Zn8Layer-Cu11Zn
Zn8Layer-Cu11Zn + 1O*
Zn8Layer-Cu11Zn + 2O*
Zn8Layer-Cu11Zn + 3O*
Zn8Layer-Cu11Zn + 4O*
Zn8Layer-Cu11Zn + 5O*
Zn8Layer-Cu11Zn + 6O*

(m)

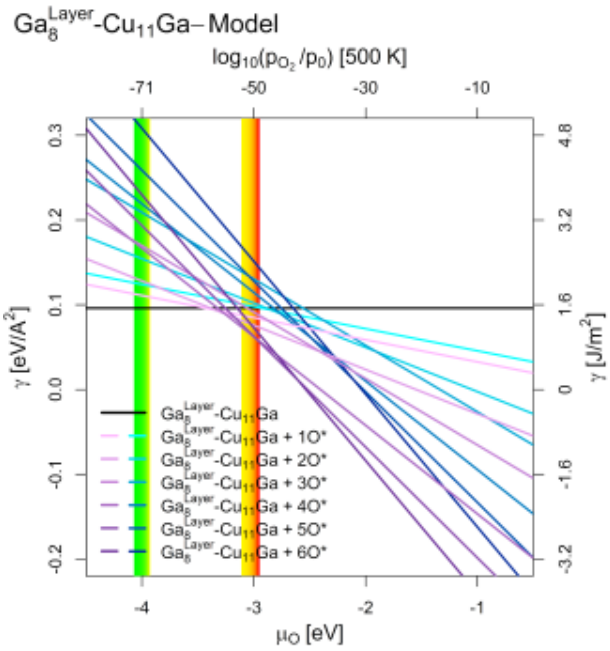
Ga8Layer-Cu11Ga– Model
log10(pO2/p0) [500 K]
-71
-50
-30
-10
γ [eV/A2]
γ [J/m2]
μO [eV]
Ga8Layer-Cu11Ga
Ga8Layer-Cu11Ga + 1O*
Ga8Layer-Cu11Ga + 2O*
Ga8Layer-Cu11Ga + 3O*
Ga8Layer-Cu11Ga + 4O*
Ga8Layer-Cu11Ga + 5O*
Ga8Layer-Cu11Ga + 6O*

(n)

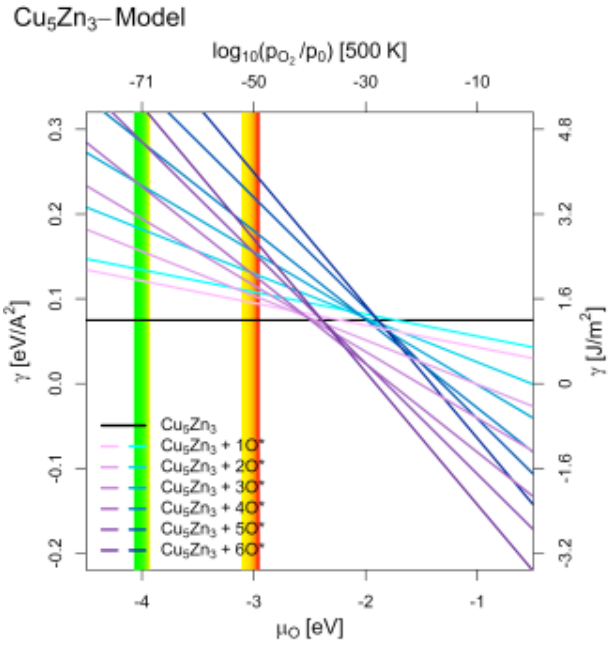
Cu5Zn3– Model
log10(pO2/p0) [500 K]
-71
-50
-30
-10
γ [eV/A2]
γ [J/m2]
μO [eV]
Cu5Zn3
Cu5Zn3 + 1O*
Cu5Zn3 + 2O*
Cu5Zn3 + 3O*
Cu5Zn3 + 4O*
Cu5Zn3 + 5O*
Cu5Zn3 + 6O*

(o)

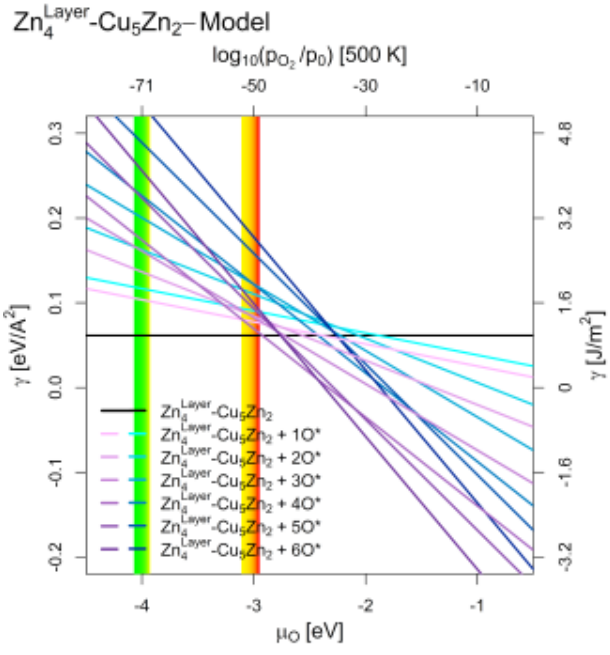
Zn4Layer-Cu5Zn2– Model
log10(pO2/p0) [500 K]
-71
-50
-30
-10
γ [eV/A2]
γ [J/m2]
μO [eV]
Zn4Layer-Cu5Zn2
Zn4Layer-Cu5Zn2 + 1O*
Zn4Layer-Cu5Zn2 + 2O*
Zn4Layer-Cu5Zn2 + 3O*
Zn4Layer-Cu5Zn2 + 4O*
Zn4Layer-Cu5Zn2 + 5O*
Zn4Layer-Cu5Zn2 + 6O*

(p)

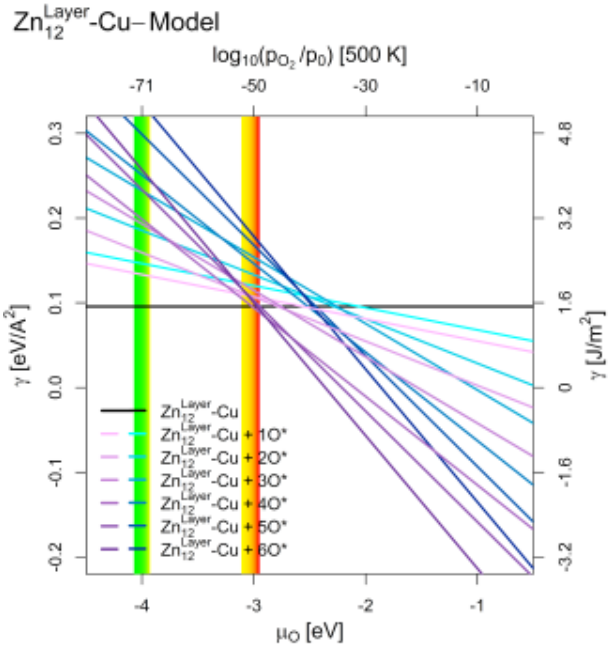
Zn12Layer-Cu−Model
log10(pO2/p0) [500 K]
-71
-50
-30
-10
γ [eV/A2]
γ [J/m2]
μO [eV]
Zn12Layer-Cu
Zn12Layer-Cu + 1O*
Zn12Layer-Cu + 2O*
Zn12Layer-Cu + 3O*
Zn12Layer-Cu + 4O*
Zn12Layer-Cu + 5O*
Zn12Layer-Cu + 6O*

(q)

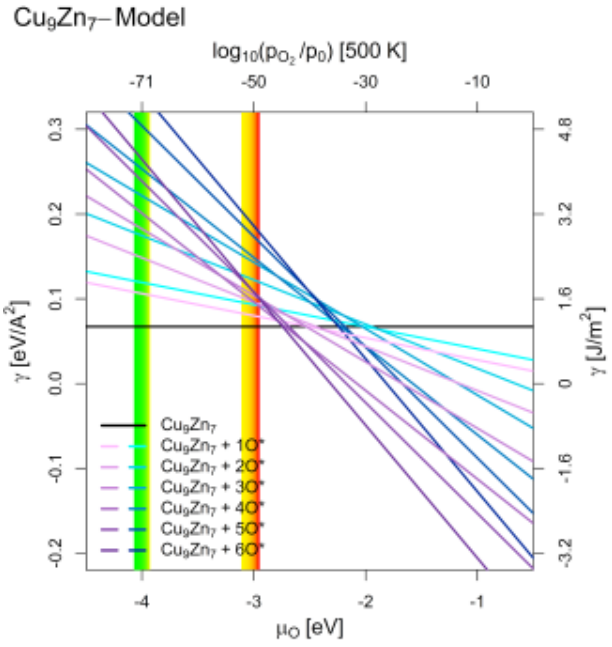
Cu9Zn7−Model
log10(pO2/p0) [500 K]
γ [eV/A2]
γ [J/m2]
μO [eV]
Cu9Zn7
Cu9Zn7 + 1O*
Cu9Zn7 + 2O*
Cu9Zn7 + 3O*
Cu9Zn7 + 4O*
Cu9Zn7 + 5O*
Cu9Zn7 + 6O*

(r)

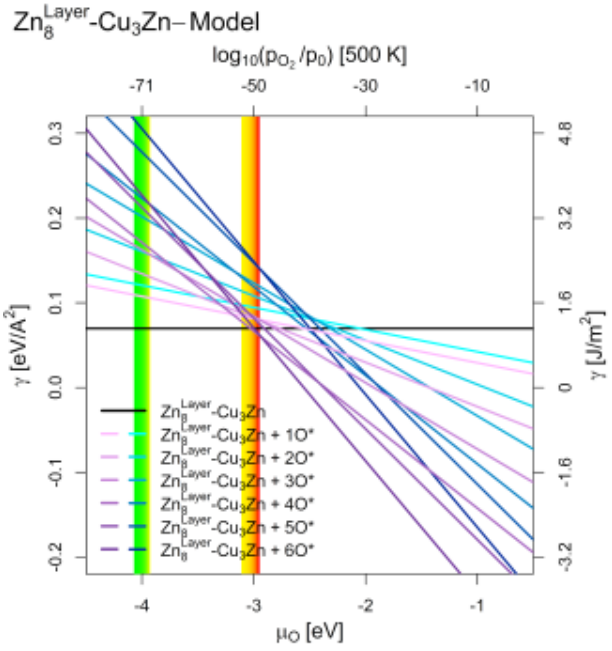
Zn8Layer-Cu3Zn−Model
log10(pO2/p0) [500 K]
γ [eV/A2]
γ [J/m2]
μO [eV]
Zn8Layer-Cu3Zn
Zn8Layer-Cu3Zn + 1O*
Zn8Layer-Cu3Zn + 2O*
Zn8Layer-Cu3Zn + 3O*
Zn8Layer-Cu3Zn + 4O*
Zn8Layer-Cu3Zn + 5O*
Zn8Layer-Cu3Zn + 6O*

(s)

Figure S7: Surface stability diagram of the (110)-facet of the investigated CuGa-/CuZn-models with both uncorrected surface energies (in blue) and corrected surface energies (in violet) depending on the chemical potential of oxygen (μ_O in eV) and the equivalent oxygen partial pressure at 500 K. The yellow-red area indicates the expected oxygen chemical potential (μ_O) under CO_2 hydrogenation conditions (-3.11 eV $< \mu_O <$ -2.92 eV, corresponding to an equivalent O_2 partial pressure bellow 10^{-48} bar) while the green-yellow area indicates the expected μ_O CO hydrogenation conditions (-4.07 eV $< \mu_O <$ -3.93 eV, equivalent to an O_2 partial pressure bellow 10^{-69} bar) with the colour gradient indicating the progressing (R)WGS reaction (yellow for low conversion, red/green for high conversion; compare Figure 1 in the main text as well as Figures S1 and S4 in the SI). Used slab models for the (110)-facet used are:
(a/b) Unlayered substoichiometric fcc-Cu_3Ga/-Cu_3Zn (12.5 % Zn/Ga).
(c/d) One Ga/Zn surface layer on pure fcc-Cu (12.5 % Ga/Zn).
(e/f) Unlayered stoichiometric fcc-Cu_3Ga/-Cu_3Zn (25 % Ga/Zn).
(g/h) One Ga/Zn surface layer on substoichiometric fcc-Cu_3Ga/-Cu_3Zn (25 % Ga/Zn).
(i/j) Two Ga/Zn surface layers on pure fcc-Cu (25 % Ga/Zn).
(k/l) Unlayered superstoichiometric fcc-Cu_3Ga/-Cu_3Zn (31.25 % Ga/Zn).
(m/n) Two Ga/Zn surface layers on substoichiometric fcc-Cu_3Ga/-Cu_3Zn (31.25 % Ga/Zn).
(o) Unlayered supersubstoichiometric fcc-Cu_3Zn (37.5 % Zn).
(p) One Zn surface layer on fcc-Cu_3Zn (37.5 % Ga/Zn).
(q) Three Zn surface layers on pure fcc-Cu (37.5 % Ga/Zn).
(r) Unlayered supersubstoichiometric fcc-Cu_3Zn (43.75 % Zn).
(s) Two Zn surface layers on fcc-Cu_3Zn (43.75 % Ga/Zn).

(111)-Facet

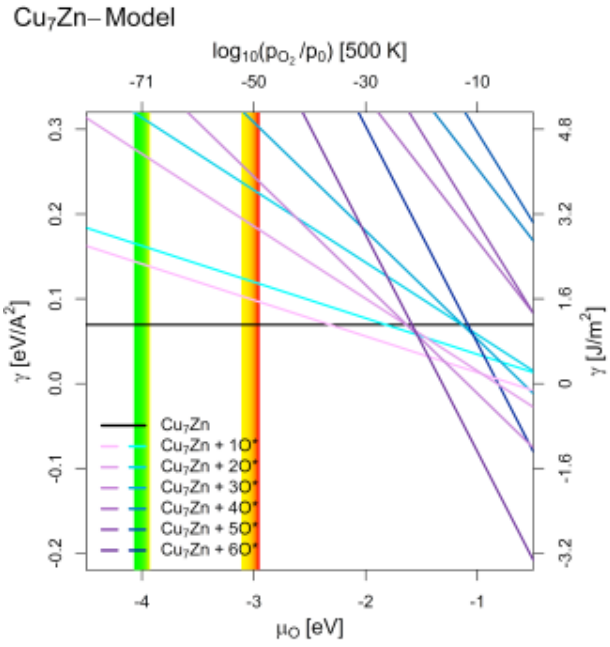

(a)

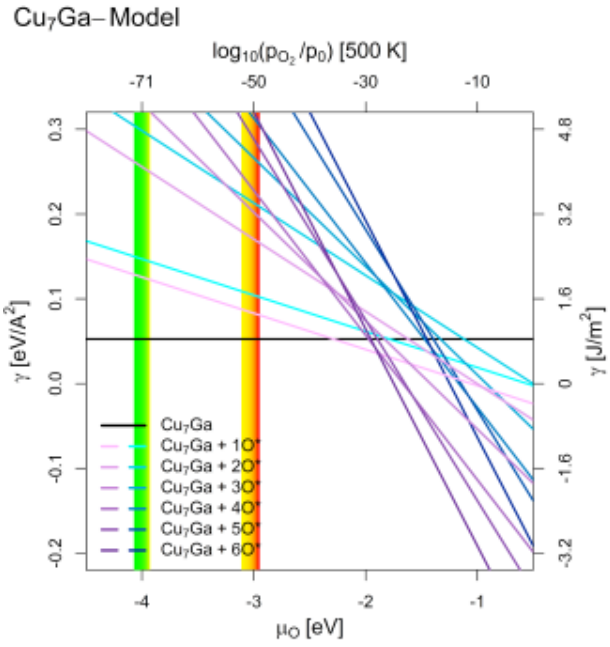

(b)

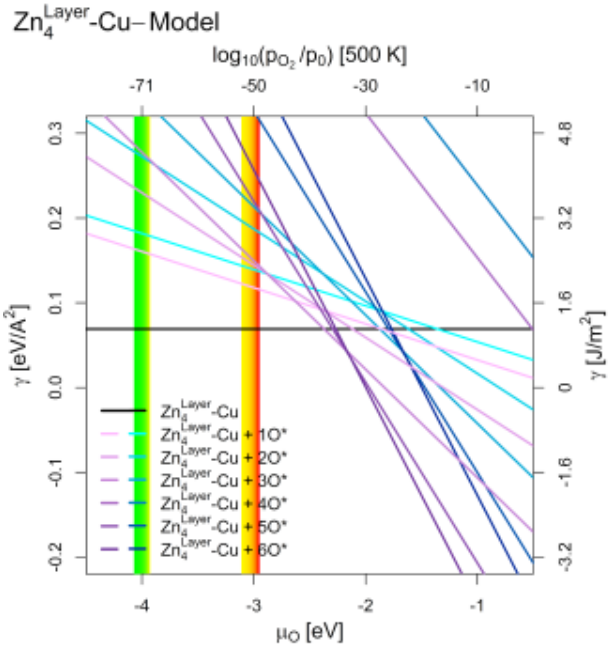

(c)

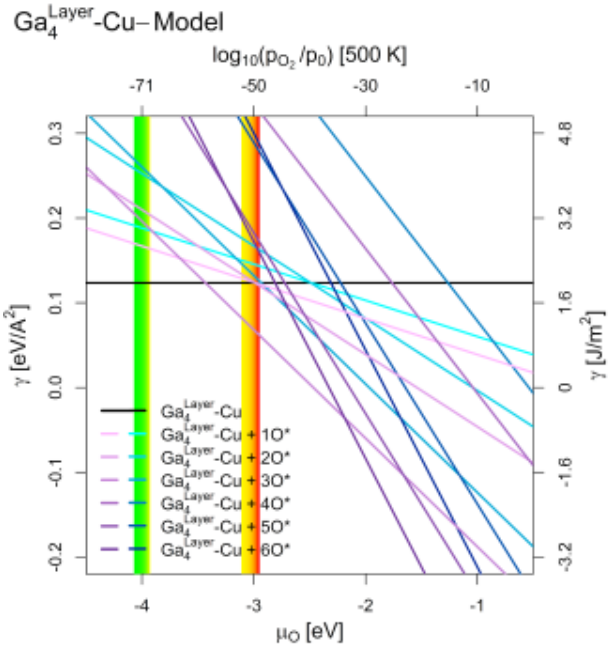

(d)

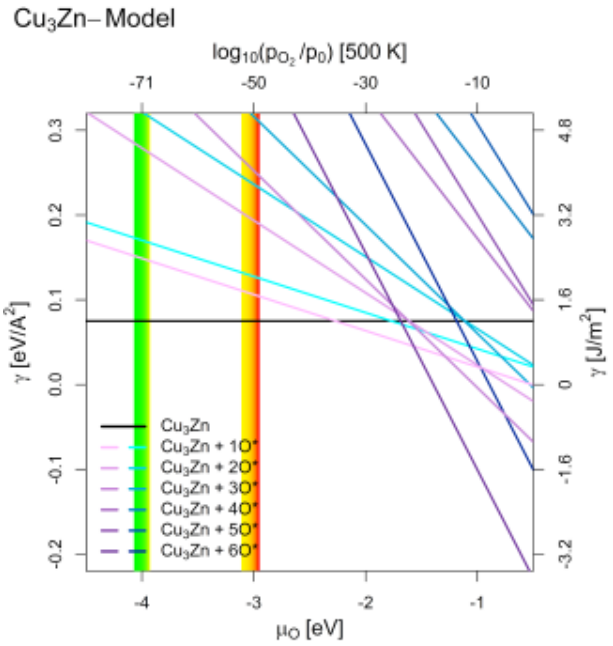
Cu3Zn– Model
log10(pO2/p0) [500 K]
-71
-50
-30
-10
γ [eV/Å2]
γ [J/m2]
μO [eV]
Cu3Zn
Cu3Zn + 1O*
Cu3Zn + 2O*
Cu3Zn + 3O*
Cu3Zn + 4O*
Cu3Zn + 5O*
Cu3Zn + 6O*

(e)

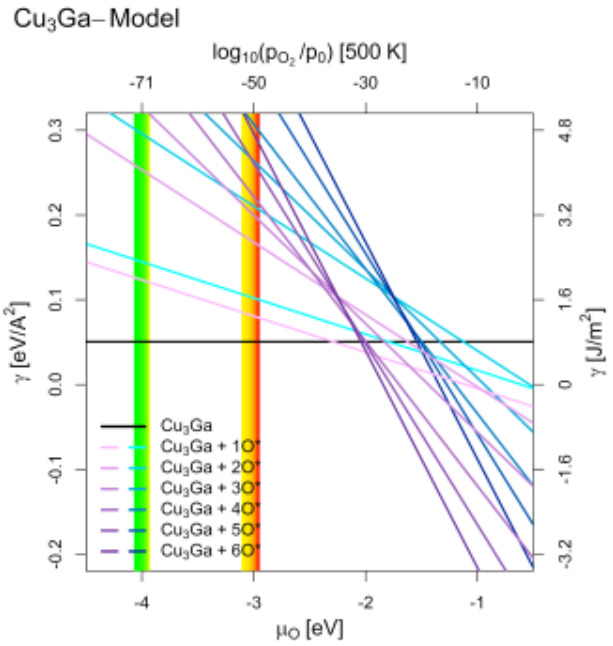
Cu3Ga– Model
log10(pO2/p0) [500 K]
-71
-50
-30
-10
γ [eV/Å2]
γ [J/m2]
μO [eV]
Cu3Ga
Cu3Ga + 1O*
Cu3Ga + 2O*
Cu3Ga + 3O*
Cu3Ga + 4O*
Cu3Ga + 5O*
Cu3Ga + 6O*

(f)

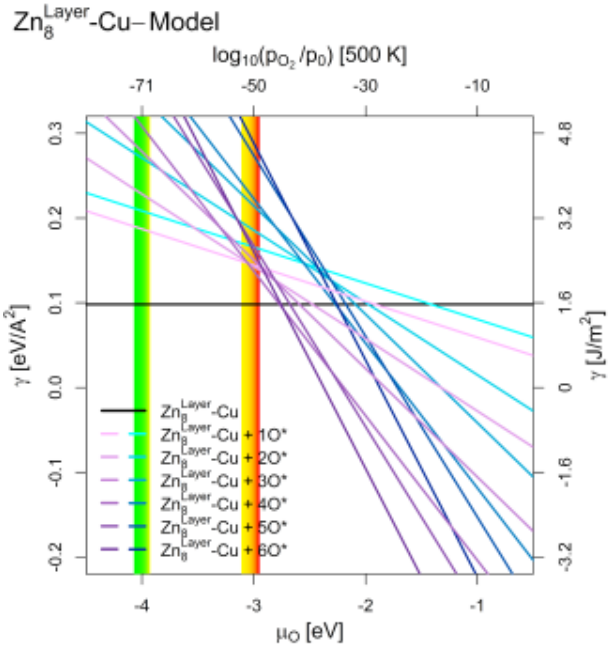
Zn8Layer-Cu– Model
log10(pO2/p0) [500 K]
-71
-50
-30
-10
γ [eV/Å2]
γ [J/m2]
μO [eV]
Zn8Layer-Cu
Zn8Layer-Cu + 1O*
Zn8Layer-Cu + 2O*
Zn8Layer-Cu + 3O*
Zn8Layer-Cu + 4O*
Zn8Layer-Cu + 5O*
Zn8Layer-Cu + 6O*

(g)

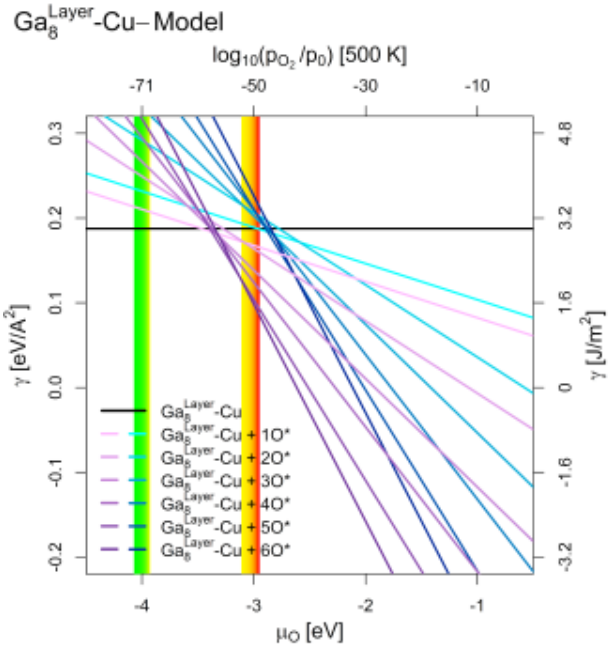
Ga8Layer-Cu– Model
log10(pO2/p0) [500 K]
-71
-50
-30
-10
γ [eV/Å2]
γ [J/m2]
μO [eV]
Ga8Layer-Cu
Ga8Layer-Cu + 1O*
Ga8Layer-Cu + 2O*
Ga8Layer-Cu + 3O*
Ga8Layer-Cu + 4O*
Ga8Layer-Cu + 5O*
Ga8Layer-Cu + 6O*

(h)

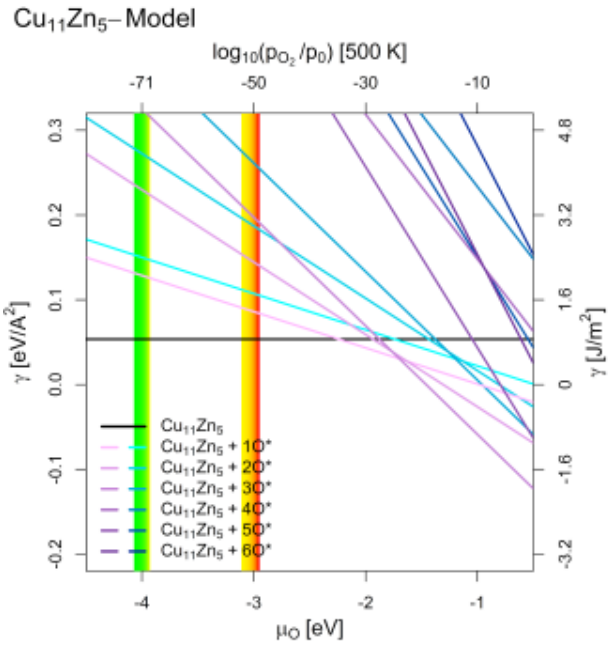
Cu11Zn5−Model
log10(pO2/p0) [500 K]
-71
-50
-30
-10
γ [eV/Å2]
γ [J/m2]
μO [eV]
Cu11Zn5
Cu11Zn5 + 1O*
Cu11Zn5 + 2O*
Cu11Zn5 + 3O*
Cu11Zn5 + 4O*
Cu11Zn5 + 5O*
Cu11Zn5 + 6O*

(i)

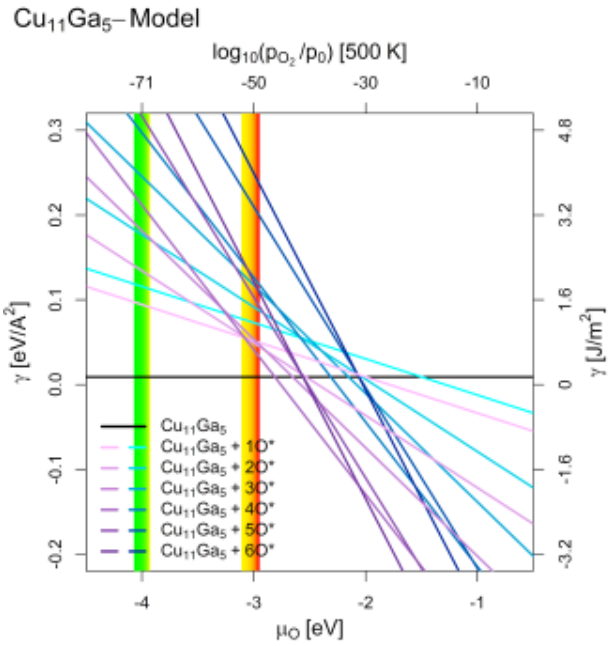
Cu11Ga5−Model
log10(pO2/p0) [500 K]
-71
-50
-30
-10
γ [eV/Å2]
γ [J/m2]
μO [eV]
Cu11Ga5
Cu11Ga5 + 1O*
Cu11Ga5 + 2O*
Cu11Ga5 + 3O*
Cu11Ga5 + 4O*
Cu11Ga5 + 5O*
Cu11Ga5 + 6O*

(j)

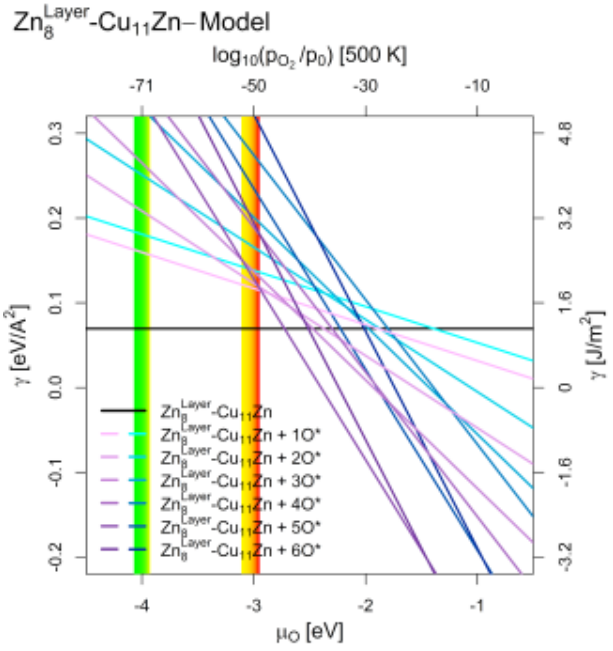
Zn8Layer-Cu11Zn−Model
log10(pO2/p0) [500 K]
-71
-50
-30
-10
γ [eV/Å2]
γ [J/m2]
μO [eV]
Zn8Layer-Cu11Zn
Zn8Layer-Cu11Zn + 1O*
Zn8Layer-Cu11Zn + 2O*
Zn8Layer-Cu11Zn + 3O*
Zn8Layer-Cu11Zn + 4O*
Zn8Layer-Cu11Zn + 5O*
Zn8Layer-Cu11Zn + 6O*

(k)

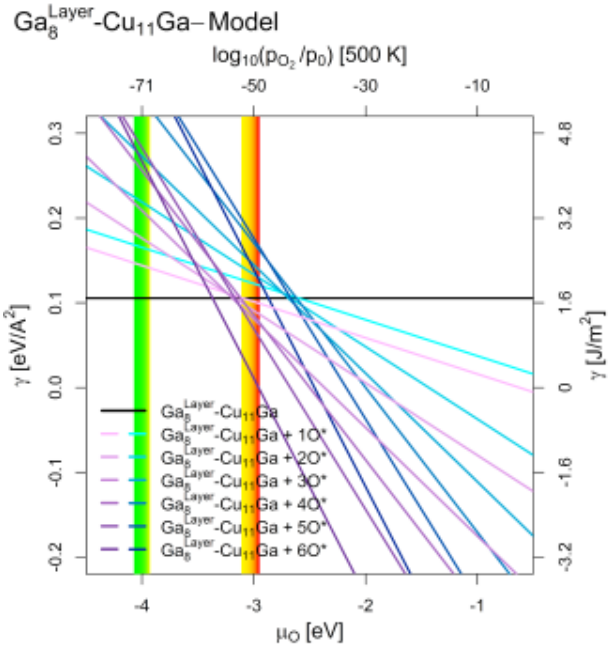
Ga8Layer-Cu11Ga−Model
log10(pO2/p0) [500 K]
-71
-50
-30
-10
γ [eV/Å2]
γ [J/m2]
μO [eV]
Ga8Layer-Cu11Ga
Ga8Layer-Cu11Ga + 1O*
Ga8Layer-Cu11Ga + 2O*
Ga8Layer-Cu11Ga + 3O*
Ga8Layer-Cu11Ga + 4O*
Ga8Layer-Cu11Ga + 5O*
Ga8Layer-Cu11Ga + 6O*

(l)

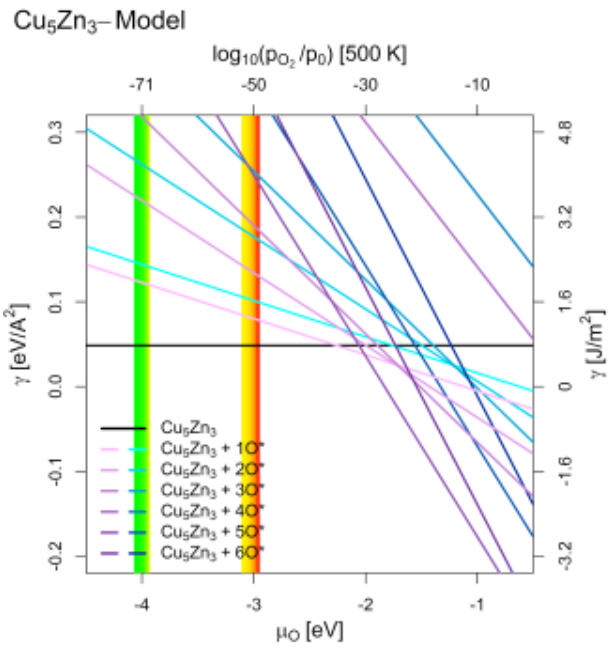
Cu5Zn3 – Model
log10(pO2/p0) [500 K]
-71
-50
-30
-10
γ [eV/Å2]
γ [J/m2]
μO [eV]
Cu5Zn3
Cu5Zn3 + 1O*
Cu5Zn3 + 2O*
Cu5Zn3 + 3O*
Cu5Zn3 + 4O*
Cu5Zn3 + 5O*
Cu5Zn3 + 6O*

(m)

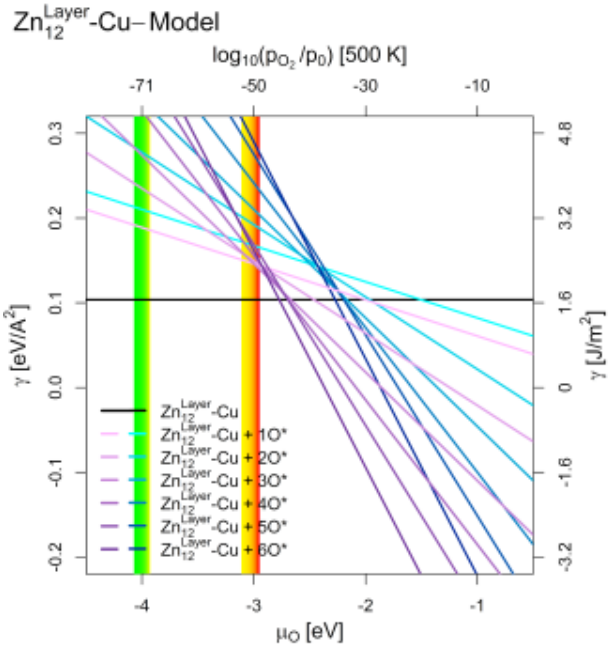
Zn12Layer-Cu – Model
log10(pO2/p0) [500 K]
γ [eV/Å2]
γ [J/m2]
μO [eV]
Zn12Layer-Cu
Zn12Layer-Cu + 1O*
Zn12Layer-Cu + 2O*
Zn12Layer-Cu + 3O*
Zn12Layer-Cu + 4O*
Zn12Layer-Cu + 5O*
Zn12Layer-Cu + 6O*

(n)

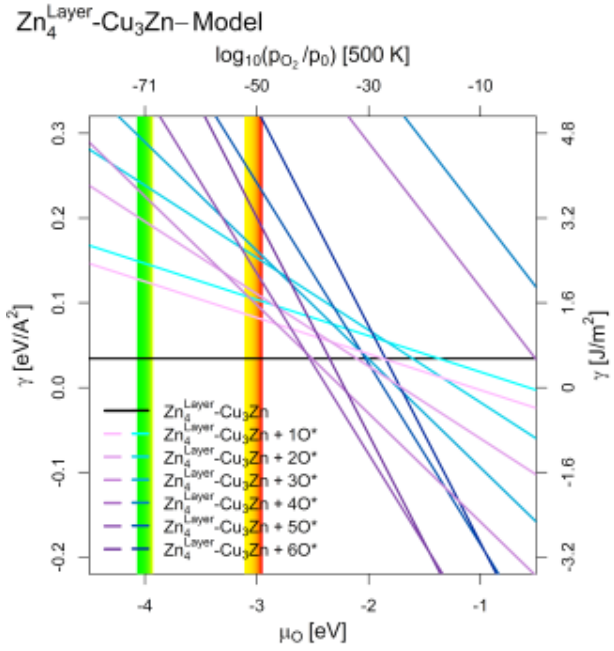
Zn4Layer-Cu3Zn – Model
log10(pO2/p0) [500 K]
γ [eV/Å2]
γ [J/m2]
μO [eV]
Zn4Layer-Cu3Zn
Zn4Layer-Cu3Zn + 1O*
Zn4Layer-Cu3Zn + 2O*
Zn4Layer-Cu3Zn + 3O*
Zn4Layer-Cu3Zn + 4O*
Zn4Layer-Cu3Zn + 5O*
Zn4Layer-Cu3Zn + 6O*

(o)

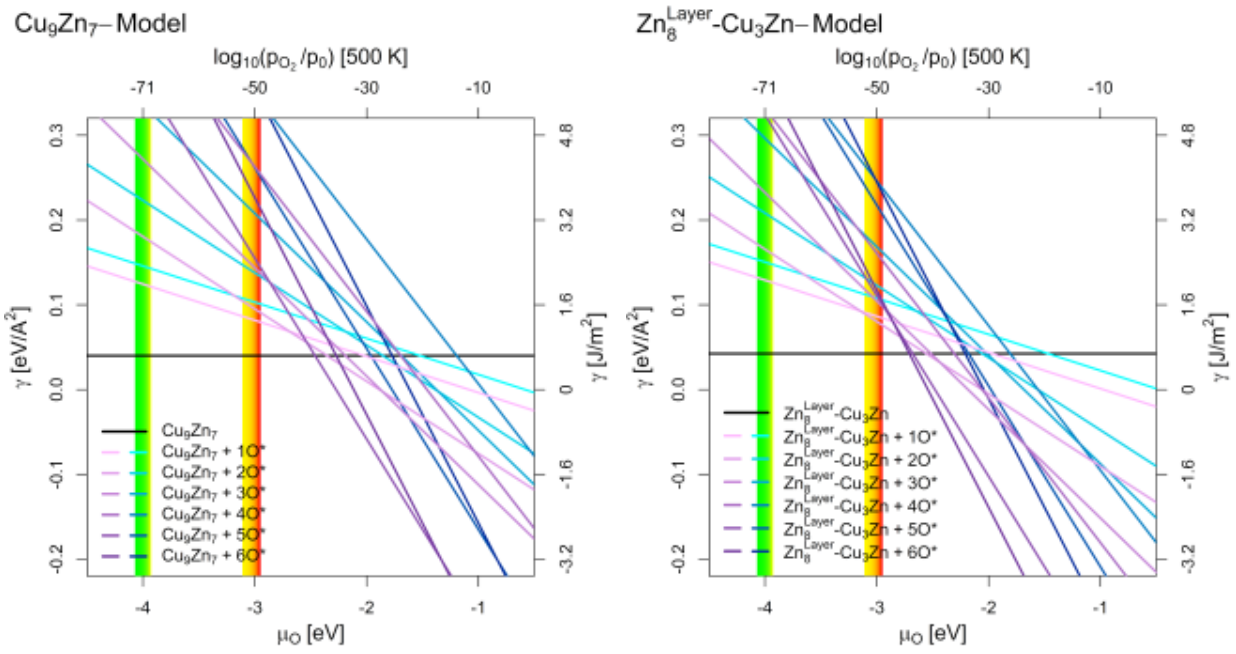

(p) (q)

Figure S8: Surface stability diagram of the (111)-facet of the investigated CuGa-/CuZn-models with both uncorrected surface energies (in blue) and corrected surface energies (in violet) depending on the chemical potential of oxygen (μ_O in eV) and the equivalent oxygen partial pressure at 500 K. The yellow-red area indicates the expected oxygen chemical potential (μ_O) under CO_2 hydrogenation conditions (-3.11 eV $< \mu_O <$ -2.92 eV, corresponding to an equivalent O_2 partial pressure bellow 10^{-48} bar) while the green-yellow area indicates the expected μ_O CO hydrogenation conditions (-4.07 eV $< \mu_O <$ -3.93 eV, equivalent to an O_2 partial pressure bellow 10^{-69} bar) with the colour gradient indicating the progressing (R)WGS reaction (yellow for low conversion, red/green for high conversion; compare Figure 1 in the main text as well as Figures S1 and S4 in the SI). Used slab models for the (111)-facet used are:
(a/b) Unlayered substoichiometric fcc-Cu_3Ga/-Cu_3Zn (12.5 % Zn/Ga).
(c/d) One Ga/Zn surface layer on pure fcc-Cu (12.5 % Ga/Zn).
(e/f) Unlayered stoichiometric fcc-Cu_3Ga/-Cu_3Zn (25 % Ga/Zn).
(g/h) Two Ga/Zn surface layers on pure fcc-Cu (25 % Ga/Zn).
(i/j) Unlayered superstoichiometric fcc-Cu_3Ga/-Cu_3Zn (31.25 % Ga/Zn).
(k/l) Two Ga/Zn surface layers on substoichiometric fcc-Cu_3Ga/-Cu_3Zn (31.25 % Ga/Zn).
(m) Unlayered supersubstoichiometric fcc-Cu_3Zn (37.5 % Zn).
(n) Three Zn surface layers on pure fcc-Cu (37.5 % Ga/Zn).
(o) One Zn surface layer on fcc-Cu_3Zn (34.375 % Ga/Zn).
(p) Unlayered supersubstoichiometric fcc-Cu_3Zn (43.75 % Zn).
(q) Two Zn surface layers on fcc-Cu_3Zn (43.75 % Ga/Zn).

3.2 Individual Surface Energies Depending on the Oxygen Chemical Potential

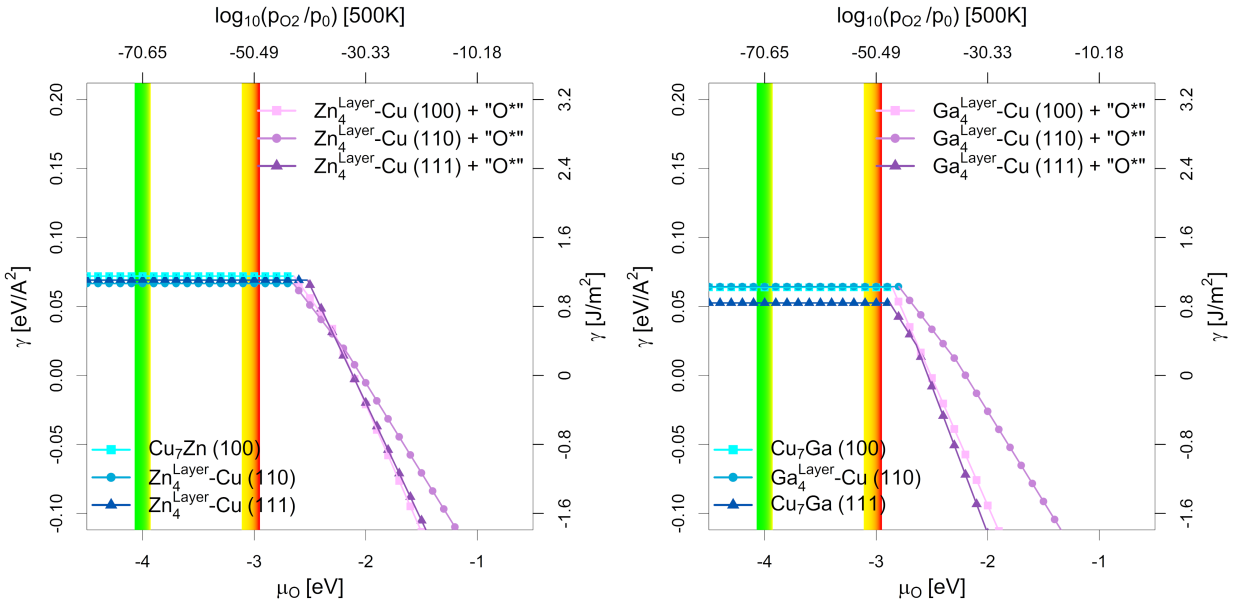

(a)

(b)

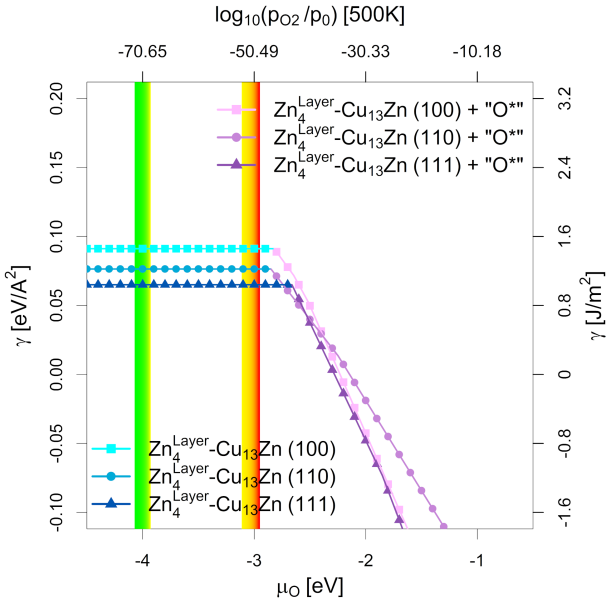

(c)

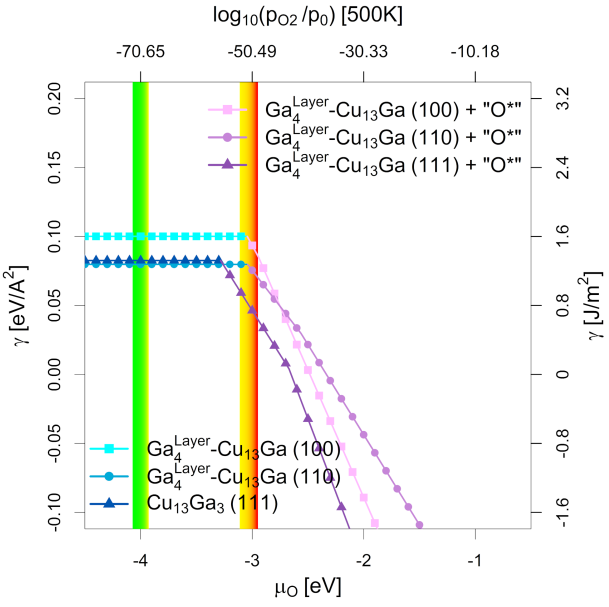

(d)

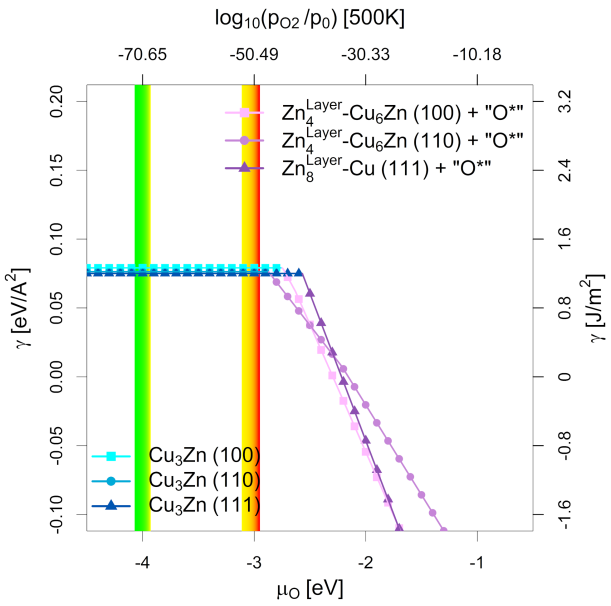
log10(pO2 /p0) [500K]
-70.65
-50.49
-30.33
-10.18
Zn4Layer-Cu6Zn (100) + "O*"
Zn4Layer-Cu6Zn (110) + "O*"
Zn8Layer-Cu (111) + "O*"
Cu3Zn (100)
Cu3Zn (110)
Cu3Zn (111)
γ [eV/A2]
γ [J/m2]
μO [eV]

(e)

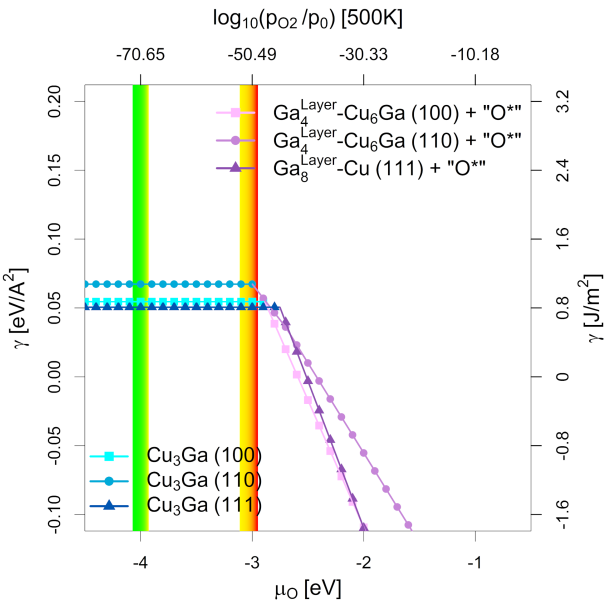
log10(pO2 /p0) [500K]
-70.65
-50.49
-30.33
-10.18
Ga4Layer-Cu6Ga (100) + "O*"
Ga4Layer-Cu6Ga (110) + "O*"
Ga8Layer-Cu (111) + "O*"
Cu3Ga (100)
Cu3Ga (110)
Cu3Ga (111)
γ [eV/A2]
γ [J/m2]
μO [eV]

(f)

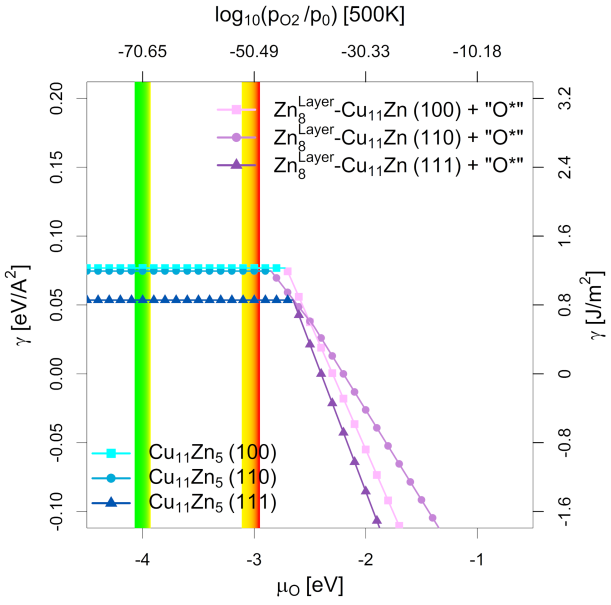
log10(pO2 /p0) [500K]
-70.65
-50.49
-30.33
-10.18
Zn8Layer-Cu11Zn (100) + "O*"
Zn8Layer-Cu11Zn (110) + "O*"
Zn8Layer-Cu11Zn (111) + "O*"
Cu11Zn5 (100)
Cu11Zn5 (110)
Cu11Zn5 (111)
γ [eV/A2]
γ [J/m2]
μO [eV]

(g)

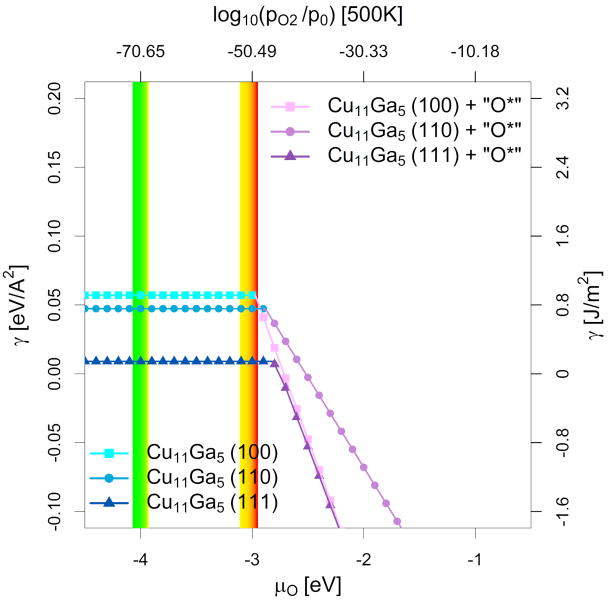
log10(pO2 /p0) [500K]
-70.65
-50.49
-30.33
-10.18
Cu11Ga5 (100) + "O*"
Cu11Ga5 (110) + "O*"
Cu11Ga5 (111) + "O*"
Cu11Ga5 (100)
Cu11Ga5 (110)
Cu11Ga5 (111)
γ [eV/A2]
γ [J/m2]
μO [eV]

(h)

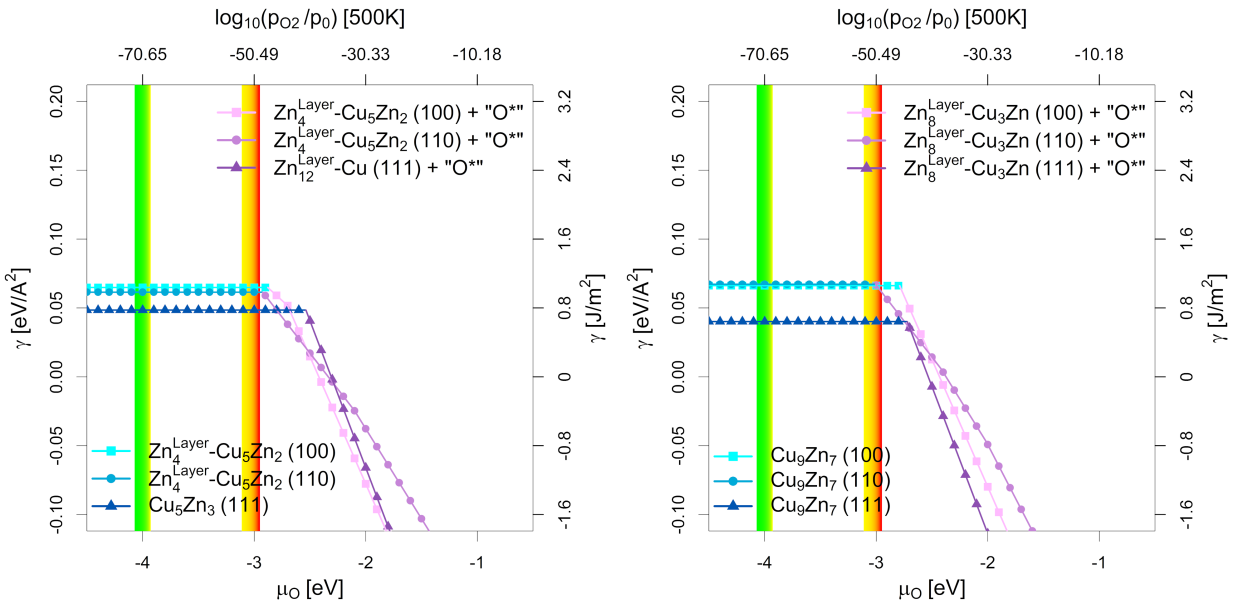

(i) (j)

Figure S9: Most stable surfaces of the fcc-Cu_3Ga/fcc-Cu_3Zn alloys with various compositions depending on the chemical potential of oxygen (μ_O in eV) and the equivalent oxygen partial pressure at 500 K including unlayered structures, partially layered structures and fully layered structures. The yellow-red area indicates the expected oxygen chemical potential (μ_O) under CO_2 hydrogenation conditions (-3.11 eV $< \mu_O < -2.92$ eV, corresponding to an equivalent O_2 partial pressure bellow 10^{-48} bar) while the green-yellow area indicates the expected μ_O CO hydrogenation conditions (-4.07 eV $< \mu_O < -3.93$ eV, equivalent to an O_2 partial pressure bellow 10^{-69} bar) with the colour gradient indicating the progressing (R)WGS reaction (yellow for low conversion, red/green for high conversion; compare Figure 1 in the main text as well as Figures S1 and S4 in the SI). The blue part without incline indicates the most stable structure in vacuum, while the violet part with incline shows the most stable structure with oxygen adsorbed. The shown promoter concentrations are:
(a/b) Substoichiometric fcc-Cu_3Ga/-Cu_3Zn (12.5 % Zn/Ga).
(c/d) Substoichiometric fcc-Cu_3Ga/-Cu_3Zn (18.75 % Zn/Ga).
(e/f) Stoichiometric fcc-Cu_3Ga/-Cu_3Zn (25 % Zn/Ga).
(g/h) Superstoichiometric fcc-Cu_3Ga/-Cu_3Zn (31.25 % Zn/Ga).
(i) Superstoichiometric fcc-Cu_3Zn (37.5 % Zn).
(j) Superstoichiometric fcc-Cu_3Zn (43.75 % Zn).

3.3 Most Stable Structures of Stoichiometric fcc-Cu_3Ga/-Cu_3Zn in Oxygen Atmosphere

3.3.1 (100)-Facet of fcc-Cu_3Ga

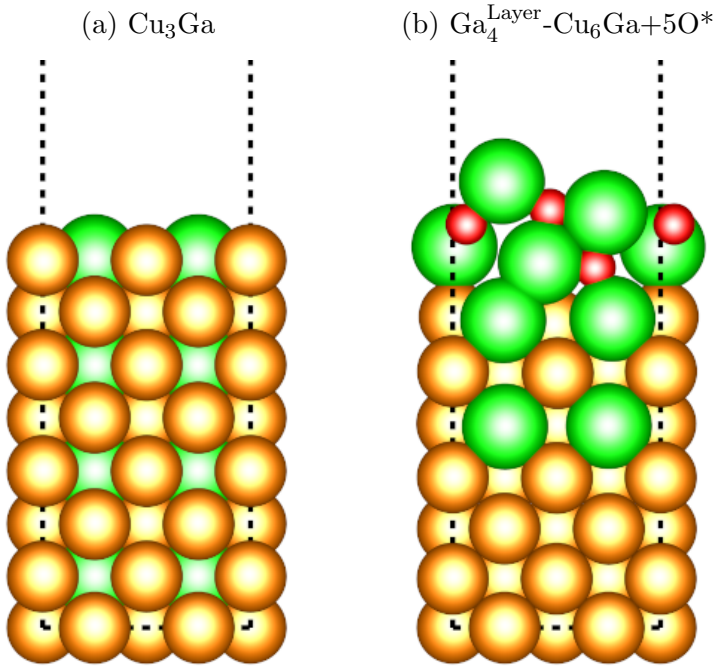

Figure S10: Surface slabs for the (100)-facet of the fcc-Cu_3Ga with the lowest surface energy for specific oxygen chemical potentials (μ_O). The clean Cu_3Ga-slab (Fig. S10a) is most stable for low μ_O (more reducing conditions) while the partially oxidised Ga_4^{Layer}-Cu_6Ga+5O*-slab (Fig. S10b) is most stable for high μ_O (more oxidising conditions). Compare Fig. 7 in the main text for the transition point (point of oxygen adsorption).

Figure S10 shows the surface slabs for the (100)-facet of the fcc-Cu_3Ga-alloy with the lowest surface energy for specific oxygen chemical potentials (μ_O). For lower μ_O, the clean, adsorbate-free surface slab has the lowest surface energy (Cu_3Ga-slab, Fig. S10a). Regarding the spatial distribution of Ga in the slab, the structures is fully alloyed with the Ga distributed over the whole particle, but Ga is slightly enriched on the particle surface resulting in surface layer with a surface concentration of 50 % Ga. If μ_O increases (more oxidising conditions), the slab partially dealloys and a GaO_X surface layer is formed on top of the partially alloyed slab (Ga_4^{Layer}-Cu_6Ga+5O*-slab, Fig. S10b). No slab model with a lower oxygen coverage has is stable, even as an intermediate structure. The structure with the

GaO_X surface layer somewhat represents the Ga_2O_3 structure, but it is not fully crystalline but rather amorphous, since the layer is only partially oxidised.

3.3.2 (110)-Facet of fcc-Cu_3Ga

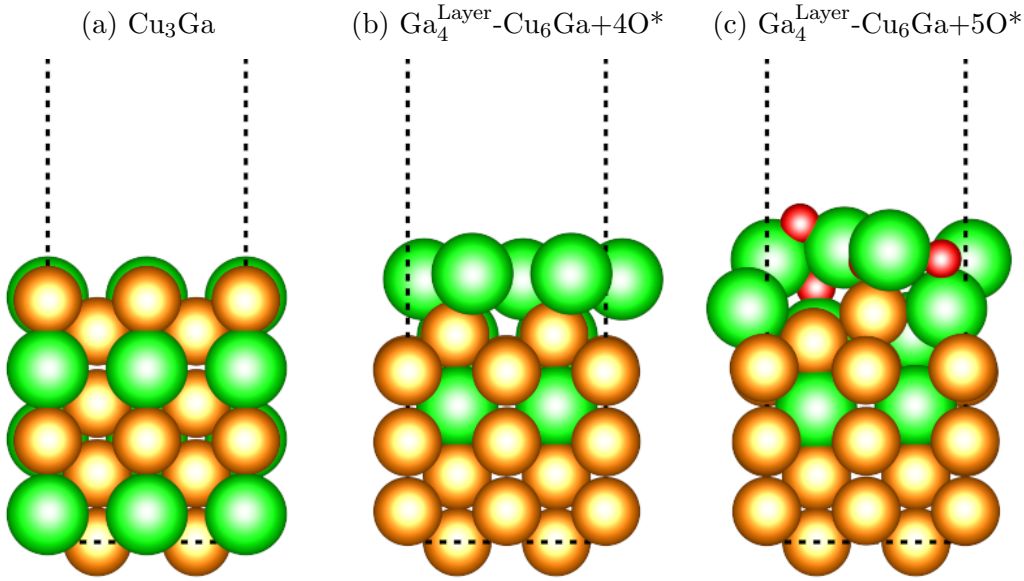

Figure S11: Surface slabs for the (110)-facet of the fcc-Cu_3Ga with the lowest surface energy for specific oxygen chemical potentials (μ_O). The clean Cu_3Ga-slab (Fig. S11a) is most stable for low μ_O (more reducing conditions), the partially oxidised Ga_4^{Layer}-Cu_6Ga+4O*-slab (Fig. S11b) is most stable for intermediate μ_O while the partially oxidised Ga_4^{Layer}-Cu_6Ga+5O*-slab (Fig. S11c) is most stable for high μ_O (more oxidising conditions). Compare Fig. 7 in the main text for the transition points (point of oxygen adsorption).

Figure S11 shows the surface slabs for the (110)-facet of the fcc-Cu_3Ga-alloy with the lowest surface energy for specific μ_O, the results are comparable to the ones for the (100)-facet: A clean, adsorbate-free surface slab (Cu_3Ga-slab, Fig. S11a) for low μ_O and a partially dealloyed slab with an amorphous GaO_X surface layer for high μ_O (Ga_4^{Layer}-Cu_6Ga+5O*-slab, Fig. S11c). But due to the specific arrangement of the atoms in the (110)-slab, there is also an intermediate structure with a more ordered introduction of the oxygen atoms between the alloy slab and the surface layer of Ga (Ga_4^{Layer}-Cu_6Ga+4O*-slab, Fig. S11b). Again, the structure with the GaO_X surface layer somewhat represents the Ga_2O_3 structure, but it is not fully crystalline, since the layer is only partially oxidised.

3.3.3 (111)-Facet of fcc-Cu_3Ga

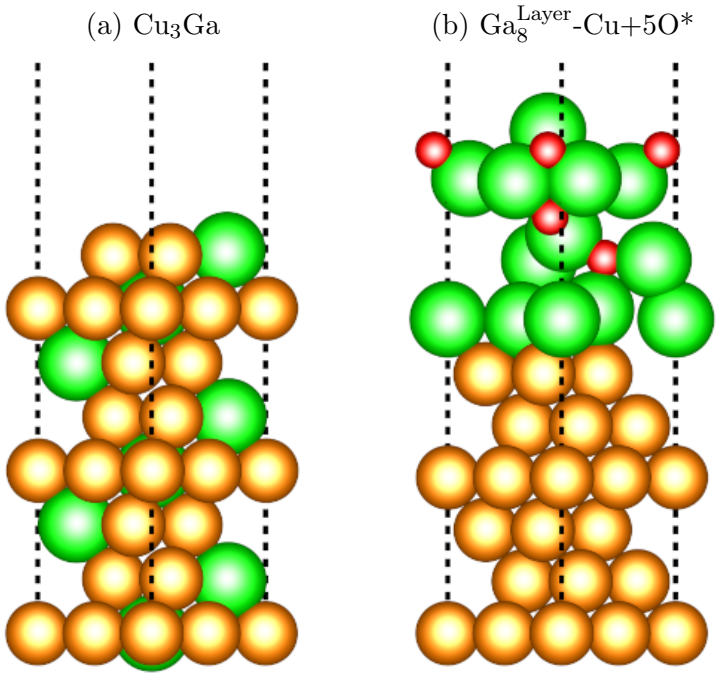

Figure S12: Surface slabs for the (111)-facet of the fcc-Cu_3Ga with the lowest surface energy for specific oxygen chemical potentials (μ_O). The clean Cu_3Ga-slab (Fig. S12a) is most stable for low μ_O (more reducing conditions) while the partially oxidised Ga_8^{Layer}-Cu+5O*-slab (Fig. S12b) is most stable for high μ_O (more oxidising conditions). Compare Fig. 7 in the main text for the transition point (point of oxygen adsorption).

Figure S12 shows the surface slabs for the (111)-facet of the fcc-Cu_3Ga-alloy with the lowest surface energy for specific μ_O. Again, comparable results to the other facets are observed: An alloyed structure under reducing conditions (low μ_O), while dealloying is observed for more oxidising conditions. But the degree of dealloying is higher for the (111)-facet when compared to the other two facets, with the formation of a double lower of Ga observed on the surface slab. This could be a result of the tighter packing of this facet compared to the other two, making it harder to introduce O* into the Ga-layer.

3.3.4 (100)-Facet of fcc-Cu_3Zn

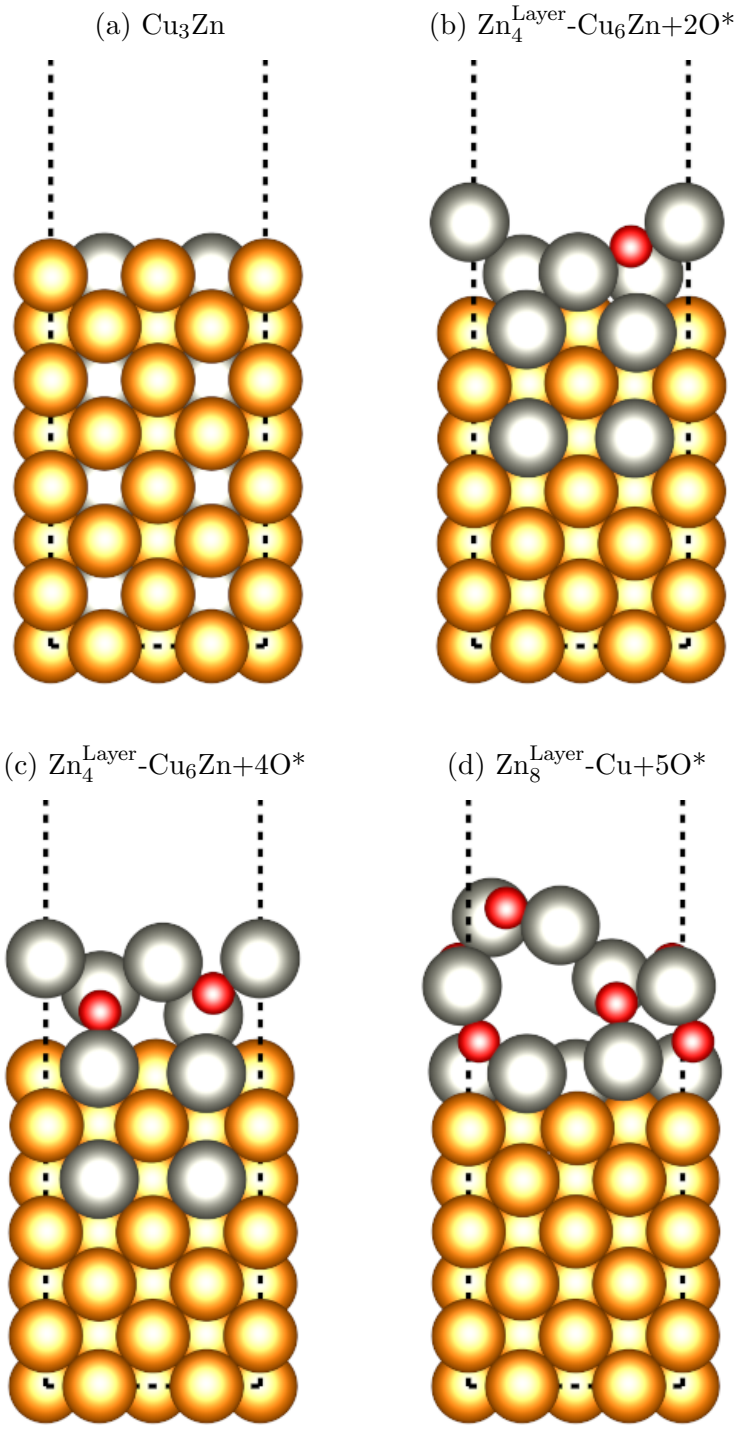

Figure S13: Surface slabs for the (100)-facet of the fcc-Cu_3Zn with the lowest surface energy for specific oxygen chemical potentials (μ_O). The clean Cu_3Zn-slab (Fig. S13a) is most stable for low μ_O (more reducing conditions), the partially oxidised Zn_4^{Layer}-Cu_6Zn+2O*- and Zn_4^{Layer}-Cu_6Zn+4O*-slab (Fig. S13b and S13c) are most stable for intermediate μ_O while the partially oxidised Zn_8^{Layer}-Cu+5O*-slab (Fig. S13d) is most stable for high μ_O (more oxidising conditions). Compare Fig. 7 in the main text for the transition points (point of oxygen adsorption).

Figure S13 shows the surface slabs for the (100)-facet of the fcc-Cu_3Zn-alloy with the lowest surface energy for specific μ_O. As for the CuGa-equivalent, it has an adsorbate-free structure at low μ_O (Cu_3Zn-slab, Fig. S13a) and a dealloyed structure at high μ_O (Zn_8^{Layer}-Cu+5O*-slab, Fig. S13d). But in contrast to the CuGa-equivalent, intermediate structures are observed (n_4^{Layer}-Cu_6Zn+2O*- and Zn_4^{Layer}-Cu_6Zn+4O*-slab, Fig. S13b and S13c) and the final structure is fully dealloyed (Fig. S13d. This can be explained by the different affinity of Ga and Zn for oxygen and the stoichiometry of their respective oxides (2:3 for Ga_2O_3 vs. 1:1 for ZnO). Regarding the structure of the surface layer, the ZnO_X structure is quite representative to the ZnO structure, but it is again rather amorphous, since the layer is only partially oxidised.

3.3.5 (110)-Facet of fcc-Cu_3Zn

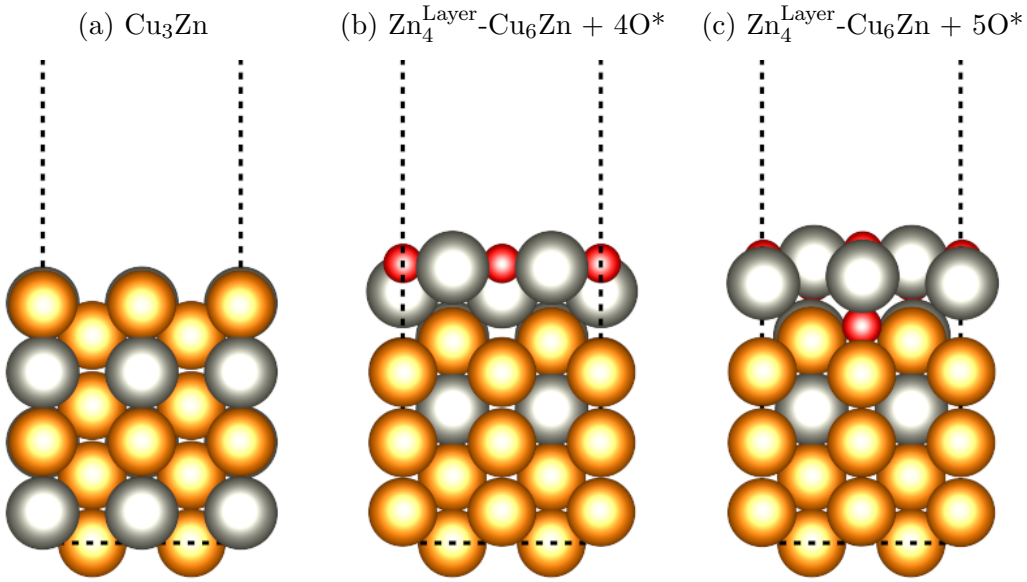

Figure S14: Surface slabs for the (110)-facet of the fcc-Cu_3Zn with the lowest surface energy for specific oxygen chemical potentials (μ_O). The clean Cu_3Zn-slab (Fig. S14a) is most stable for low μ_O (more reducing conditions), the partially oxidised Zn_4^{Layer}-Cu_6Zn+4O*-slab (Fig. S14b) is most stable for intermediate μ_O while the partially oxidised Zn_4^{Layer}-Cu_6Zn+5O*-slab (Fig. S14c) is most stable for high μ_O (more oxidising conditions). Compare Fig. 7 in the main text for the transition points (point of oxygen adsorption).

Figure S14 shows the surface slabs for the (110)-facet of the fcc-Cu_3Zn with the lowest

surface energy for specific μ_O. The slabs for the CuZn-system are very similar to the CuGa-system: An adsorbate-free surface (Cu_3Ga-slab, Fig. S14a) for low μ_O, an intermediate structure with a more ordered introduction of the oxygen atoms between the alloy slab and the surface layer of Zn (Zn_4^{Layer}-Cu_6Zn + 4O*-slab, Fig. S14c) and a partially dealloyed slab with an amorphous ZnO_X surface layer for high μ_O (Zn_4^{Layer}-Cu_6Zn + 5O*-slab, Fig. S14c).

3.3.6 (111)-Facet of fcc-Cu_3Zn

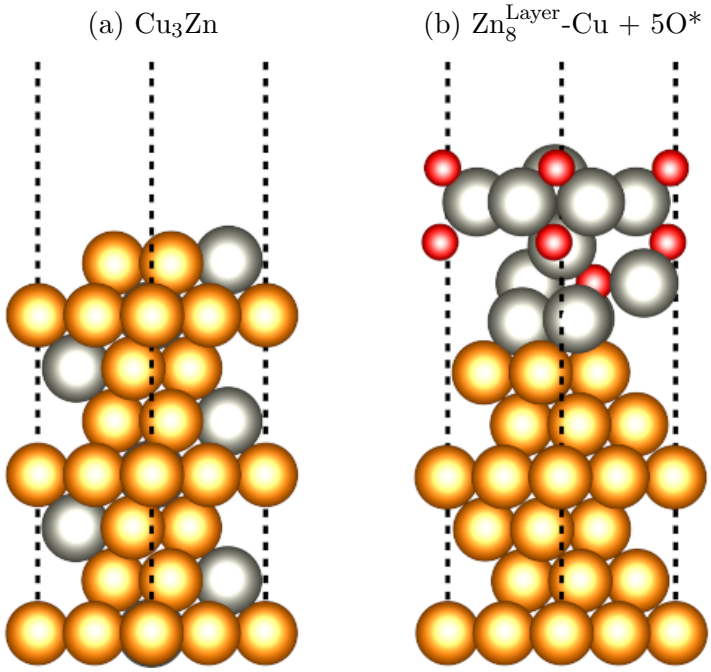

Figure S15: Surface slabs for the (111)-facet of the fcc-Cu_3Zn with the lowest surface energy for specific oxygen chemical potentials (μ_O). The clean Cu_3Zn-slab (Fig. S15a) is most stable for low μ_O (more reducing conditions) while the partially oxidised Zn_8^{Layer}-Cu+5O*-slab (Fig. S15b) is most stable for high μ_O (more oxidising conditions). Compare Fig. 7 in the main text for the transition point (point of oxygen adsorption).

Finally, Figure S15 shows the surface slabs for the (111)-facet of the fcc-Cu_3Zn-alloy with the lowest surface energy for specific μ_O. As for the (110)-facet, the slabs are very similar to the CuGa-system; the slab is alloyed under reducing conditions (low μ_O, Cu_3Zn-slab, Fig. S15a) and a completely dealloyed structure under oxidising conditions (high μ_O, Zn_8^{Layer}-Cu + 5O*, Fig. S15b). The layer oxided layer is again structurally similar to the ZnO-structure.

4 Surface Stability Diagrams in Hydrogen Atmosphere

4.1 Individual Surface Stability Diagrams in Hydrogen Atmosphere

(100)-Facet

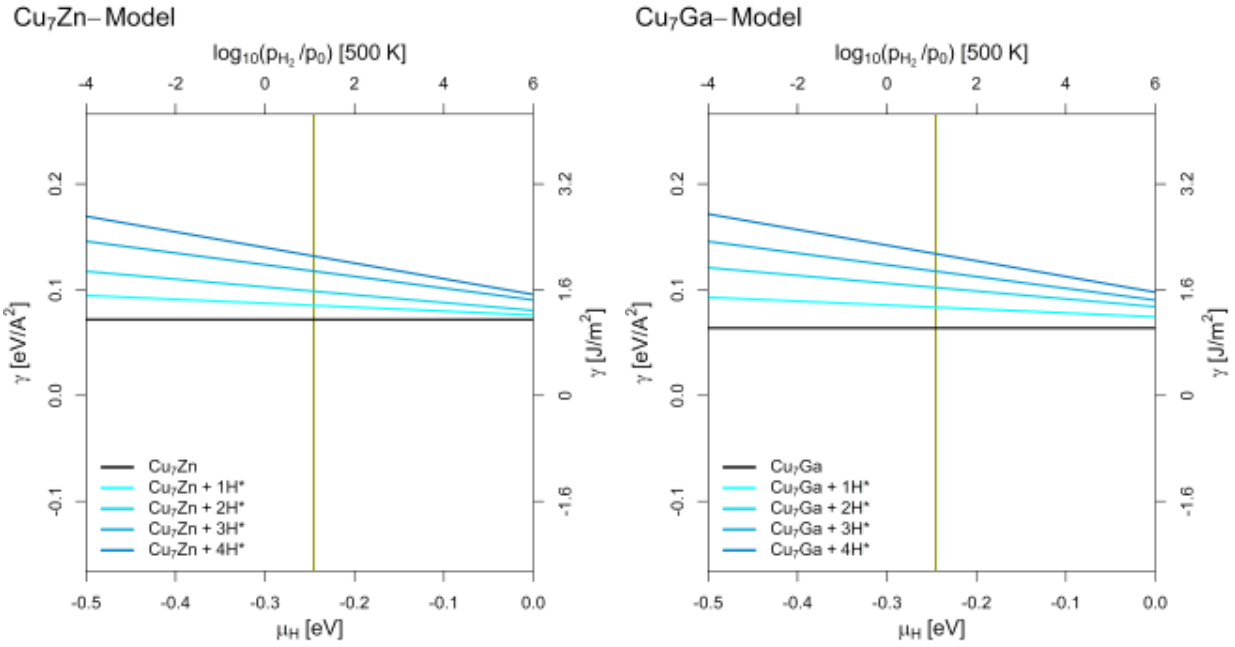

(a) (b)

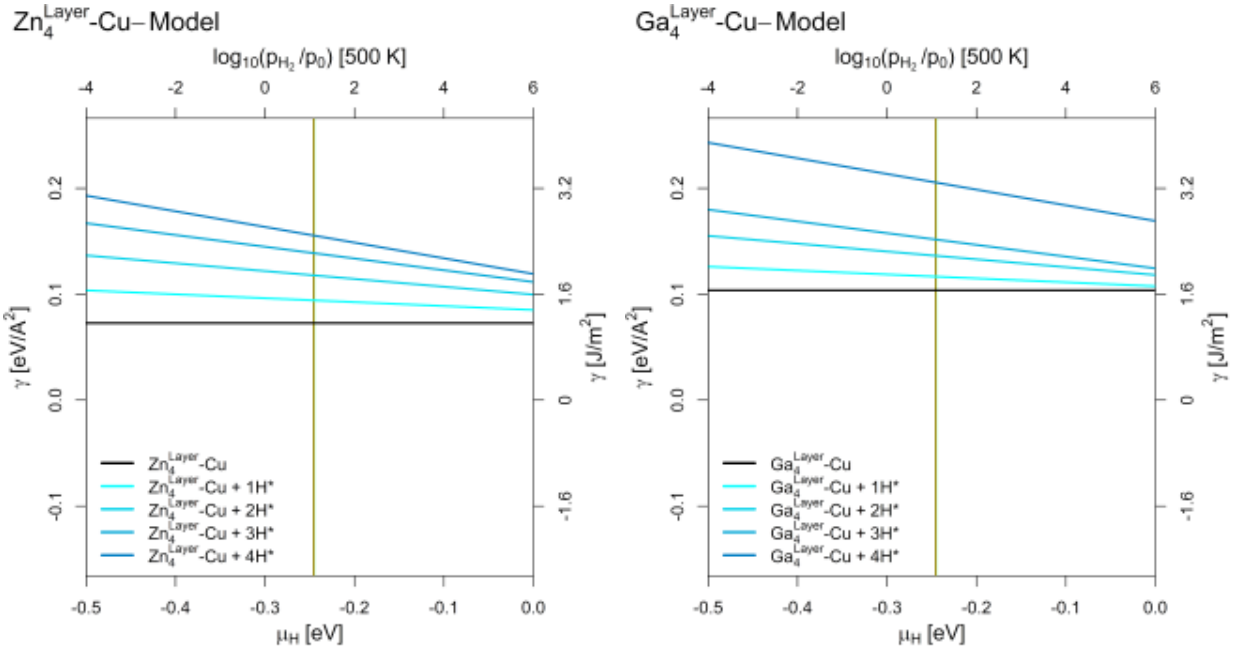

(c) (d)

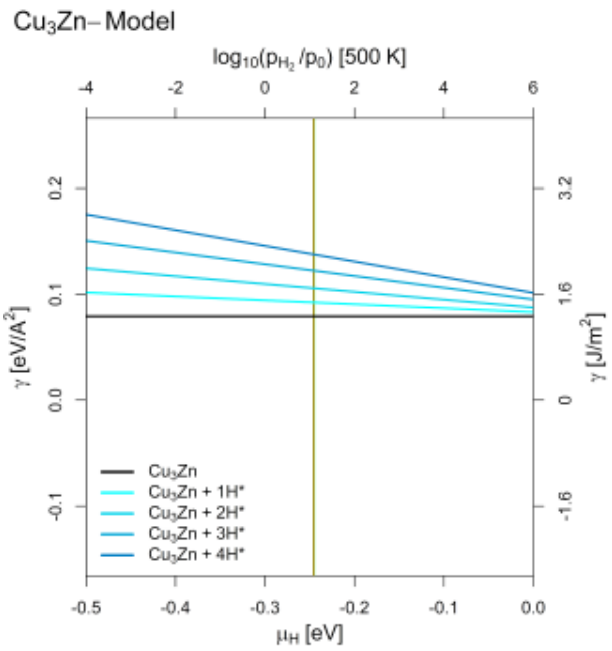
Cu3Zn – Model
log10(pH2 /p0) [500 K]
γ [eV/Å2]
γ [J/m2]
μH [eV]
Cu3Zn
Cu3Zn + 1H*
Cu3Zn + 2H*
Cu3Zn + 3H*
Cu3Zn + 4H*

(e)

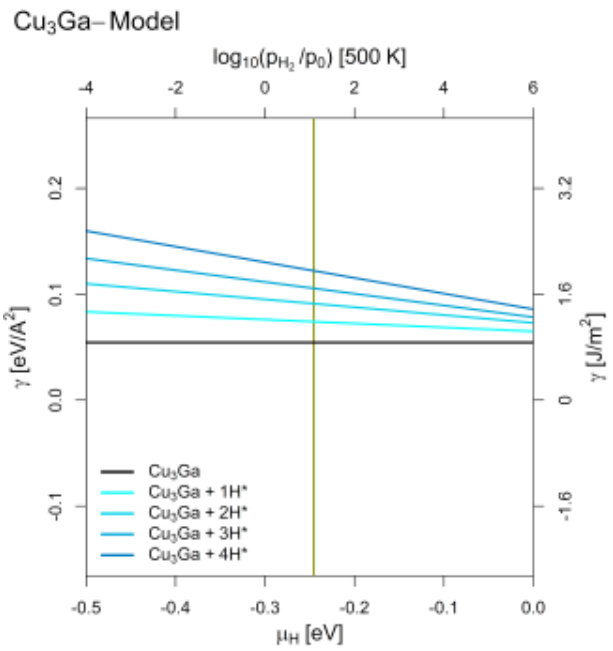
Cu3Ga – Model
log10(pH2 /p0) [500 K]
γ [eV/Å2]
γ [J/m2]
μH [eV]
Cu3Ga
Cu3Ga + 1H*
Cu3Ga + 2H*
Cu3Ga + 3H*
Cu3Ga + 4H*

(f)

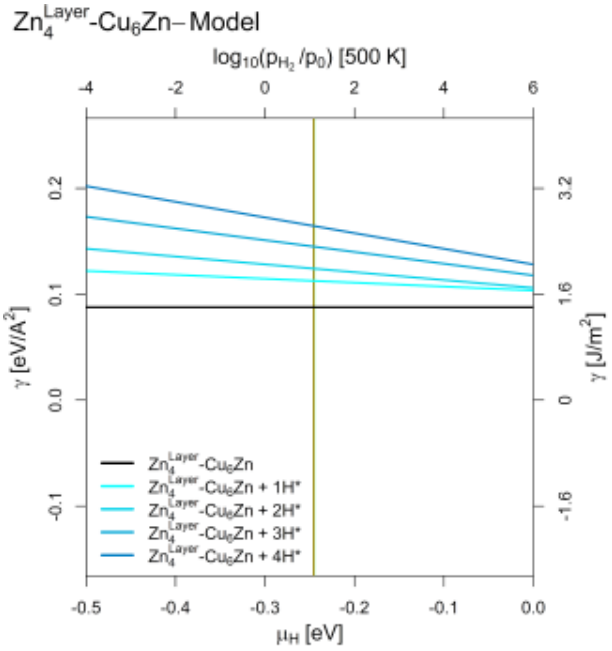
Zn4Layer-Cu6Zn – Model
log10(pH2 /p0) [500 K]
γ [eV/Å2]
γ [J/m2]
μH [eV]
Zn4Layer-Cu6Zn
Zn4Layer-Cu6Zn + 1H*
Zn4Layer-Cu6Zn + 2H*
Zn4Layer-Cu6Zn + 3H*
Zn4Layer-Cu6Zn + 4H*

(g)

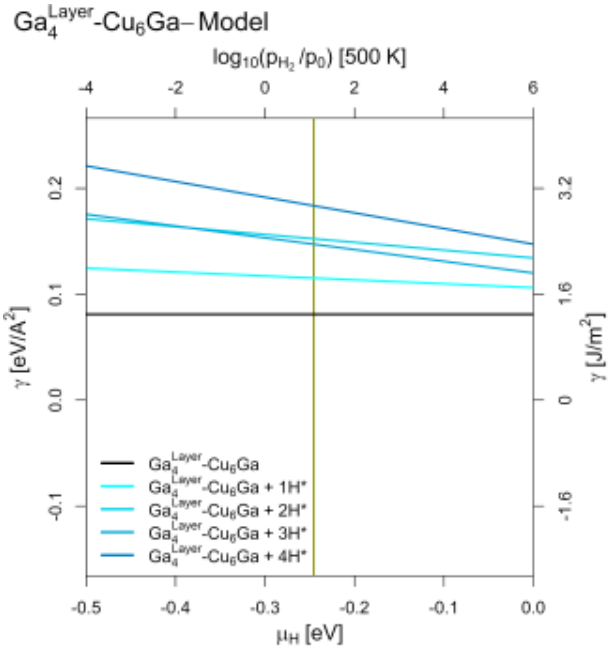
Ga4Layer-Cu6Ga – Model
log10(pH2 /p0) [500 K]
γ [eV/Å2]
γ [J/m2]
μH [eV]
Ga4Layer-Cu6Ga
Ga4Layer-Cu6Ga + 1H*
Ga4Layer-Cu6Ga + 2H*
Ga4Layer-Cu6Ga + 3H*
Ga4Layer-Cu6Ga + 4H*

(h)

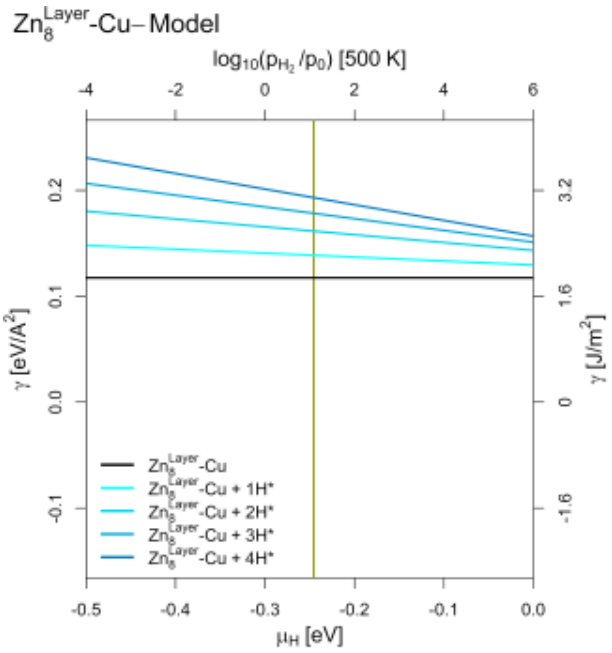
Zn_8^{Layer}-Cu–Model
$\log_{10}(p_{H_2}/p_0)$ [500 K]
γ [eV/Å^2]
γ [J/m^2]
μ_H [eV]
Zn_8^{Layer}-Cu
Zn_8^{Layer}-Cu + 1H*
Zn_8^{Layer}-Cu + 2H*
Zn_8^{Layer}-Cu + 3H*
Zn_8^{Layer}-Cu + 4H*

(i)

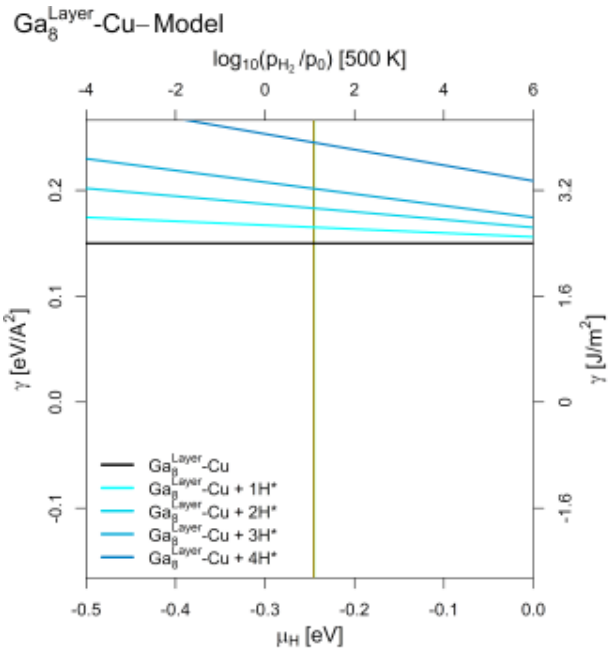
Ga_8^{Layer}-Cu–Model
$\log_{10}(p_{H_2}/p_0)$ [500 K]
γ [eV/Å^2]
γ [J/m^2]
μ_H [eV]
Ga_8^{Layer}-Cu
Ga_8^{Layer}-Cu + 1H*
Ga_8^{Layer}-Cu + 2H*
Ga_8^{Layer}-Cu + 3H*
Ga_8^{Layer}-Cu + 4H*

(j)

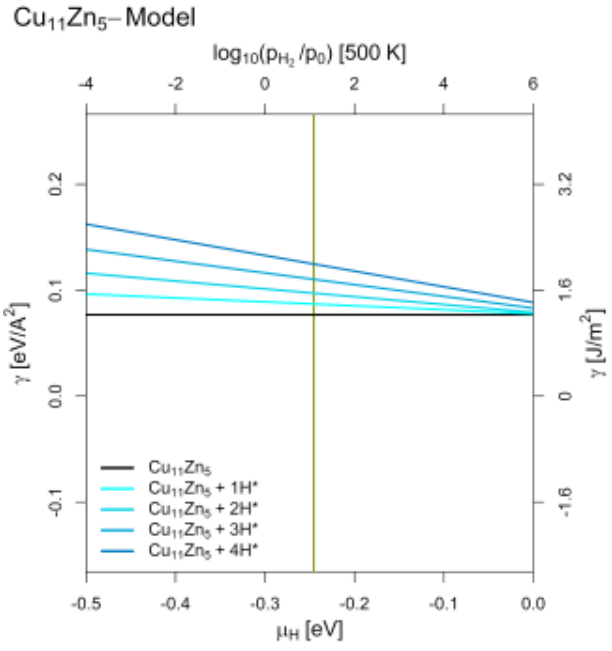
$Cu_{11}Zn_5$–Model
$\log_{10}(p_{H_2}/p_0)$ [500 K]
γ [eV/Å^2]
γ [J/m^2]
μ_H [eV]
$Cu_{11}Zn_5$
$Cu_{11}Zn_5$ + 1H*
$Cu_{11}Zn_5$ + 2H*
$Cu_{11}Zn_5$ + 3H*
$Cu_{11}Zn_5$ + 4H*

(k)

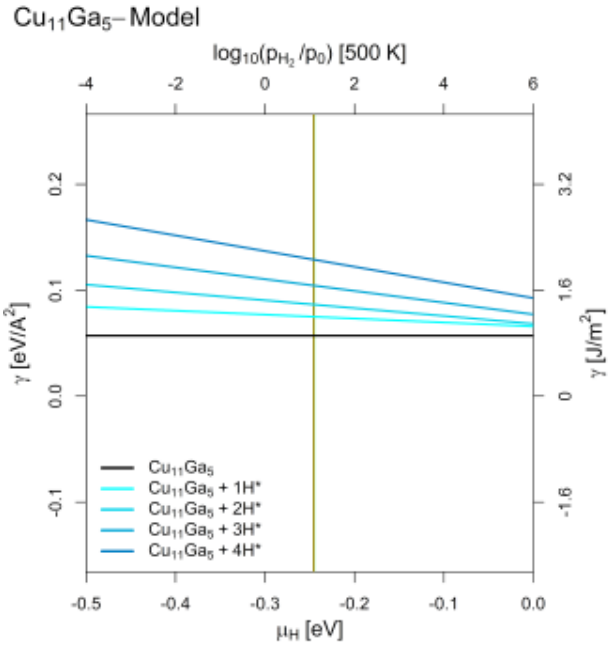
$Cu_{11}Ga_5$–Model
$\log_{10}(p_{H_2}/p_0)$ [500 K]
γ [eV/Å^2]
γ [J/m^2]
μ_H [eV]
$Cu_{11}Ga_5$
$Cu_{11}Ga_5$ + 1H*
$Cu_{11}Ga_5$ + 2H*
$Cu_{11}Ga_5$ + 3H*
$Cu_{11}Ga_5$ + 4H*

(l)

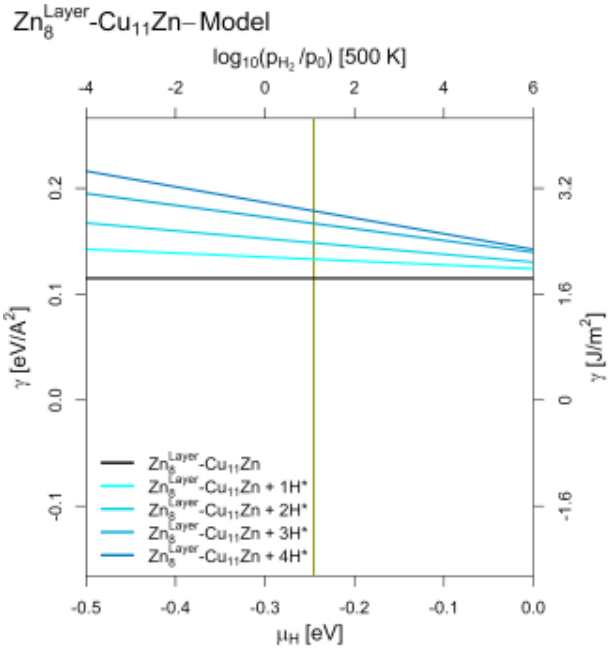
Zn_8^{Layer}-$Cu_{11}Zn$ – Model
$\log_{10}(p_{H_2}/p_0)$ [500 K]
γ [eV/A^2]
γ [J/m^2]
μ_H [eV]
Zn_8^{Layer}-$Cu_{11}Zn$
Zn_8^{Layer}-$Cu_{11}Zn$ + 1H*
Zn_8^{Layer}-$Cu_{11}Zn$ + 2H*
Zn_8^{Layer}-$Cu_{11}Zn$ + 3H*
Zn_8^{Layer}-$Cu_{11}Zn$ + 4H*

(m)

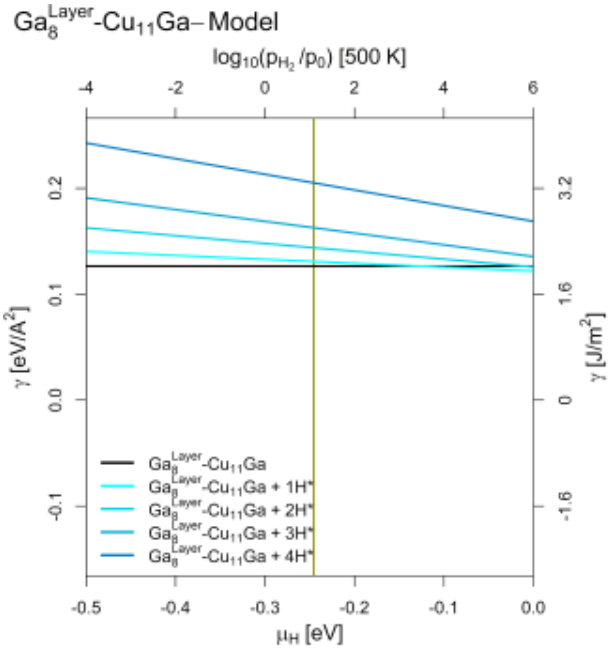
Ga_8^{Layer}-$Cu_{11}Ga$ – Model
$\log_{10}(p_{H_2}/p_0)$ [500 K]
γ [eV/A^2]
γ [J/m^2]
μ_H [eV]
Ga_8^{Layer}-$Cu_{11}Ga$
Ga_8^{Layer}-$Cu_{11}Ga$ + 1H*
Ga_8^{Layer}-$Cu_{11}Ga$ + 2H*
Ga_8^{Layer}-$Cu_{11}Ga$ + 3H*
Ga_8^{Layer}-$Cu_{11}Ga$ + 4H*

(n)

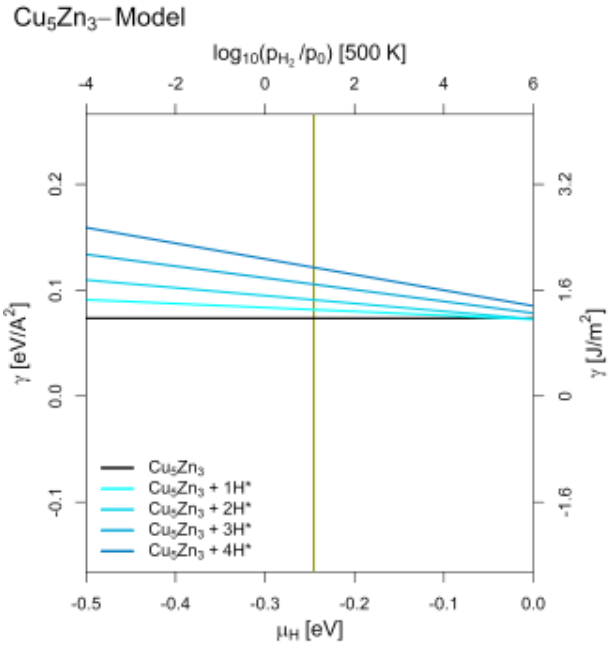
Cu_5Zn_3 – Model
$\log_{10}(p_{H_2}/p_0)$ [500 K]
γ [eV/A^2]
γ [J/m^2]
μ_H [eV]
Cu_5Zn_3
Cu_5Zn_3 + 1H*
Cu_5Zn_3 + 2H*
Cu_5Zn_3 + 3H*
Cu_5Zn_3 + 4H*

(o)

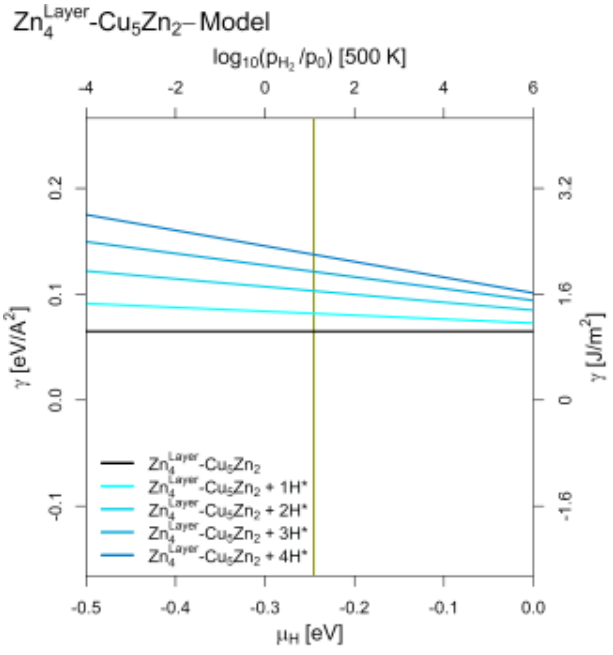
Zn_4^{Layer}-Cu_5Zn_2 – Model
$\log_{10}(p_{H_2}/p_0)$ [500 K]
γ [eV/A^2]
γ [J/m^2]
μ_H [eV]
Zn_4^{Layer}-Cu_5Zn_2
Zn_4^{Layer}-Cu_5Zn_2 + 1H*
Zn_4^{Layer}-Cu_5Zn_2 + 2H*
Zn_4^{Layer}-Cu_5Zn_2 + 3H*
Zn_4^{Layer}-Cu_5Zn_2 + 4H*

(p)

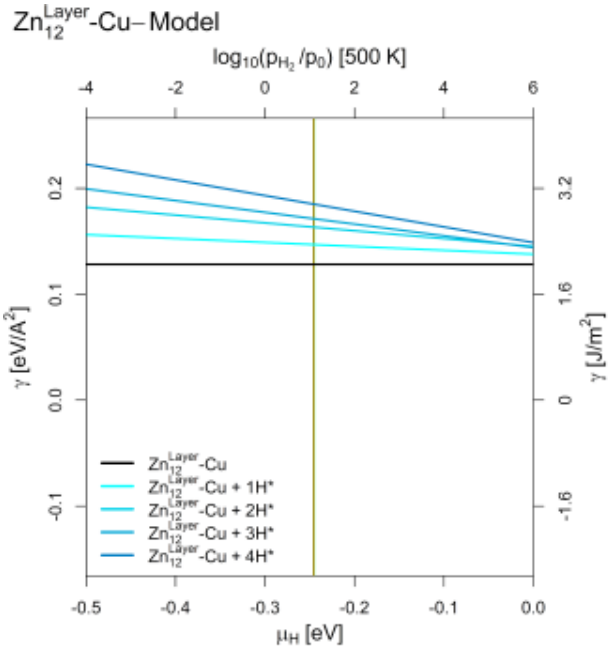
Zn12Layer-Cu– Model
log10(pH2 /p0) [500 K]
γ [eV/A2]
γ [J/m2]
μH [eV]
Zn12Layer-Cu
Zn12Layer-Cu + 1H*
Zn12Layer-Cu + 2H*
Zn12Layer-Cu + 3H*
Zn12Layer-Cu + 4H*

(q)

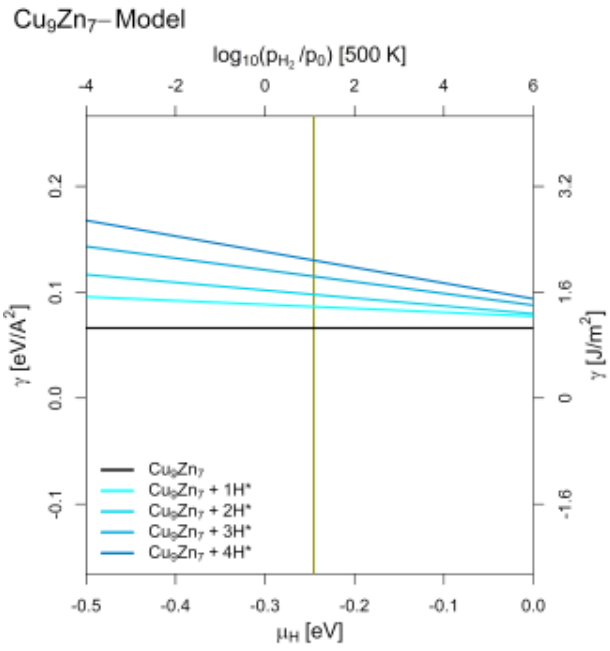
Cu9Zn7– Model
log10(pH2 /p0) [500 K]
γ [eV/A2]
γ [J/m2]
μH [eV]
Cu9Zn7
Cu9Zn7 + 1H*
Cu9Zn7 + 2H*
Cu9Zn7 + 3H*
Cu9Zn7 + 4H*

(r)

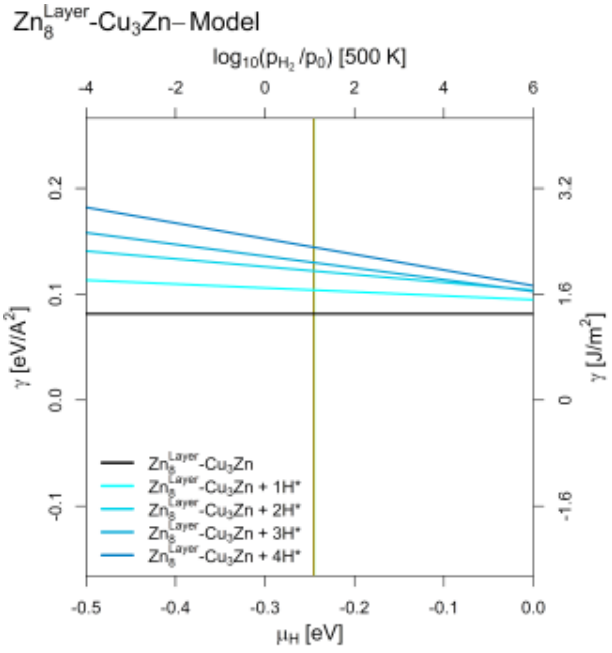
Zn8Layer-Cu3Zn– Model
log10(pH2 /p0) [500 K]
γ [eV/A2]
γ [J/m2]
μH [eV]
Zn8Layer-Cu3Zn
Zn8Layer-Cu3Zn + 1H*
Zn8Layer-Cu3Zn + 2H*
Zn8Layer-Cu3Zn + 3H*
Zn8Layer-Cu3Zn + 4H*

(s)

Figure S16: Surface stability diagram of the (100)-facet of the investigated CuGa-/CuZn-models depending on the chemical potential of hydrogen (μ_H in eV) and the equivalent hydrogen partial pressure at 500 K. The red/green line indicates μ_H expected under CO_2 or CO hydrogenation conditions (-0.235 eV $< \mu_H <$ -0.234 eV).[S2] Used slab models for the (100)-facet used are:
(a/b) Unlayered substoichiometric fcc-Cu_3Ga/-Cu_3Zn (12.5 % Zn/Ga).
(c/d) One Ga/Zn surface layer on pure fcc-Cu (12.5 % Ga/Zn).
(e/f) Unlayered stoichiometric fcc-Cu_3Ga/-Cu_3Zn (25 % Ga/Zn).
(g/h) One Ga/Zn surface layer on substoichiometric fcc-Cu_3Ga/-Cu_3Zn (25 % Ga/Zn).
(i/j) Two Ga/Zn surface layers on pure fcc-Cu (25 % Ga/Zn).
(k/l) Unlayered superstoichiometric fcc-Cu_3Ga/-Cu_3Zn (31.25 % Ga/Zn).
(m/n) Two Ga/Zn surface layers on substoichiometric fcc-Cu_3Ga/-Cu_3Zn (31.25 % Ga/Zn).
(o) Unlayered supersubstoichiometric fcc-Cu_3Zn (37.5 % Zn).
(p) One Zn surface layer on fcc-Cu_3Zn (37.5 % Ga/Zn).
(q) Three Zn surface layers on pure fcc-Cu (37.5 % Ga/Zn).
(r) Unlayered supersubstoichiometric fcc-Cu_3Zn (43.75 % Zn).
(s) Two Zn surface layers on fcc-Cu_3Zn (43.75 % Ga/Zn).

(110)-Facet

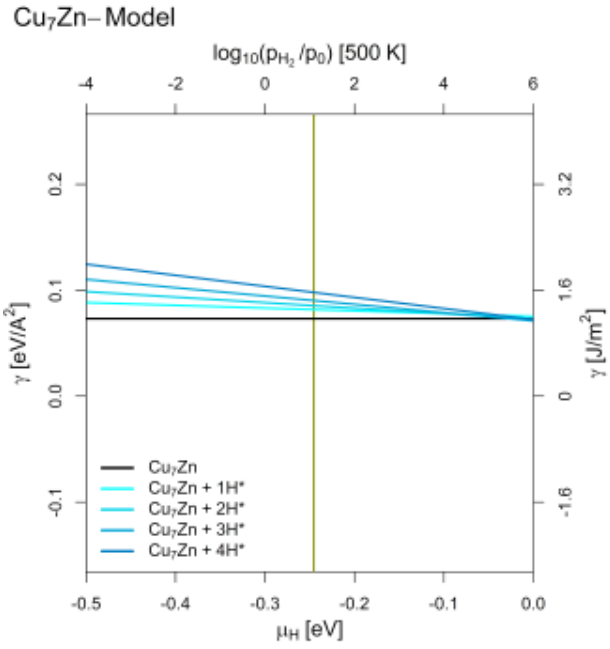

(a)

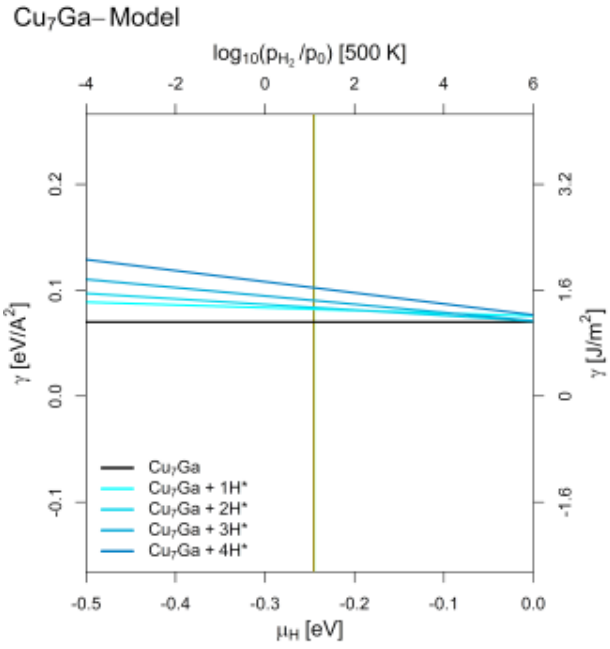

(b)

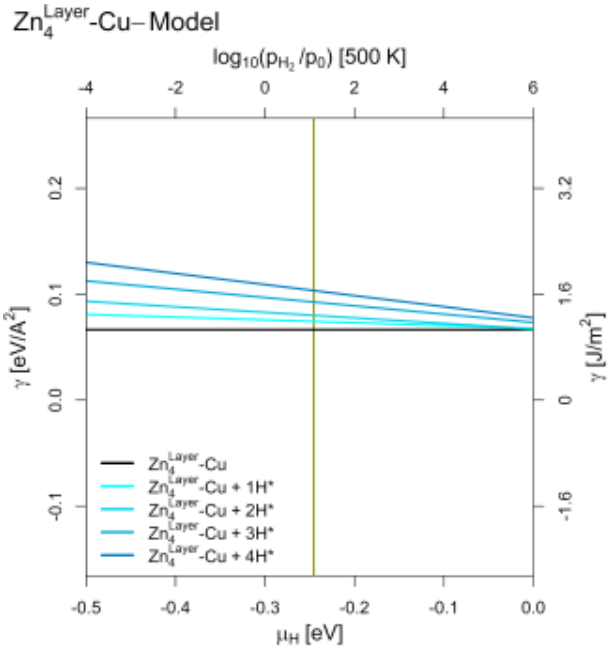

(c)

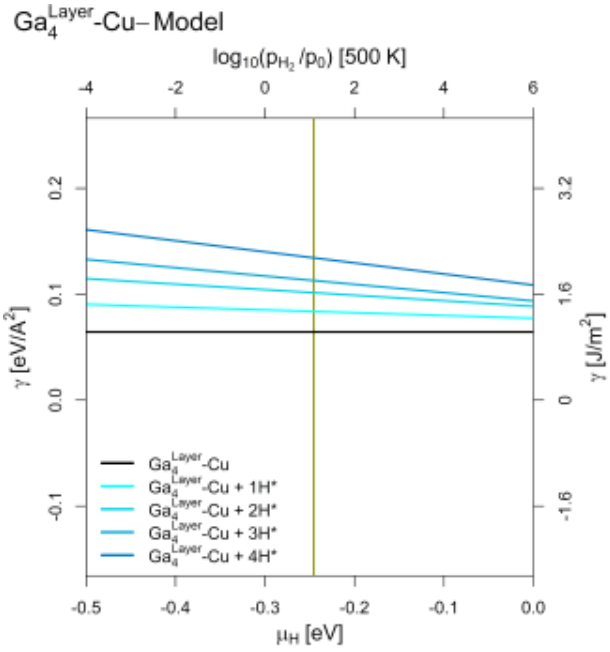

(d)

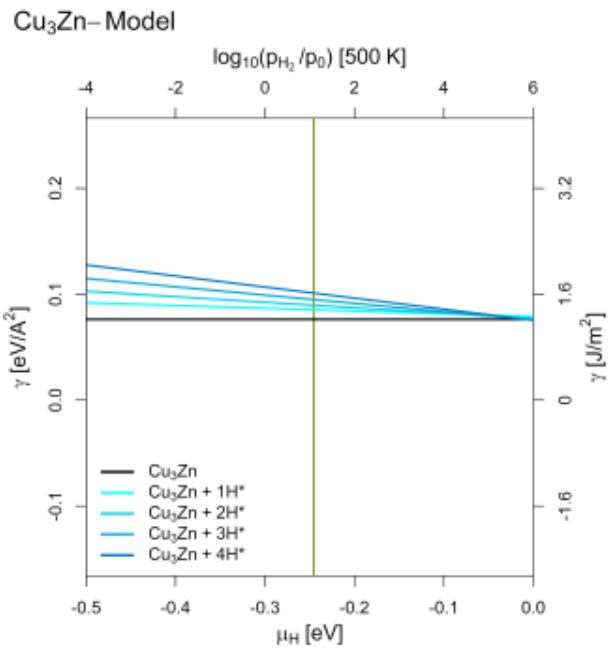
Cu3Zn – Model
log10(pH2 /p0) [500 K]
γ [eV/Å2]
γ [J/m2]
μH [eV]
Cu3Zn
Cu3Zn + 1H*
Cu3Zn + 2H*
Cu3Zn + 3H*
Cu3Zn + 4H*

(e)

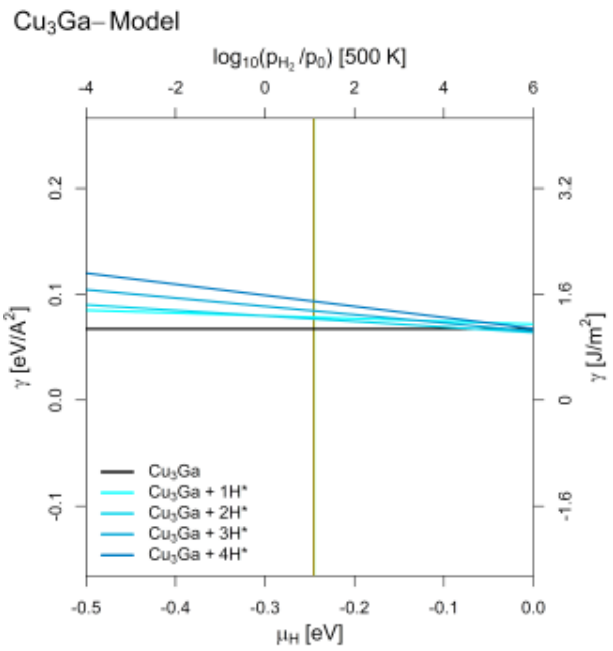
Cu3Ga – Model
log10(pH2 /p0) [500 K]
γ [eV/Å2]
γ [J/m2]
μH [eV]
Cu3Ga
Cu3Ga + 1H*
Cu3Ga + 2H*
Cu3Ga + 3H*
Cu3Ga + 4H*

(f)

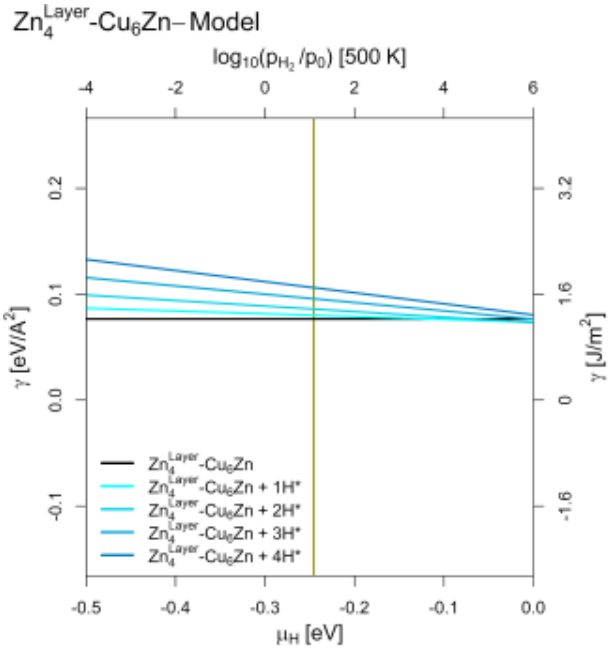
Zn4Layer-Cu6Zn – Model
log10(pH2 /p0) [500 K]
γ [eV/Å2]
γ [J/m2]
μH [eV]
Zn4Layer-Cu6Zn
Zn4Layer-Cu6Zn + 1H*
Zn4Layer-Cu6Zn + 2H*
Zn4Layer-Cu6Zn + 3H*
Zn4Layer-Cu6Zn + 4H*

(g)

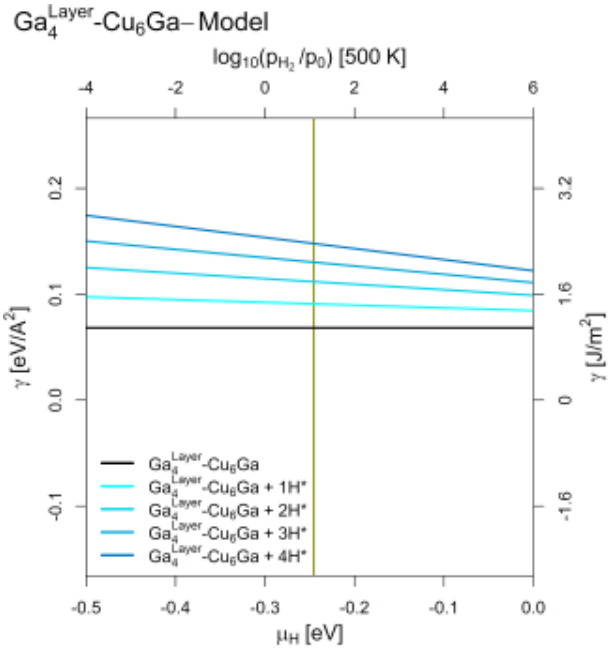
Ga4Layer-Cu6Ga – Model
log10(pH2 /p0) [500 K]
γ [eV/Å2]
γ [J/m2]
μH [eV]
Ga4Layer-Cu6Ga
Ga4Layer-Cu6Ga + 1H*
Ga4Layer-Cu6Ga + 2H*
Ga4Layer-Cu6Ga + 3H*
Ga4Layer-Cu6Ga + 4H*

(h)

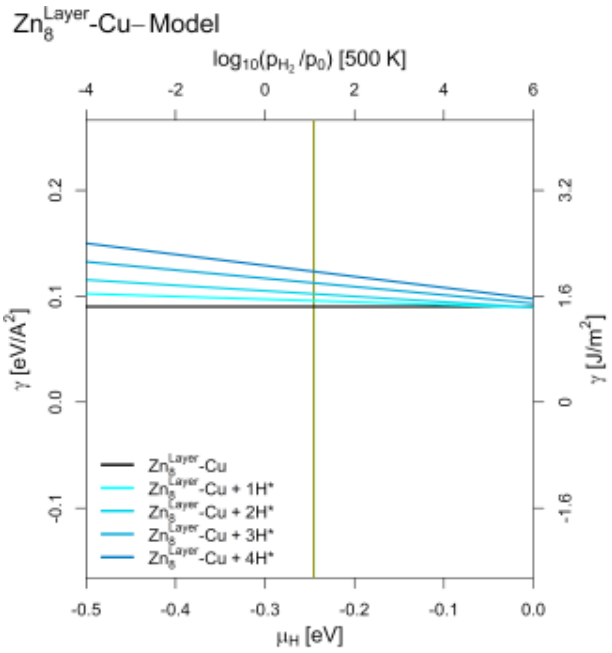
Zn_8^{Layer}-Cu– Model
$\log_{10}(p_{H_2}/p_0)$ [500 K]
-4 -2 0 2 4 6
γ [eV/A²]
γ [J/m²]
0.2 0.1 0.0 -0.1
3.2 1.6 0 -1.6
Zn_8^{Layer}-Cu
Zn_8^{Layer}-Cu + 1H*
Zn_8^{Layer}-Cu + 2H*
Zn_8^{Layer}-Cu + 3H*
Zn_8^{Layer}-Cu + 4H*
-0.5 -0.4 -0.3 -0.2 -0.1 0.0
μ_H [eV]

(i)

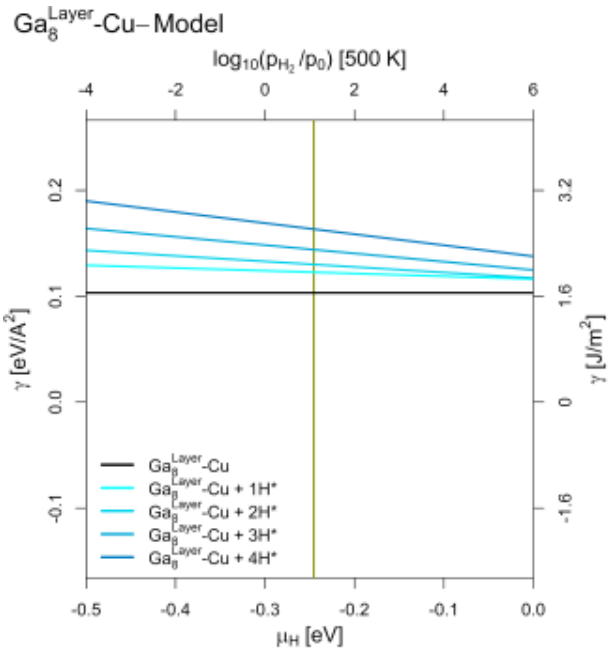
Ga_8^{Layer}-Cu– Model
$\log_{10}(p_{H_2}/p_0)$ [500 K]
-4 -2 0 2 4 6
γ [eV/A²]
γ [J/m²]
0.2 0.1 0.0 -0.1
3.2 1.6 0 -1.6
Ga_8^{Layer}-Cu
Ga_8^{Layer}-Cu + 1H*
Ga_8^{Layer}-Cu + 2H*
Ga_8^{Layer}-Cu + 3H*
Ga_8^{Layer}-Cu + 4H*
-0.5 -0.4 -0.3 -0.2 -0.1 0.0
μ_H [eV]

(j)

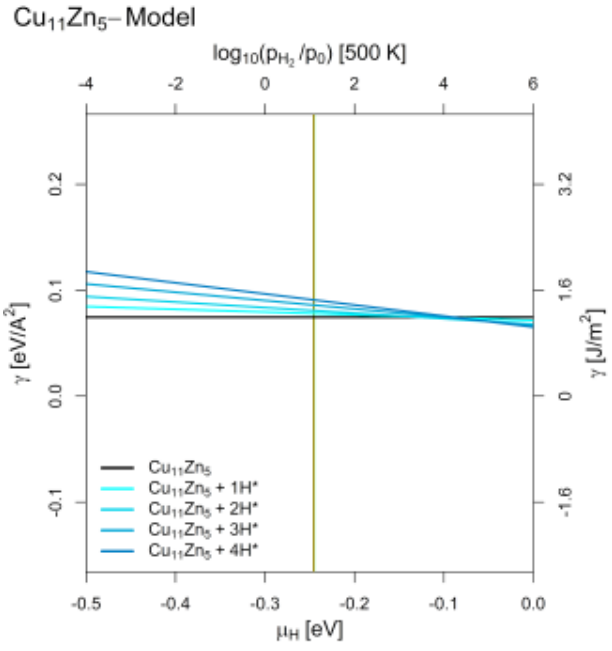
$Cu_{11}Zn_5$– Model
$\log_{10}(p_{H_2}/p_0)$ [500 K]
-4 -2 0 2 4 6
γ [eV/A²]
γ [J/m²]
0.2 0.1 0.0 -0.1
3.2 1.6 0 -1.6
$Cu_{11}Zn_5$
$Cu_{11}Zn_5$ + 1H*
$Cu_{11}Zn_5$ + 2H*
$Cu_{11}Zn_5$ + 3H*
$Cu_{11}Zn_5$ + 4H*
-0.5 -0.4 -0.3 -0.2 -0.1 0.0
μ_H [eV]

(k)

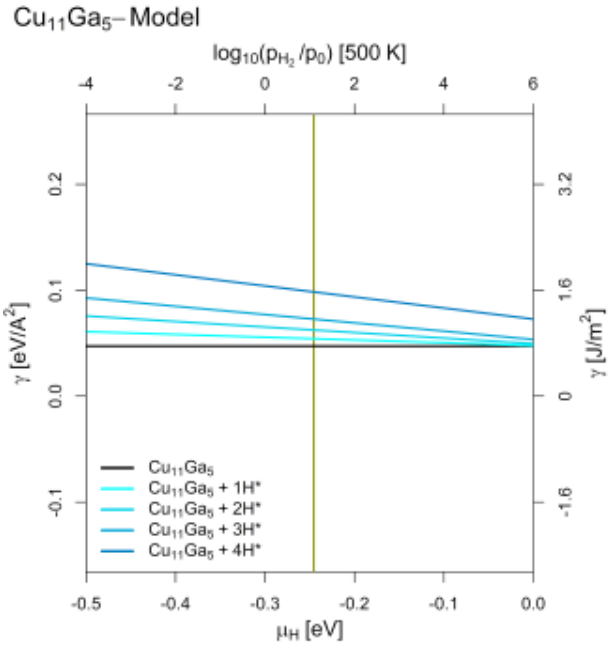
$Cu_{11}Ga_5$– Model
$\log_{10}(p_{H_2}/p_0)$ [500 K]
-4 -2 0 2 4 6
γ [eV/A²]
γ [J/m²]
0.2 0.1 0.0 -0.1
3.2 1.6 0 -1.6
$Cu_{11}Ga_5$
$Cu_{11}Ga_5$ + 1H*
$Cu_{11}Ga_5$ + 2H*
$Cu_{11}Ga_5$ + 3H*
$Cu_{11}Ga_5$ + 4H*
-0.5 -0.4 -0.3 -0.2 -0.1 0.0
μ_H [eV]

(l)

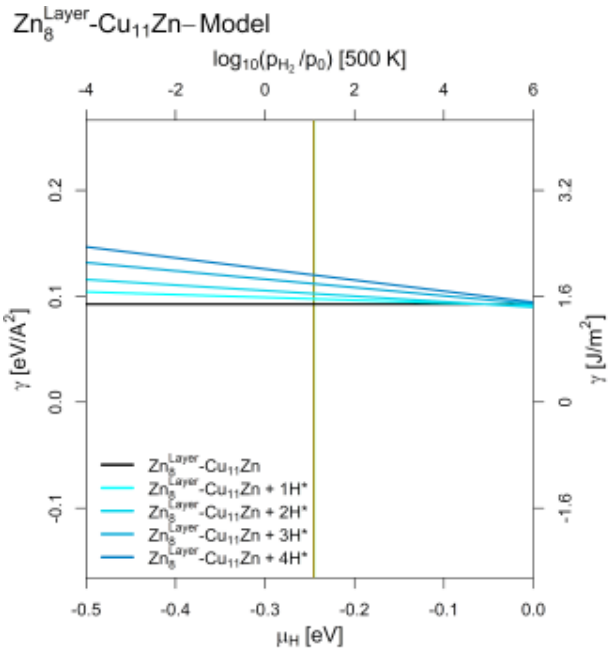
Zn_8^{Layer}-$Cu_{11}Zn$ – Model
$\log_{10}(p_{H_2}/p_0)$ [500 K]
γ [eV/Å^2]
γ [J/m^2]
μ_H [eV]
Zn_8^{Layer}-$Cu_{11}Zn$
Zn_8^{Layer}-$Cu_{11}Zn$ + 1H*
Zn_8^{Layer}-$Cu_{11}Zn$ + 2H*
Zn_8^{Layer}-$Cu_{11}Zn$ + 3H*
Zn_8^{Layer}-$Cu_{11}Zn$ + 4H*

(m)

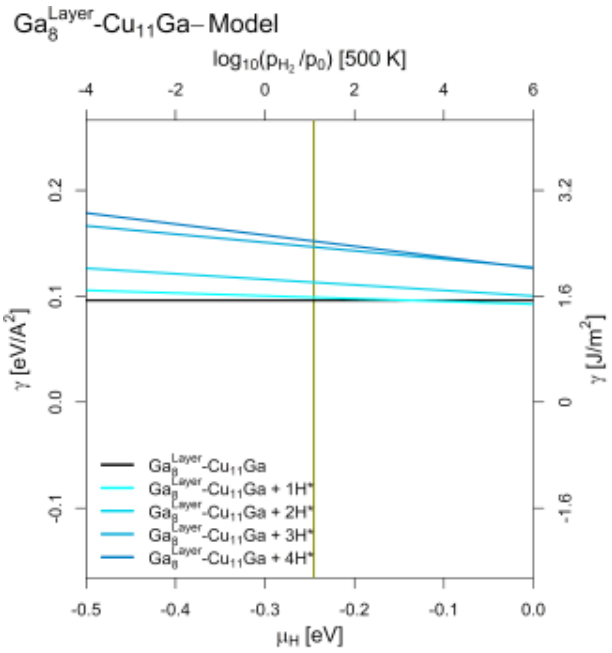
Ga_8^{Layer}-$Cu_{11}Ga$ – Model
$\log_{10}(p_{H_2}/p_0)$ [500 K]
γ [eV/Å^2]
γ [J/m^2]
μ_H [eV]
Ga_8^{Layer}-$Cu_{11}Ga$
Ga_8^{Layer}-$Cu_{11}Ga$ + 1H*
Ga_8^{Layer}-$Cu_{11}Ga$ + 2H*
Ga_8^{Layer}-$Cu_{11}Ga$ + 3H*
Ga_8^{Layer}-$Cu_{11}Ga$ + 4H*

(n)

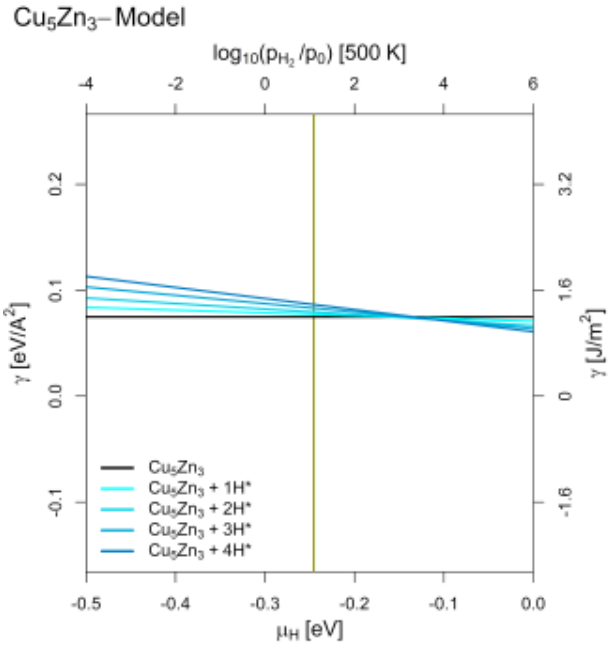
Cu_5Zn_3 – Model
$\log_{10}(p_{H_2}/p_0)$ [500 K]
γ [eV/Å^2]
γ [J/m^2]
μ_H [eV]
Cu_5Zn_3
Cu_5Zn_3 + 1H*
Cu_5Zn_3 + 2H*
Cu_5Zn_3 + 3H*
Cu_5Zn_3 + 4H*

(o)

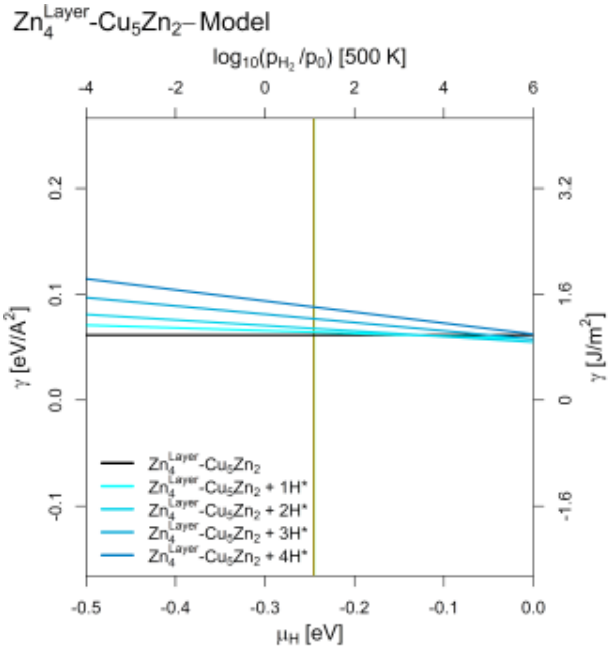
Zn_4^{Layer}-Cu_5Zn_2 – Model
$\log_{10}(p_{H_2}/p_0)$ [500 K]
γ [eV/Å^2]
γ [J/m^2]
μ_H [eV]
Zn_4^{Layer}-Cu_5Zn_2
Zn_4^{Layer}-Cu_5Zn_2 + 1H*
Zn_4^{Layer}-Cu_5Zn_2 + 2H*
Zn_4^{Layer}-Cu_5Zn_2 + 3H*
Zn_4^{Layer}-Cu_5Zn_2 + 4H*

(p)

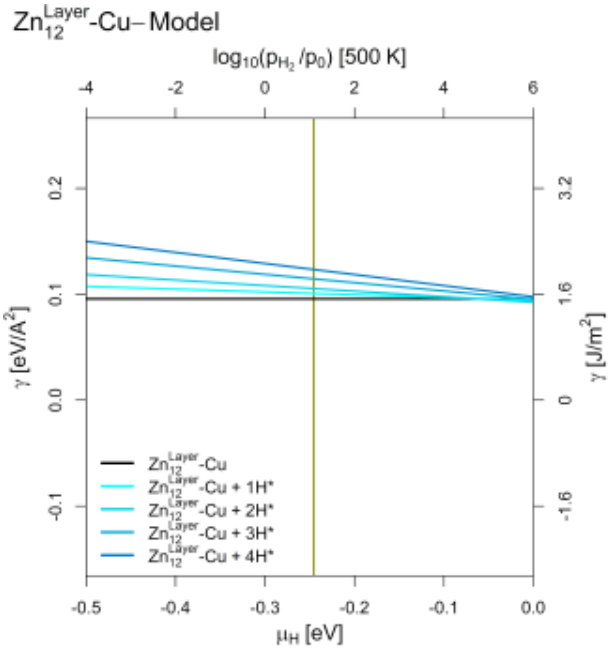
Zn12Layer-Cu– Model
log10(pH2 /p0) [500 K]
γ [eV/A2]
γ [J/m2]
μH [eV]
Zn12Layer-Cu
Zn12Layer-Cu + 1H*
Zn12Layer-Cu + 2H*
Zn12Layer-Cu + 3H*
Zn12Layer-Cu + 4H*

(q)

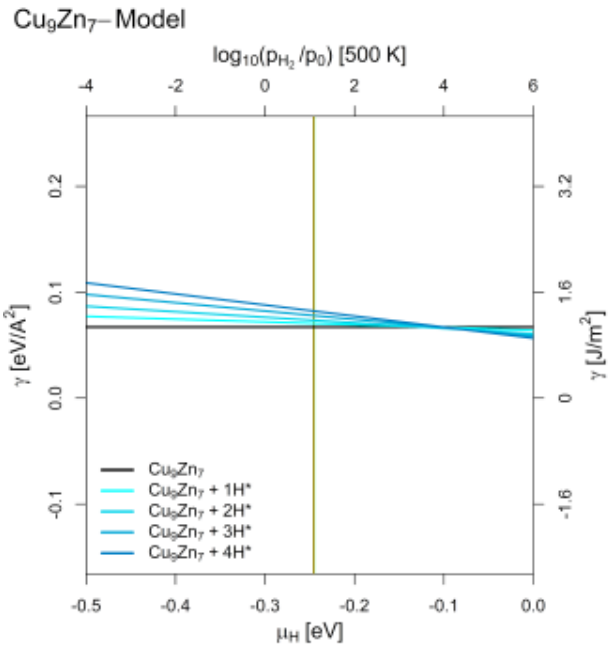
Cu9Zn7– Model
log10(pH2 /p0) [500 K]
γ [eV/A2]
γ [J/m2]
μH [eV]
Cu9Zn7
Cu9Zn7 + 1H*
Cu9Zn7 + 2H*
Cu9Zn7 + 3H*
Cu9Zn7 + 4H*

(r)

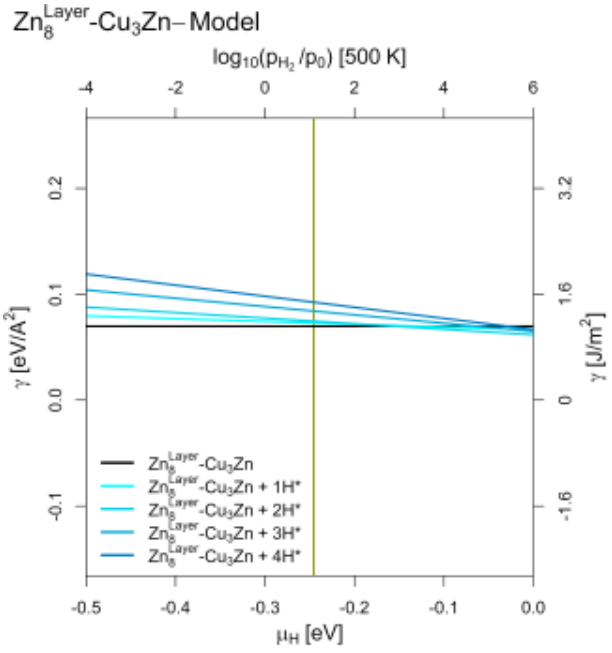
Zn8Layer-Cu3Zn– Model
log10(pH2 /p0) [500 K]
γ [eV/A2]
γ [J/m2]
μH [eV]
Zn8Layer-Cu3Zn
Zn8Layer-Cu3Zn + 1H*
Zn8Layer-Cu3Zn + 2H*
Zn8Layer-Cu3Zn + 3H*
Zn8Layer-Cu3Zn + 4H*

(s)

Figure S17: Surface stability diagram of the (110)-facet of the investigated CuGa-/CuZn-models depending on the chemical potential of hydrogen (μ_H in eV) and the equivalent hydrogen partial pressure at 500 K. The red/green line indicates μ_H expected under CO_2 or CO hydrogenation conditions (-0.235 eV $< \mu_H <$ -0.234 eV).[S2] Used slab models for the (110)-facet used are:
(a/b) Unlayered substoichiometric fcc-Cu_3Ga/-Cu_3Zn (12.5 % Zn/Ga).
(c/d) One Ga/Zn surface layer on pure fcc-Cu (12.5 % Ga/Zn).
(e/f) Unlayered stoichiometric fcc-Cu_3Ga/-Cu_3Zn (25 % Ga/Zn).
(g/h) One Ga/Zn surface layer on substoichiometric fcc-Cu_3Ga/-Cu_3Zn (25 % Ga/Zn).
(i/j) Two Ga/Zn surface layers on pure fcc-Cu (25 % Ga/Zn).
(k/l) Unlayered superstoichiometric fcc-Cu_3Ga/-Cu_3Zn (31.25 % Ga/Zn).
(m/n) Two Ga/Zn surface layers on substoichiometric fcc-Cu_3Ga/-Cu_3Zn (31.25 % Ga/Zn).
(o) Unlayered supersubstoichiometric fcc-Cu_3Zn (37.5 % Zn).
(p) One Zn surface layer on fcc-Cu_3Zn (37.5 % Ga/Zn).
(q) Three Zn surface layers on pure fcc-Cu (37.5 % Ga/Zn).
(r) Unlayered supersubstoichiometric fcc-Cu_3Zn (43.75 % Zn).
(s) Two Zn surface layers on fcc-Cu_3Zn (43.75 % Ga/Zn).

(111)-Facet

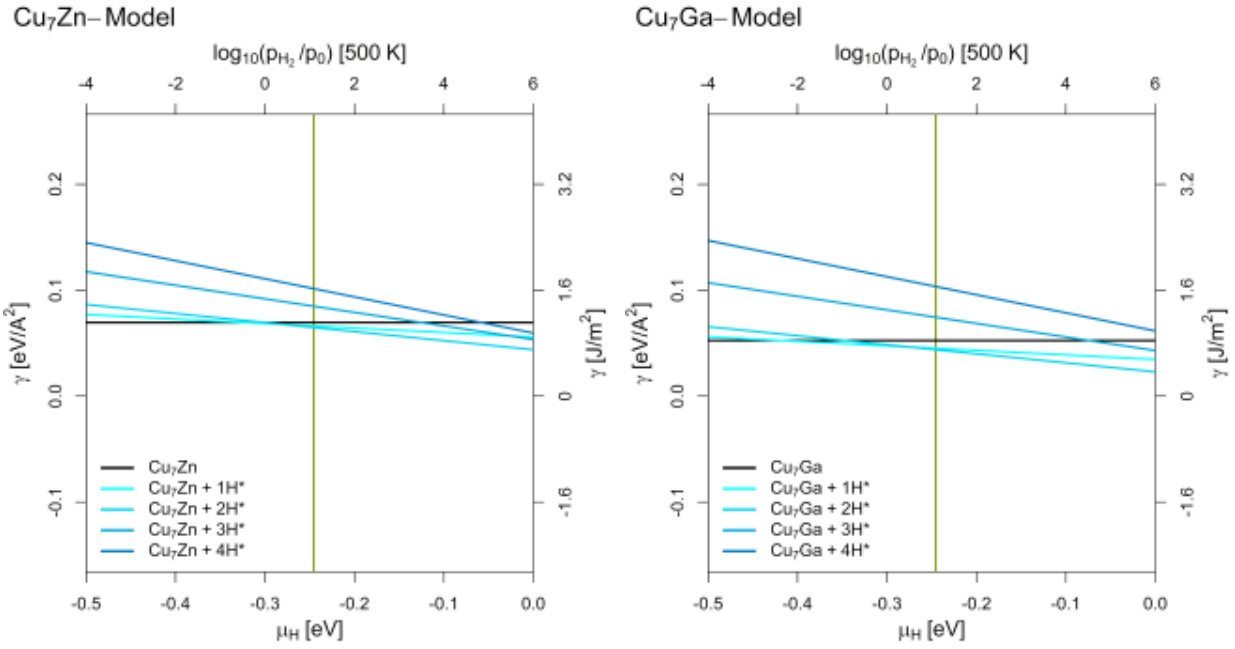

(a)

(b)

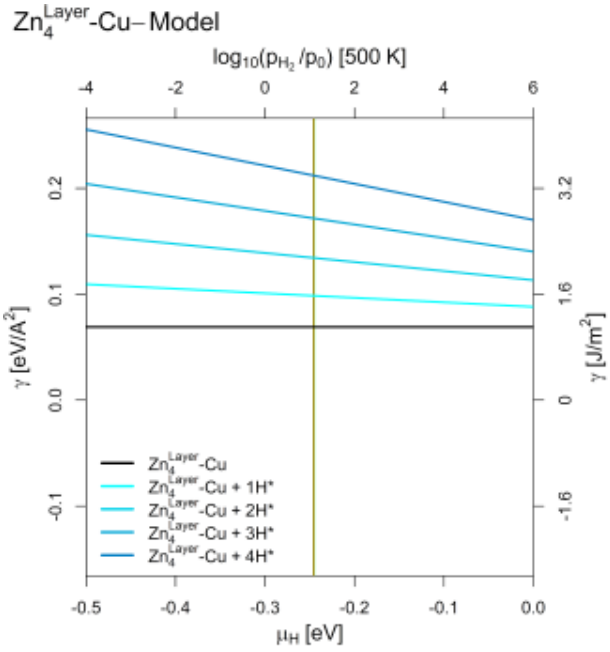

(c)

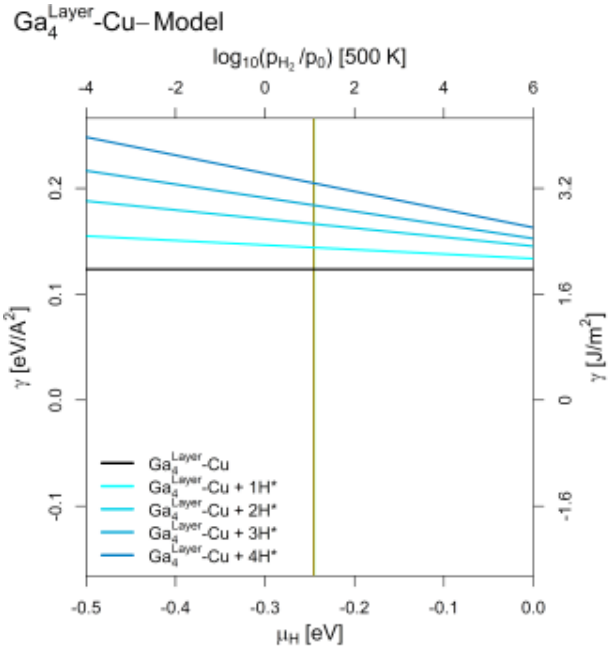

(d)

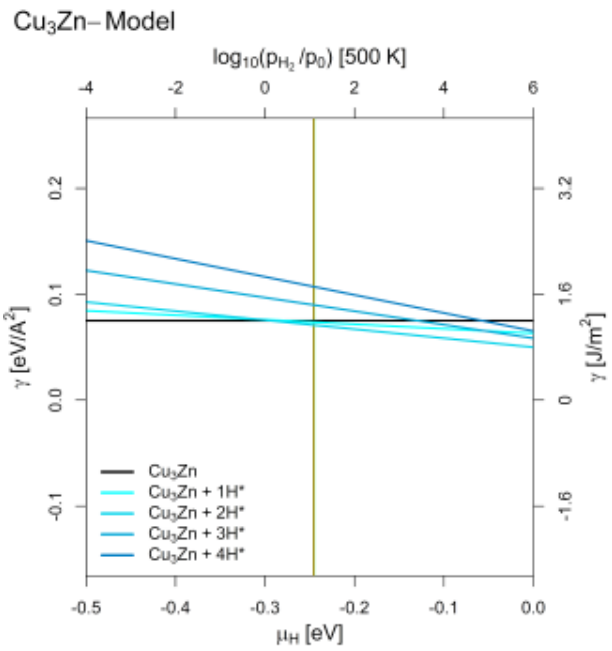
Cu3Zn – Model
log10(pH2 /p0) [500 K]
γ [eV/Å2]
γ [J/m2]
μH [eV]
Cu3Zn
Cu3Zn + 1H*
Cu3Zn + 2H*
Cu3Zn + 3H*
Cu3Zn + 4H*

(e)

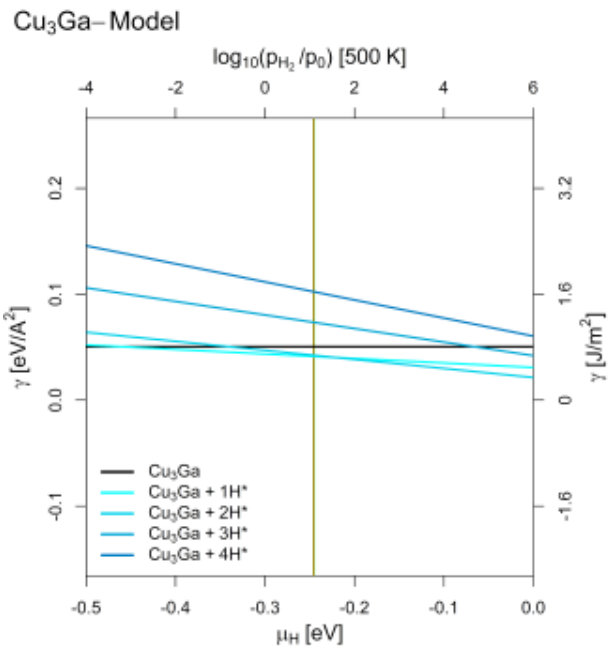
Cu3Ga – Model
log10(pH2 /p0) [500 K]
γ [eV/Å2]
γ [J/m2]
μH [eV]
Cu3Ga
Cu3Ga + 1H*
Cu3Ga + 2H*
Cu3Ga + 3H*
Cu3Ga + 4H*

(f)

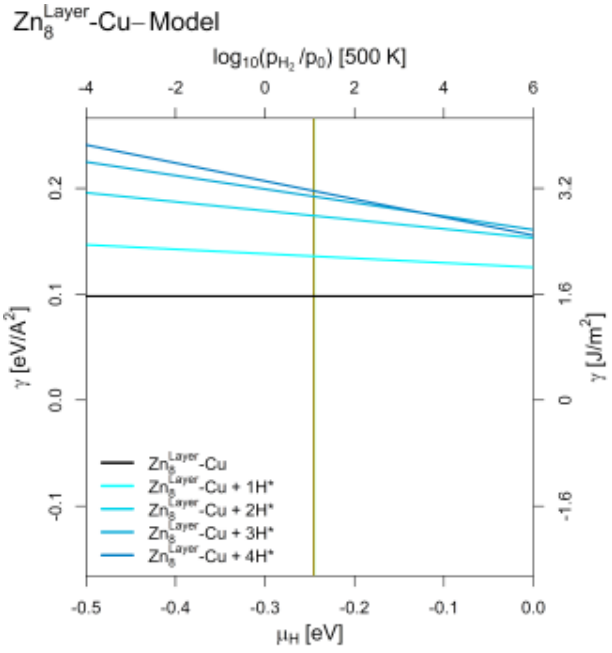
Zn8Layer-Cu – Model
log10(pH2 /p0) [500 K]
γ [eV/Å2]
γ [J/m2]
μH [eV]
Zn8Layer-Cu
Zn8Layer-Cu + 1H*
Zn8Layer-Cu + 2H*
Zn8Layer-Cu + 3H*
Zn8Layer-Cu + 4H*

(g)

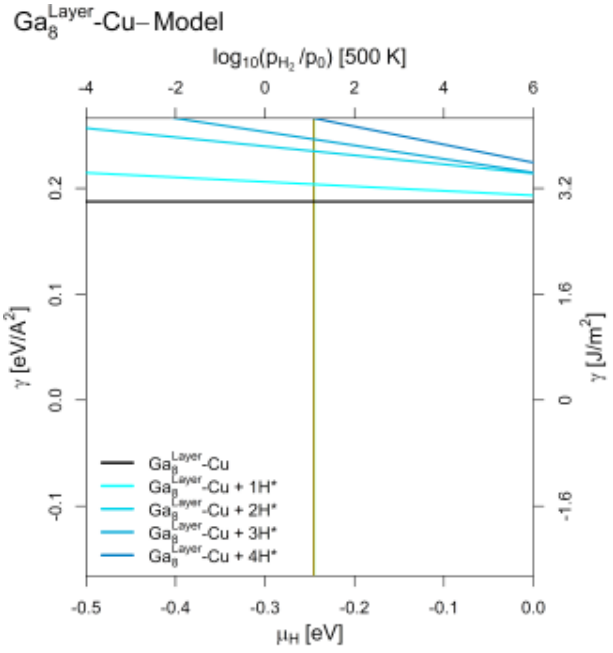
Ga8Layer-Cu – Model
log10(pH2 /p0) [500 K]
γ [eV/Å2]
γ [J/m2]
μH [eV]
Ga8Layer-Cu
Ga8Layer-Cu + 1H*
Ga8Layer-Cu + 2H*
Ga8Layer-Cu + 3H*
Ga8Layer-Cu + 4H*

(h)

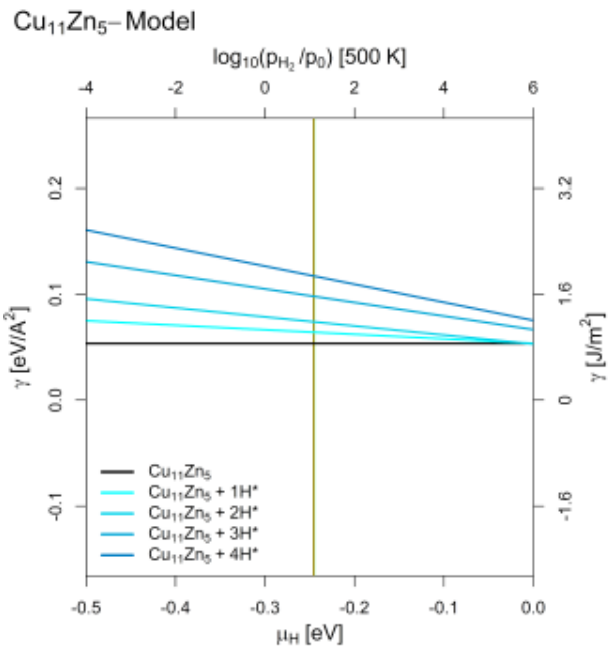
Cu11Zn5 – Model
log10(pH2 /p0) [500 K]
γ [eV/Å2]
γ [J/m2]
μH [eV]
Cu11Zn5
Cu11Zn5 + 1H*
Cu11Zn5 + 2H*
Cu11Zn5 + 3H*
Cu11Zn5 + 4H*

(i)

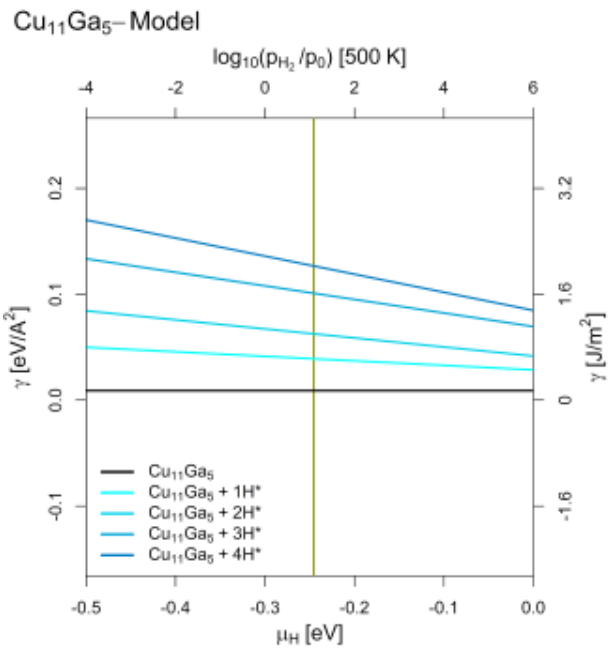
Cu11Ga5 – Model
log10(pH2 /p0) [500 K]
γ [eV/Å2]
γ [J/m2]
μH [eV]
Cu11Ga5
Cu11Ga5 + 1H*
Cu11Ga5 + 2H*
Cu11Ga5 + 3H*
Cu11Ga5 + 4H*

(j)

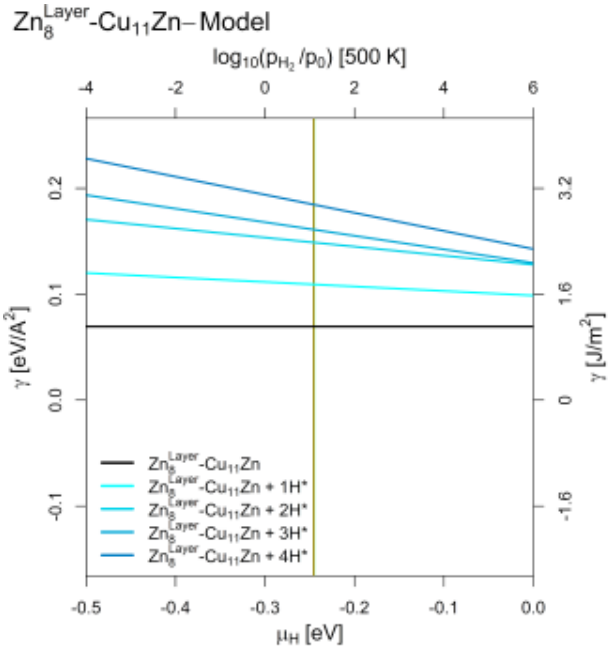
Zn8Layer-Cu11Zn – Model
log10(pH2 /p0) [500 K]
γ [eV/Å2]
γ [J/m2]
μH [eV]
Zn8Layer-Cu11Zn
Zn8Layer-Cu11Zn + 1H*
Zn8Layer-Cu11Zn + 2H*
Zn8Layer-Cu11Zn + 3H*
Zn8Layer-Cu11Zn + 4H*

(k)

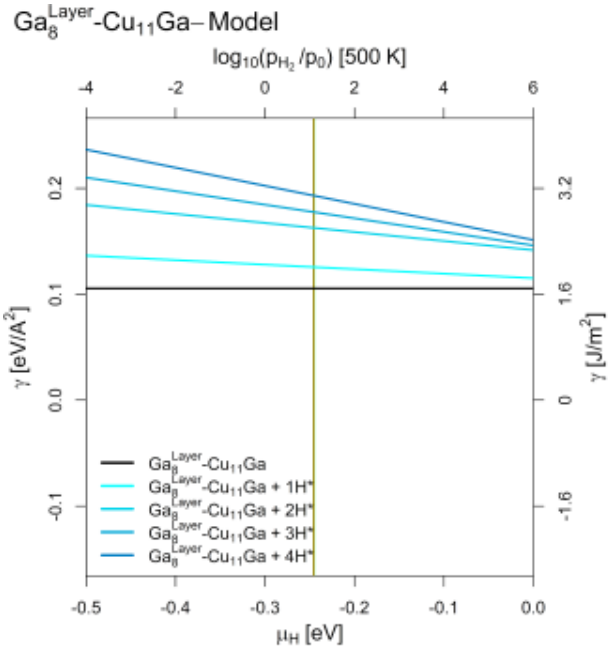
Ga8Layer-Cu11Ga – Model
log10(pH2 /p0) [500 K]
γ [eV/Å2]
γ [J/m2]
μH [eV]
Ga8Layer-Cu11Ga
Ga8Layer-Cu11Ga + 1H*
Ga8Layer-Cu11Ga + 2H*
Ga8Layer-Cu11Ga + 3H*
Ga8Layer-Cu11Ga + 4H*

(l)

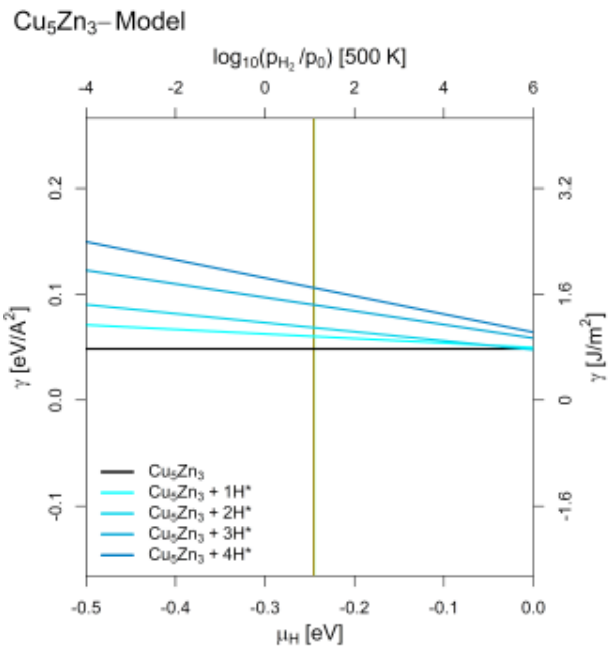
Cu5Zn3 – Model
log10(pH2 /p0) [500 K]
γ [eV/A2]
γ [J/m2]
μH [eV]
Cu5Zn3
Cu5Zn3 + 1H*
Cu5Zn3 + 2H*
Cu5Zn3 + 3H*
Cu5Zn3 + 4H*

(m)

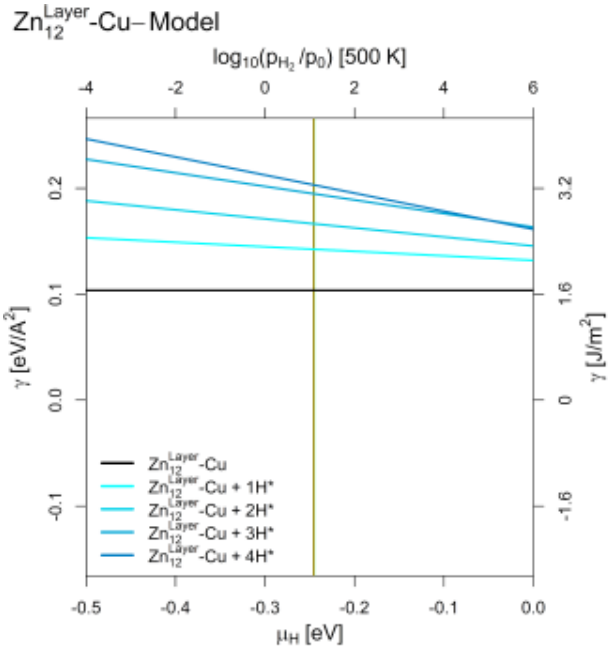
Zn12Layer-Cu – Model
log10(pH2 /p0) [500 K]
γ [eV/A2]
γ [J/m2]
μH [eV]
Zn12Layer-Cu
Zn12Layer-Cu + 1H*
Zn12Layer-Cu + 2H*
Zn12Layer-Cu + 3H*
Zn12Layer-Cu + 4H*

(n)

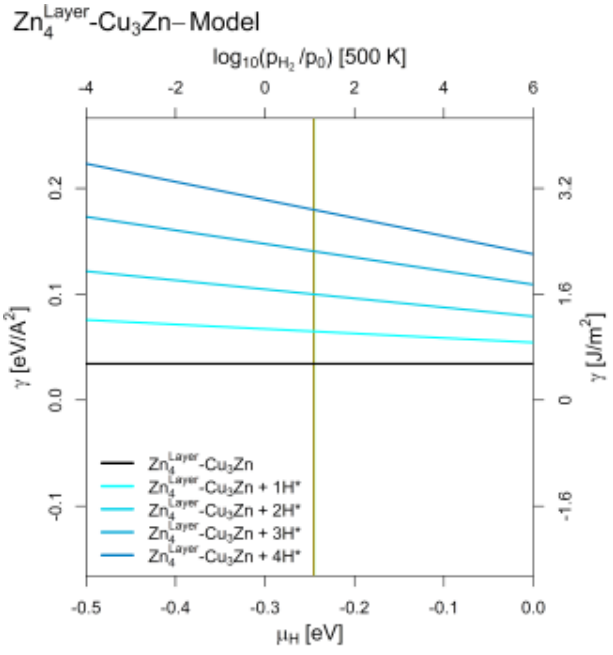
Zn4Layer-Cu3Zn – Model
log10(pH2 /p0) [500 K]
γ [eV/A2]
γ [J/m2]
μH [eV]
Zn4Layer-Cu3Zn
Zn4Layer-Cu3Zn + 1H*
Zn4Layer-Cu3Zn + 2H*
Zn4Layer-Cu3Zn + 3H*
Zn4Layer-Cu3Zn + 4H*

(o)

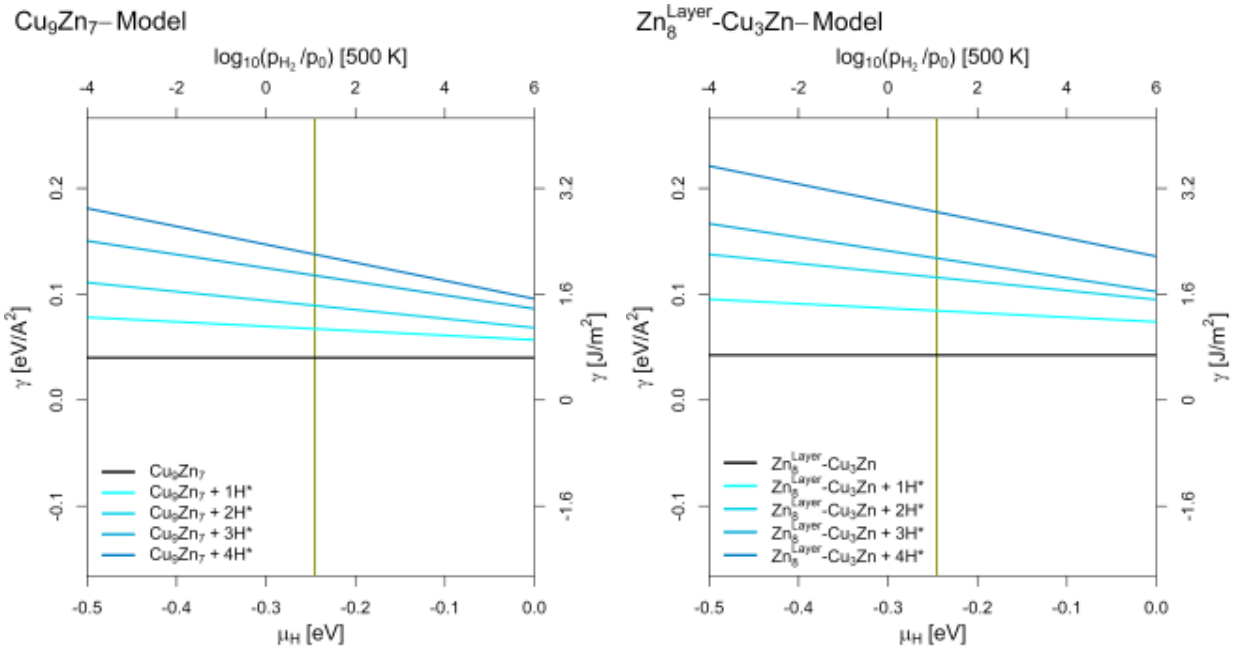

(p) (q)

Figure S18: Surface stability diagram of the (111)-facet of the investigated CuGa-/CuZn-models depending on the chemical potential of hydrogen (μ_H in eV) and the equivalent hydrogen partial pressure at 500 K. The red/green line indicates μ_H expected under CO_2 or CO hydrogenation conditions (-0.235 eV $< \mu_H <$ -0.234 eV).[S2] Used slab models for the (111)-facet used are:
(a/b) Unlayered substoichiometric fcc-Cu_3Ga/-Cu_3Zn (12.5 % Zn/Ga).
(c/d) One Ga/Zn surface layer on pure fcc-Cu (12.5 % Ga/Zn).
(e/f) Unlayered stoichiometric fcc-Cu_3Ga/-Cu_3Zn (25 % Ga/Zn).
(g/h) Two Ga/Zn surface layers on pure fcc-Cu (25 % Ga/Zn).
(i/j) Unlayered superstoichiometric fcc-Cu_3Ga/-Cu_3Zn (31.25 % Ga/Zn).
(k/l) Two Ga/Zn surface layers on substoichiometric fcc-Cu_3Ga/-Cu_3Zn (31.25 % Ga/Zn).
(m) Unlayered supersubstoichiometric fcc-Cu_3Zn (37.5 % Zn).
(n) Three Zn surface layers on pure fcc-Cu (37.5 % Ga/Zn).
(o) One Zn surface layer on fcc-Cu_3Zn (34.375 % Ga/Zn).
(p) Unlayered supersubstoichiometric fcc-Cu_3Zn (43.75 % Zn).
(q) Two Zn surface layers on fcc-Cu_3Zn (43.75 % Ga/Zn).

4.2 Individual Surface Energies Depending on the Hydrogen Chemical Potential

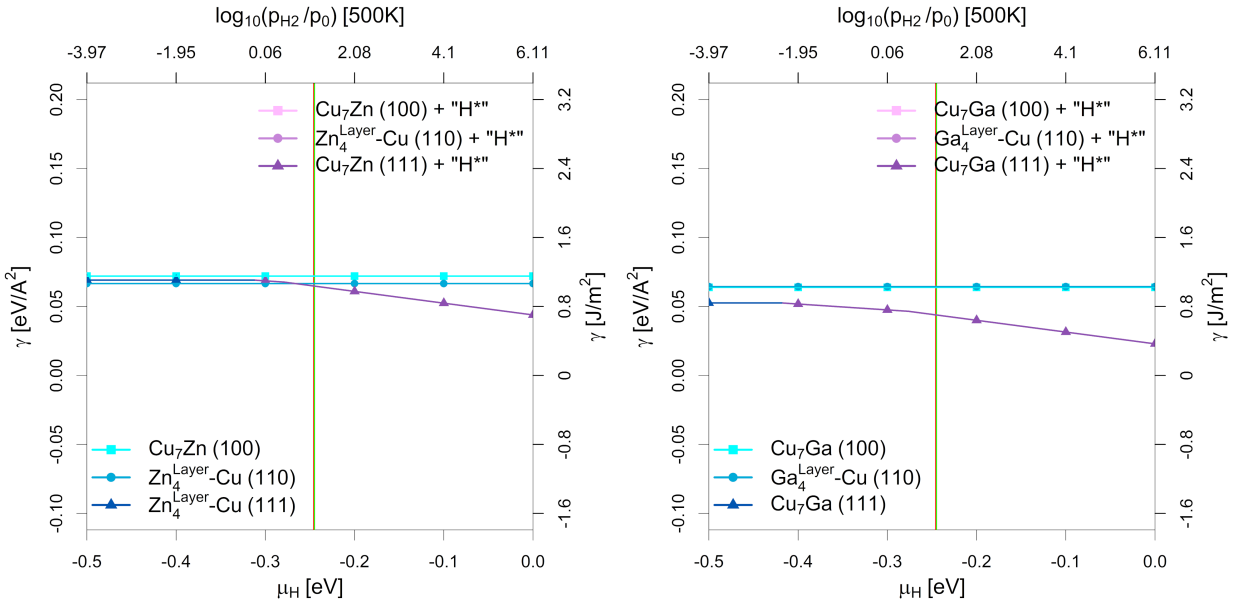

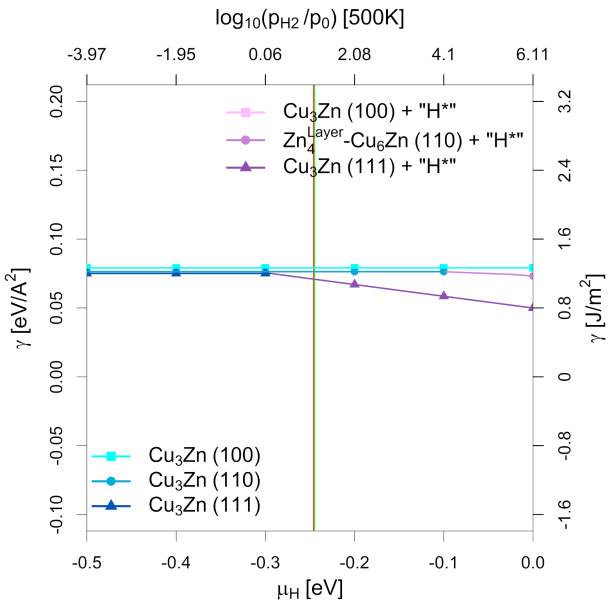
log10(pH2 /p0) [500K]
-3.97
-1.95
0.06
2.08
4.1
6.11
Cu3Zn (100) + "H*"
Zn4Layer-Cu6Zn (110) + "H*"
Cu3Zn (111) + "H*"
Cu3Zn (100)
Cu3Zn (110)
Cu3Zn (111)
γ [eV/A2]
γ [J/m2]
μH [eV]

(e)

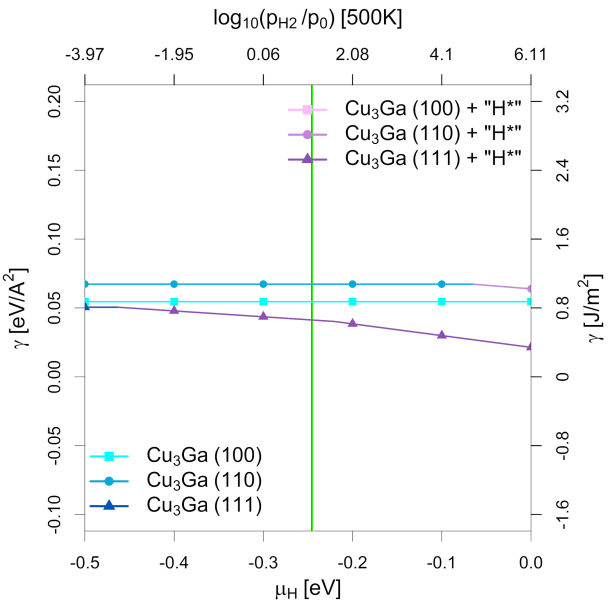
log10(pH2 /p0) [500K]
-3.97
-1.95
0.06
2.08
4.1
6.11
Cu3Ga (100) + "H*"
Cu3Ga (110) + "H*"
Cu3Ga (111) + "H*"
Cu3Ga (100)
Cu3Ga (110)
Cu3Ga (111)
γ [eV/A2]
γ [J/m2]
μH [eV]

(f)

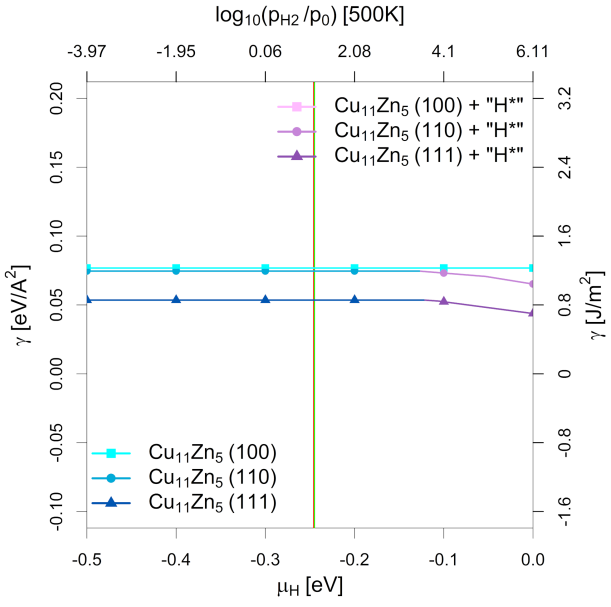
log10(pH2 /p0) [500K]
-3.97
-1.95
0.06
2.08
4.1
6.11
Cu11Zn5 (100) + "H*"
Cu11Zn5 (110) + "H*"
Cu11Zn5 (111) + "H*"
Cu11Zn5 (100)
Cu11Zn5 (110)
Cu11Zn5 (111)
γ [eV/A2]
γ [J/m2]
μH [eV]

(g)

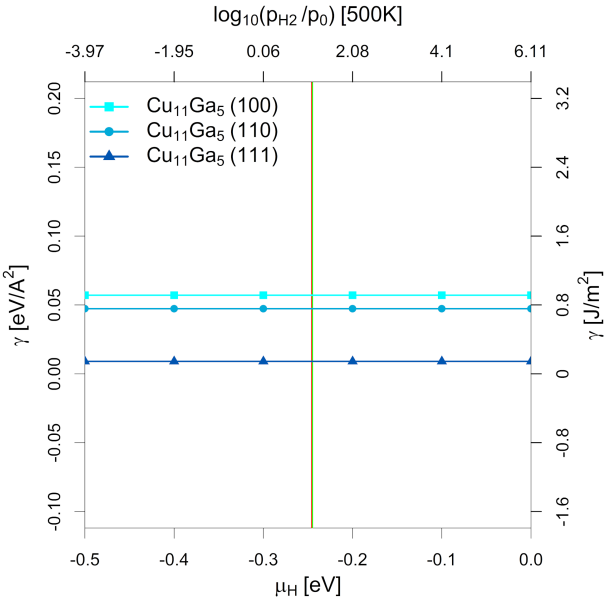
log10(pH2 /p0) [500K]
-3.97
-1.95
0.06
2.08
4.1
6.11
Cu11Ga5 (100)
Cu11Ga5 (110)
Cu11Ga5 (111)
γ [eV/A2]
γ [J/m2]
μH [eV]

(h)

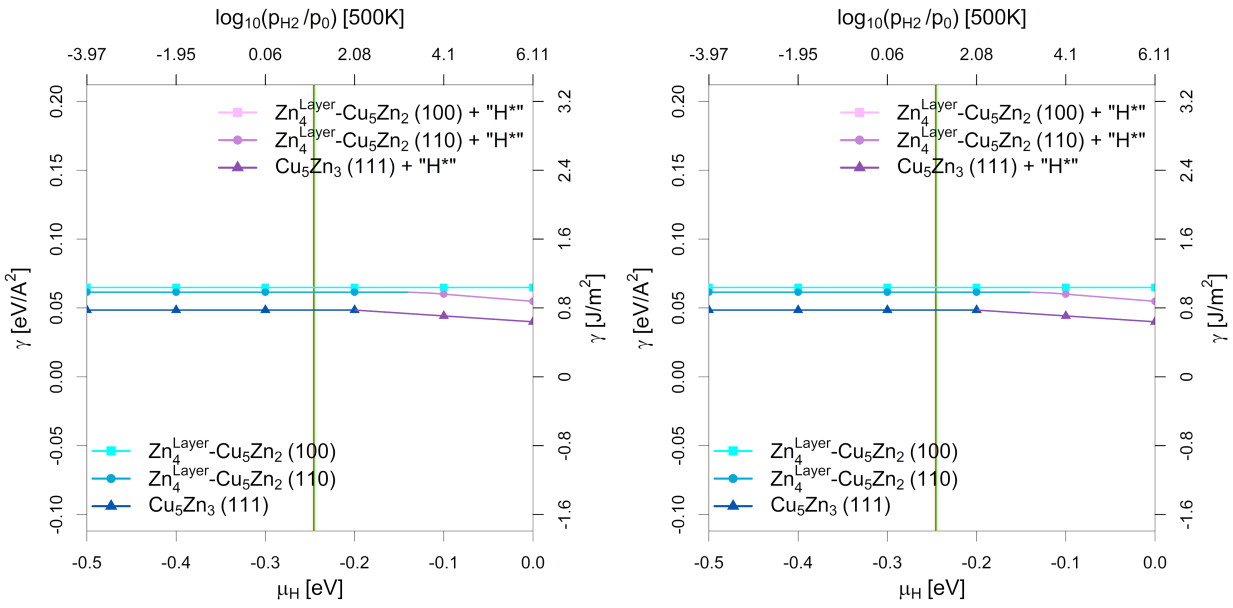

Figure S19: Most stable surfaces of the fcc-Cu_3Ga/fcc-Cu_3Zn alloys with various compositions depending on the chemical potential of hydrogen (μ_H in eV) and the equivalent hydrogen partial pressure at 500 K including unlayered structures, partially layered structures and fully layered structures. The red/green line indicates μ_H expected under CO_2 or CO hydrogenation conditions (-0.235 eV $< \mu_H <$ -0.234 eV).[S2] The blue part without incline indicates the most stable structure in vacuum, while the violet part with incline shows the most stable structure with oxygen adsorbed. The shown promoter concentrations are:
(a/b) Substoichiometric fcc-Cu_3Ga/-Cu_3Zn (12.5 % Zn/Ga).
(c/d) Substoichiometric fcc-Cu_3Ga/-Cu_3Zn (18.75 % Zn/Ga).
(e/f) Stoichiometric fcc-Cu_3Ga/-Cu_3Zn (25 % Zn/Ga).
(g/h) Superstoichiometric fcc-Cu_3Ga/-Cu_3Zn (31.25 % Zn/Ga).
(i) Superstoichiometric fcc-Cu_3Zn (37.5 % Zn).
(j) Superstoichiometric fcc-Cu_3Zn (43.75 % Zn).

5 Surface Stability Diagrams in CO Atmosphere

5.1 Individual Surface Stability Diagrams in CO Atmosphere

(100)-Facet

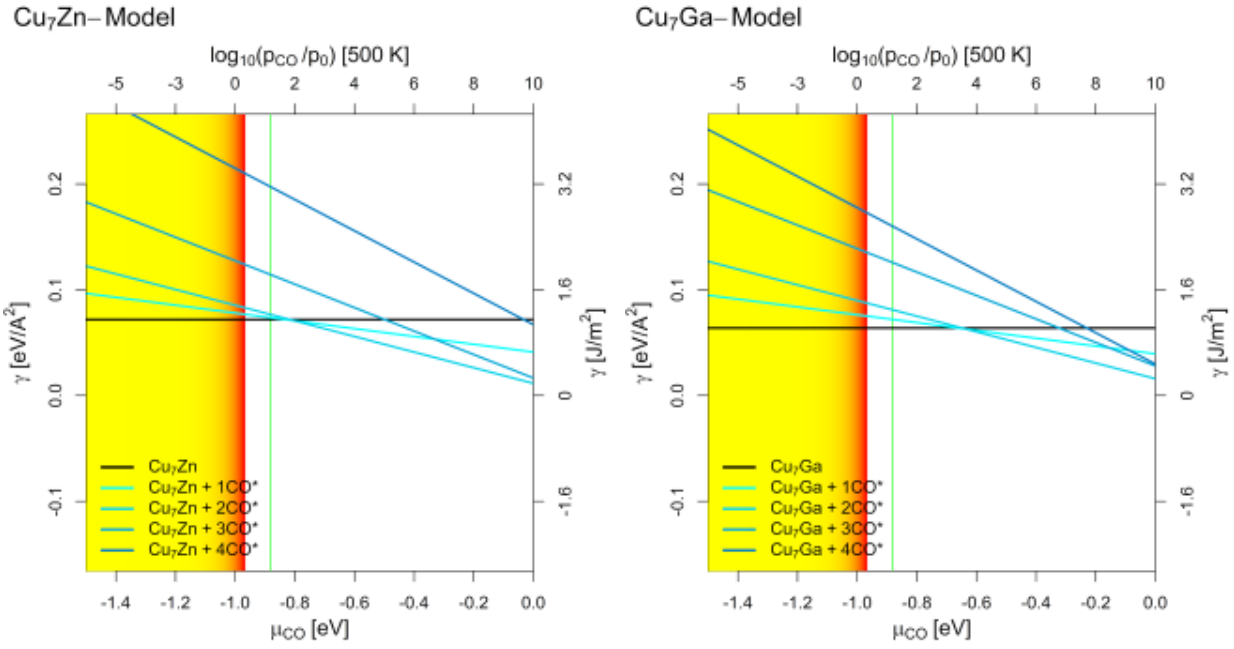

(a)

(b)

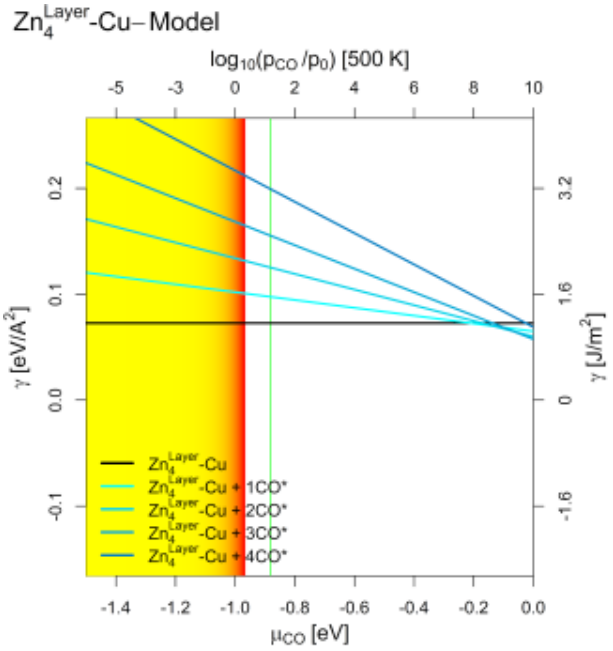

(c)

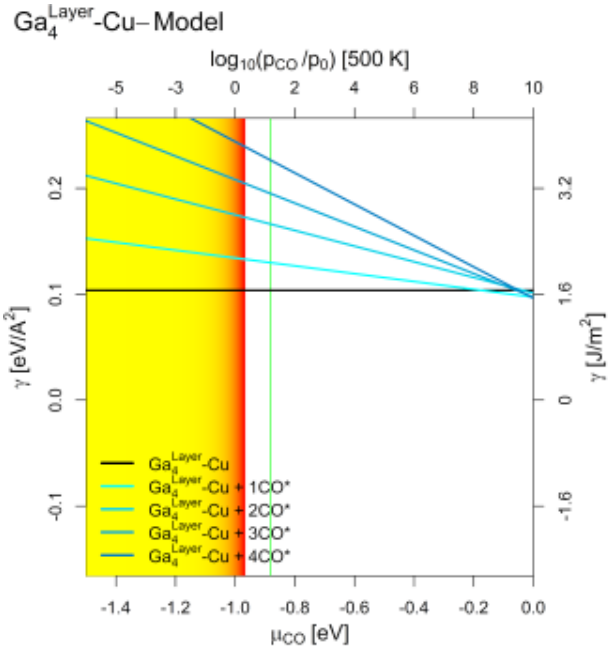

(d)

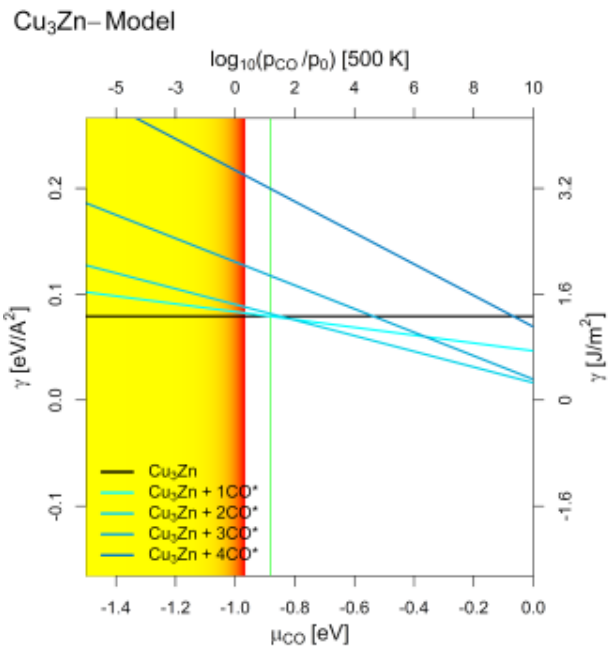
Cu3Zn – Model
log10(pCO /p0) [500 K]
-5 -3 0 2 4 6 8 10
γ [eV/Å2]
γ [J/m2]
0.2 0.1 0.0 -0.1
3.2 1.6 0 -1.6
Cu3Zn
Cu3Zn + 1CO*
Cu3Zn + 2CO*
Cu3Zn + 3CO*
Cu3Zn + 4CO*
-1.4 -1.2 -1.0 -0.8 -0.6 -0.4 -0.2 0.0
μCO [eV]

(e)

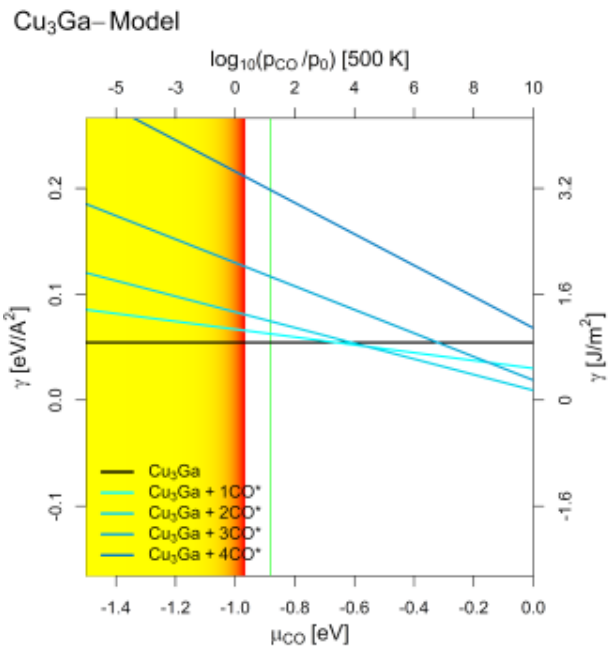
Cu3Ga – Model
log10(pCO /p0) [500 K]
-5 -3 0 2 4 6 8 10
γ [eV/Å2]
γ [J/m2]
0.2 0.1 0.0 -0.1
3.2 1.6 0 -1.6
Cu3Ga
Cu3Ga + 1CO*
Cu3Ga + 2CO*
Cu3Ga + 3CO*
Cu3Ga + 4CO*
-1.4 -1.2 -1.0 -0.8 -0.6 -0.4 -0.2 0.0
μCO [eV]

(f)

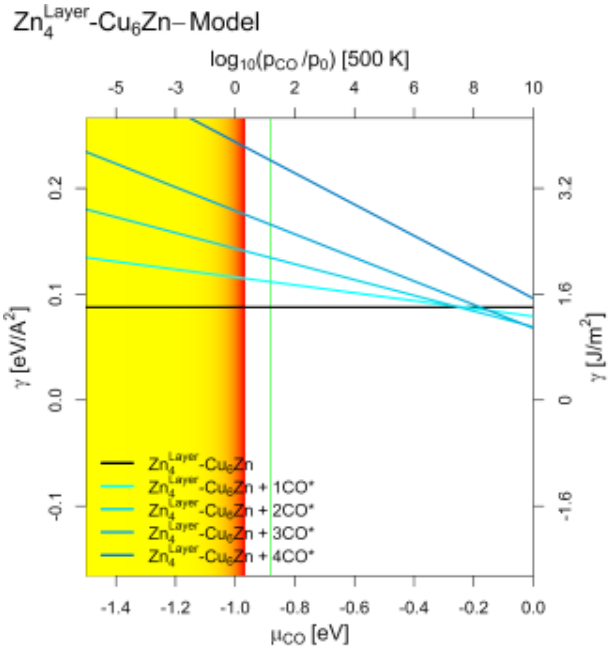
Zn4Layer-Cu6Zn – Model
log10(pCO /p0) [500 K]
-5 -3 0 2 4 6 8 10
γ [eV/Å2]
γ [J/m2]
0.2 0.1 0.0 -0.1
3.2 1.6 0 -1.6
Zn4Layer-Cu6Zn
Zn4Layer-Cu6Zn + 1CO*
Zn4Layer-Cu6Zn + 2CO*
Zn4Layer-Cu6Zn + 3CO*
Zn4Layer-Cu6Zn + 4CO*
-1.4 -1.2 -1.0 -0.8 -0.6 -0.4 -0.2 0.0
μCO [eV]

(g)

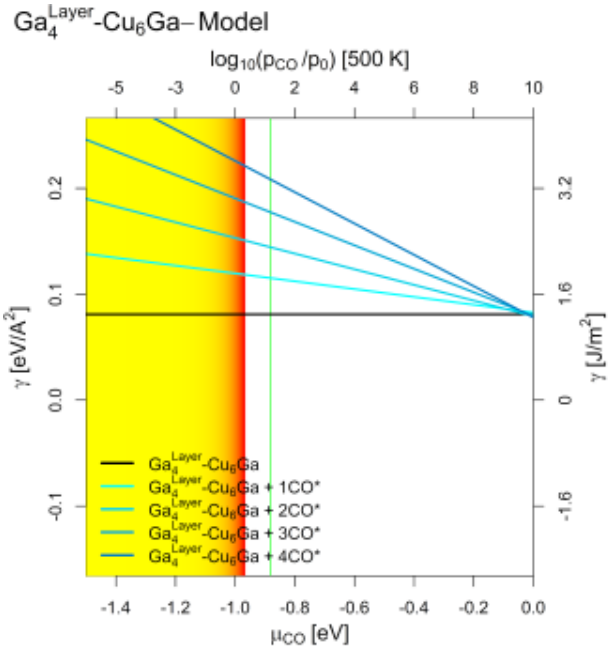
Ga4Layer-Cu6Ga – Model
log10(pCO /p0) [500 K]
-5 -3 0 2 4 6 8 10
γ [eV/Å2]
γ [J/m2]
0.2 0.1 0.0 -0.1
3.2 1.6 0 -1.6
Ga4Layer-Cu6Ga
Ga4Layer-Cu6Ga + 1CO*
Ga4Layer-Cu6Ga + 2CO*
Ga4Layer-Cu6Ga + 3CO*
Ga4Layer-Cu6Ga + 4CO*
-1.4 -1.2 -1.0 -0.8 -0.6 -0.4 -0.2 0.0
μCO [eV]

(h)

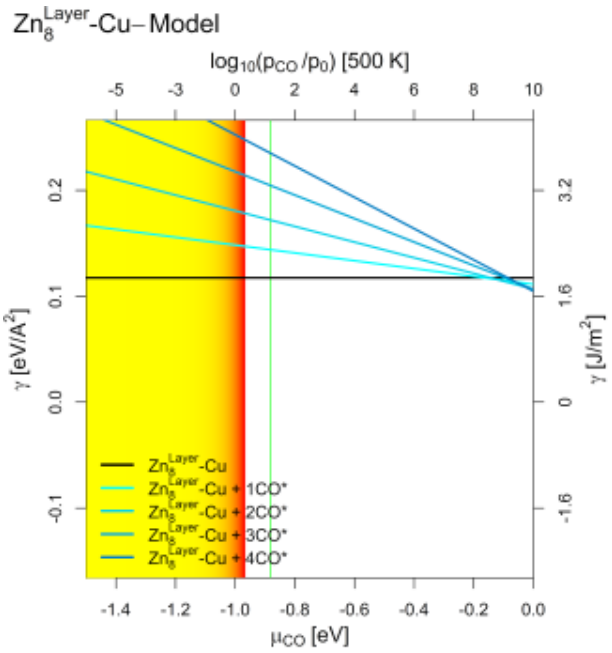
Zn_8^{Layer}-Cu–Model
$\log_{10}(p_{CO}/p_0)$ [500 K]
-5 -3 0 2 4 6 8 10
0.2 0.1 0.0 -0.1
3.2 1.6 0 -1.6
γ [eV/Å²]
γ [J/m²]
Zn_8^{Layer}-Cu
Zn_8^{Layer}-Cu + 1CO*
Zn_8^{Layer}-Cu + 2CO*
Zn_8^{Layer}-Cu + 3CO*
Zn_8^{Layer}-Cu + 4CO*
-1.4 -1.2 -1.0 -0.8 -0.6 -0.4 -0.2 0.0
μ_{CO} [eV]

(i)

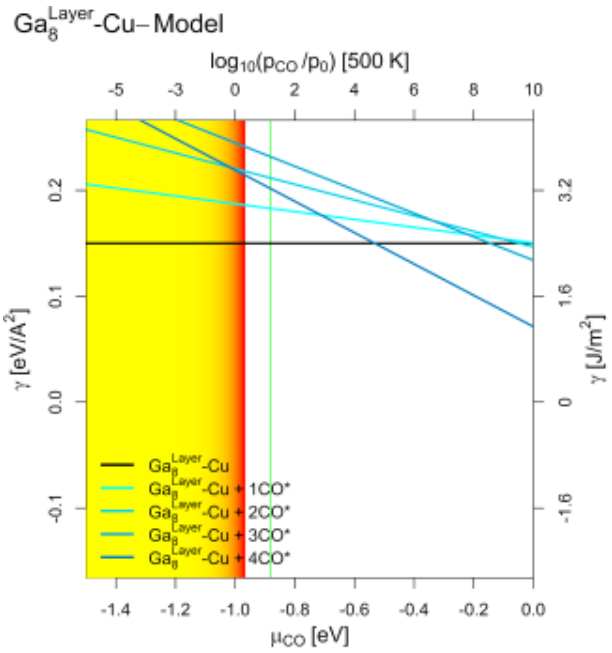
Ga_8^{Layer}-Cu–Model
$\log_{10}(p_{CO}/p_0)$ [500 K]
-5 -3 0 2 4 6 8 10
0.2 0.1 0.0 -0.1
3.2 1.6 0 -1.6
γ [eV/Å²]
γ [J/m²]
Ga_8^{Layer}-Cu
Ga_8^{Layer}-Cu + 1CO*
Ga_8^{Layer}-Cu + 2CO*
Ga_8^{Layer}-Cu + 3CO*
Ga_8^{Layer}-Cu + 4CO*
-1.4 -1.2 -1.0 -0.8 -0.6 -0.4 -0.2 0.0
μ_{CO} [eV]

(j)

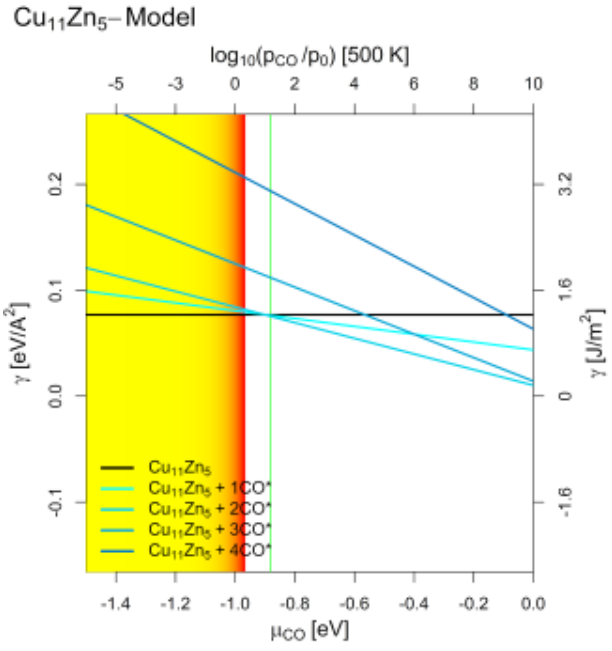
$Cu_{11}Zn_5$–Model
$\log_{10}(p_{CO}/p_0)$ [500 K]
-5 -3 0 2 4 6 8 10
0.2 0.1 0.0 -0.1
3.2 1.6 0 -1.6
γ [eV/Å²]
γ [J/m²]
$Cu_{11}Zn_5$
$Cu_{11}Zn_5$ + 1CO*
$Cu_{11}Zn_5$ + 2CO*
$Cu_{11}Zn_5$ + 3CO*
$Cu_{11}Zn_5$ + 4CO*
-1.4 -1.2 -1.0 -0.8 -0.6 -0.4 -0.2 0.0
μ_{CO} [eV]

(k)

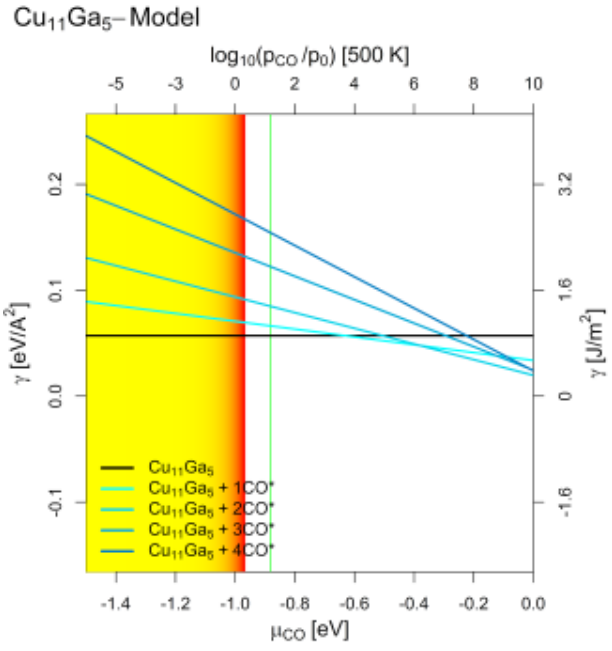
$Cu_{11}Ga_5$–Model
$\log_{10}(p_{CO}/p_0)$ [500 K]
-5 -3 0 2 4 6 8 10
0.2 0.1 0.0 -0.1
3.2 1.6 0 -1.6
γ [eV/Å²]
γ [J/m²]
$Cu_{11}Ga_5$
$Cu_{11}Ga_5$ + 1CO*
$Cu_{11}Ga_5$ + 2CO*
$Cu_{11}Ga_5$ + 3CO*
$Cu_{11}Ga_5$ + 4CO*
-1.4 -1.2 -1.0 -0.8 -0.6 -0.4 -0.2 0.0
μ_{CO} [eV]

(l)

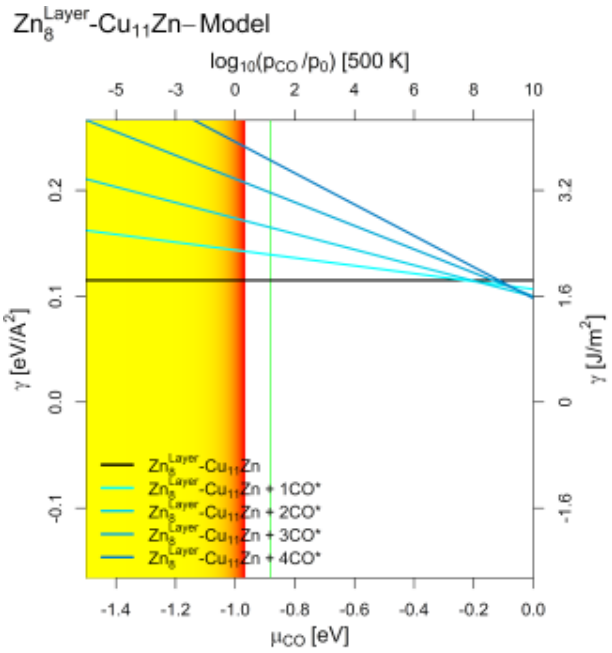
Zn_8^{Layer}-$Cu_{11}Zn$ – Model
$\log_{10}(p_{CO}/p_0)$ [500 K]
γ [eV/Å^2]
γ [J/m^2]
μ_{CO} [eV]
Zn_8^{Layer}-$Cu_{11}Zn$
Zn_8^{Layer}-$Cu_{11}Zn$ + 1CO*
Zn_8^{Layer}-$Cu_{11}Zn$ + 2CO*
Zn_8^{Layer}-$Cu_{11}Zn$ + 3CO*
Zn_8^{Layer}-$Cu_{11}Zn$ + 4CO*

(m)

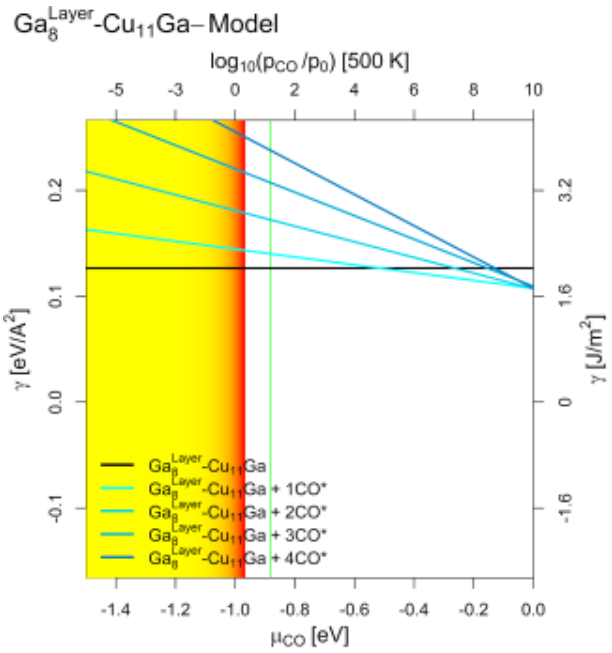
Ga_8^{Layer}-$Cu_{11}Ga$ – Model
$\log_{10}(p_{CO}/p_0)$ [500 K]
γ [eV/Å^2]
γ [J/m^2]
μ_{CO} [eV]
Ga_8^{Layer}-$Cu_{11}Ga$
Ga_8^{Layer}-$Cu_{11}Ga$ + 1CO*
Ga_8^{Layer}-$Cu_{11}Ga$ + 2CO*
Ga_8^{Layer}-$Cu_{11}Ga$ + 3CO*
Ga_8^{Layer}-$Cu_{11}Ga$ + 4CO*

(n)

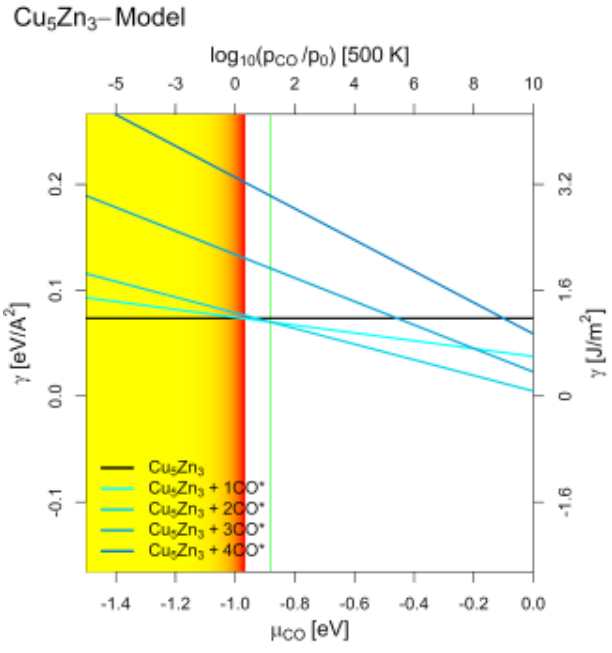
Cu_5Zn_3 – Model
$\log_{10}(p_{CO}/p_0)$ [500 K]
γ [eV/Å^2]
γ [J/m^2]
μ_{CO} [eV]
Cu_5Zn_3
Cu_5Zn_3 + 1CO*
Cu_5Zn_3 + 2CO*
Cu_5Zn_3 + 3CO*
Cu_5Zn_3 + 4CO*

(o)

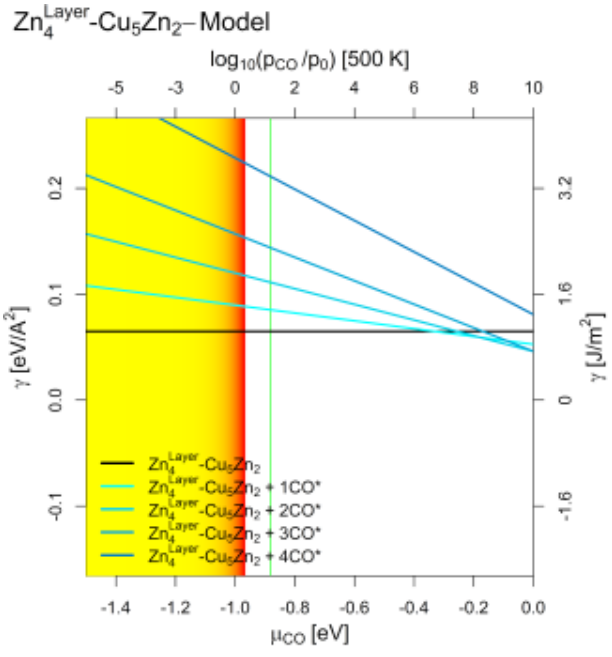
Zn_4^{Layer}-Cu_5Zn_2 – Model
$\log_{10}(p_{CO}/p_0)$ [500 K]
γ [eV/Å^2]
γ [J/m^2]
μ_{CO} [eV]
Zn_4^{Layer}-Cu_5Zn_2
Zn_4^{Layer}-Cu_5Zn_2 + 1CO*
Zn_4^{Layer}-Cu_5Zn_2 + 2CO*
Zn_4^{Layer}-Cu_5Zn_2 + 3CO*
Zn_4^{Layer}-Cu_5Zn_2 + 4CO*

(p)

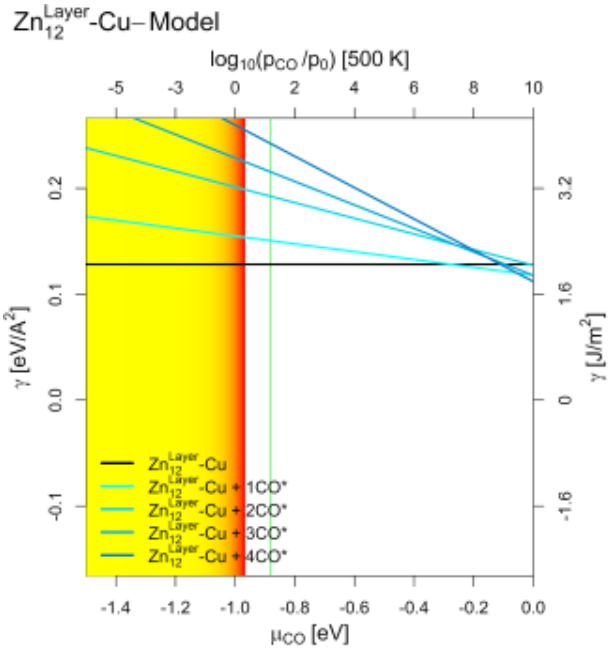
Zn12Layer-Cu– Model
log10(pCO /p0) [500 K]
γ [eV/Å2]
γ [J/m2]
μCO [eV]
Zn12Layer-Cu
Zn12Layer-Cu + 1CO*
Zn12Layer-Cu + 2CO*
Zn12Layer-Cu + 3CO*
Zn12Layer-Cu + 4CO*

(q)

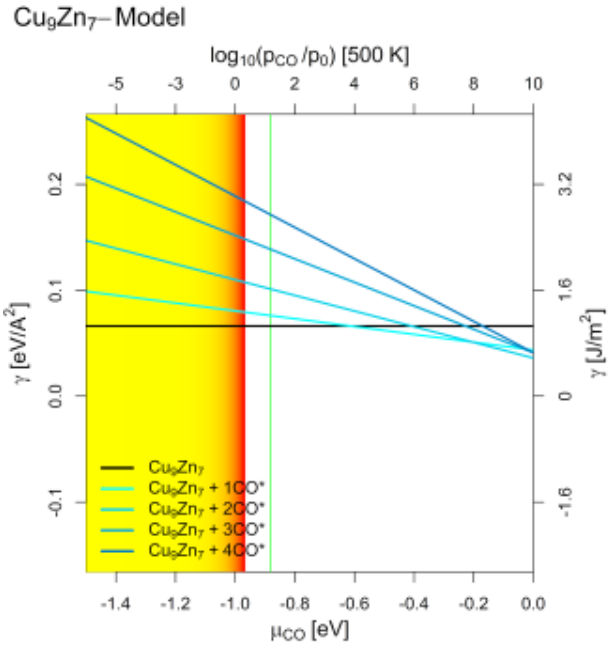
Cu9Zn7– Model
log10(pCO /p0) [500 K]
γ [eV/Å2]
γ [J/m2]
μCO [eV]
Cu9Zn7
Cu9Zn7 + 1CO*
Cu9Zn7 + 2CO*
Cu9Zn7 + 3CO*
Cu9Zn7 + 4CO*

(r)

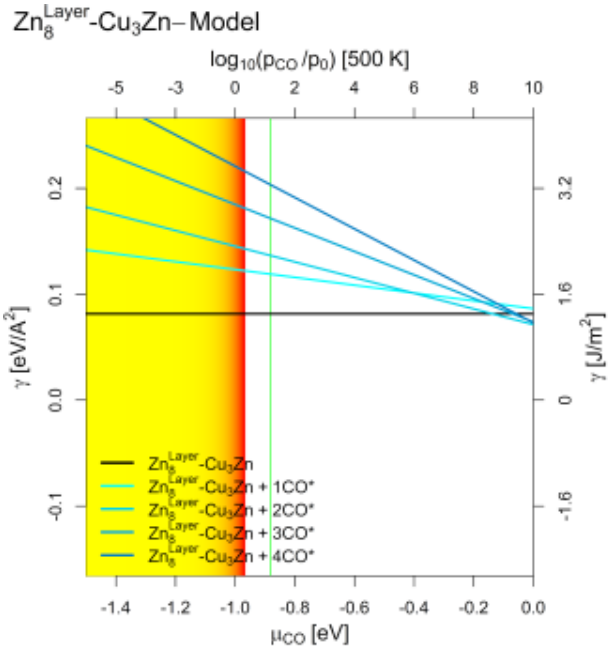
Zn8Layer-Cu3Zn– Model
log10(pCO /p0) [500 K]
γ [eV/Å2]
γ [J/m2]
μCO [eV]
Zn8Layer-Cu3Zn
Zn8Layer-Cu3Zn + 1CO*
Zn8Layer-Cu3Zn + 2CO*
Zn8Layer-Cu3Zn + 3CO*
Zn8Layer-Cu3Zn + 4CO*

(s)

Figure S20: Surface stability diagram of the (100)-facet of the investigated CuGa-/CuZn-models depending on the chemical potential of CO (μ_{CO} in eV) and the equivalent CO partial pressure at 500 K. The yellow-red area indicates μ_{CO} expected under CO_2 hydrogenation conditions (X_{CO_2} = 1, -2.00 eV < μ_{CO} < -0.96 eV) with the colour gradient indicating the progressing RWGS reaction (yellow for low conversion, red for high conversion; μ_{CO} increases with increasing RWGS-conversion). The green line indicates the expected μ_{CO} under CO hydrogenation conditions (X_{CO_2} = 0, μ_{CO} = -0.882) with no changes for μ_{CO} with progressing WGS-conversion. Used slab models for the (100)-facet used are:
(a/b) Unlayered substoichiometric fcc-Cu_3Ga/-Cu_3Zn (12.5 % Zn/Ga).
(c/d) One Ga/Zn surface layer on pure fcc-Cu (12.5 % Ga/Zn).
(e/f) Unlayered stoichiometric fcc-Cu_3Ga/-Cu_3Zn (25 % Ga/Zn).
(g/h) One Ga/Zn surface layer on substoichiometric fcc-Cu_3Ga/-Cu_3Zn (25 % Ga/Zn).
(i/j) Two Ga/Zn surface layers on pure fcc-Cu (25 % Ga/Zn).
(k/l) Unlayered superstoichiometric fcc-Cu_3Ga/-Cu_3Zn (31.25 % Ga/Zn).
(m/n) Two Ga/Zn surface layers on substoichiometric fcc-Cu_3Ga/-Cu_3Zn (31.25 % Ga/Zn).
(o) Unlayered supersubstoichiometric fcc-Cu_3Zn (37.5 % Zn).
(p) One Zn surface layer on fcc-Cu_3Zn (37.5 % Ga/Zn).
(q) Three Zn surface layers on pure fcc-Cu (37.5 % Ga/Zn).
(r) Unlayered supersubstoichiometric fcc-Cu_3Zn (43.75 % Zn).
(s) Two Zn surface layers on fcc-Cu_3Zn (43.75 % Ga/Zn).

(110)-Facet

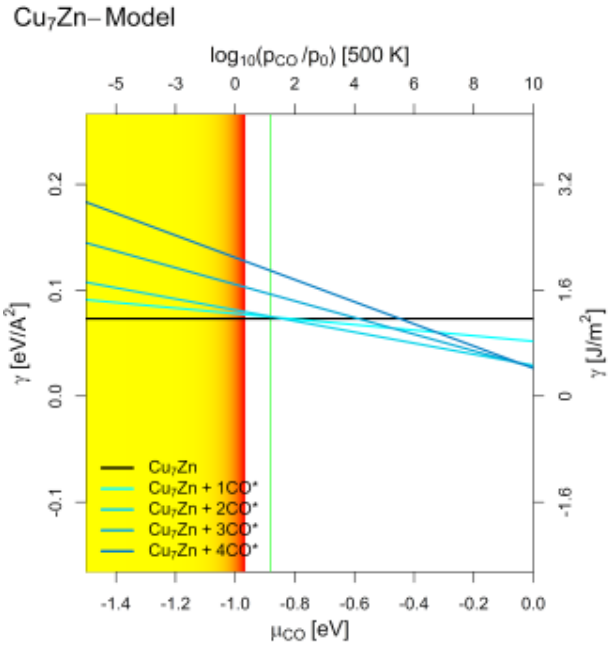

(a)

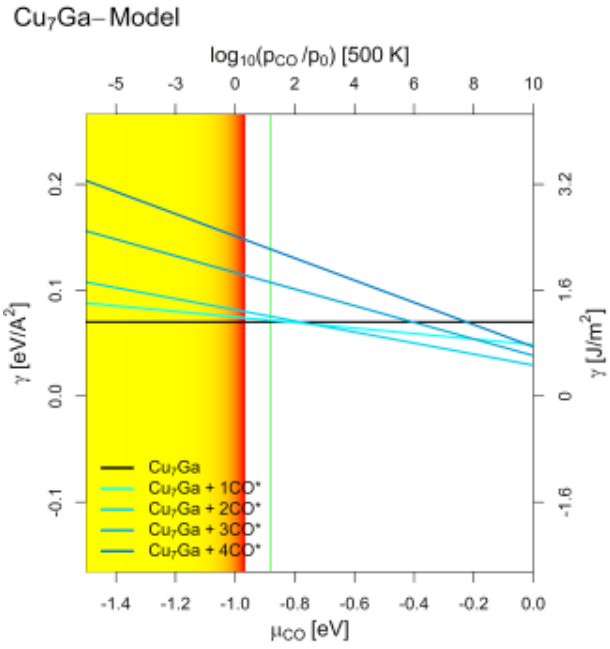

(b)

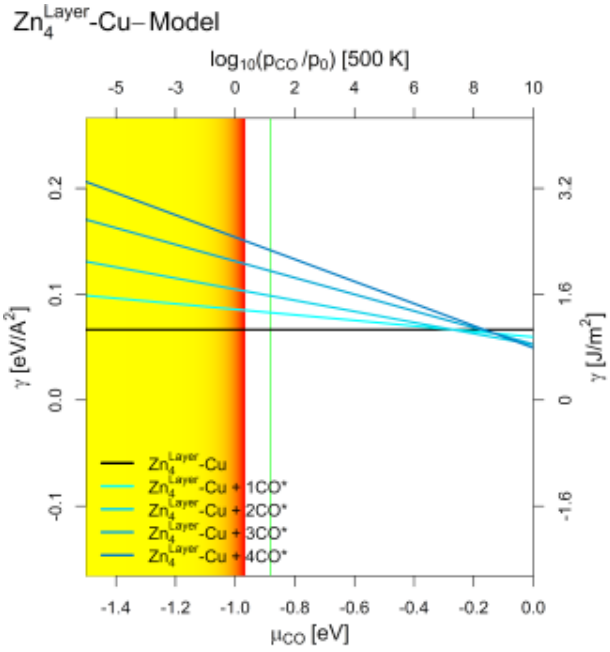

(c)

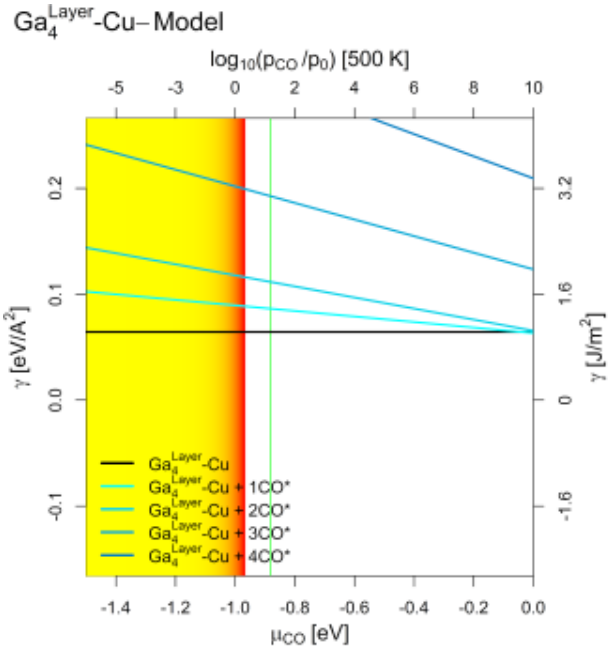

(d)

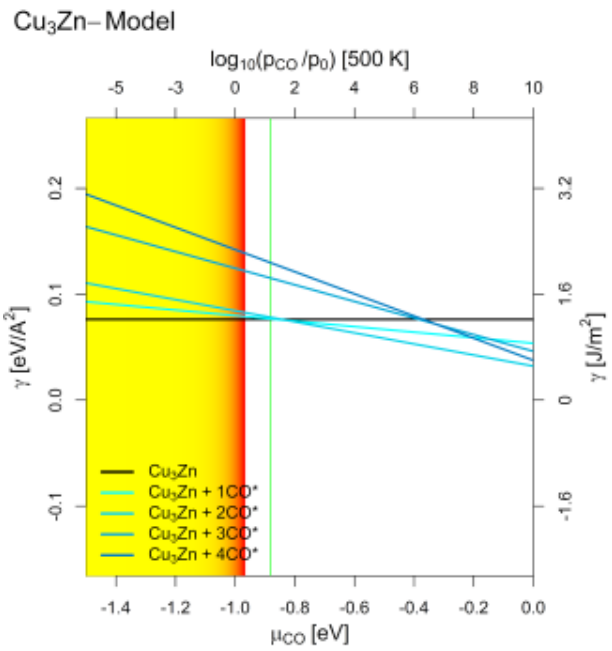
Cu3Zn−Model
log10(pCO /p0) [500 K]
-5 -3 0 2 4 6 8 10
γ [eV/Å2]
γ [J/m2]
0.2 0.1 0.0 -0.1
3.2 1.6 0 -1.6
Cu3Zn
Cu3Zn + 1CO*
Cu3Zn + 2CO*
Cu3Zn + 3CO*
Cu3Zn + 4CO*
-1.4 -1.2 -1.0 -0.8 -0.6 -0.4 -0.2 0.0
μCO [eV]

(e)

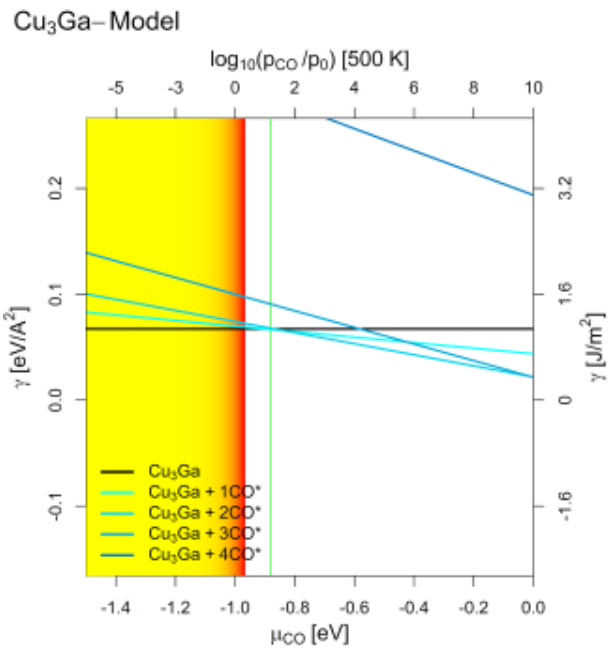
Cu3Ga−Model
log10(pCO /p0) [500 K]
-5 -3 0 2 4 6 8 10
γ [eV/Å2]
γ [J/m2]
0.2 0.1 0.0 -0.1
3.2 1.6 0 -1.6
Cu3Ga
Cu3Ga + 1CO*
Cu3Ga + 2CO*
Cu3Ga + 3CO*
Cu3Ga + 4CO*
-1.4 -1.2 -1.0 -0.8 -0.6 -0.4 -0.2 0.0
μCO [eV]

(f)

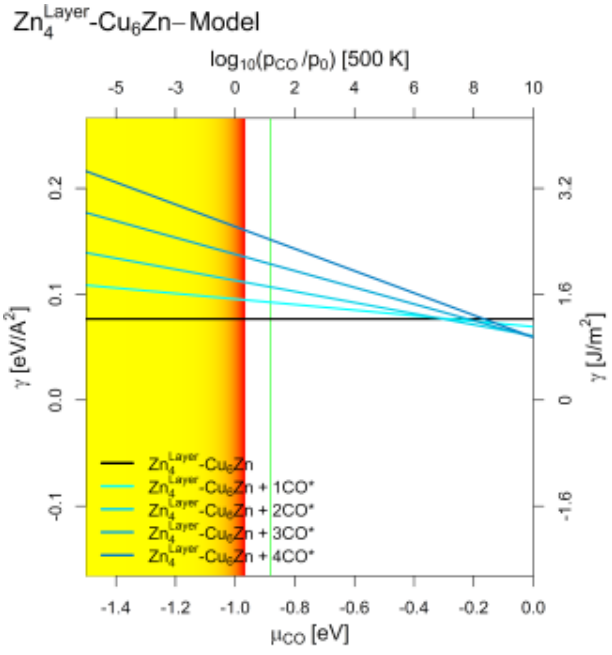
Zn4Layer-Cu6Zn−Model
log10(pCO /p0) [500 K]
-5 -3 0 2 4 6 8 10
γ [eV/Å2]
γ [J/m2]
0.2 0.1 0.0 -0.1
3.2 1.6 0 -1.6
Zn4Layer-Cu6Zn
Zn4Layer-Cu6Zn + 1CO*
Zn4Layer-Cu6Zn + 2CO*
Zn4Layer-Cu6Zn + 3CO*
Zn4Layer-Cu6Zn + 4CO*
-1.4 -1.2 -1.0 -0.8 -0.6 -0.4 -0.2 0.0
μCO [eV]

(g)

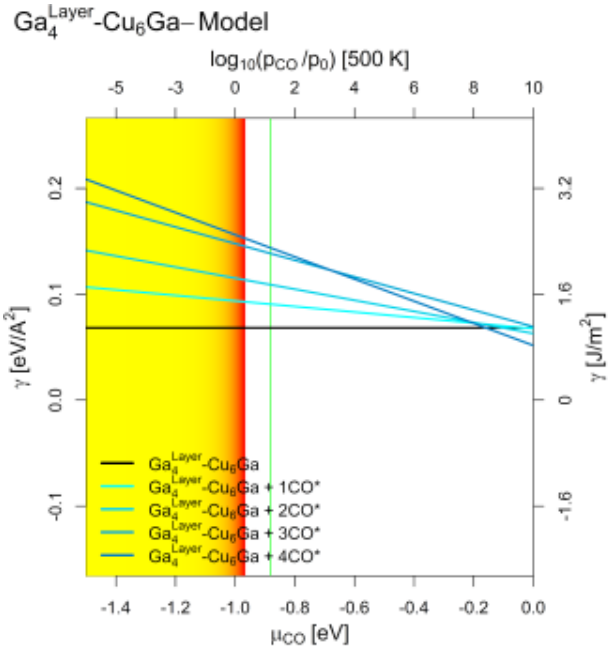
Ga4Layer-Cu6Ga−Model
log10(pCO /p0) [500 K]
-5 -3 0 2 4 6 8 10
γ [eV/Å2]
γ [J/m2]
0.2 0.1 0.0 -0.1
3.2 1.6 0 -1.6
Ga4Layer-Cu6Ga
Ga4Layer-Cu6Ga + 1CO*
Ga4Layer-Cu6Ga + 2CO*
Ga4Layer-Cu6Ga + 3CO*
Ga4Layer-Cu6Ga + 4CO*
-1.4 -1.2 -1.0 -0.8 -0.6 -0.4 -0.2 0.0
μCO [eV]

(h)

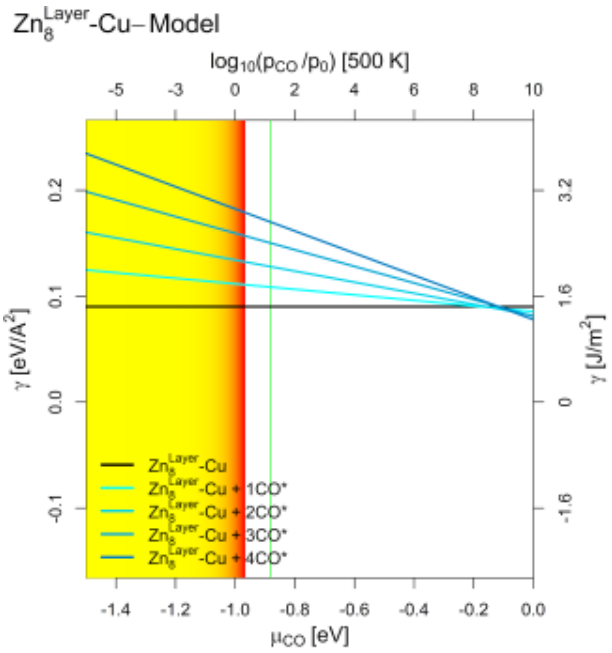
Zn8Layer-Cu– Model
log10(pCO /p0) [500 K]
-5 -3 0 2 4 6 8 10
γ [eV/A2]
γ [J/m2]
0.2 0.1 0.0 -0.1
3.2 1.6 0 -1.6
Zn8Layer-Cu
Zn8Layer-Cu + 1CO*
Zn8Layer-Cu + 2CO*
Zn8Layer-Cu + 3CO*
Zn8Layer-Cu + 4CO*
-1.4 -1.2 -1.0 -0.8 -0.6 -0.4 -0.2 0.0
μCO [eV]

(i)

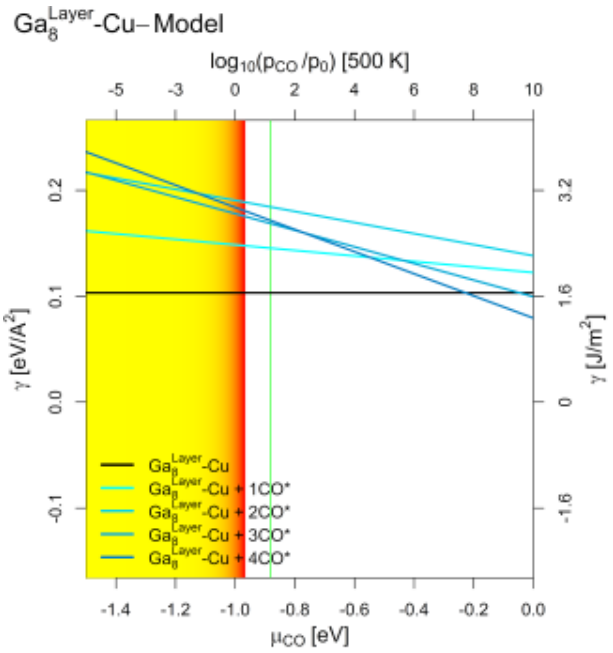
Ga8Layer-Cu– Model
log10(pCO /p0) [500 K]
-5 -3 0 2 4 6 8 10
γ [eV/A2]
γ [J/m2]
0.2 0.1 0.0 -0.1
3.2 1.6 0 -1.6
Ga8Layer-Cu
Ga8Layer-Cu + 1CO*
Ga8Layer-Cu + 2CO*
Ga8Layer-Cu + 3CO*
Ga8Layer-Cu + 4CO*
-1.4 -1.2 -1.0 -0.8 -0.6 -0.4 -0.2 0.0
μCO [eV]

(j)

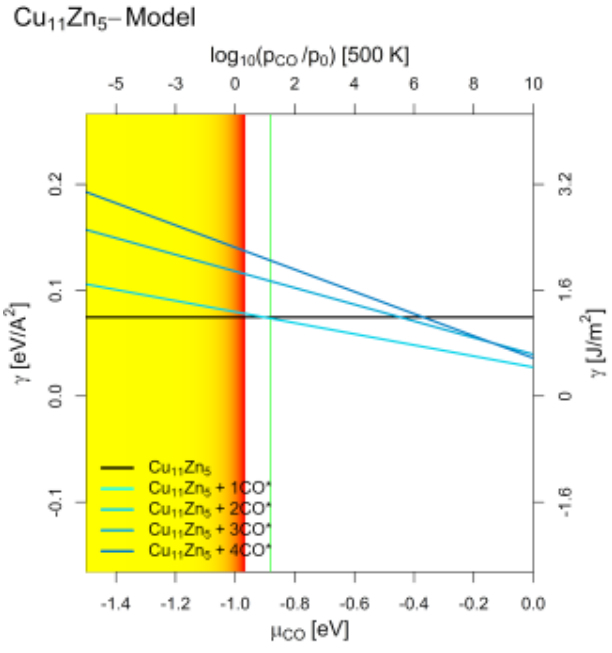
Cu11Zn5– Model
log10(pCO /p0) [500 K]
-5 -3 0 2 4 6 8 10
γ [eV/A2]
γ [J/m2]
0.2 0.1 0.0 -0.1
3.2 1.6 0 -1.6
Cu11Zn5
Cu11Zn5 + 1CO*
Cu11Zn5 + 2CO*
Cu11Zn5 + 3CO*
Cu11Zn5 + 4CO*
-1.4 -1.2 -1.0 -0.8 -0.6 -0.4 -0.2 0.0
μCO [eV]

(k)

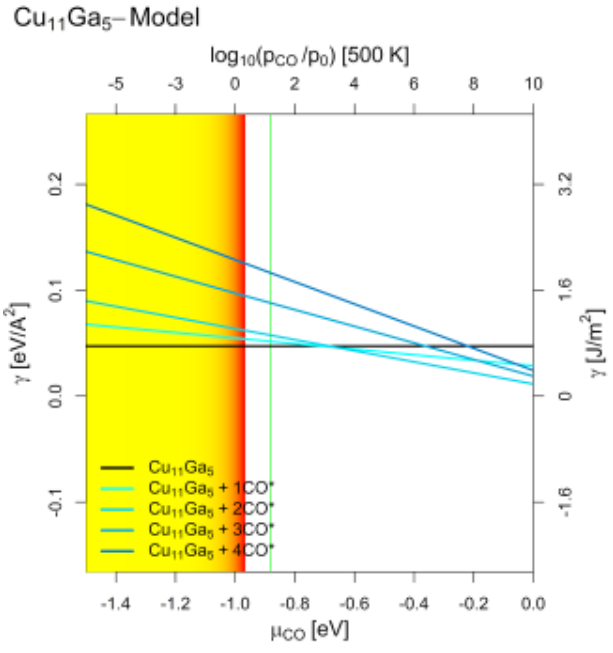
Cu11Ga5– Model
log10(pCO /p0) [500 K]
-5 -3 0 2 4 6 8 10
γ [eV/A2]
γ [J/m2]
0.2 0.1 0.0 -0.1
3.2 1.6 0 -1.6
Cu11Ga5
Cu11Ga5 + 1CO*
Cu11Ga5 + 2CO*
Cu11Ga5 + 3CO*
Cu11Ga5 + 4CO*
-1.4 -1.2 -1.0 -0.8 -0.6 -0.4 -0.2 0.0
μCO [eV]

(l)

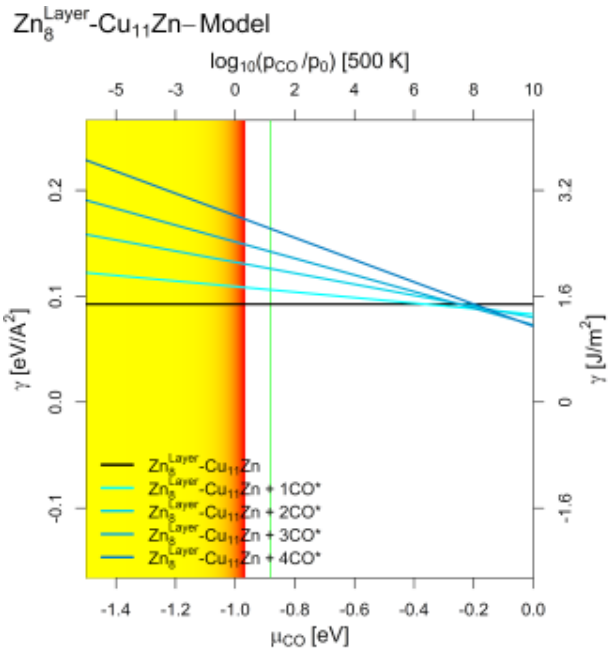
Zn_8^{Layer}-$Cu_{11}Zn$ – Model
$\log_{10}(p_{CO}/p_0)$ [500 K]
-5 -3 0 2 4 6 8 10
γ [eV/Å²]
γ [J/m²]
Zn_8^{Layer}-$Cu_{11}Zn$
Zn_8^{Layer}-$Cu_{11}Zn$ + 1CO*
Zn_8^{Layer}-$Cu_{11}Zn$ + 2CO*
Zn_8^{Layer}-$Cu_{11}Zn$ + 3CO*
Zn_8^{Layer}-$Cu_{11}Zn$ + 4CO*
-1.4 -1.2 -1.0 -0.8 -0.6 -0.4 -0.2 0.0
μ_{CO} [eV]

(m)

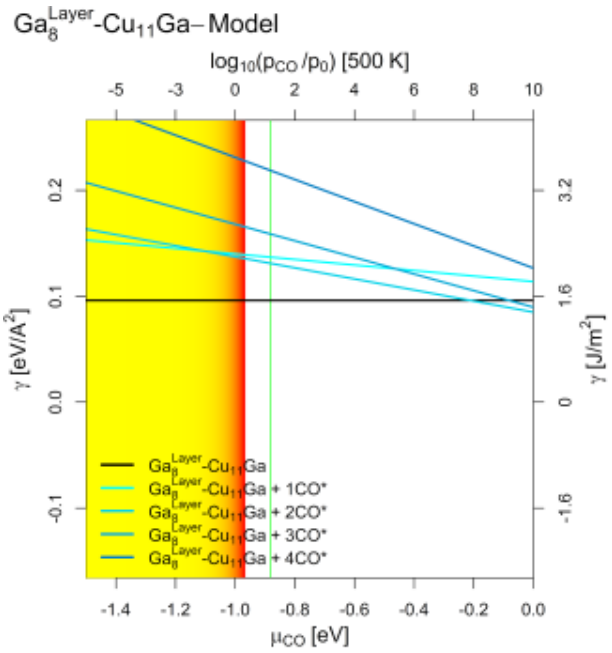
Ga_8^{Layer}-$Cu_{11}Ga$ – Model
$\log_{10}(p_{CO}/p_0)$ [500 K]
-5 -3 0 2 4 6 8 10
γ [eV/Å²]
γ [J/m²]
Ga_8^{Layer}-$Cu_{11}Ga$
Ga_8^{Layer}-$Cu_{11}Ga$ + 1CO*
Ga_8^{Layer}-$Cu_{11}Ga$ + 2CO*
Ga_8^{Layer}-$Cu_{11}Ga$ + 3CO*
Ga_8^{Layer}-$Cu_{11}Ga$ + 4CO*
-1.4 -1.2 -1.0 -0.8 -0.6 -0.4 -0.2 0.0
μ_{CO} [eV]

(n)

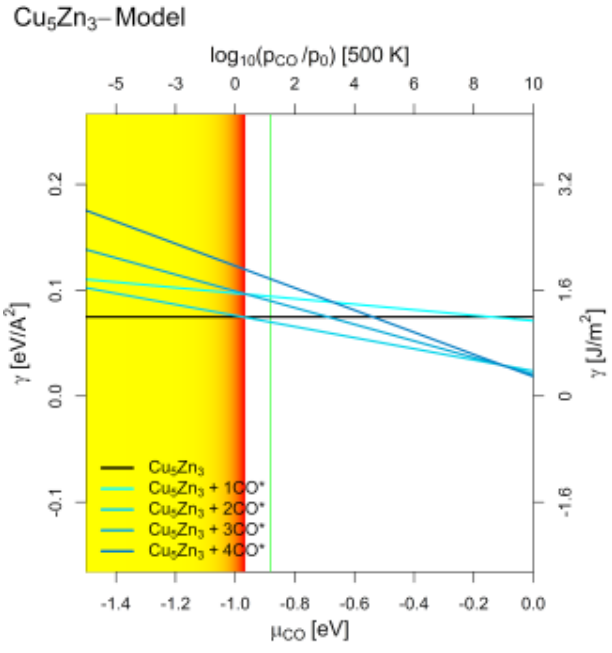
Cu_5Zn_3 – Model
$\log_{10}(p_{CO}/p_0)$ [500 K]
-5 -3 0 2 4 6 8 10
γ [eV/Å²]
γ [J/m²]
Cu_5Zn_3
Cu_5Zn_3 + 1CO*
Cu_5Zn_3 + 2CO*
Cu_5Zn_3 + 3CO*
Cu_5Zn_3 + 4CO*
-1.4 -1.2 -1.0 -0.8 -0.6 -0.4 -0.2 0.0
μ_{CO} [eV]

(o)

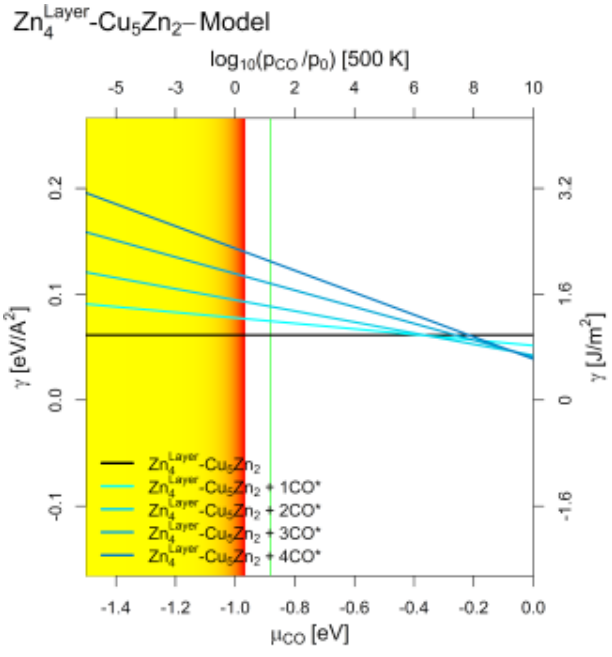
Zn_4^{Layer}-Cu_5Zn_2 – Model
$\log_{10}(p_{CO}/p_0)$ [500 K]
-5 -3 0 2 4 6 8 10
γ [eV/Å²]
γ [J/m²]
Zn_4^{Layer}-Cu_5Zn_2
Zn_4^{Layer}-Cu_5Zn_2 + 1CO*
Zn_4^{Layer}-Cu_5Zn_2 + 2CO*
Zn_4^{Layer}-Cu_5Zn_2 + 3CO*
Zn_4^{Layer}-Cu_5Zn_2 + 4CO*
-1.4 -1.2 -1.0 -0.8 -0.6 -0.4 -0.2 0.0
μ_{CO} [eV]

(p)

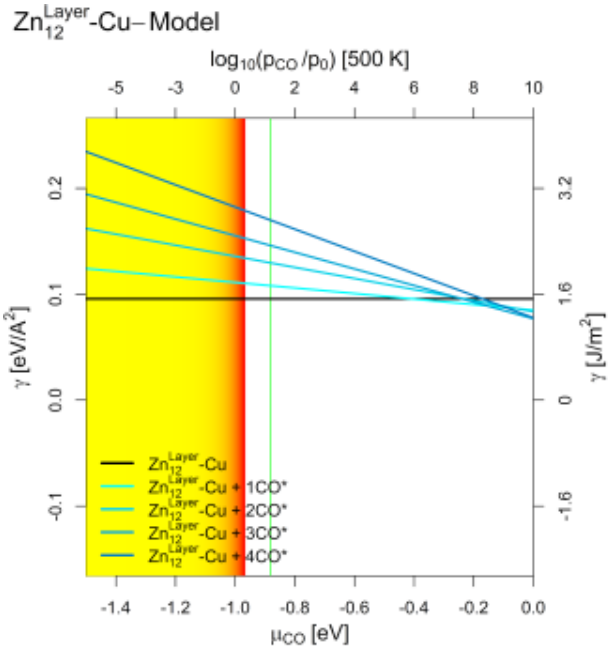
Zn12Layer-Cu– Model
log10(pCO /p0) [500 K]
γ [eV/A2]
γ [J/m2]
μCO [eV]
Zn12Layer-Cu
Zn12Layer-Cu + 1CO*
Zn12Layer-Cu + 2CO*
Zn12Layer-Cu + 3CO*
Zn12Layer-Cu + 4CO*

(q)

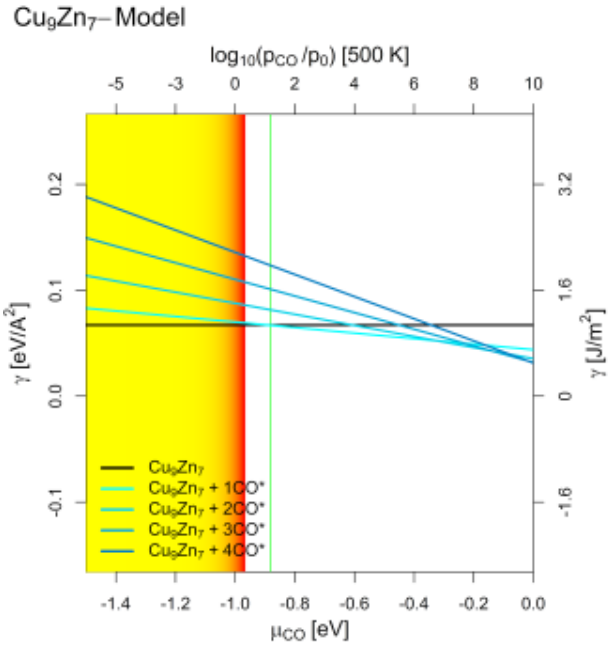
Cu9Zn7– Model
log10(pCO /p0) [500 K]
γ [eV/A2]
γ [J/m2]
μCO [eV]
Cu9Zn7
Cu9Zn7 + 1CO*
Cu9Zn7 + 2CO*
Cu9Zn7 + 3CO*
Cu9Zn7 + 4CO*

(r)

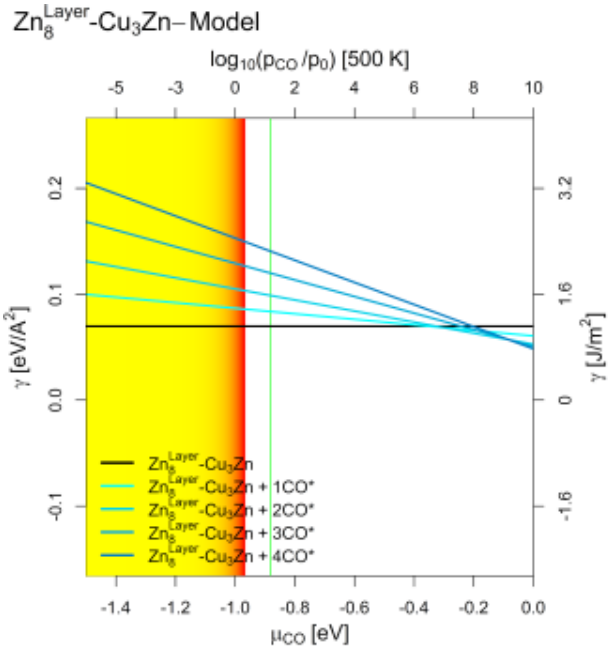
Zn8Layer-Cu3Zn– Model
log10(pCO /p0) [500 K]
γ [eV/A2]
γ [J/m2]
μCO [eV]
Zn8Layer-Cu3Zn
Zn8Layer-Cu3Zn + 1CO*
Zn8Layer-Cu3Zn + 2CO*
Zn8Layer-Cu3Zn + 3CO*
Zn8Layer-Cu3Zn + 4CO*

(s)

Figure S21: Surface stability diagram of the (110)-facet of the investigated CuGa-/CuZn-models depending on the chemical potential of CO (μ_{CO} in eV) and the equivalent CO partial pressure at 500 K. The yellow-red area indicates μ_{CO} expected under CO_2 hydrogenation conditions (X_{CO_2} = 1, -2.00 eV < μ_{CO} < -0.96 eV) with the colour gradient indicating the progressing RWGS reaction (yellow for low conversion, red for high conversion; μ_{CO} increases with increasing RWGS-conversion). The green line indicates the expected μ_{CO} under CO hydrogenation conditions (X_{CO_2} = 0, μ_{CO} = -0.882) with no changes for μ_{CO} with progressing WGS-conversion. Used slab models for the (110)-facet used are:
(a/b) Unlayered substoichiometric fcc-Cu_3Ga/-Cu_3Zn (12.5 % Zn/Ga).
(c/d) One Ga/Zn surface layer on pure fcc-Cu (12.5 % Ga/Zn).
(e/f) Unlayered stoichiometric fcc-Cu_3Ga/-Cu_3Zn (25 % Ga/Zn).
(g/h) One Ga/Zn surface layer on substoichiometric fcc-Cu_3Ga/-Cu_3Zn (25 % Ga/Zn).
(i/j) Two Ga/Zn surface layers on pure fcc-Cu (25 % Ga/Zn).
(k/l) Unlayered superstoichiometric fcc-Cu_3Ga/-Cu_3Zn (31.25 % Ga/Zn).
(m/n) Two Ga/Zn surface layers on substoichiometric fcc-Cu_3Ga/-Cu_3Zn (31.25 % Ga/Zn).
(o) Unlayered supersubstoichiometric fcc-Cu_3Zn (37.5 % Zn).
(p) One Zn surface layer on fcc-Cu_3Zn (37.5 % Ga/Zn).
(q) Three Zn surface layers on pure fcc-Cu (37.5 % Ga/Zn).
(r) Unlayered supersubstoichiometric fcc-Cu_3Zn (43.75 % Zn).
(s) Two Zn surface layers on fcc-Cu_3Zn (43.75 % Ga/Zn).

(111)-Facet

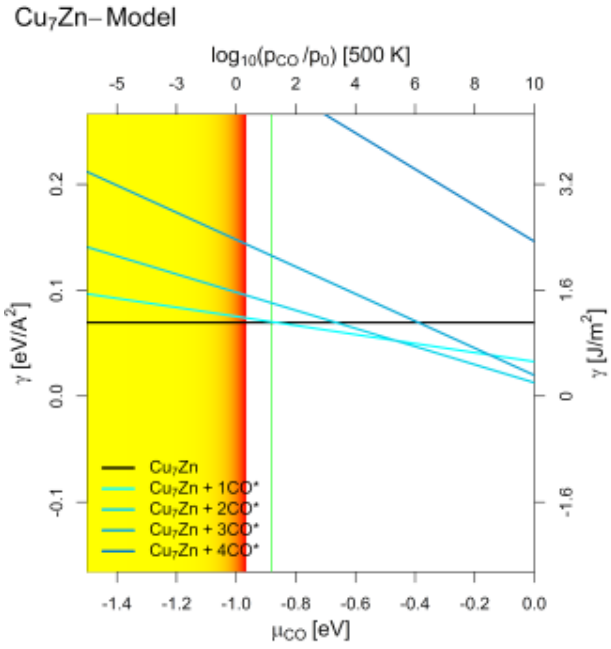

(a)

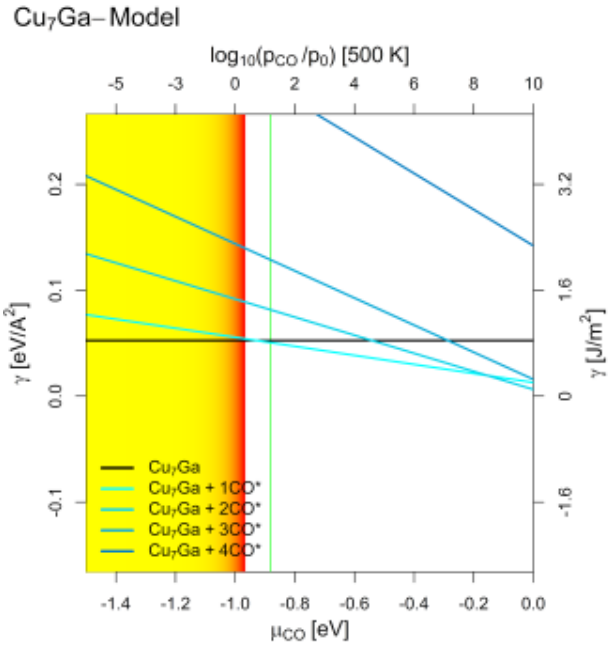

(b)

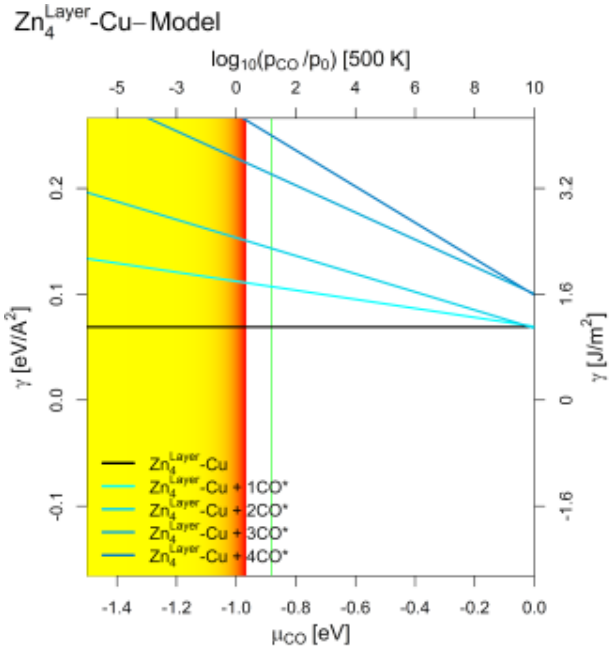

(c)

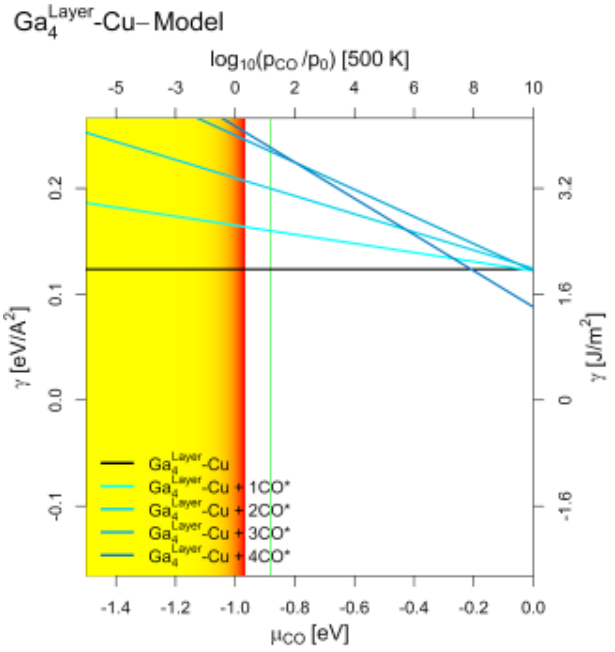

(d)

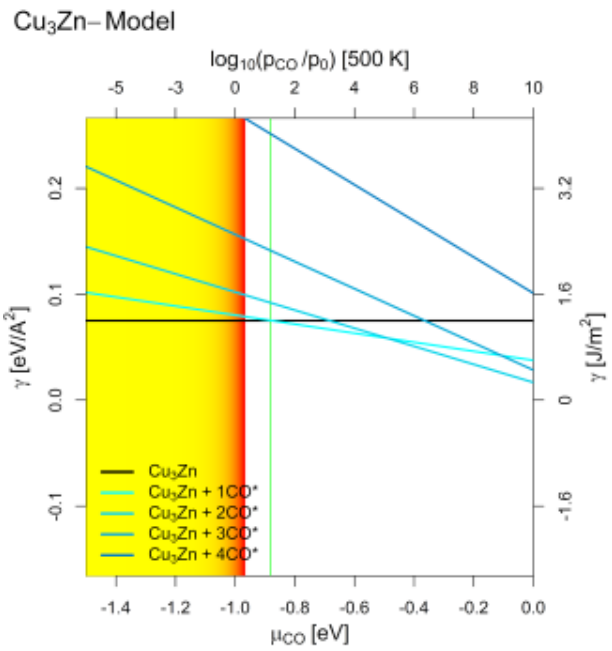
Cu3Zn−Model
log10(pCO /p0) [500 K]
-5 -3 0 2 4 6 8 10
γ [eV/Å2]
γ [J/m2]
0.2 0.1 0.0 -0.1
3.2 1.6 0 -1.6
Cu3Zn
Cu3Zn + 1CO*
Cu3Zn + 2CO*
Cu3Zn + 3CO*
Cu3Zn + 4CO*
-1.4 -1.2 -1.0 -0.8 -0.6 -0.4 -0.2 0.0
μCO [eV]

(e)

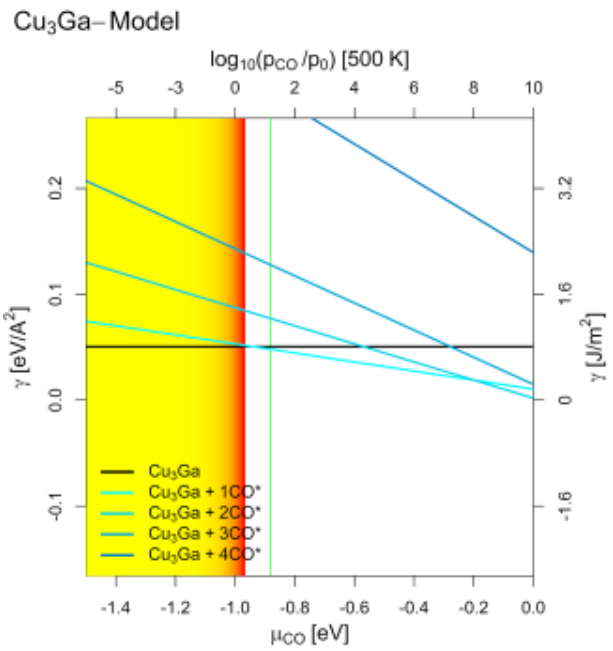
Cu3Ga−Model
log10(pCO /p0) [500 K]
-5 -3 0 2 4 6 8 10
γ [eV/Å2]
γ [J/m2]
0.2 0.1 0.0 -0.1
3.2 1.6 0 -1.6
Cu3Ga
Cu3Ga + 1CO*
Cu3Ga + 2CO*
Cu3Ga + 3CO*
Cu3Ga + 4CO*
-1.4 -1.2 -1.0 -0.8 -0.6 -0.4 -0.2 0.0
μCO [eV]

(f)

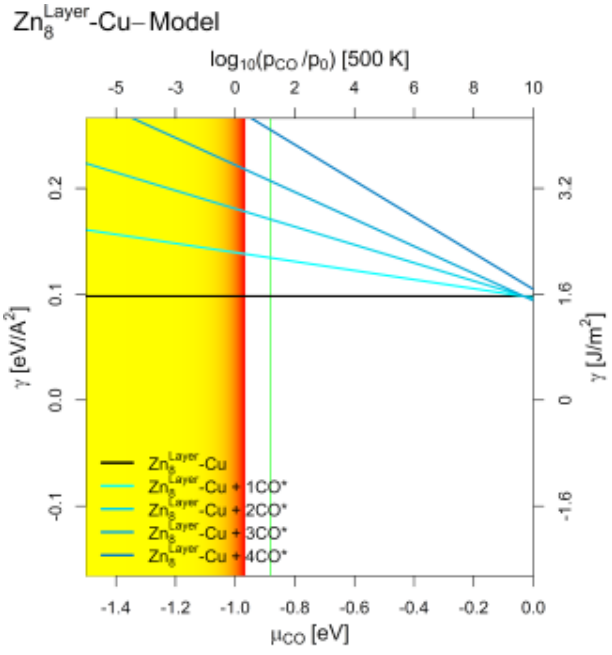
Zn8Layer-Cu−Model
log10(pCO /p0) [500 K]
-5 -3 0 2 4 6 8 10
γ [eV/Å2]
γ [J/m2]
0.2 0.1 0.0 -0.1
3.2 1.6 0 -1.6
Zn8Layer-Cu
Zn8Layer-Cu + 1CO*
Zn8Layer-Cu + 2CO*
Zn8Layer-Cu + 3CO*
Zn8Layer-Cu + 4CO*
-1.4 -1.2 -1.0 -0.8 -0.6 -0.4 -0.2 0.0
μCO [eV]

(g)

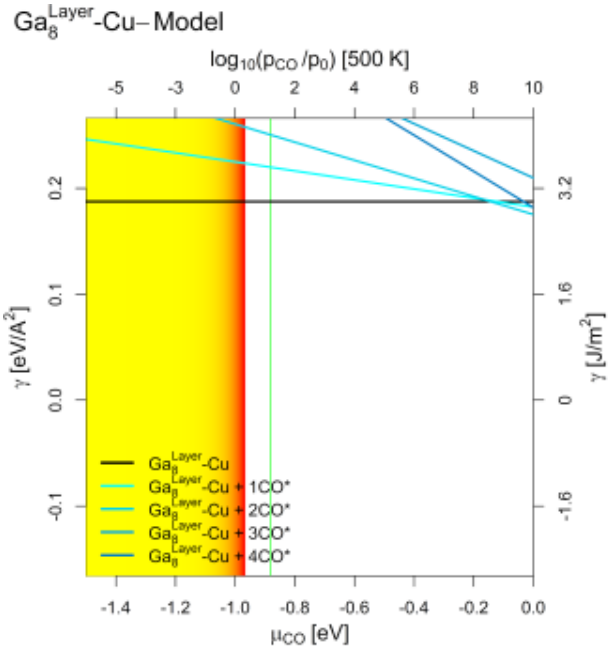
Ga8Layer-Cu−Model
log10(pCO /p0) [500 K]
-5 -3 0 2 4 6 8 10
γ [eV/Å2]
γ [J/m2]
0.2 0.1 0.0 -0.1
3.2 1.6 0 -1.6
Ga8Layer-Cu
Ga8Layer-Cu + 1CO*
Ga8Layer-Cu + 2CO*
Ga8Layer-Cu + 3CO*
Ga8Layer-Cu + 4CO*
-1.4 -1.2 -1.0 -0.8 -0.6 -0.4 -0.2 0.0
μCO [eV]

(h)

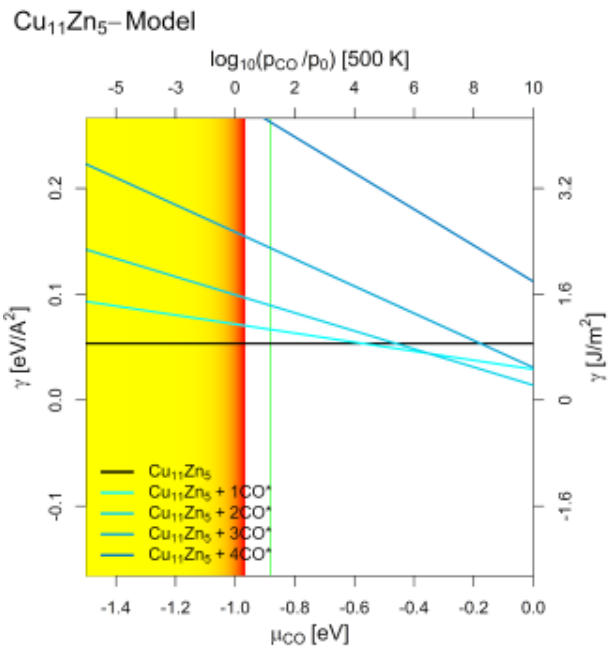
Cu11Zn5 – Model
log10(pCO /p0) [500 K]
γ [eV/Å2]
γ [J/m2]
μCO [eV]
Cu11Zn5
Cu11Zn5 + 1CO*
Cu11Zn5 + 2CO*
Cu11Zn5 + 3CO*
Cu11Zn5 + 4CO*

(i)

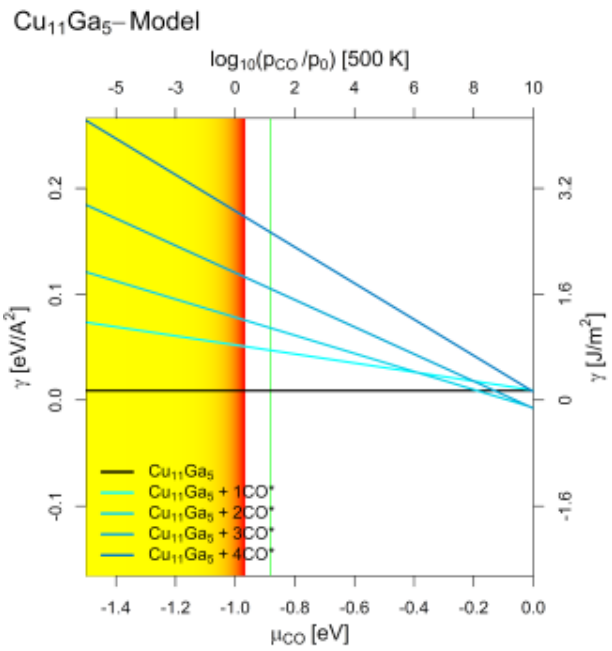
Cu11Ga5 – Model
log10(pCO /p0) [500 K]
γ [eV/Å2]
γ [J/m2]
μCO [eV]
Cu11Ga5
Cu11Ga5 + 1CO*
Cu11Ga5 + 2CO*
Cu11Ga5 + 3CO*
Cu11Ga5 + 4CO*

(j)

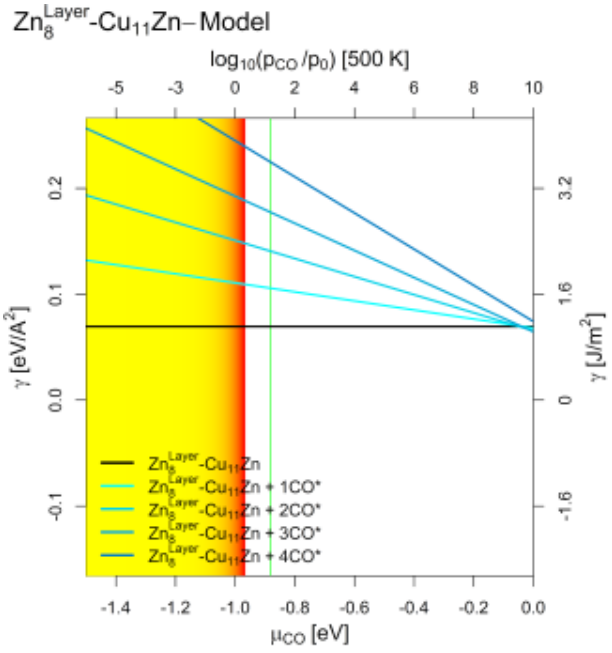
Zn8Layer-Cu11Zn – Model
log10(pCO /p0) [500 K]
γ [eV/Å2]
γ [J/m2]
μCO [eV]
Zn8Layer-Cu11Zn
Zn8Layer-Cu11Zn + 1CO*
Zn8Layer-Cu11Zn + 2CO*
Zn8Layer-Cu11Zn + 3CO*
Zn8Layer-Cu11Zn + 4CO*

(k)

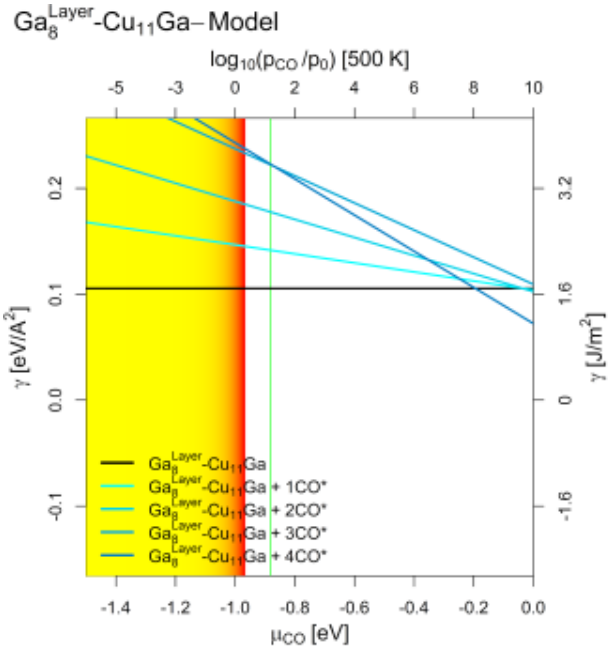
Ga8Layer-Cu11Ga – Model
log10(pCO /p0) [500 K]
γ [eV/Å2]
γ [J/m2]
μCO [eV]
Ga8Layer-Cu11Ga
Ga8Layer-Cu11Ga + 1CO*
Ga8Layer-Cu11Ga + 2CO*
Ga8Layer-Cu11Ga + 3CO*
Ga8Layer-Cu11Ga + 4CO*

(l)

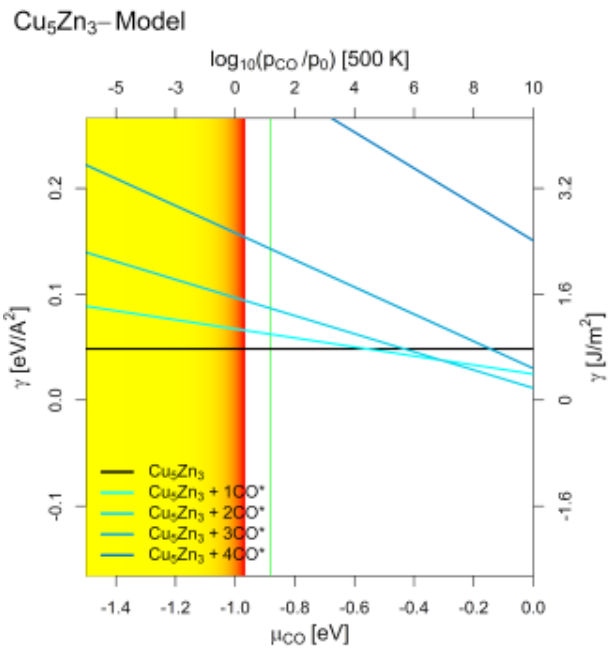
Cu5Zn3 – Model
log10(pCO /p0) [500 K]
γ [eV/Å2]
γ [J/m2]
μCO [eV]
Cu5Zn3
Cu5Zn3 + 1CO*
Cu5Zn3 + 2CO*
Cu5Zn3 + 3CO*
Cu5Zn3 + 4CO*

(m)

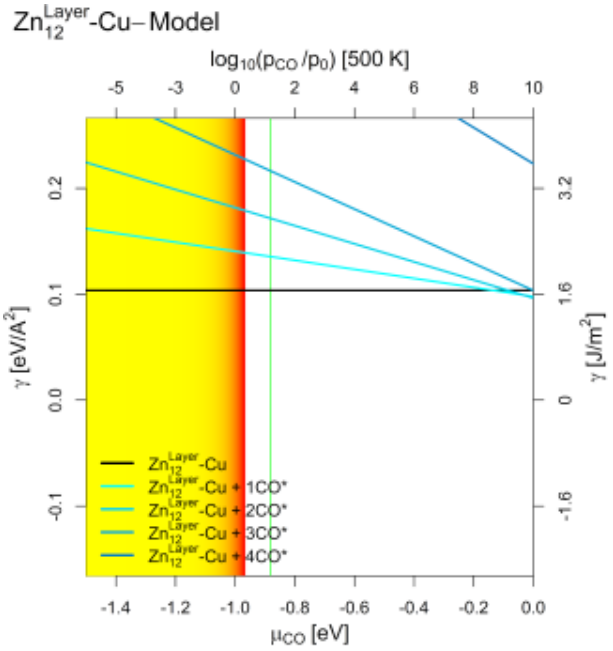
Zn12Layer-Cu – Model
log10(pCO /p0) [500 K]
γ [eV/Å2]
γ [J/m2]
μCO [eV]
Zn12Layer-Cu
Zn12Layer-Cu + 1CO*
Zn12Layer-Cu + 2CO*
Zn12Layer-Cu + 3CO*
Zn12Layer-Cu + 4CO*

(n)

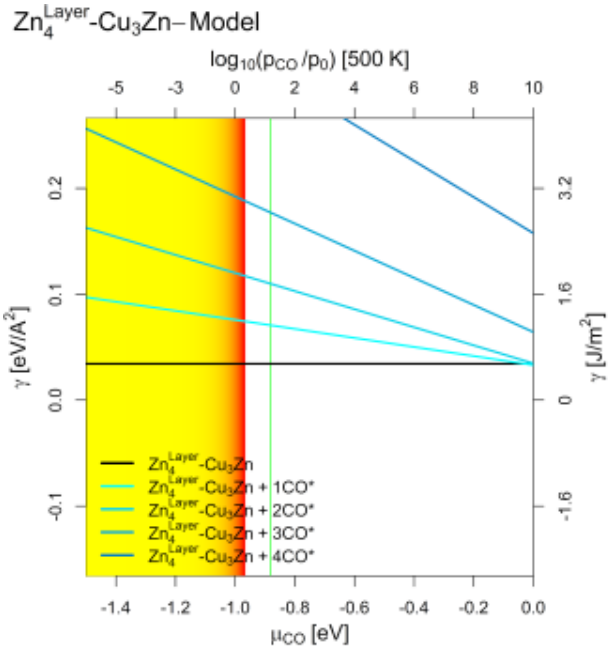
Zn4Layer-Cu3Zn – Model
log10(pCO /p0) [500 K]
γ [eV/Å2]
γ [J/m2]
μCO [eV]
Zn4Layer-Cu3Zn
Zn4Layer-Cu3Zn + 1CO*
Zn4Layer-Cu3Zn + 2CO*
Zn4Layer-Cu3Zn + 3CO*
Zn4Layer-Cu3Zn + 4CO*

(o)

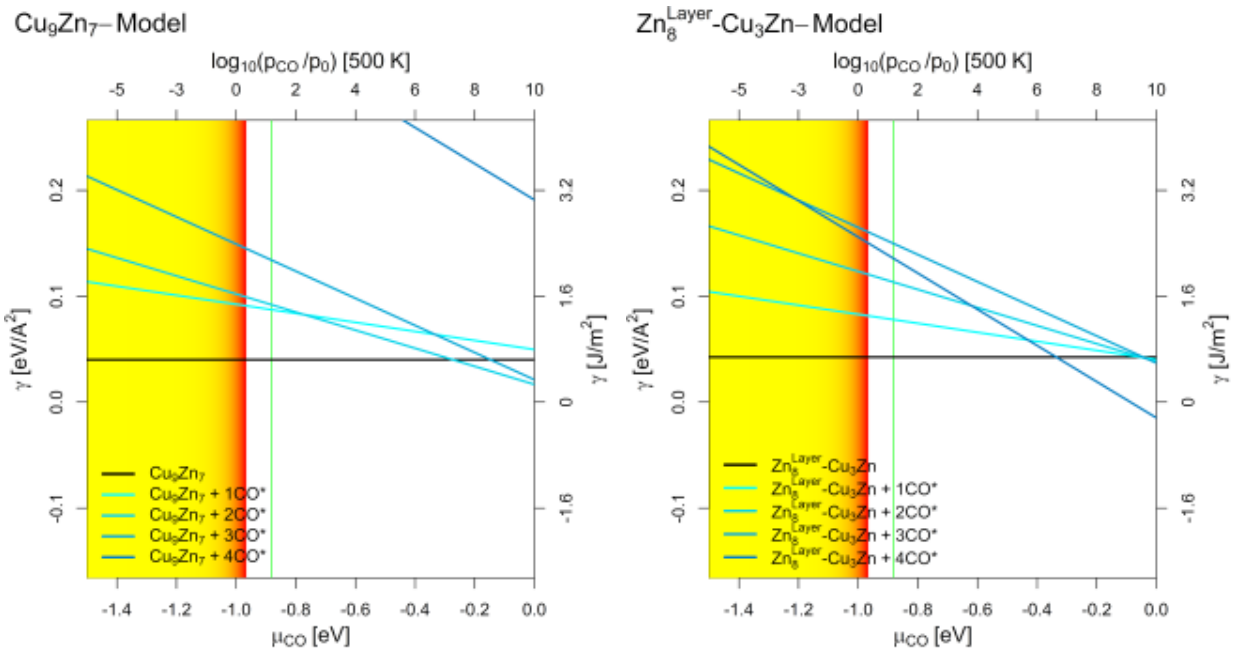

(p) (q)

Figure S22: Surface stability diagram of the (111)-facet of the investigated CuGa-/CuZn-models depending on the chemical potential of CO (μ_{CO} in eV) and the equivalent CO partial pressure at 500 K. The yellow-red area indicates μ_{CO} expected under CO_2 hydrogenation conditions (X_{CO_2} = 1, -2.00 eV < μ_{CO} < -0.96 eV) with the colour gradient indicating the progressing RWGS reaction (yellow for low conversion, red for high conversion; μ_{CO} increases with increasing RWGS-conversion). The green line indicates the expected μ_{CO} under CO hydrogenation conditions (X_{CO_2} = 0, μ_{CO} = -0.882) with no changes for μ_{CO} with progressing WGS-conversion. Used slab models for the (111)-facet used are:
(a/b) Unlayered substoichiometric fcc-Cu_3Ga/-Cu_3Zn (12.5 % Zn/Ga).
(c/d) One Ga/Zn surface layer on pure fcc-Cu (12.5 % Ga/Zn).
(e/f) Unlayered stoichiometric fcc-Cu_3Ga/-Cu_3Zn (25 % Ga/Zn).
(g/h) Two Ga/Zn surface layers on pure fcc-Cu (25 % Ga/Zn).
(i/j) Unlayered superstoichiometric fcc-Cu_3Ga/-Cu_3Zn (31.25 % Ga/Zn).
(k/l) Two Ga/Zn surface layers on substoichiometric fcc-Cu_3Ga/-Cu_3Zn (31.25 % Ga/Zn).
(m) Unlayered supersubstoichiometric fcc-Cu_3Zn (37.5 % Zn).
(n) Three Zn surface layers on pure fcc-Cu (37.5 % Ga/Zn).
(o) One Zn surface layer on fcc-Cu_3Zn (34.375 % Ga/Zn).
(p) Unlayered supersubstoichiometric fcc-Cu_3Zn (43.75 % Zn).
(q) Two Zn surface layers on fcc-Cu_3Zn (43.75 % Ga/Zn).

5.2 Individual Surface Energies Depending on the CO Chemical Potential

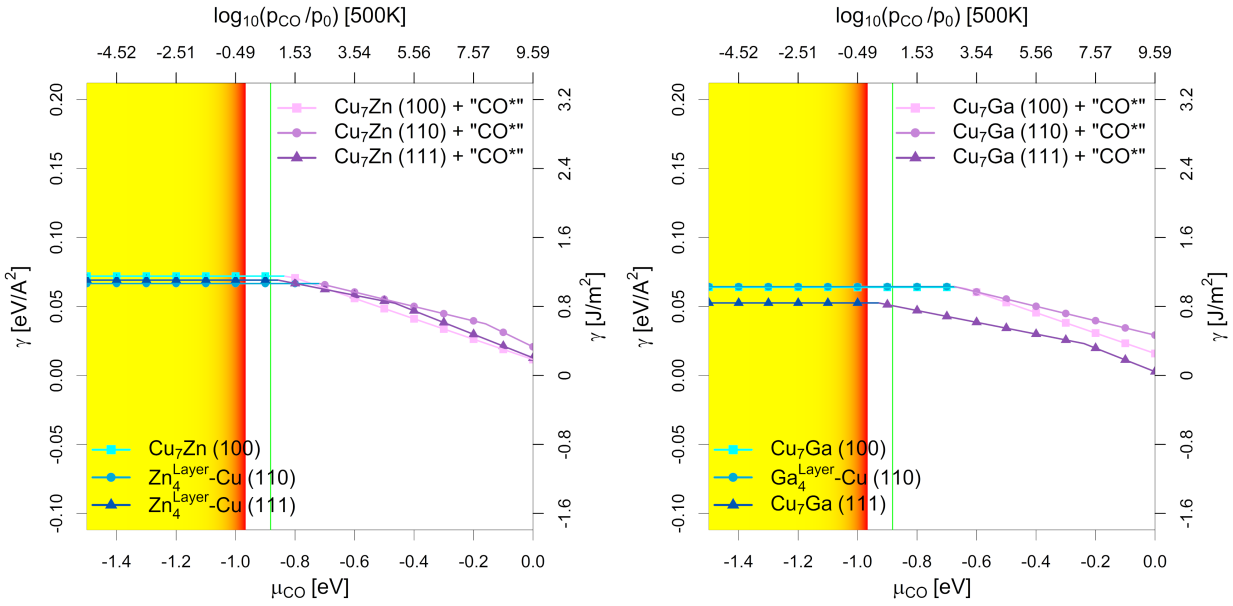

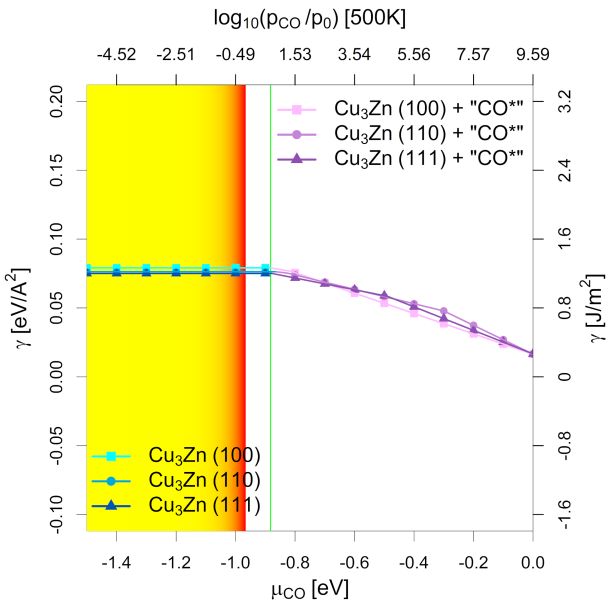
log10(pCO /p0) [500K]
-4.52 -2.51 -0.49 1.53 3.54 5.56 7.57 9.59
Cu3Zn (100) + "CO*"
Cu3Zn (110) + "CO*"
Cu3Zn (111) + "CO*"
Cu3Zn (100)
Cu3Zn (110)
Cu3Zn (111)
γ [eV/A2]
γ [J/m2]
μCO [eV]

(e)

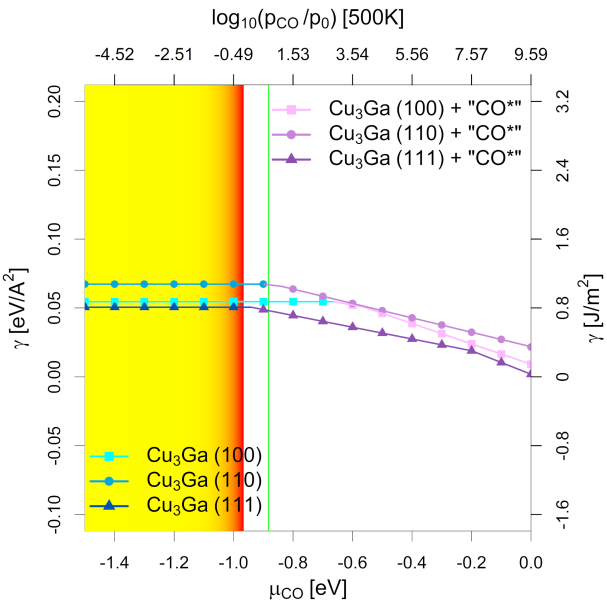
log10(pCO /p0) [500K]
-4.52 -2.51 -0.49 1.53 3.54 5.56 7.57 9.59
Cu3Ga (100) + "CO*"
Cu3Ga (110) + "CO*"
Cu3Ga (111) + "CO*"
Cu3Ga (100)
Cu3Ga (110)
Cu3Ga (111)
γ [eV/A2]
γ [J/m2]
μCO [eV]

(f)

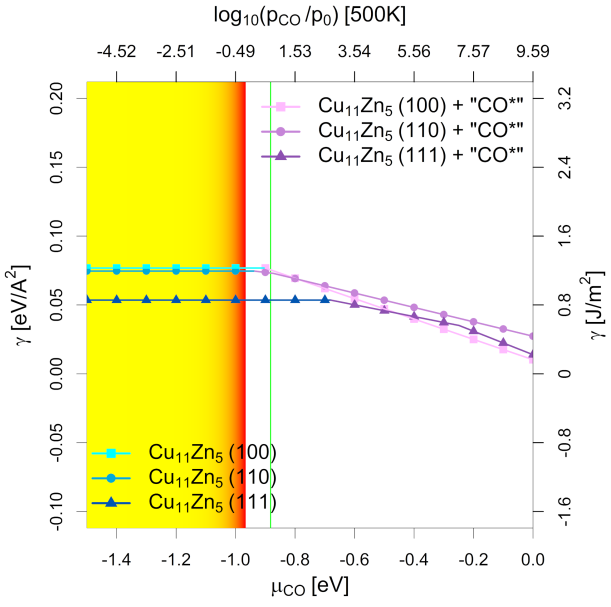
log10(pCO /p0) [500K]
-4.52 -2.51 -0.49 1.53 3.54 5.56 7.57 9.59
Cu11Zn5 (100) + "CO*"
Cu11Zn5 (110) + "CO*"
Cu11Zn5 (111) + "CO*"
Cu11Zn5 (100)
Cu11Zn5 (110)
Cu11Zn5 (111)
γ [eV/A2]
γ [J/m2]
μCO [eV]

(g)

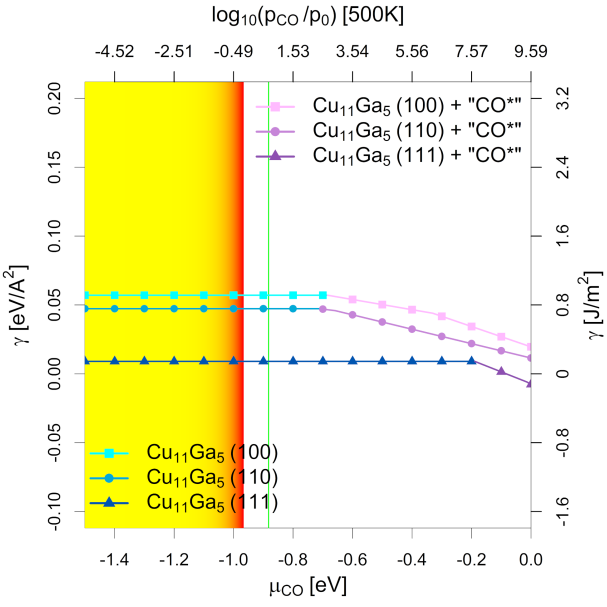
log10(pCO /p0) [500K]
-4.52 -2.51 -0.49 1.53 3.54 5.56 7.57 9.59
Cu11Ga5 (100) + "CO*"
Cu11Ga5 (110) + "CO*"
Cu11Ga5 (111) + "CO*"
Cu11Ga5 (100)
Cu11Ga5 (110)
Cu11Ga5 (111)
γ [eV/A2]
γ [J/m2]
μCO [eV]

(h)

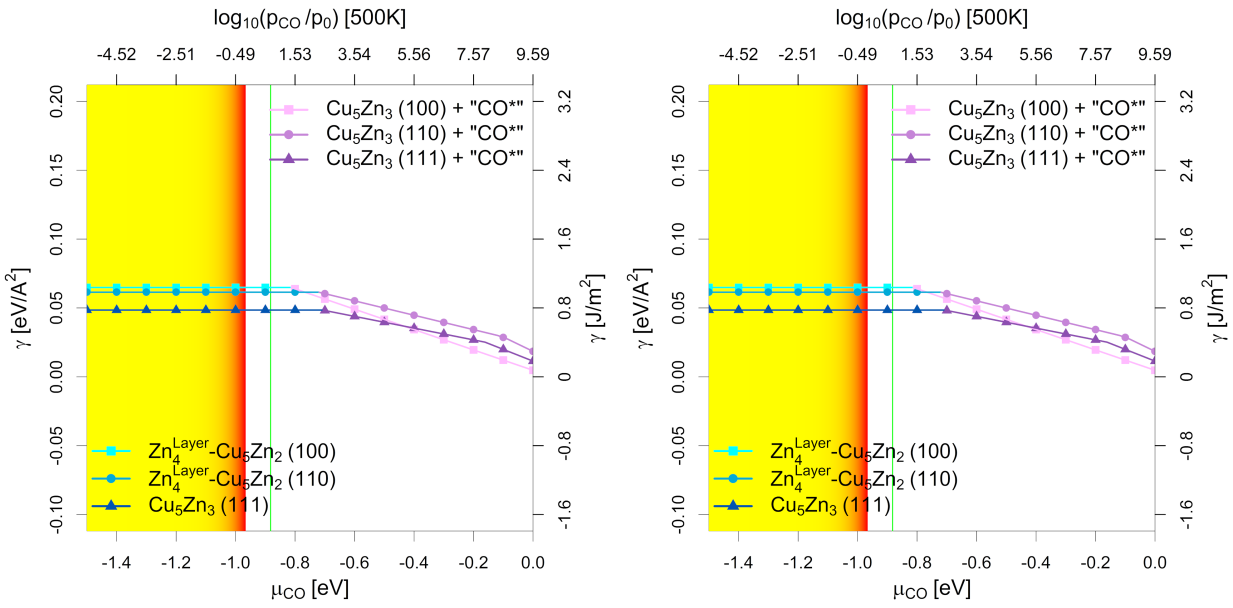

Figure S23: Most stable surfaces of the fcc-Cu_3Ga/fcc-Cu_3Zn alloys with various compositions depending on the chemical potential of CO (μ_{CO} in eV) and the equivalent CO partial pressure at 500 K including unlayered structures, partially layered structures and fully layered structures. The yellow-red area indicates μ_{CO} expected under CO_2 hydrogenation conditions (X_{CO_2} = 1, -2.00 eV < μ_{CO} < -0.96 eV) with the colour gradient indicating the progressing RWGS reaction (yellow for low conversion, red for high conversion; μ_{CO} increases with increasing RWGS-conversion). The green line indicates the expected μ_{CO} under CO hydrogenation conditions (X_{CO_2} = 0, μ_{CO} = -0.882) with no changes for μ_{CO} with progressing WGS-conversion. The blue part without incline indicates the most stable structure in vacuum, while the violet part with incline shows the most stable structure with oxygen adsorbed. The shown promoter concentrations are:
(a/b) Substoichiometric fcc-Cu_3Ga/-Cu_3Zn (12.5 % Zn/Ga).
(c/d) Substoichiometric fcc-Cu_3Ga/-Cu_3Zn (18.75 % Zn/Ga).
(e/f) Stoichiometric fcc-Cu_3Ga/-Cu_3Zn (25 % Zn/Ga).
(g/h) Superstoichiometric fcc-Cu_3Ga/-Cu_3Zn (31.25 % Zn/Ga).
(i) Superstoichiometric fcc-Cu_3Zn (37.5 % Zn).
(j) Superstoichiometric fcc-Cu_3Zn (43.75 % Zn).

6 Surface Stability Diagrams in CO_2 Atmosphere

6.1 Individual Surface Stability Diagrams in CO_2 Atmosphere

(100)-Facet

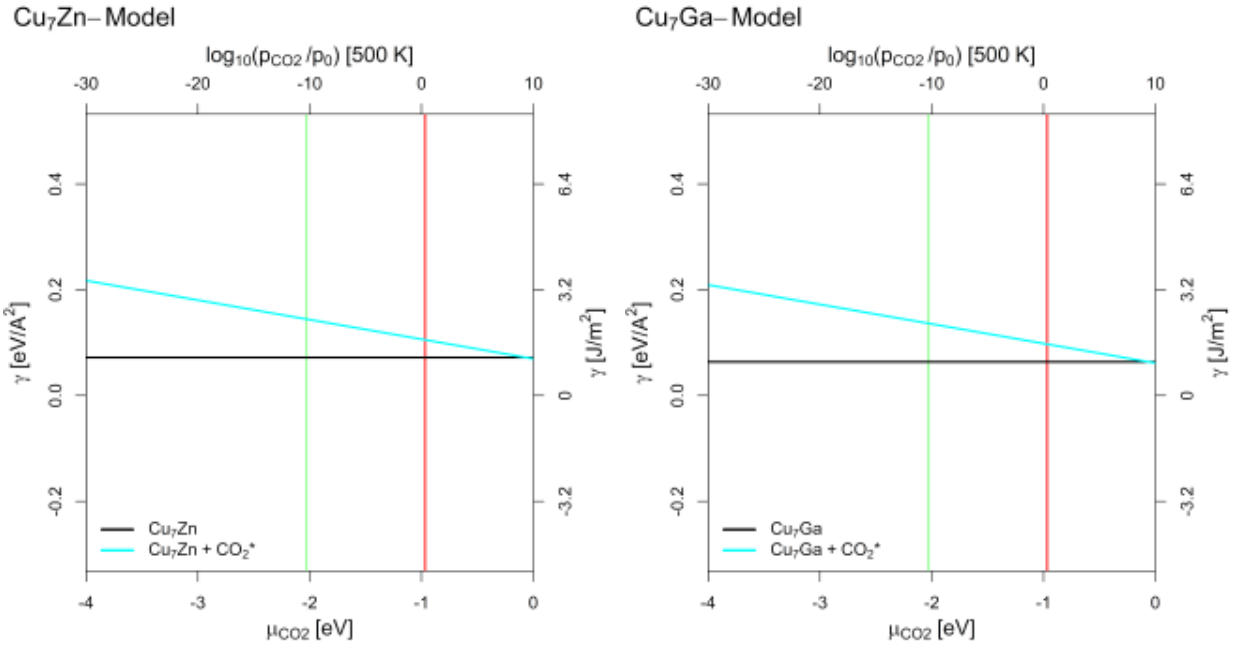

(a)

(b)

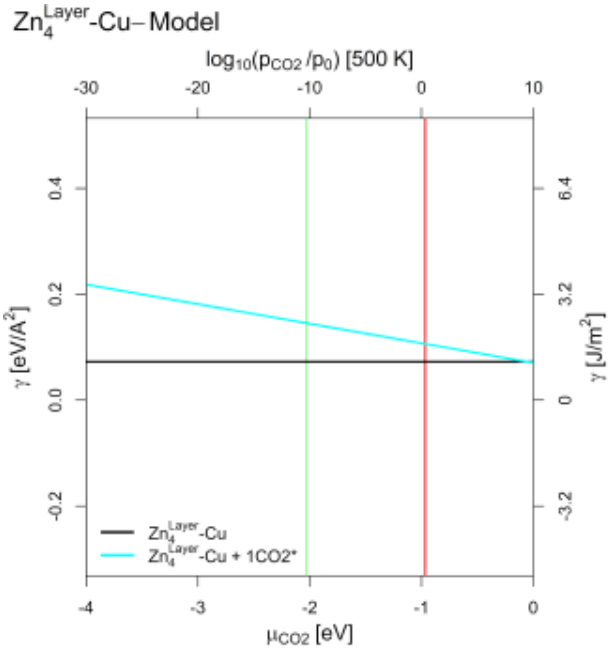

(c)

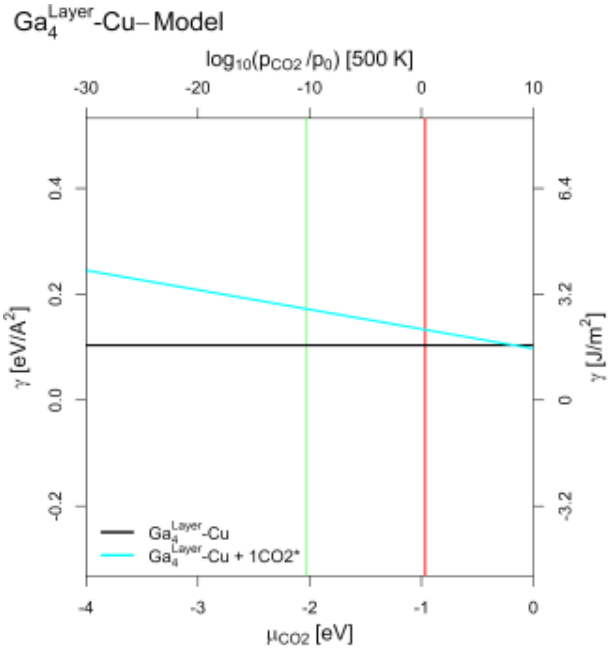

(d)

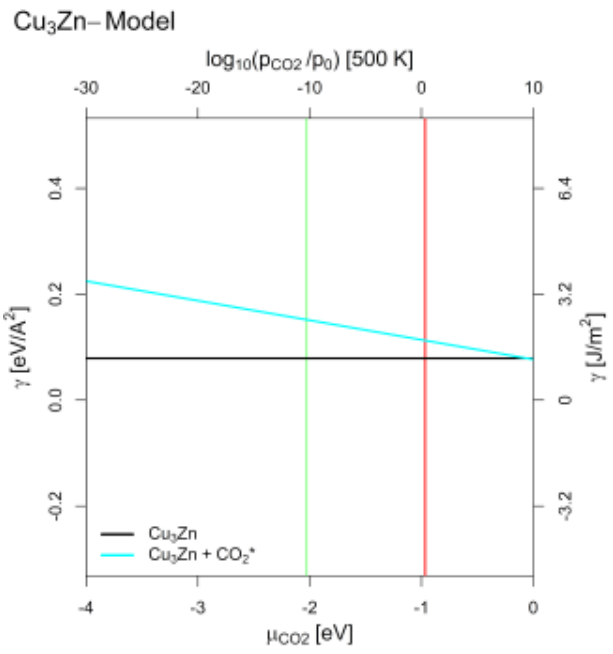
Cu3Zn – Model
log10(pCO2 /p0) [500 K]
-30
-20
-10
0
10
0.4
0.2
0.0
-0.2
γ [eV/Å2]
6.4
3.2
0
-3.2
γ [J/m2]
Cu3Zn
Cu3Zn + CO2*
-4
-3
-2
-1
0
μCO2 [eV]

(e)

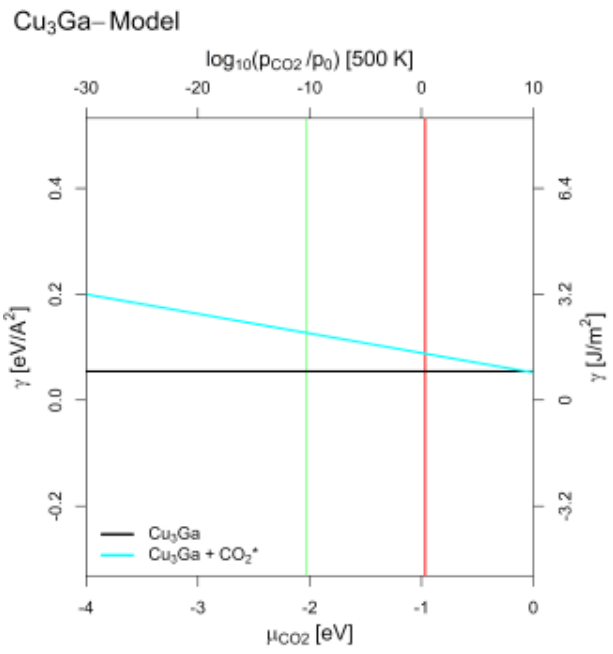
Cu3Ga – Model
log10(pCO2 /p0) [500 K]
-30
-20
-10
0
10
0.4
0.2
0.0
-0.2
γ [eV/Å2]
6.4
3.2
0
-3.2
γ [J/m2]
Cu3Ga
Cu3Ga + CO2*
-4
-3
-2
-1
0
μCO2 [eV]

(f)

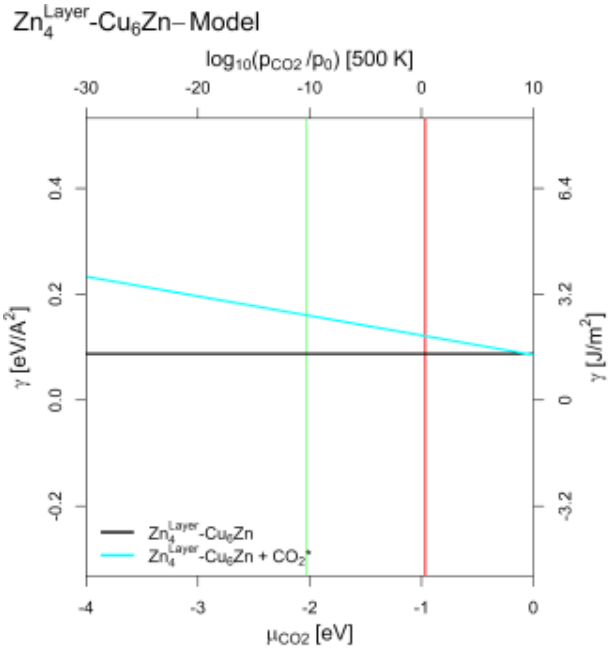
Zn4Layer-Cu6Zn – Model
log10(pCO2 /p0) [500 K]
-30
-20
-10
0
10
0.4
0.2
0.0
-0.2
γ [eV/Å2]
6.4
3.2
0
-3.2
γ [J/m2]
Zn4Layer-Cu6Zn
Zn4Layer-Cu6Zn + CO2*
-4
-3
-2
-1
0
μCO2 [eV]

(g)

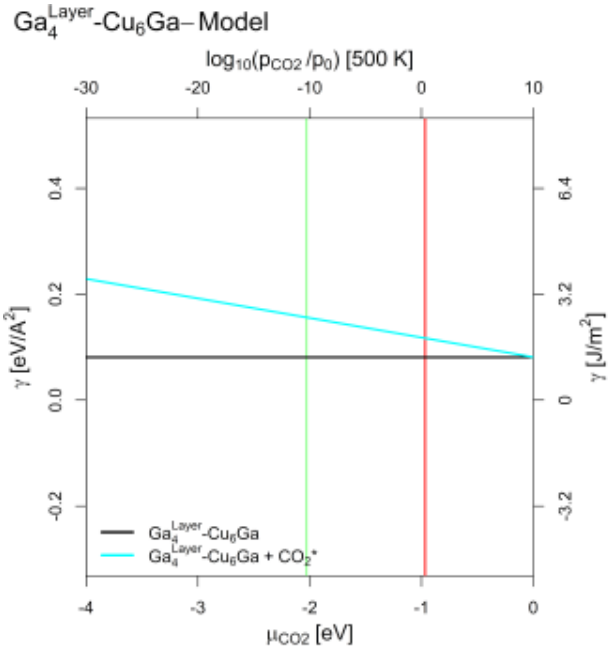
Ga4Layer-Cu6Ga – Model
log10(pCO2 /p0) [500 K]
-30
-20
-10
0
10
0.4
0.2
0.0
-0.2
γ [eV/Å2]
6.4
3.2
0
-3.2
γ [J/m2]
Ga4Layer-Cu6Ga
Ga4Layer-Cu6Ga + CO2*
-4
-3
-2
-1
0
μCO2 [eV]

(h)

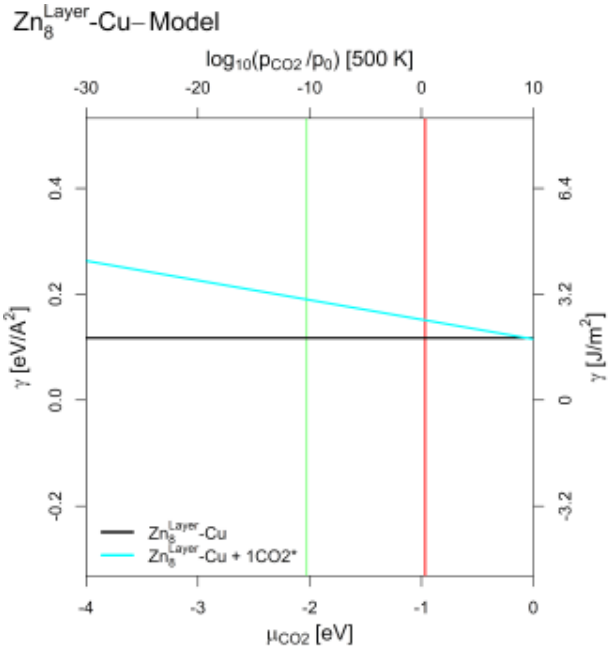
Zn_8^{Layer}-Cu– Model
$\log_{10}(p_{CO2}/p_0)$ [500 K]
-30 -20 -10 0 10
0.4 0.2 0.0 -0.2
6.4 3.2 0 -3.2
γ [eV/A²]
γ [J/m²]
Zn_8^{Layer}-Cu
Zn_8^{Layer}-Cu + 1CO2*
-4 -3 -2 -1 0
μ_{CO2} [eV]

(i)

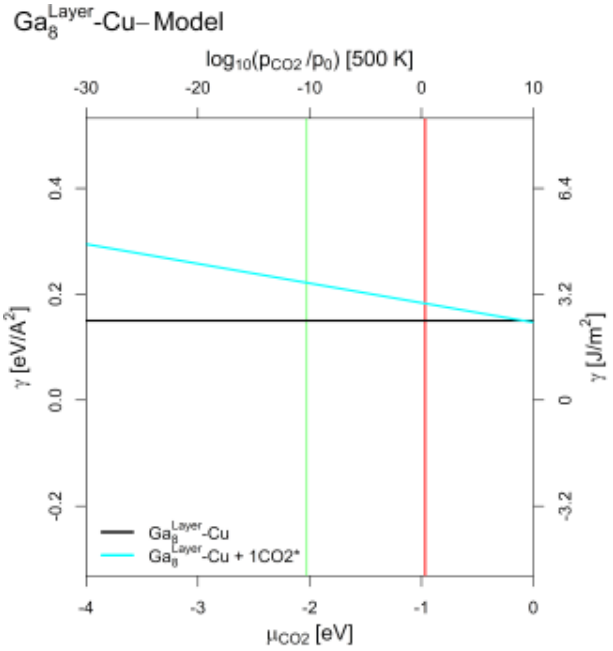
Ga_8^{Layer}-Cu– Model
$\log_{10}(p_{CO2}/p_0)$ [500 K]
-30 -20 -10 0 10
0.4 0.2 0.0 -0.2
6.4 3.2 0 -3.2
γ [eV/A²]
γ [J/m²]
Ga_8^{Layer}-Cu
Ga_8^{Layer}-Cu + 1CO2*
-4 -3 -2 -1 0
μ_{CO2} [eV]

(j)

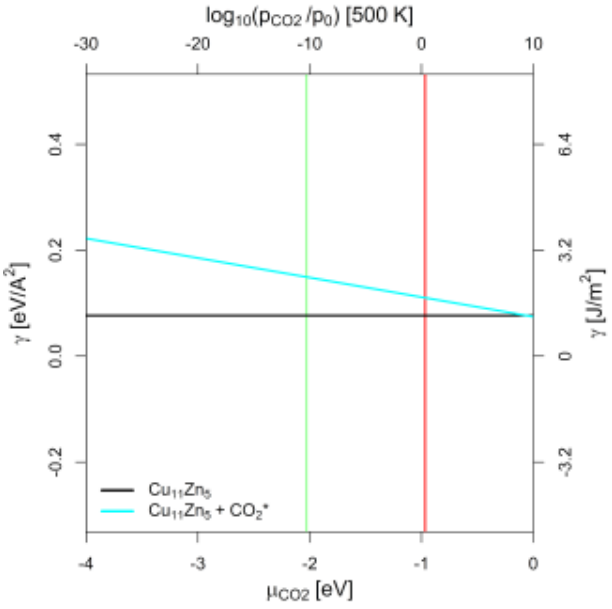
$Cu_{11}Zn_5$– Model
$\log_{10}(p_{CO2}/p_0)$ [500 K]
-30 -20 -10 0 10
0.4 0.2 0.0 -0.2
6.4 3.2 0 -3.2
γ [eV/A²]
γ [J/m²]
$Cu_{11}Zn_5$
$Cu_{11}Zn_5$ + CO_2*
-4 -3 -2 -1 0
μ_{CO2} [eV]

(k)

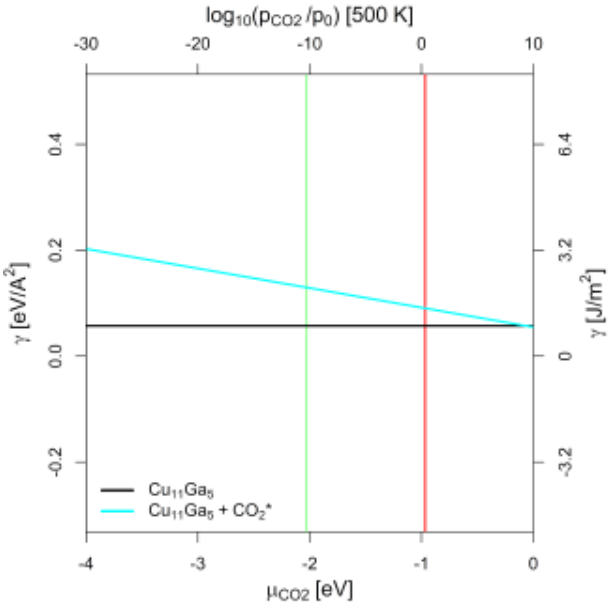
$Cu_{11}Ga_5$– Model
$\log_{10}(p_{CO2}/p_0)$ [500 K]
-30 -20 -10 0 10
0.4 0.2 0.0 -0.2
6.4 3.2 0 -3.2
γ [eV/A²]
γ [J/m²]
$Cu_{11}Ga_5$
$Cu_{11}Ga_5$ + CO_2*
-4 -3 -2 -1 0
μ_{CO2} [eV]

(l)

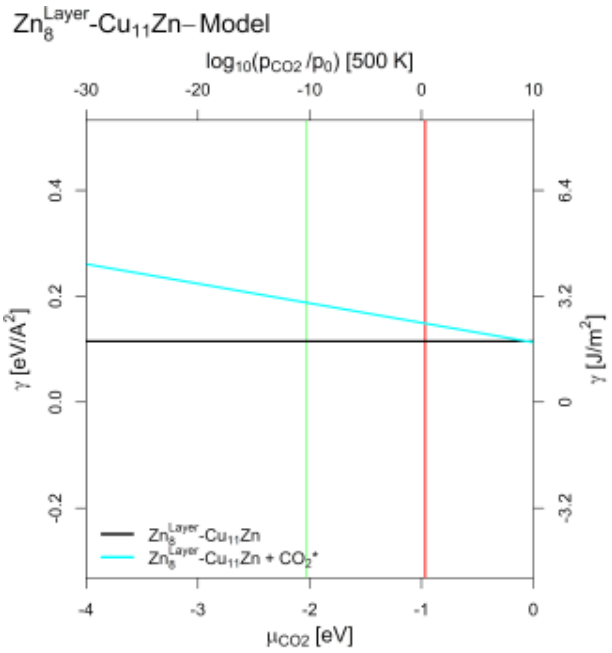
Zn_8^{Layer}-$Cu_{11}Zn$ – Model
$\log_{10}(p_{CO2}/p_0)$ [500 K]
-30 -20 -10 0 10
0.4 0.2 0.0 -0.2
6.4 3.2 0 -3.2
γ [eV/Å^2]
γ [J/m^2]
Zn_8^{Layer}-$Cu_{11}Zn$
Zn_8^{Layer}-$Cu_{11}Zn$ + CO_2*
-4 -3 -2 -1 0
μ_{CO2} [eV]

(m)

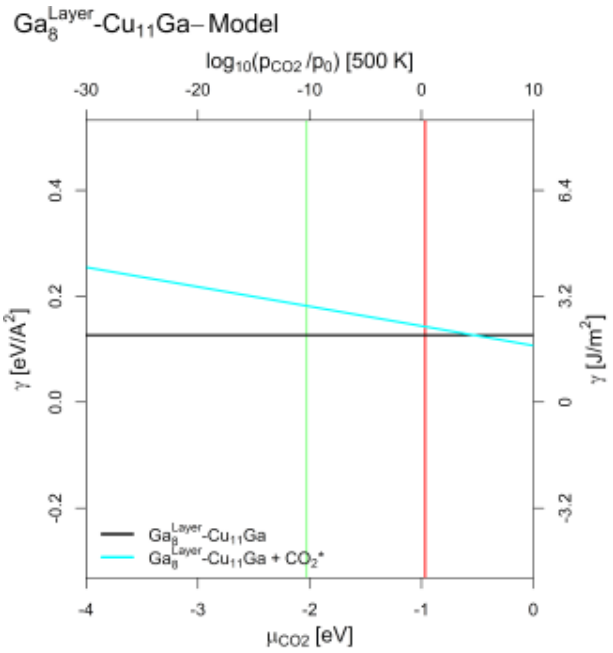
Ga_8^{Layer}-$Cu_{11}Ga$ – Model
$\log_{10}(p_{CO2}/p_0)$ [500 K]
-30 -20 -10 0 10
0.4 0.2 0.0 -0.2
6.4 3.2 0 -3.2
γ [eV/Å^2]
γ [J/m^2]
Ga_8^{Layer}-$Cu_{11}Ga$
Ga_8^{Layer}-$Cu_{11}Ga$ + CO_2*
-4 -3 -2 -1 0
μ_{CO2} [eV]

(n)

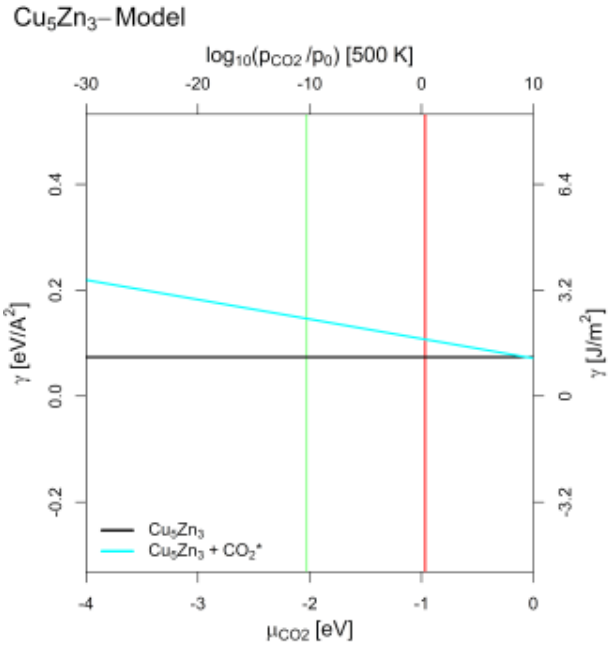
Cu_5Zn_3 – Model
$\log_{10}(p_{CO2}/p_0)$ [500 K]
-30 -20 -10 0 10
0.4 0.2 0.0 -0.2
6.4 3.2 0 -3.2
γ [eV/Å^2]
γ [J/m^2]
Cu_5Zn_3
Cu_5Zn_3 + CO_2*
-4 -3 -2 -1 0
μ_{CO2} [eV]

(o)

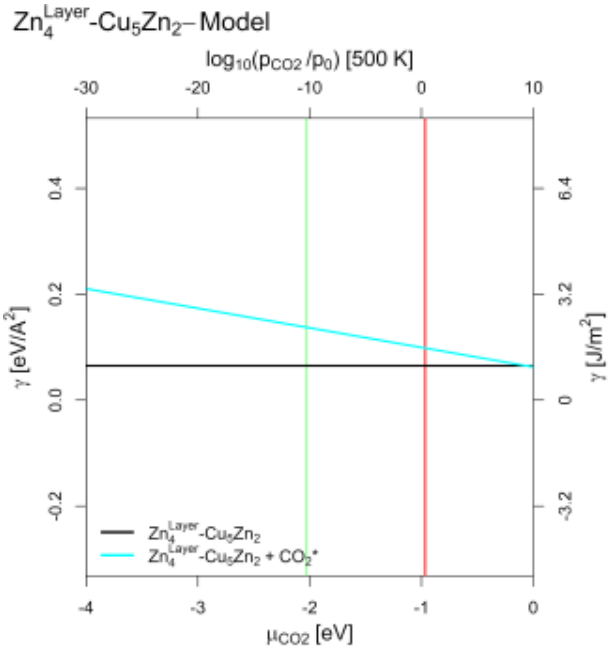
Zn_4^{Layer}-Cu_5Zn_2 – Model
$\log_{10}(p_{CO2}/p_0)$ [500 K]
-30 -20 -10 0 10
0.4 0.2 0.0 -0.2
6.4 3.2 0 -3.2
γ [eV/Å^2]
γ [J/m^2]
Zn_4^{Layer}-Cu_5Zn_2
Zn_4^{Layer}-Cu_5Zn_2 + CO_2*
-4 -3 -2 -1 0
μ_{CO2} [eV]

(p)

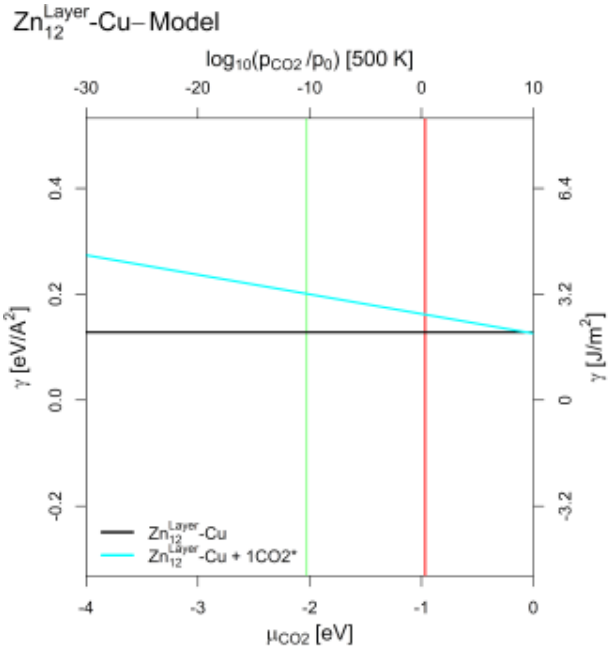
Zn12Layer-Cu– Model
log10(pCO2 /p0) [500 K]
-30
-20
-10
0
10
0.4
0.2
0.0
-0.2
γ [eV/A2]
6.4
3.2
0
-3.2
γ [J/m2]
Zn12Layer-Cu
Zn12Layer-Cu + 1CO2*
-4
-3
-2
-1
0
μCO2 [eV]

(q)

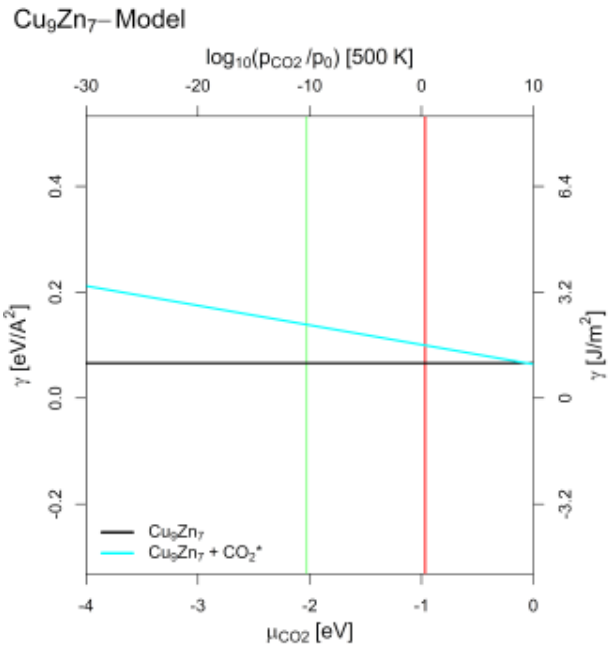
Cu9Zn7– Model
log10(pCO2 /p0) [500 K]
-30
-20
-10
0
10
0.4
0.2
0.0
-0.2
γ [eV/A2]
6.4
3.2
0
-3.2
γ [J/m2]
Cu9Zn7
Cu9Zn7 + CO2*
-4
-3
-2
-1
0
μCO2 [eV]

(r)

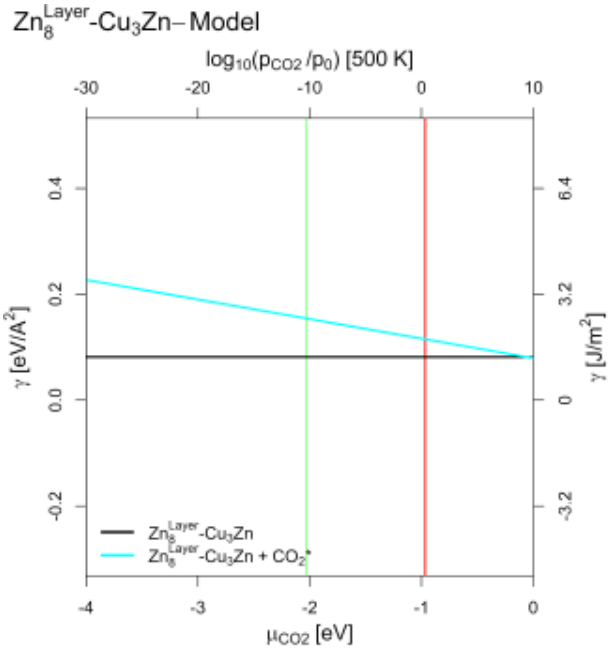
Zn8Layer-Cu3Zn– Model
log10(pCO2 /p0) [500 K]
-30
-20
-10
0
10
0.4
0.2
0.0
-0.2
γ [eV/A2]
6.4
3.2
0
-3.2
γ [J/m2]
Zn8Layer-Cu3Zn
Zn8Layer-Cu3Zn + CO2*
-4
-3
-2
-1
0
μCO2 [eV]

(s)

Figure S24: Surface stability diagram of the (100)-facet of the investigated CuGa-/CuZn-models depending on the chemical potential of CO_2 (μ_{CO_2} in eV) and the equivalent CO_2 partial pressure at 500 K. The red area indicates μ_{CO_2} expected under CO_2 hydrogenation conditions ($X_{CO_2} = 1$, -0.97 eV $\mu_{CO_2} < -0.96$ eV). The green area indicates the expected μ_{CO_2} under CO_2 hydrogenation conditions ($X_{CO_2} = 0$, -2.03 eV $< \mu_{CO_2} < -2.00$ eV). No CO_2 adsorption is expected for any of the investigated stoichiometries and facets. Used slab models for the (100)-facet used are:
(a/b) Unlayered substoichiometric fcc-Cu_3Ga/-Cu_3Zn (12.5 % Zn/Ga).
(c/d) One Ga/Zn surface layer on pure fcc-Cu (12.5 % Ga/Zn).
(e/f) Unlayered stoichiometric fcc-Cu_3Ga/-Cu_3Zn (25 % Ga/Zn).
(g/h) One Ga/Zn surface layer on substoichiometric fcc-Cu_3Ga/-Cu_3Zn (25 % Ga/Zn).
(i/j) Two Ga/Zn surface layers on pure fcc-Cu (25 % Ga/Zn).
(k/l) Unlayered superstoichiometric fcc-Cu_3Ga/-Cu_3Zn (31.25 % Ga/Zn).
(m/n) Two Ga/Zn surface layers on substoichiometric fcc-Cu_3Ga/-Cu_3Zn (31.25 % Ga/Zn).
(o) Unlayered supersubstoichiometric fcc-Cu_3Zn (37.5 % Zn).
(p) One Zn surface layer on fcc-Cu_3Zn (37.5 % Ga/Zn).
(q) Three Zn surface layers on pure fcc-Cu (37.5 % Ga/Zn).
(r) Unlayered supersubstoichiometric fcc-Cu_3Zn (43.75 % Zn).
(s) Two Zn surface layers on fcc-Cu_3Zn (43.75 % Ga/Zn).

(110)-Facet

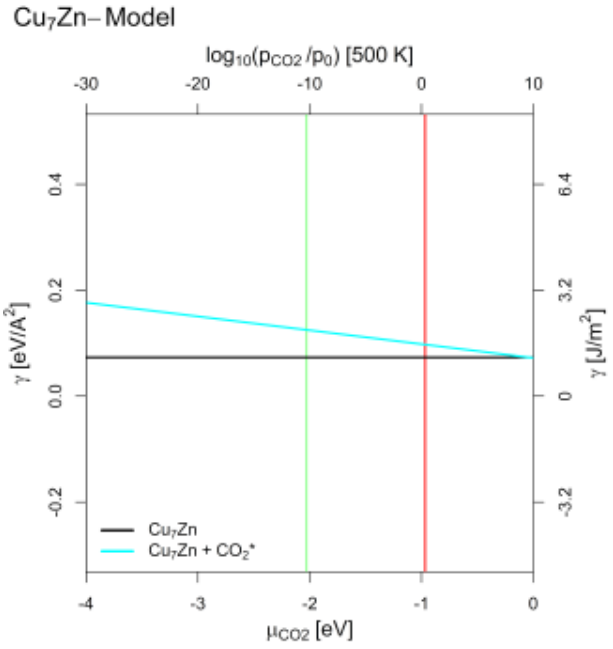

(a)

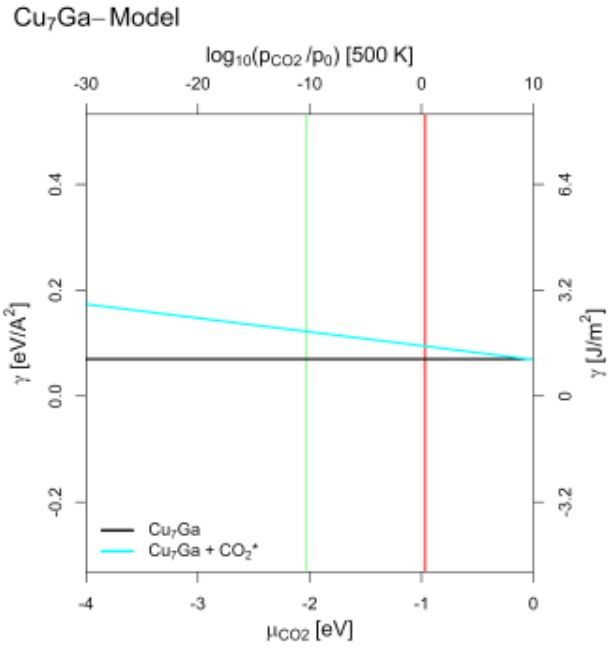

(b)

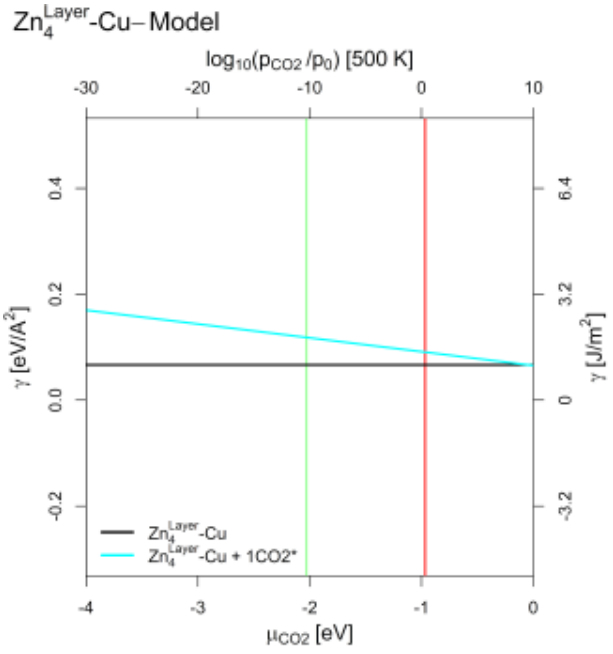

(c)

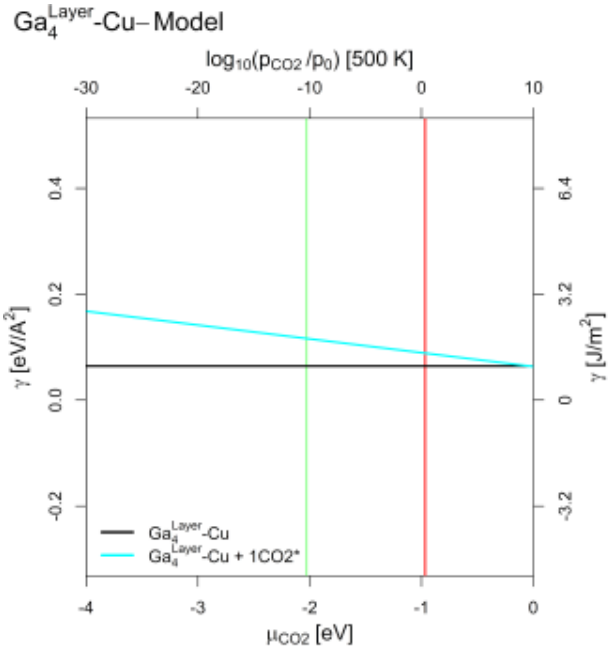

(d)

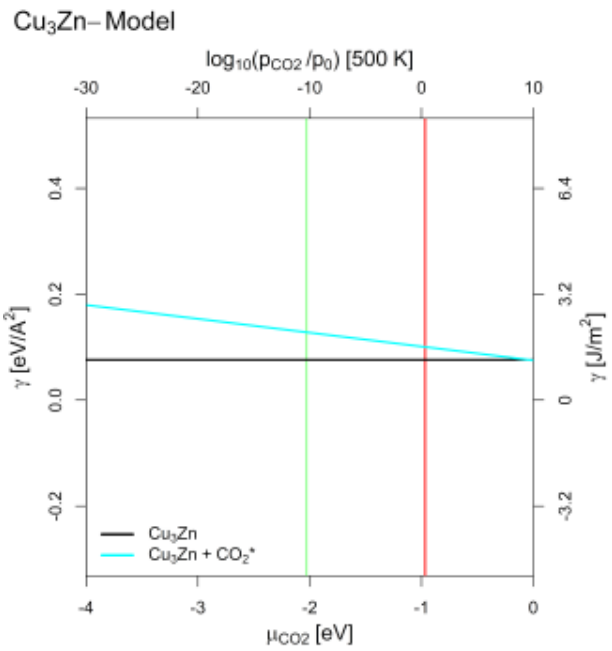
Cu3Zn−Model
log10(pCO2/p0) [500 K]
-30
-20
-10
0
10
0.4
0.2
0.0
-0.2
γ [eV/A2]
6.4
3.2
0
-3.2
γ [J/m2]
Cu3Zn
Cu3Zn + CO2*
-4
-3
-2
-1
0
μCO2 [eV]

(e)

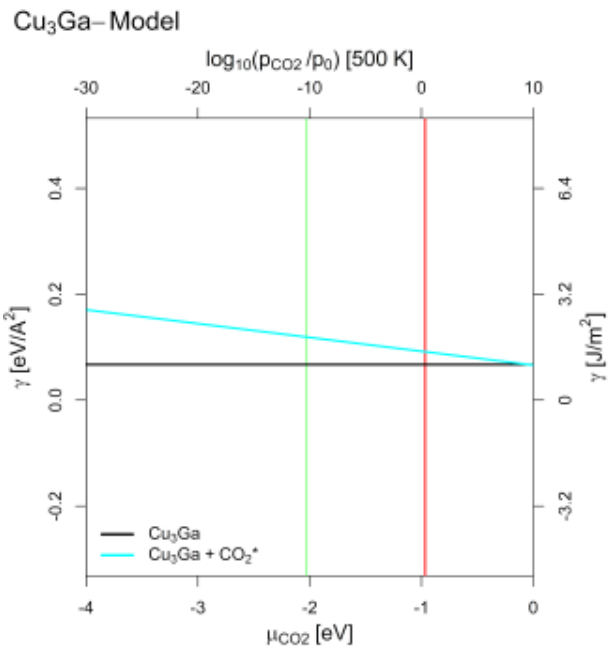
Cu3Ga−Model
log10(pCO2/p0) [500 K]
-30
-20
-10
0
10
0.4
0.2
0.0
-0.2
γ [eV/A2]
6.4
3.2
0
-3.2
γ [J/m2]
Cu3Ga
Cu3Ga + CO2*
-4
-3
-2
-1
0
μCO2 [eV]

(f)

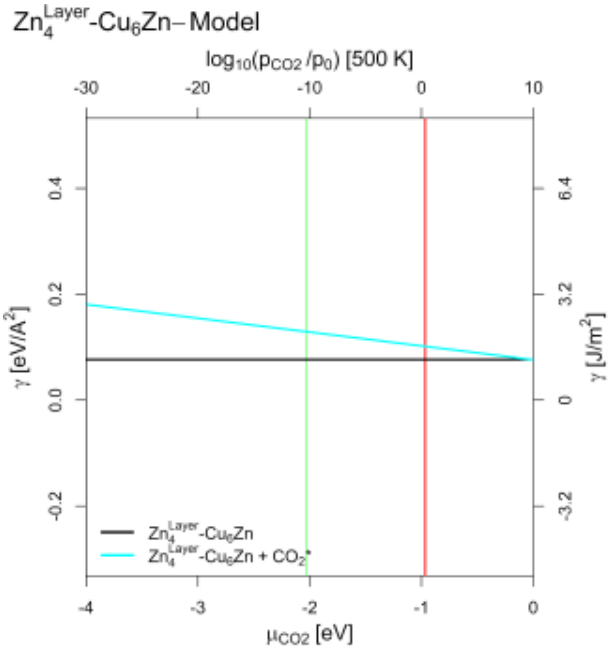
Zn4Layer-Cu6Zn−Model
log10(pCO2/p0) [500 K]
-30
-20
-10
0
10
0.4
0.2
0.0
-0.2
γ [eV/A2]
6.4
3.2
0
-3.2
γ [J/m2]
Zn4Layer-Cu6Zn
Zn4Layer-Cu6Zn + CO2*
-4
-3
-2
-1
0
μCO2 [eV]

(g)

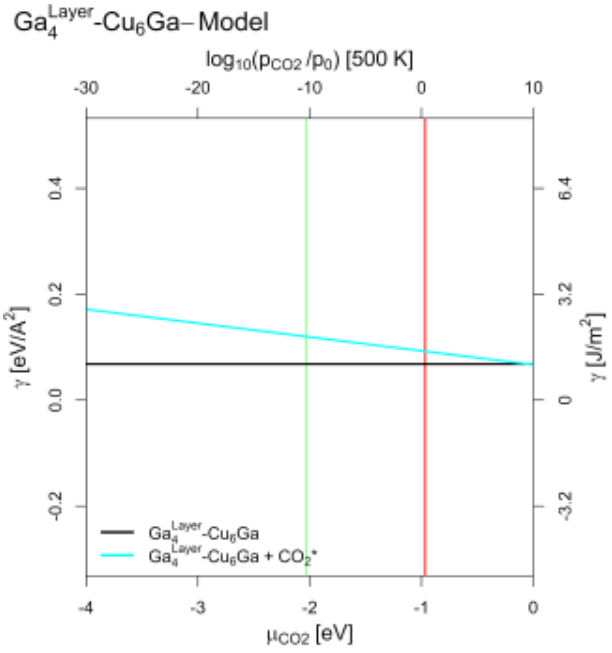
Ga4Layer-Cu6Ga−Model
log10(pCO2/p0) [500 K]
-30
-20
-10
0
10
0.4
0.2
0.0
-0.2
γ [eV/A2]
6.4
3.2
0
-3.2
γ [J/m2]
Ga4Layer-Cu6Ga
Ga4Layer-Cu6Ga + CO2*
-4
-3
-2
-1
0
μCO2 [eV]

(h)

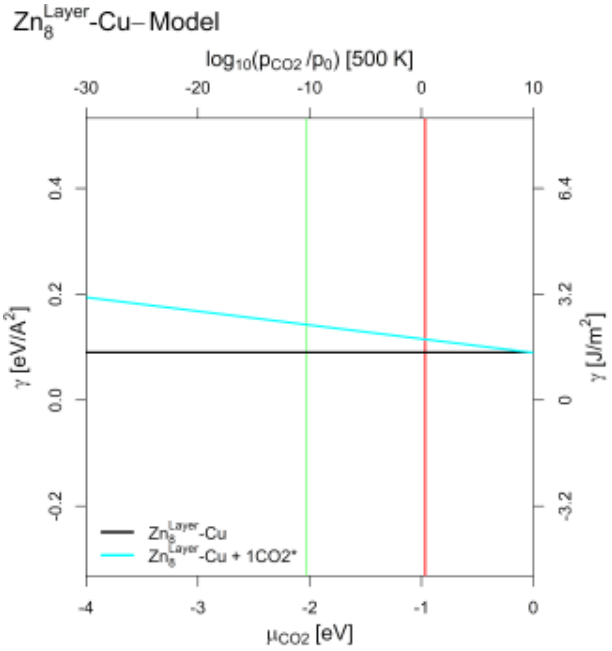
Zn_8^{Layer}-Cu– Model
$\log_{10}(p_{CO2}/p_0)$ [500 K]
-30 -20 -10 0 10
0.4 0.2 0.0 -0.2
6.4 3.2 0 -3.2
γ [eV/A²]
γ [J/m²]
Zn_8^{Layer}-Cu
Zn_8^{Layer}-Cu + 1CO2*
-4 -3 -2 -1 0
μ_{CO2} [eV]

(i)

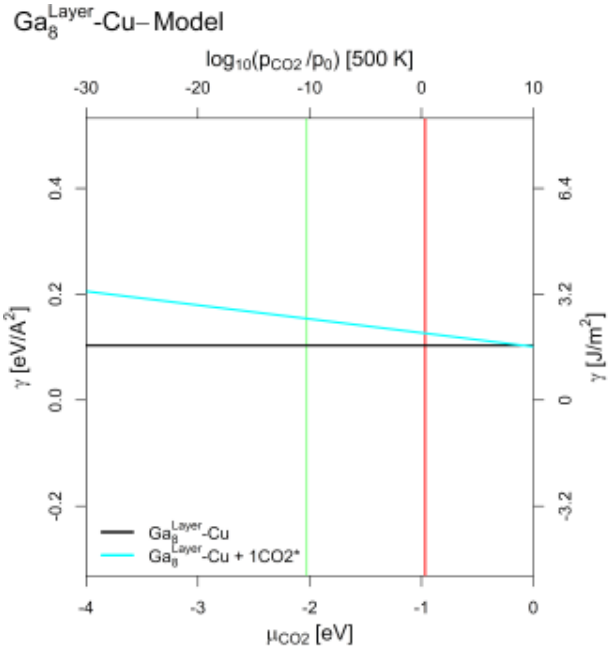
Ga_8^{Layer}-Cu– Model
$\log_{10}(p_{CO2}/p_0)$ [500 K]
-30 -20 -10 0 10
0.4 0.2 0.0 -0.2
6.4 3.2 0 -3.2
γ [eV/A²]
γ [J/m²]
Ga_8^{Layer}-Cu
Ga_8^{Layer}-Cu + 1CO2*
-4 -3 -2 -1 0
μ_{CO2} [eV]

(j)

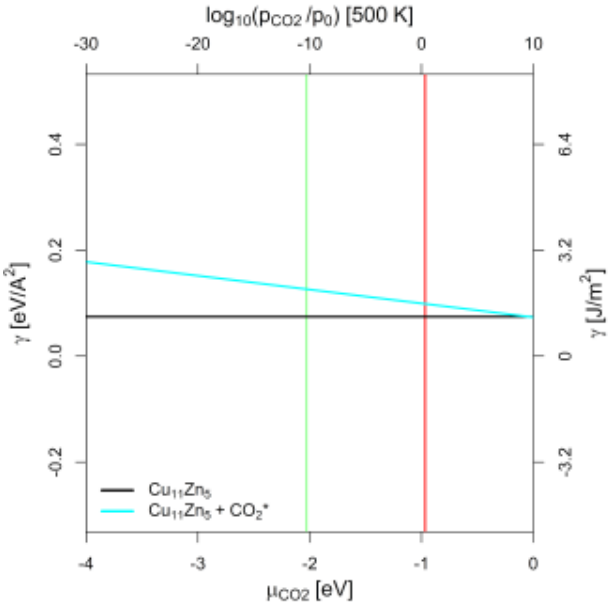
$Cu_{11}Zn_5$– Model
$\log_{10}(p_{CO2}/p_0)$ [500 K]
-30 -20 -10 0 10
0.4 0.2 0.0 -0.2
6.4 3.2 0 -3.2
γ [eV/A²]
γ [J/m²]
$Cu_{11}Zn_5$
$Cu_{11}Zn_5$ + CO_2*
-4 -3 -2 -1 0
μ_{CO2} [eV]

(k)

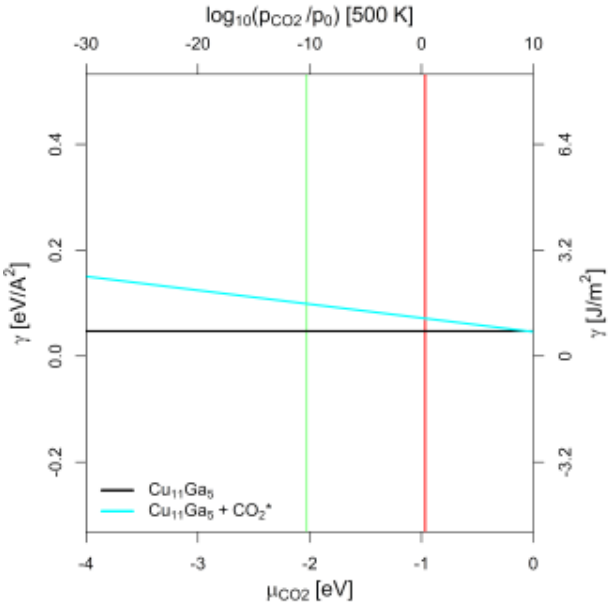
$Cu_{11}Ga_5$– Model
$\log_{10}(p_{CO2}/p_0)$ [500 K]
-30 -20 -10 0 10
0.4 0.2 0.0 -0.2
6.4 3.2 0 -3.2
γ [eV/A²]
γ [J/m²]
$Cu_{11}Ga_5$
$Cu_{11}Ga_5$ + CO_2*
-4 -3 -2 -1 0
μ_{CO2} [eV]

(l)

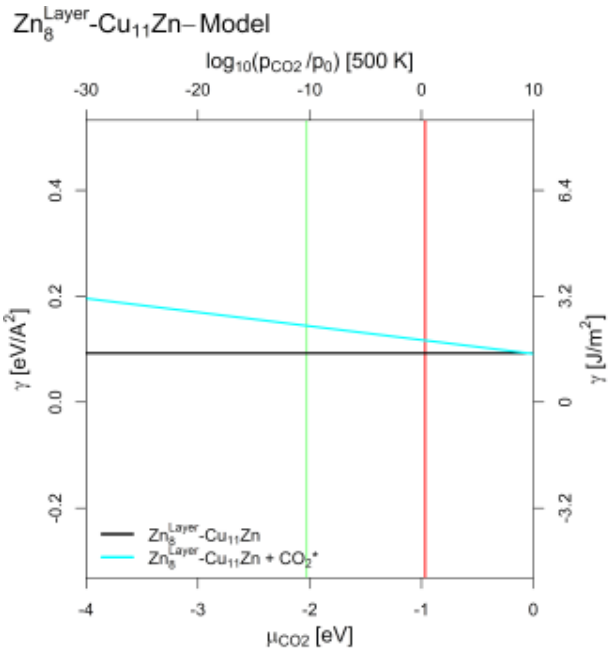
Zn_8^{Layer}-$Cu_{11}Zn$ – Model
$\log_{10}(p_{CO2}/p_0)$ [500 K]
-30 -20 -10 0 10
0.4 0.2 0.0 -0.2
6.4 3.2 0 -3.2
γ [eV/Å^2]
γ [J/m^2]
Zn_8^{Layer}-$Cu_{11}Zn$
Zn_8^{Layer}-$Cu_{11}Zn$ + CO_2*
-4 -3 -2 -1 0
μ_{CO2} [eV]

(m)

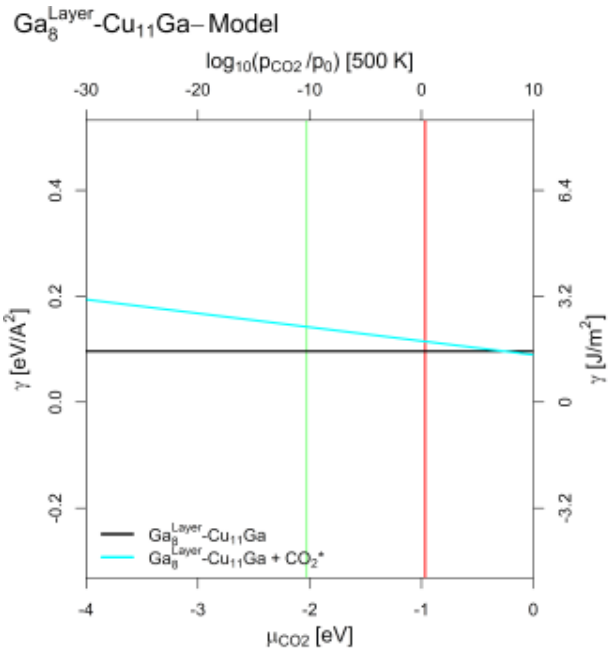
Ga_8^{Layer}-$Cu_{11}Ga$ – Model
$\log_{10}(p_{CO2}/p_0)$ [500 K]
-30 -20 -10 0 10
0.4 0.2 0.0 -0.2
6.4 3.2 0 -3.2
γ [eV/Å^2]
γ [J/m^2]
Ga_8^{Layer}-$Cu_{11}Ga$
Ga_8^{Layer}-$Cu_{11}Ga$ + CO_2*
-4 -3 -2 -1 0
μ_{CO2} [eV]

(n)

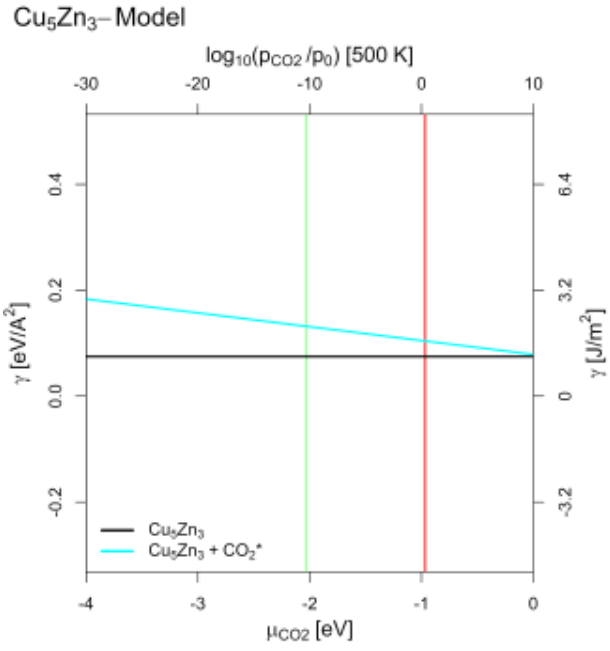
Cu_5Zn_3 – Model
$\log_{10}(p_{CO2}/p_0)$ [500 K]
-30 -20 -10 0 10
0.4 0.2 0.0 -0.2
6.4 3.2 0 -3.2
γ [eV/Å^2]
γ [J/m^2]
Cu_5Zn_3
Cu_5Zn_3 + CO_2*
-4 -3 -2 -1 0
μ_{CO2} [eV]

(o)

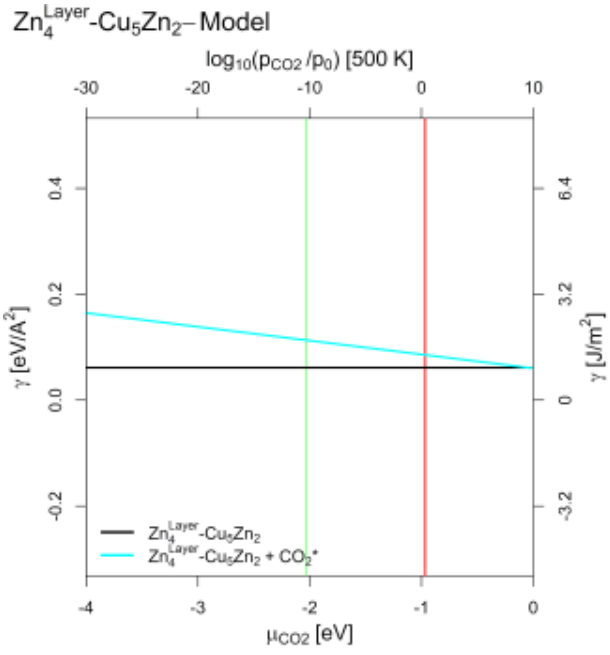
Zn_4^{Layer}-Cu_5Zn_2 – Model
$\log_{10}(p_{CO2}/p_0)$ [500 K]
-30 -20 -10 0 10
0.4 0.2 0.0 -0.2
6.4 3.2 0 -3.2
γ [eV/Å^2]
γ [J/m^2]
Zn_4^{Layer}-Cu_5Zn_2
Zn_4^{Layer}-Cu_5Zn_2 + CO_2*
-4 -3 -2 -1 0
μ_{CO2} [eV]

(p)

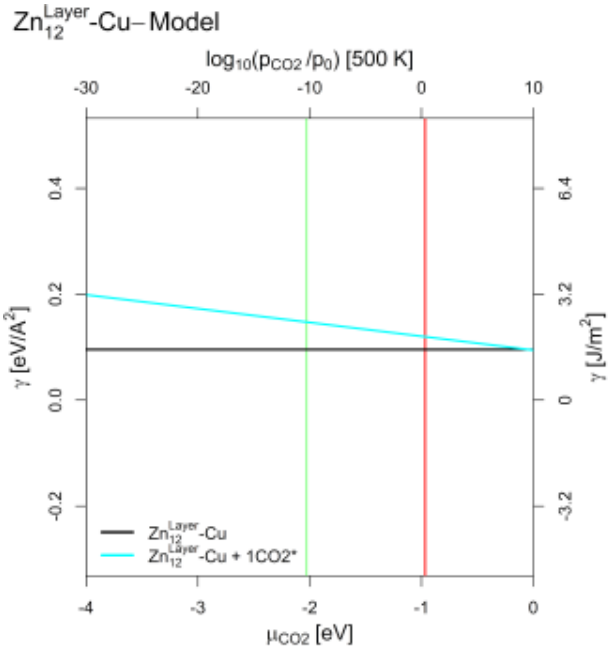
Zn_{12}^{Layer}-Cu– Model
$\log_{10}(p_{CO2}/p_0)$ [500 K]
-30
-20
-10
0
10
0.4
0.2
0.0
-0.2
6.4
3.2
0
-3.2
γ [eV/A²]
γ [J/m²]
Zn_{12}^{Layer}-Cu
Zn_{12}^{Layer}-Cu + 1CO2*
-4
-3
-2
-1
0
μ_{CO2} [eV]

(q)

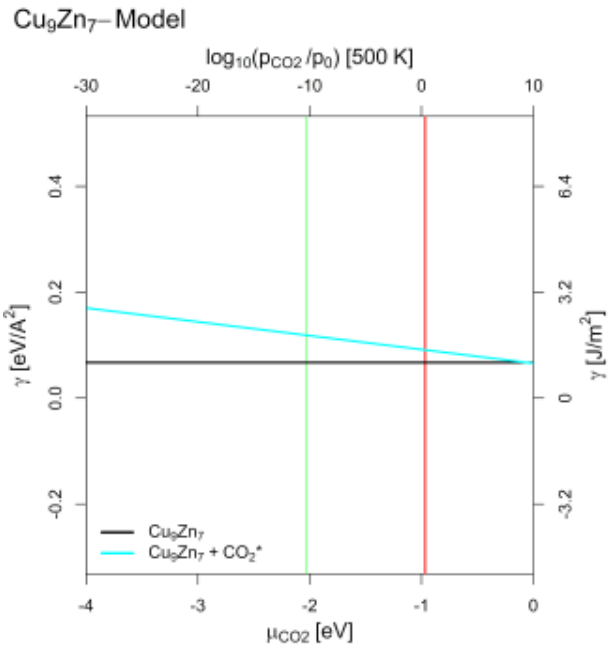
Cu_9Zn_7– Model
$\log_{10}(p_{CO2}/p_0)$ [500 K]
-30
-20
-10
0
10
0.4
0.2
0.0
-0.2
6.4
3.2
0
-3.2
γ [eV/A²]
γ [J/m²]
Cu_9Zn_7
Cu_9Zn_7 + CO_2*
-4
-3
-2
-1
0
μ_{CO2} [eV]

(r)

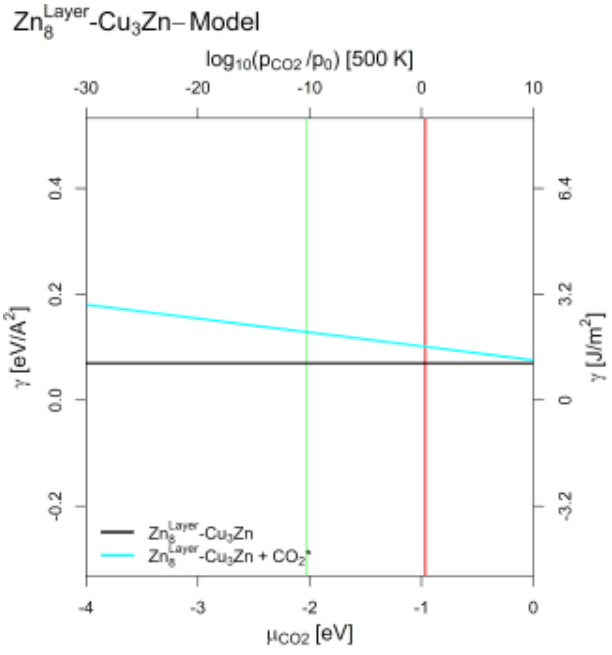
Zn_8^{Layer}-Cu_3Zn– Model
$\log_{10}(p_{CO2}/p_0)$ [500 K]
-30
-20
-10
0
10
0.4
0.2
0.0
-0.2
6.4
3.2
0
-3.2
γ [eV/A²]
γ [J/m²]
Zn_8^{Layer}-Cu_3Zn
Zn_8^{Layer}-Cu_3Zn + CO_2*
-4
-3
-2
-1
0
μ_{CO2} [eV]

(s)

Figure S25: Surface stability diagram of the (110)-facet of the investigated CuGa-/CuZn-models depending on the chemical potential of CO_2 (μ_{CO_2} in eV) and the equivalent CO_2 partial pressure at 500 K. The red area indicates μ_{CO_2} expected under CO_2 hydrogenation conditions ($X_{CO_2} = 1$, -0.97 eV $\mu_{CO_2} < -0.96$ eV). The green area indicates the expected μ_{CO_2} under CO_2 hydrogenation conditions ($X_{CO_2} = 0$, -2.03 eV $< \mu_{CO_2} < -2.00$ eV). No CO_2 adsorption is expected for any of the investigated stoichiometries and facets. Used slab models for the (110)-facet used are:
(a/b) Unlayered substoichiometric fcc-Cu_3Ga/-Cu_3Zn (12.5 % Zn/Ga).
(c/d) One Ga/Zn surface layer on pure fcc-Cu (12.5 % Ga/Zn).
(e/f) Unlayered stoichiometric fcc-Cu_3Ga/-Cu_3Zn (25 % Ga/Zn).
(g/h) One Ga/Zn surface layer on substoichiometric fcc-Cu_3Ga/-Cu_3Zn (25 % Ga/Zn).
(i/j) Two Ga/Zn surface layers on pure fcc-Cu (25 % Ga/Zn).
(k/l) Unlayered superstoichiometric fcc-Cu_3Ga/-Cu_3Zn (31.25 % Ga/Zn).
(m/n) Two Ga/Zn surface layers on substoichiometric fcc-Cu_3Ga/-Cu_3Zn (31.25 % Ga/Zn).
(o) Unlayered supersubstoichiometric fcc-Cu_3Zn (37.5 % Zn).
(p) One Zn surface layer on fcc-Cu_3Zn (37.5 % Ga/Zn).
(q) Three Zn surface layers on pure fcc-Cu (37.5 % Ga/Zn).
(r) Unlayered supersubstoichiometric fcc-Cu_3Zn (43.75 % Zn).
(s) Two Zn surface layers on fcc-Cu_3Zn (43.75 % Ga/Zn).

(111)-Facet

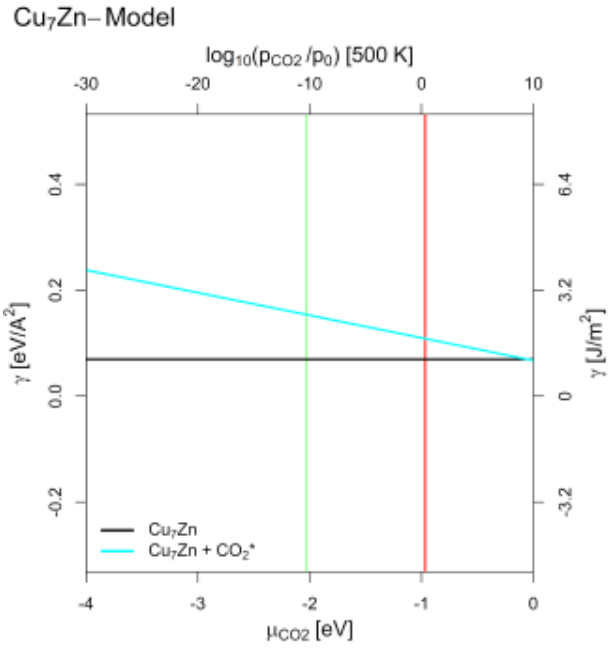

(a)

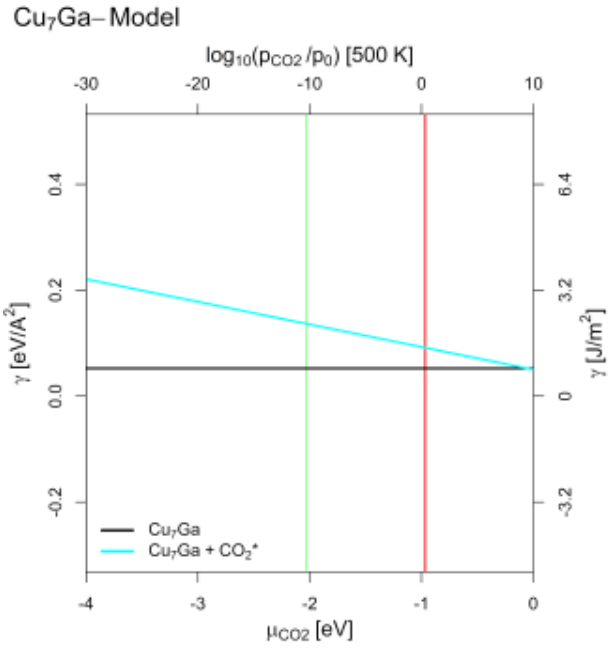

(b)

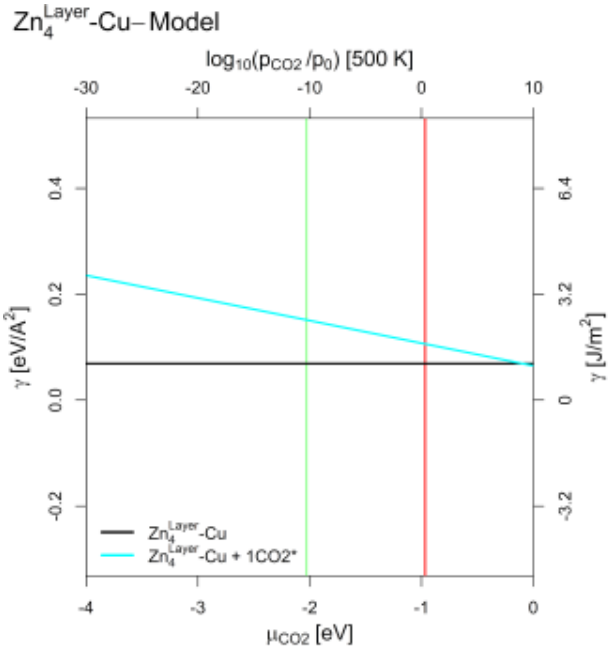

(c)

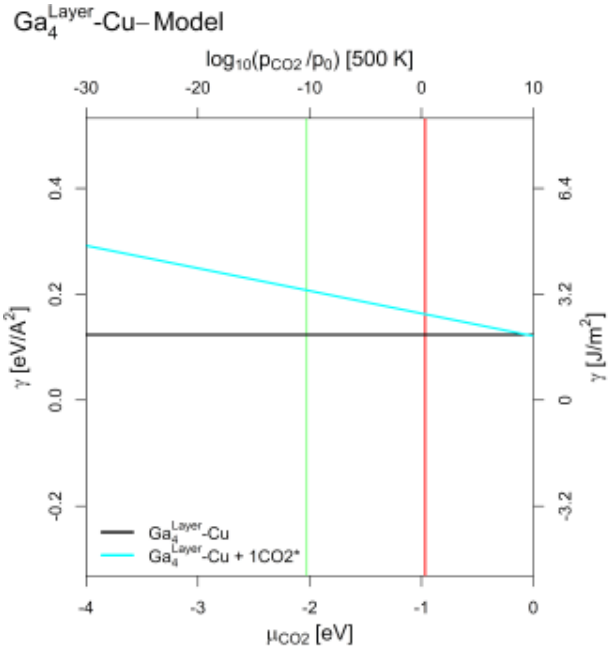

(d)

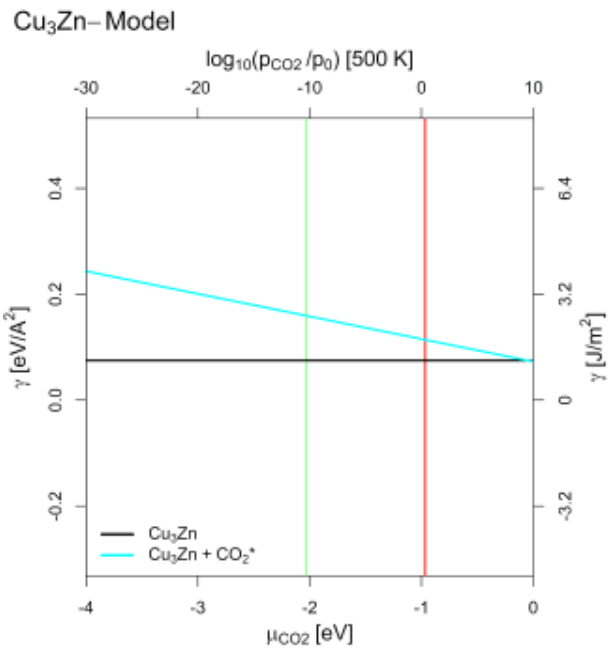
Cu3Zn – Model
log10(pCO2/p0) [500 K]
-30
-20
-10
0
10
0.4
0.2
0.0
-0.2
γ [eV/A2]
6.4
3.2
0
-3.2
γ [J/m2]
Cu3Zn
Cu3Zn + CO2*
-4
-3
-2
-1
0
μCO2 [eV]

(e)

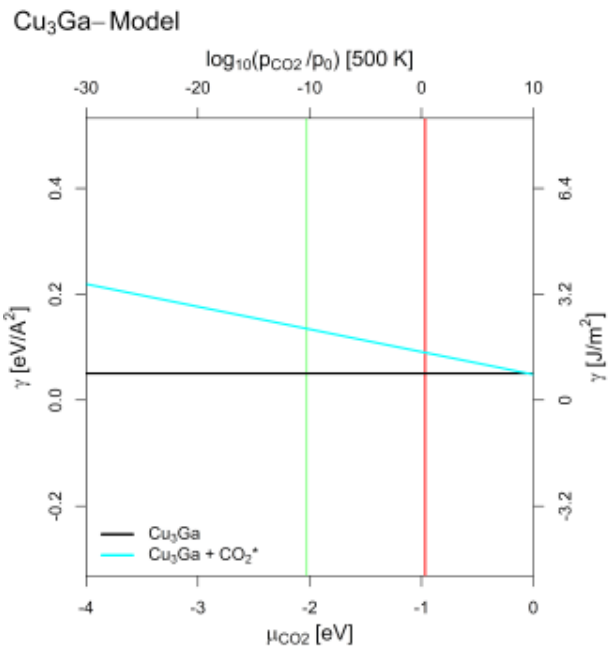
Cu3Ga – Model
log10(pCO2/p0) [500 K]
-30
-20
-10
0
10
0.4
0.2
0.0
-0.2
γ [eV/A2]
6.4
3.2
0
-3.2
γ [J/m2]
Cu3Ga
Cu3Ga + CO2*
-4
-3
-2
-1
0
μCO2 [eV]

(f)

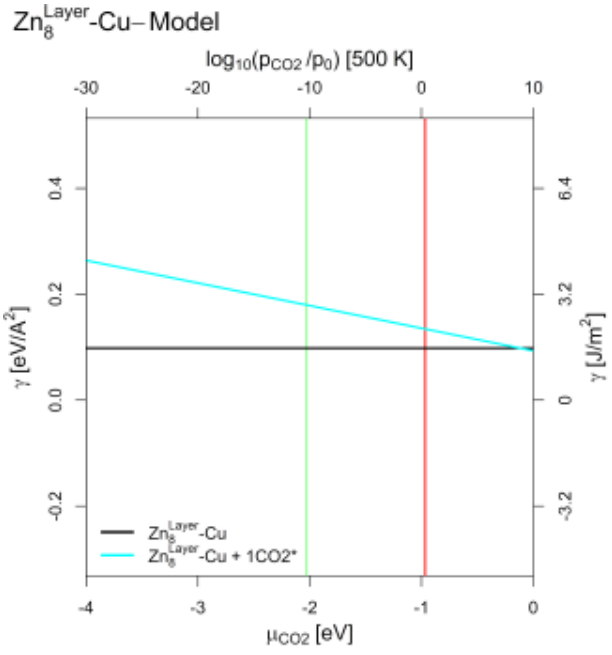
Zn8Layer-Cu – Model
log10(pCO2/p0) [500 K]
-30
-20
-10
0
10
0.4
0.2
0.0
-0.2
γ [eV/A2]
6.4
3.2
0
-3.2
γ [J/m2]
Zn8Layer-Cu
Zn8Layer-Cu + 1CO2*
-4
-3
-2
-1
0
μCO2 [eV]

(g)

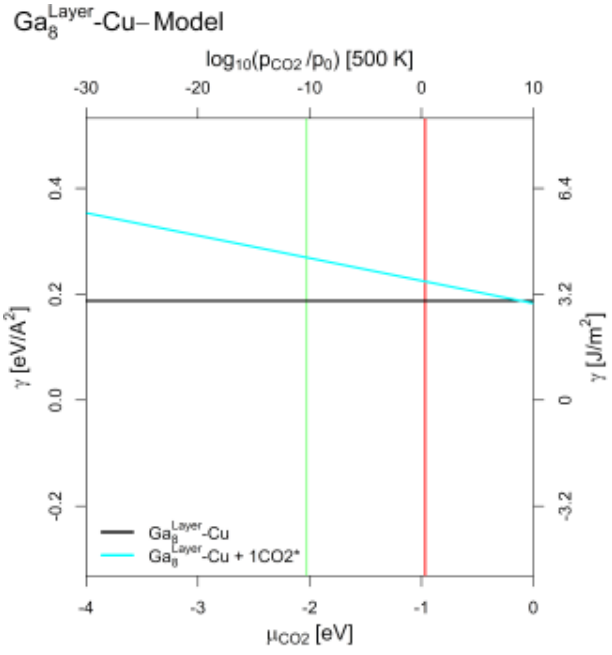
Ga8Layer-Cu – Model
log10(pCO2/p0) [500 K]
-30
-20
-10
0
10
0.4
0.2
0.0
-0.2
γ [eV/A2]
6.4
3.2
0
-3.2
γ [J/m2]
Ga8Layer-Cu
Ga8Layer-Cu + 1CO2*
-4
-3
-2
-1
0
μCO2 [eV]

(h)

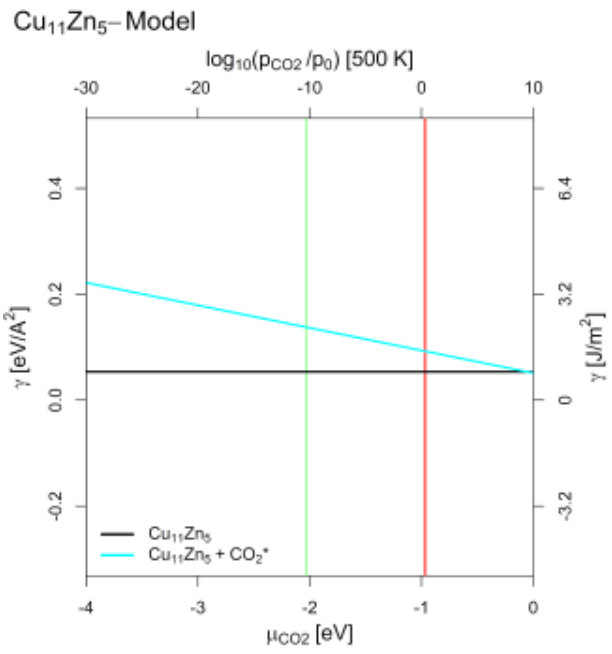
Cu11Zn5 – Model
log10(pCO2/p0) [500 K]
-30
-20
-10
0
10
0.4
0.2
0.0
-0.2
γ [eV/A2]
6.4
3.2
0
-3.2
γ [J/m2]
Cu11Zn5
Cu11Zn5 + CO2*
-4
-3
-2
-1
0
μCO2 [eV]

(i)

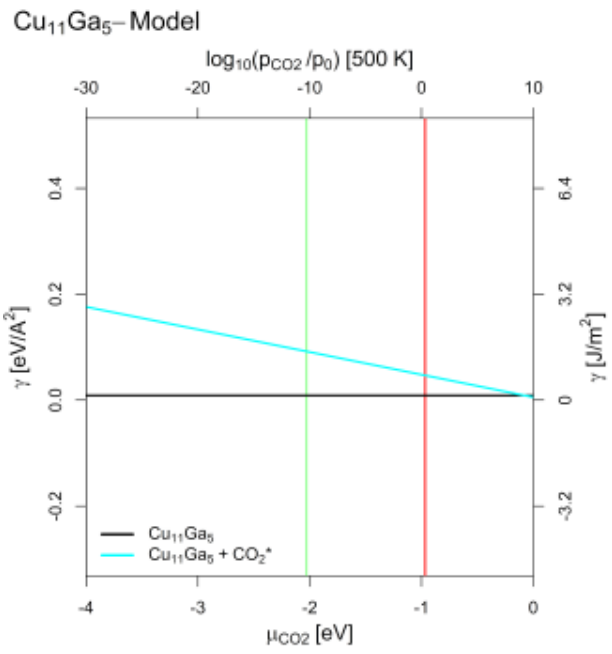
Cu11Ga5 – Model
log10(pCO2/p0) [500 K]
-30
-20
-10
0
10
0.4
0.2
0.0
-0.2
γ [eV/A2]
6.4
3.2
0
-3.2
γ [J/m2]
Cu11Ga5
Cu11Ga5 + CO2*
-4
-3
-2
-1
0
μCO2 [eV]

(j)

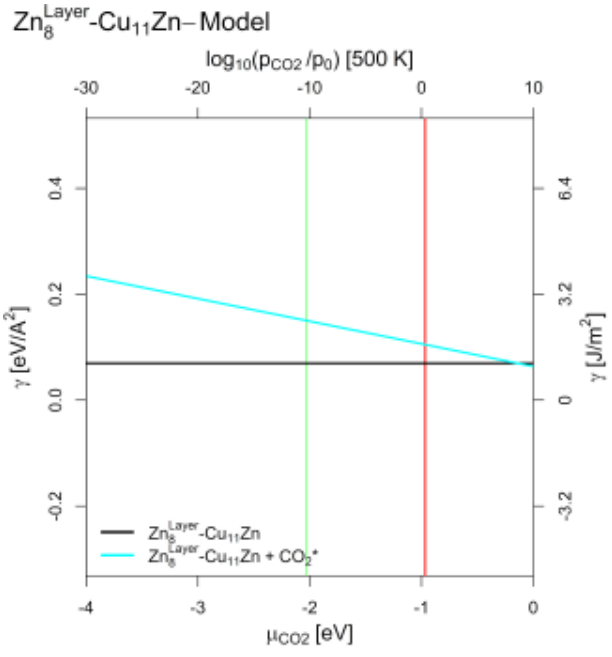
Zn8Layer-Cu11Zn – Model
log10(pCO2/p0) [500 K]
-30
-20
-10
0
10
0.4
0.2
0.0
-0.2
γ [eV/A2]
6.4
3.2
0
-3.2
γ [J/m2]
Zn8Layer-Cu11Zn
Zn8Layer-Cu11Zn + CO2*
-4
-3
-2
-1
0
μCO2 [eV]

(k)

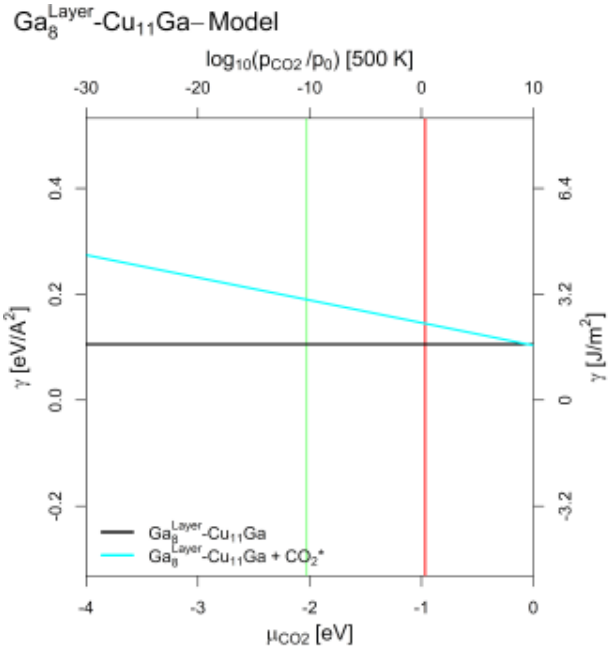
Ga8Layer-Cu11Ga – Model
log10(pCO2/p0) [500 K]
-30
-20
-10
0
10
0.4
0.2
0.0
-0.2
γ [eV/A2]
6.4
3.2
0
-3.2
γ [J/m2]
Ga8Layer-Cu11Ga
Ga8Layer-Cu11Ga + CO2*
-4
-3
-2
-1
0
μCO2 [eV]

(l)

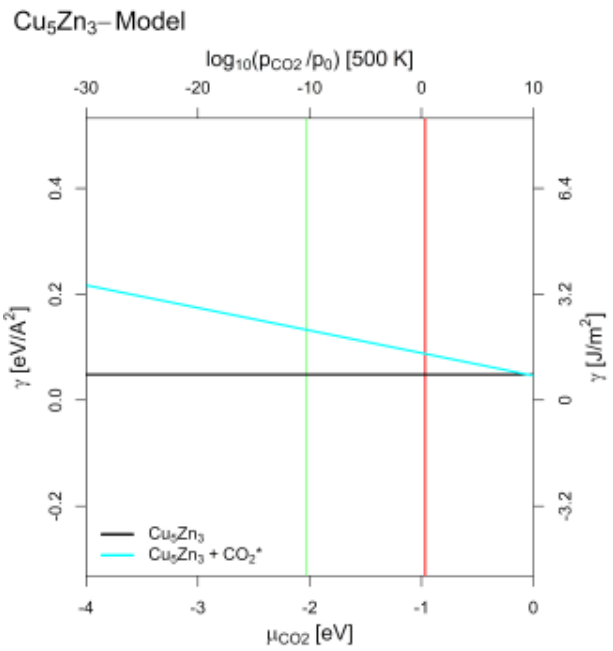
Cu5Zn3 – Model
log10(pCO2/p0) [500 K]
-30
-20
-10
0
10
0.4
0.2
0.0
-0.2
6.4
3.2
0
-3.2
γ [eV/A2]
γ [J/m2]
Cu5Zn3
Cu5Zn3 + CO2*
-4
-3
-2
-1
0
μCO2 [eV]

(m)

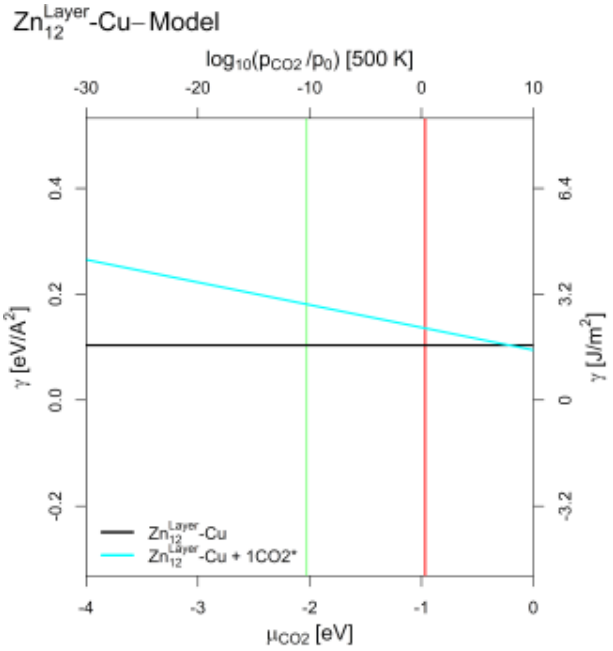
Zn12Layer-Cu – Model
log10(pCO2/p0) [500 K]
-30
-20
-10
0
10
0.4
0.2
0.0
-0.2
6.4
3.2
0
-3.2
γ [eV/A2]
γ [J/m2]
Zn12Layer-Cu
Zn12Layer-Cu + 1CO2*
-4
-3
-2
-1
0
μCO2 [eV]

(n)

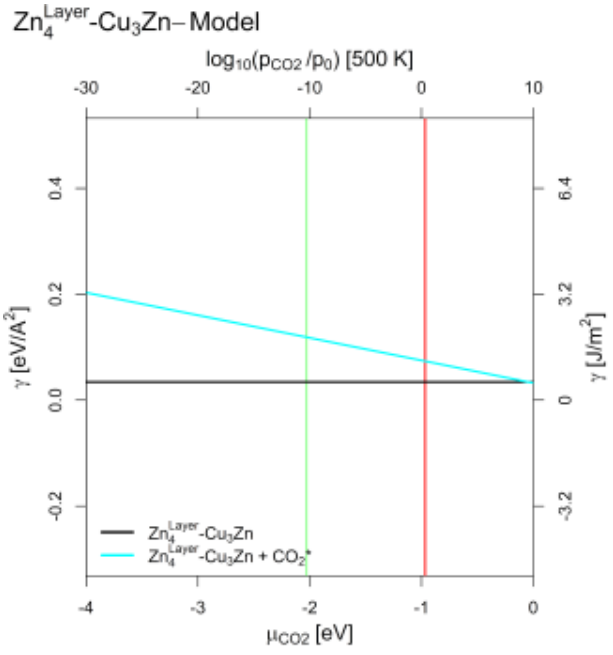
Zn4Layer-Cu3Zn – Model
log10(pCO2/p0) [500 K]
-30
-20
-10
0
10
0.4
0.2
0.0
-0.2
6.4
3.2
0
-3.2
γ [eV/A2]
γ [J/m2]
Zn4Layer-Cu3Zn
Zn4Layer-Cu3Zn + CO2*
-4
-3
-2
-1
0
μCO2 [eV]

(o)

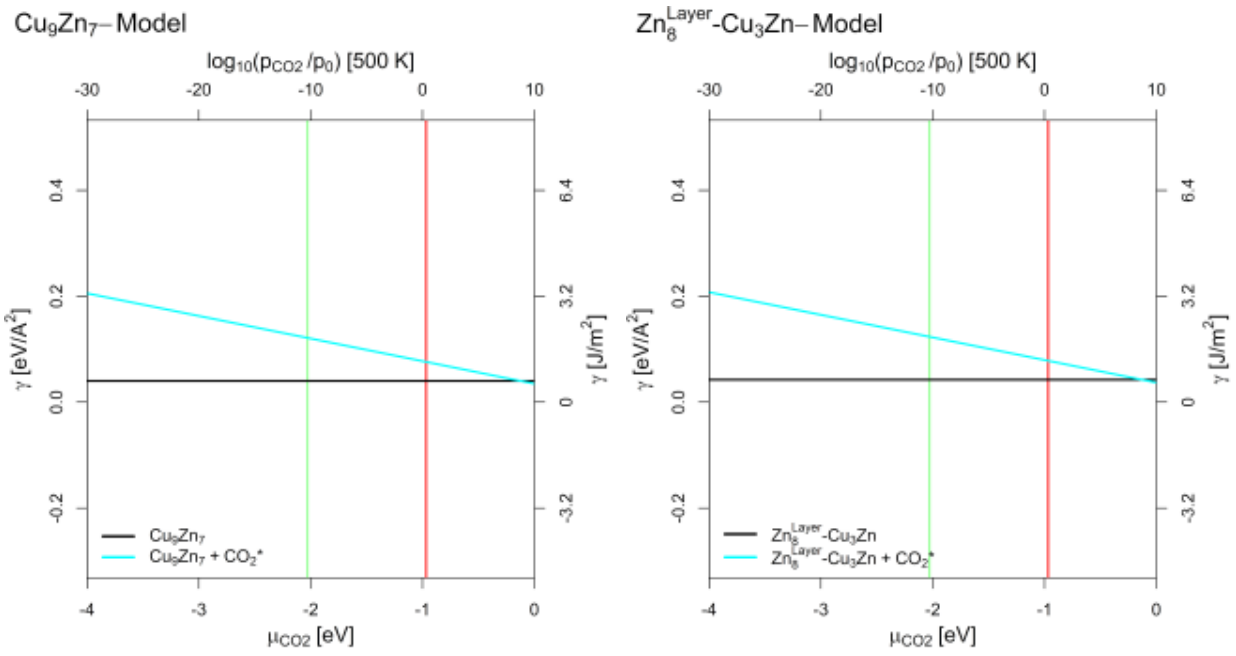

(p) (q)

Figure S26: Surface stability diagram of the (111)-facet of the investigated CuGa-/CuZn-models depending on the chemical potential of CO_2 (μ_{CO_2} in eV) and the equivalent CO_2 partial pressure at 500 K. The red area indicates μ_{CO_2} expected under CO_2 hydrogenation conditions ($X_{CO_2} = 1$, -0.97 eV $\mu_{CO_2} < -0.96$ eV). The green area indicates the expected μ_{CO_2} under CO_2 hydrogenation conditions ($X_{CO_2} = 0$, -2.03 eV $< \mu_{CO_2} < -2.00$ eV). No CO_2 adsorption is expected for any of the investigated stoichiometries and facets. Used slab models for the (111)-facet used are:
(a/b) Unlayered substoichiometric fcc-Cu_3Ga/-Cu_3Zn (12.5 % Zn/Ga).
(c/d) One Ga/Zn surface layer on pure fcc-Cu (12.5 % Ga/Zn).
(e/f) Unlayered stoichiometric fcc-Cu_3Ga/-Cu_3Zn (25 % Ga/Zn).
(g/h) Two Ga/Zn surface layers on pure fcc-Cu (25 % Ga/Zn).
(i/j) Unlayered superstoichiometric fcc-Cu_3Ga/-Cu_3Zn (31.25 % Ga/Zn).
(k/l) Two Ga/Zn surface layers on substoichiometric fcc-Cu_3Ga/-Cu_3Zn (31.25 % Ga/Zn).
(m) Unlayered supersubstoichiometric fcc-Cu_3Zn (37.5 % Zn).
(n) Three Zn surface layers on pure fcc-Cu (37.5 % Ga/Zn).
(o) One Zn surface layer on fcc-Cu_3Zn (34.375 % Ga/Zn).
(p) Unlayered supersubstoichiometric fcc-Cu_3Zn (43.75 % Zn).
(q) Two Zn surface layers on fcc-Cu_3Zn (43.75 % Ga/Zn).

6.2 Individual Surface Energies Depending on the CO_2 Chemical Potential

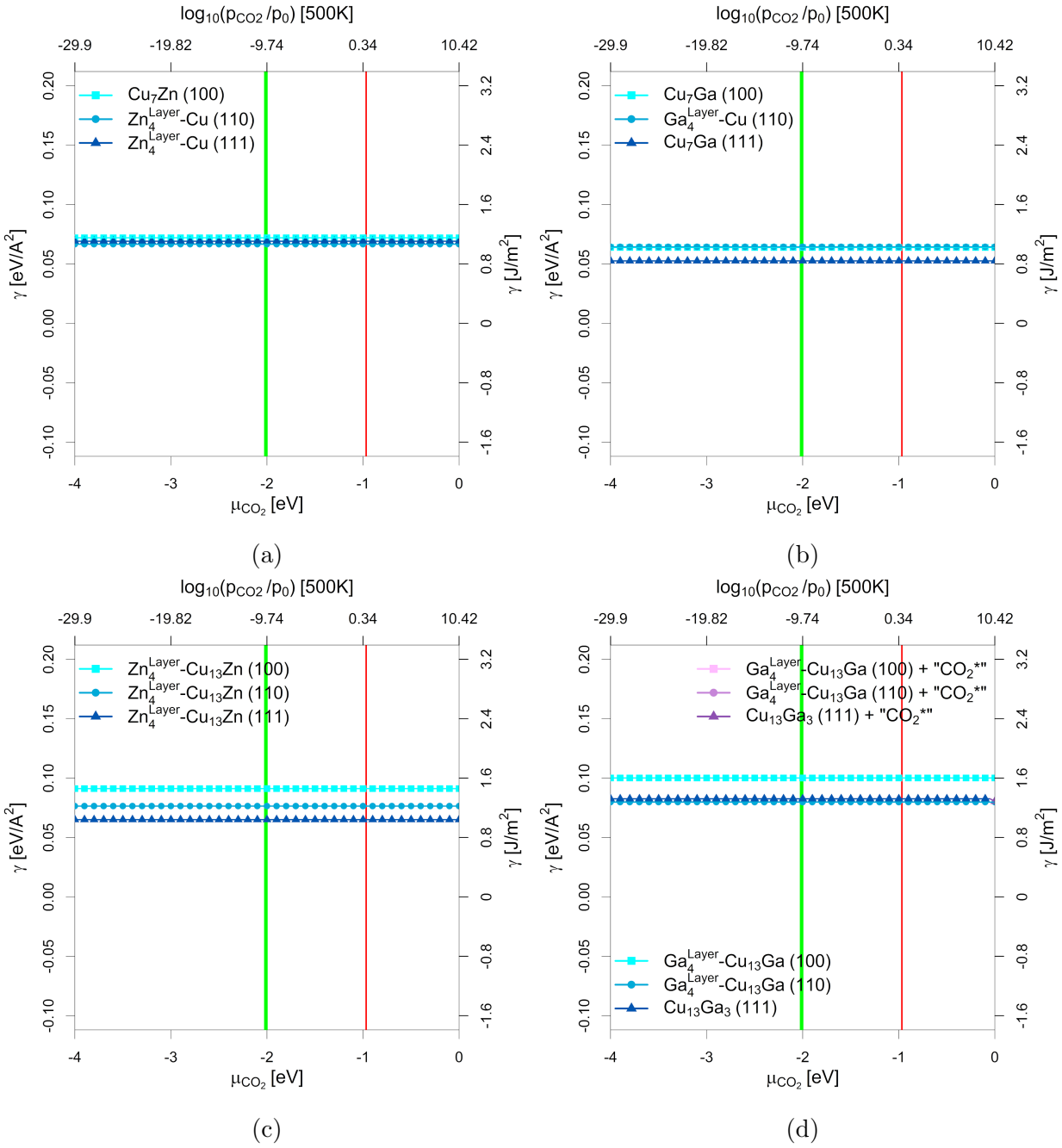

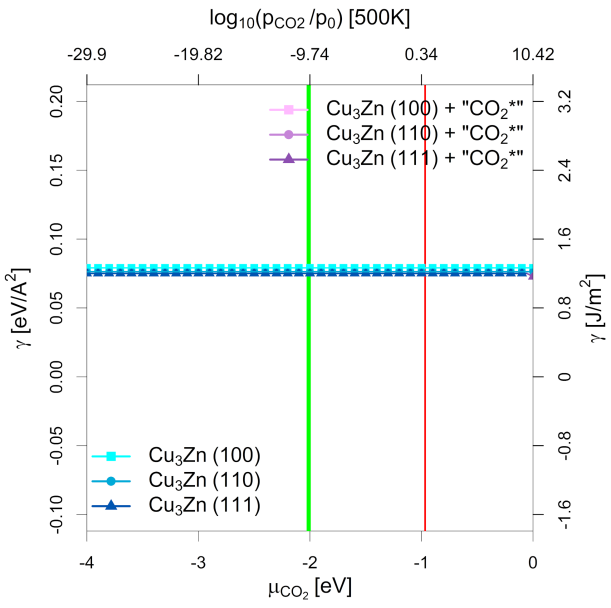
log10(pCO2 /p0) [500K]
-29.9
-19.82
-9.74
0.34
10.42
Cu3Zn (100) + "CO2*"
Cu3Zn (110) + "CO2*"
Cu3Zn (111) + "CO2*"
Cu3Zn (100)
Cu3Zn (110)
Cu3Zn (111)
γ [eV/A2]
γ [J/m2]
μCO2 [eV]

(e)

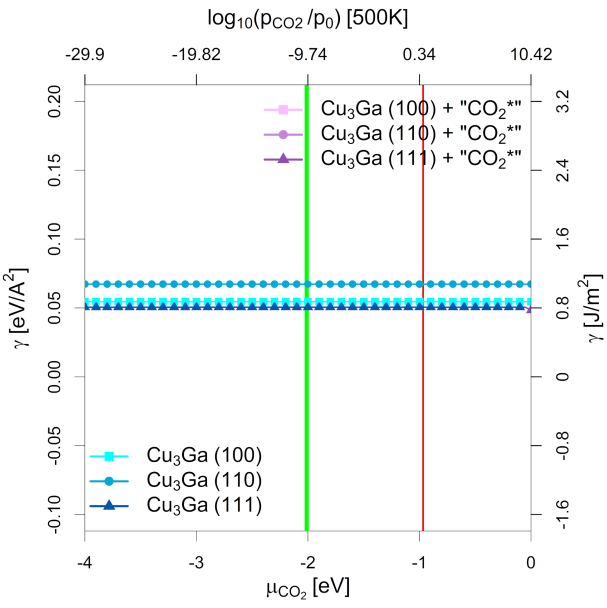
log10(pCO2 /p0) [500K]
-29.9
-19.82
-9.74
0.34
10.42
Cu3Ga (100) + "CO2*"
Cu3Ga (110) + "CO2*"
Cu3Ga (111) + "CO2*"
Cu3Ga (100)
Cu3Ga (110)
Cu3Ga (111)
γ [eV/A2]
γ [J/m2]
μCO2 [eV]

(f)

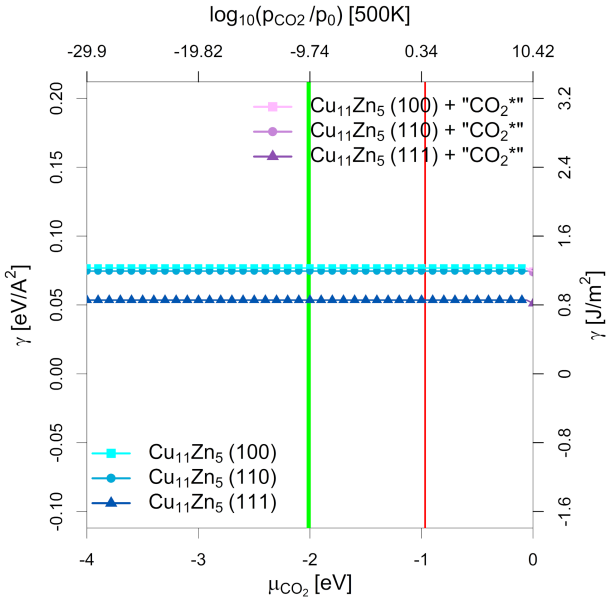
log10(pCO2 /p0) [500K]
-29.9
-19.82
-9.74
0.34
10.42
Cu11Zn5 (100) + "CO2*"
Cu11Zn5 (110) + "CO2*"
Cu11Zn5 (111) + "CO2*"
Cu11Zn5 (100)
Cu11Zn5 (110)
Cu11Zn5 (111)
γ [eV/A2]
γ [J/m2]
μCO2 [eV]

(g)

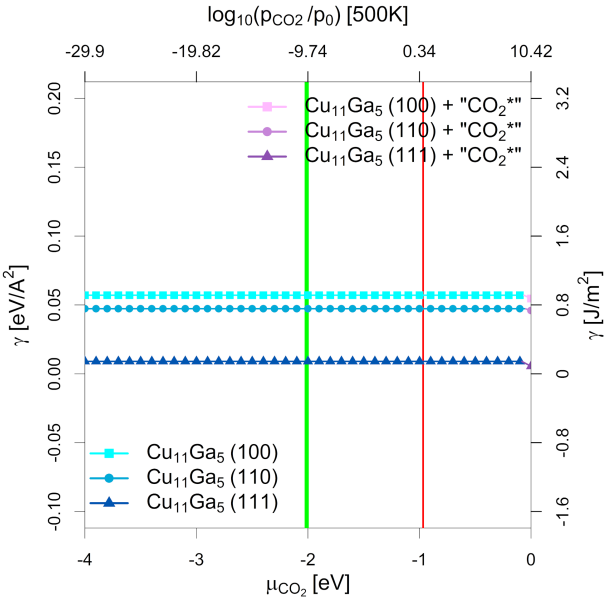
log10(pCO2 /p0) [500K]
-29.9
-19.82
-9.74
0.34
10.42
Cu11Ga5 (100) + "CO2*"
Cu11Ga5 (110) + "CO2*"
Cu11Ga5 (111) + "CO2*"
Cu11Ga5 (100)
Cu11Ga5 (110)
Cu11Ga5 (111)
γ [eV/A2]
γ [J/m2]
μCO2 [eV]

(h)

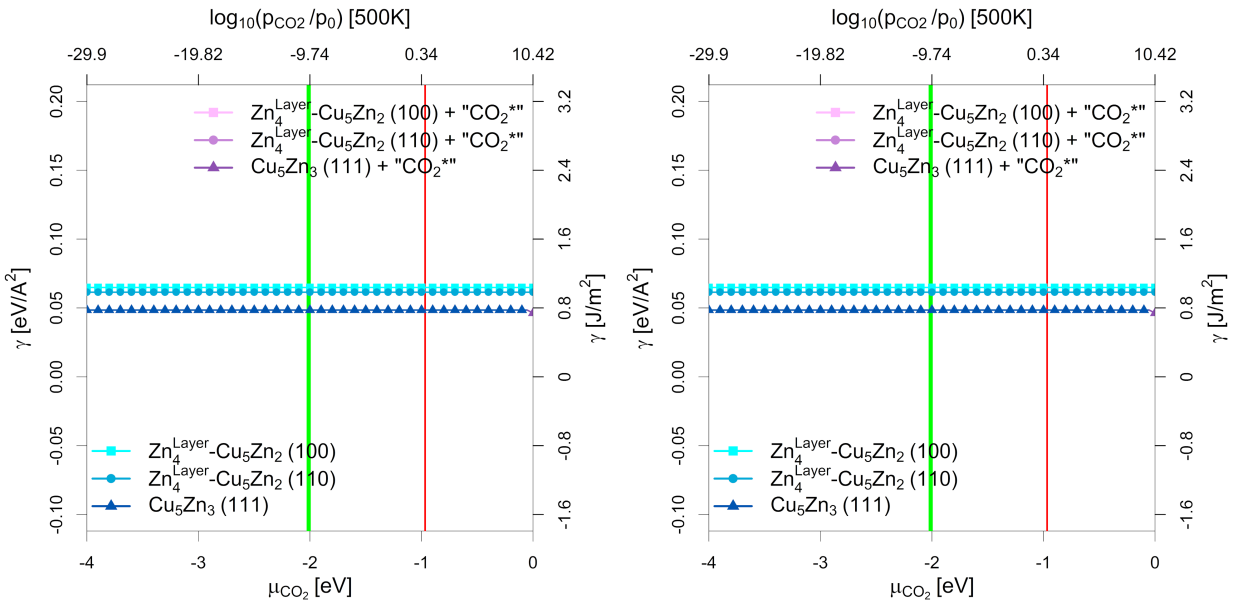

Figure S27: Most stable surfaces of the fcc-Cu_3Ga/fcc-Cu_3Zn alloys with various compositions depending on the chemical potential of CO_2 (μ_{CO_2} in eV) and the equivalent oxygen partial pressure at 500 K including unlayered structures, partially layered structures and fully layered structures. The red area indicates μ_{CO_2} expected under CO_2 hydrogenation conditions ($X_{CO_2} = 1$, -0.97 eV $\mu_{CO_2} < -0.96$ eV). The green area indicates the expected μ_{CO_2} under CO_2 hydrogenation conditions ($X_{CO_2} = 0$, -2.03 eV $< \mu_{CO_2} < -2.00$ eV). The blue part without incline indicates the most stable structure in vacuum, while the violet part with incline shows the most stable structure with oxygen adsorbed. The shown promoter concentrations are:
(a/b) Substoichiometric fcc-Cu_3Ga/-Cu_3Zn (12.5 % Zn/Ga).
(c/d) Substoichiometric fcc-Cu_3Ga/-Cu_3Zn (18.75 % Zn/Ga).
(e/f) Stoichiometric fcc-Cu_3Ga/-Cu_3Zn (25 % Zn/Ga).
(g/h) Superstoichiometric fcc-Cu_3Ga/-Cu_3Zn (31.25 % Zn/Ga).
(i) Superstoichiometric fcc-Cu_3Zn (37.5 % Zn).
(j) Superstoichiometric fcc-Cu_3Zn (43.75 % Zn).

References

(S1) Chase Jr., M. W. In *NIST-JANAF Thermochemical Tables, Fourth Edition*; of Standards, N. I., (U.S.), T., Eds.; Journal of Physical and Chemical Reference Data, Monograph 9: Gaihersburt, Maryland 20899-0001, 1998.

(S2) Müller, A.; Comas-Vives, A.; Copéret, C. Shape and Surface Morphology of Copper Nanoparticles under CO2 Hydrogenation Conditions from First Principles. *The Journal of Physical Chemistry C* **2021**, *125*, 396–409.